MINIATURE PIEZOCONE TESTS
AND EFFECTS OF SMEAR DUE TO VERTICAL PENETRATION
IN LAYERED SOILS

by

Note Sangtian

A thesis submitted to The University of Sheffield

Department of Civil and Structural Engineering

for the degree of Doctor of Philosophy

September, 2001

To my beloved parents

Mr. Cherm Sangtian

and

Mrs. Sompong Sangtian

ACKNOWLEDGEMENTS

The author would like to express his deepest thanks and gratitude to his supervisor, Dr. C. C. Hird, for his invaluable suggestions, comments and guidance throughout the research, without which the research would not be accomplished.

Technical support given by Mr. P. L. Osborne and Mr. M. J. Foster during the experimental work is gratefully acknowledged.

Special thanks are due to Dr. V. J. Moseley for his kind guidance on the experimental work at the beginning of the research, Mr. A. Oram for his help at the initial stages of making sintered glass tip filters for the piezocone and Mr. P. Johnson for his suggestions during a part of the piezocone dissipation analysis. Thanks are also due to his colleagues in Geotechnics Research Group and all his Thai friends in Sheffield for their precious friendship.

Appreciation is gratefully expressed to Dr. T. H. Seah, in Thailand, for his kind encouragement and suggestions.

At personal level, profound thankfulness is due to his girlfriend, Mrs. Narisara Buakhaw for her exhaustive patience and support throughout the research period.

Finally, he is particularly indebted to The Government of Thailand for giving a chance to carry out this research, sponsoring the tuition fees and all life expenses in England.

ABSTRACT

Knowledge of the soil profile is necessary for ground engineering projects and piezocones are widely used in situ test devices that can supply some of this knowledge. This thesis describes an investigation of the performance of a specific piezocone when used in thinly layered soil.

A miniature piezocone, with a cross sectional area of 1cm^2, was driven at a speed of 20mm/sec into artificial layered soil samples that were constructed in the laboratory and consolidated under a vertical pressure in a 254mm diameter test cell. The layered samples contained alternating layers of pre-consolidated Speswhite kaolin clay about 20mm thick and layers of more permeable, silty or sandy soil about 2mm thick. The pore pressure filter of the piezocone was located either at the cone tip or cone shoulder. During driving, the cone resistance and pore pressure responses were recorded at a rate of at least 200 readings/sec. Once the piezocone was stopped, in a clay layer, the dissipation of excess pore water pressure was monitored.

In terms of the pore pressure response, though not the cone resistance, the piezocone was able to detect the more permeable layers located between the clay layers. Both dilation and localised drainage in the more permeable layers, deformed during penetration, could have significantly influenced the pore pressure responses. Despite the proximity of permeable layers, values of the coefficient of consolidation obtained from pore pressure dissipation at the piezocone tip agreed fairly well with values obtained independently during unloading or reloading of the clay in one-dimensional consolidation tests. At the cone shoulder, the permeable layers had some influence and larger values were obtained.

The layered soil samples used for piezocone testing were also used for investigating the effects of soil disturbance, or "smear", caused by vertical penetration of objects with different sectional shapes in the context of permeability measurement and soil drainage. A mandrel carrying a vertical drain, either circular (23.5mm diameter) or rectangular (50x6.5mm) in section, was driven into the centre of the soil sample at a speed of 5mm/sec. The effects of smear were evaluated by performing radial flow permeability tests in which pressure distributions across sample were recorded.

The effect of smear increased substantially as the permeability of the more permeable layers increased, but only when it exceeded the permeability of the clay by a factor of about 100. For a given layer combination, the rectangular drain always produced a significantly smaller smear effect than the circular drain.

CONTENTS

LIST OF FIGURES

LIST OF TABLES

LIST OF SYMBOLS

A_c	=	projected area of the piezocone
a	=	cone area ratio
b	=	width of band drain
B_q	=	pore water pressure coefficient
c_v	=	vertical coefficient of consolidation
c_h	=	horizontal coefficient of consolidation
D	=	thickness of permeable layer or clay layer
d_w	=	diameter of circular drain or equivalent diameter of band drain
e	=	void ratio
f_s	=	piezocone sleeve friction
G	=	shear modulus
I_r	=	rigidity index
k_h	=	horizontal permeability
k_v	=	vertical permeability
k_r	=	permeability ratio (k_h of layering material / k_h of kaolin)
k_s	=	horizontal permeability of smear zone
k_m	=	measured horizontal permeability
m	=	measured initial gradient of a dissipation curve
m_v	=	coefficient of one-dimensional volume compressibility
M	=	measured initial theoretical gradient of a dissipation curve
n	=	vertical drain spacing ratio (= r_e/r_w)
N_{kt}	=	empirical cone factor
Δp	=	differential pressure across sample
q	=	flow rate
q_c	=	uncorrected cone resistance
q_t	=	corrected cone resistance

Q_t	=	normalised cone resistance
r_c	=	radius of piezocone
r_w	=	radius of vertical drain (equivalent for band drain)
r_e	=	radius of equivalent soil cylinder
r_k	=	ratio of horizontal permeability to vertical permeability (= k_h/k_v)
r_s	=	radius of smear zone or reduction of permeability of soil sample
R	=	radius of soil sample
S	=	normalised smear zone radius (= r_s / r_w)
s_u	=	undrained shear strength
t	=	consolidation time or dissipation time or thickness of band drain
T	=	theoretical consolidation time factor
T^*	=	modified theoretical consolidation time factor
Δu	=	excess pore pressure
U	=	degree of consolidation
u_1	=	pore pressure measured at cone tip
u_2	=	pore pressure measured at cone shoulder
u_{cf}	=	pore pressure measure at cone face
u_d	=	datum pore pressure before a piezocone test
u_o	=	final measured pore pressure after a piezocone dissipation test
u_{max}	=	maximum pore pressure before a dissipation test
Δu_n	=	normalised excess pore pressure during a dissipation test
w	=	water content
η	=	ratio of horizontal permeability to permeability of smear zone(= k_h/k_v)
σ_{vo}	=	total over burden stress
σ'_v	=	vertical effective stress

CHAPTER 1

INTRODUCTION AND RESEARCH METHODS

1.1 Background

Natural soils in many parts of the world are layered or laminated. Most commonly this is due to differential rates of settling of soil particles, with different grain sizes, after transportation by wind or water. Layering can produce a variation (i.e. anisotropy) in values of certain properties, e.g. shear strength and permeability. The arrangement of layers having different particle sizes is part of the soil "fabric". The term fabric is used to describe the arrangement of the layers along with other structural features.

It is important to record soil fabric during soil exploration. Rowe (1972) stated that the fabric must be described because classification by index tests and grading alone is not indicative of the engineering performance of natural deposits in situ. Rowe also highlighted the significance of layered fabric to engineering, e.g. its influence on the consolidation rate of soil beneath foundations and embankments, the rate of swelling and effective stress change in soil around excavations, retaining walls and cast in situ piles.

Steenhuis et al. (1990) stated that the way soil is layered affects how water and solutes leaking from landfills flow down to the ground water. In open excavations, water-bearing sandy or silty soils are particularly troublesome when interbedded with layers of clay (Tomlinson, 1995). The silt or sand eroding from the face can cause undermining and collapse of more stable clay layers. Ladd (1990) suggested that most normally consolidated soils exhibit significant anisotropy of undrained shear strength which generally becomes more important in lean clays. Varved clays could present unusually low strengths on horizontal shear planes.

Soil profiling information is generally obtained by making shallow excavations (trial pits) in the field or drilling boreholes to collect samples using tube

samplers. The physical description of soils in trial pits or tube samples and the determination of their engineering properties are both necessary for ground engineering projects. However, a major problem of testing soil samples collected from the field is the disturbance caused by sampling, transportation and setting up the sample in laboratory. Furthermore, these procedures can also be time-consuming and expensive. Therefore, in-situ testing has been developed for ground exploration and there is now a wide range of such tests.

The piezocone, a cone penetrometer with measurement of pore water pressure, is one of the most widely used in-situ test devices. With an ability to measure soil resistance and pore water pressure, normally at the cone tip (u1) or shoulder (u2), simultaneously during penetration, the piezocone provides a profile of soil type and soil shear strength. From dissipation tests when penetration is halted, consolidation properties of the soils can be determined. However, generally, the piezocone is used to explore stratigraphy or macroscopic features of the ground. Determining fabric detail, in the form of thin layers or lenses, using the piezocone is not prevalent.

Soil fabric does not only influence the behaviour of natural soil in situ but also causes difficulties and uncertainties in soil property determination, both in the laboratory and in the field. In laboratory tests, small samples collected from the same region with variations of fabric can have very different performances in terms of shear resistance and consolidation. In in-situ tests, installation of the in-situ testing devices generally disturbs the soil to a degree. As reported by Tavenas et al. (1986) and DeGroot & Lutenegger (1994), for in-situ permeability determination conducted by installing a piezometer, the disturbed soil surrounding the piezometer, known as the "smear zone", can reduce the measured permeability of layered soil significantly. During the penetration of a piezocone, disturbance, or smearing, of the soil potentially affects the pore water pressure response, especially when the measurement is taken at the cone shoulder where the surrounding soil is disturbed more that at the cone tip. Disturbance of the soil could also affect dissipation test results.

The smear zone does not only cause problems during in-situ tests but also during ground improvement using vertical drains. For construction on soft soils, consolidation time is an important design issue and vertical drains are often installed

into the ground to speed up the consolidation of the soil. Once the ground is subjected to load, the pore water flows horizontally to the vertical drains. This is encouraged by soil layering which naturally causes the overall horizontal permeability to be greater than the overall vertical permeability. In the vertical drains, the water is then directed upwards to the ground surface and led away. However, the smear zone surrounding the drains, caused by installation, can reduce their effectiveness.

Despite the common occurrence of smear in layered soils, relatively little is known about its effects in quantitative terms. One of the first systematic studies was conducted by Moseley (1998) at the University of Sheffield and this provided a platform for further research described in this thesis.

1.2 Research Aims

Building on previous work, Moseley (1998), the present research aims to:

a) investigate the performance of a miniature piezocone in detecting thin soil layers with different permeabilities within clay deposits.
b) investigate the influence of more permeable layers on the measurement of the coefficient of consolidation in clay layers using the piezocone .
c) investigate the influence on smear of the relative permeabilities of the clay layers and the more permeable layers.
d) investigate the effects of the sectional shape of the penetrating object on smear in layered soils.

The last of these aims was in recognition of the fact that many vertical drains are rectangular rather than circular in shape, and that the mandrels used to install them vary similarly. Only circular penetrating objects were used by Moseley (1998).

1.3 Research Methods

To achieve the research aims, artificial layered soil samples, containing layers of consolidated Speswhite kaolin clay and more permeable soil, were constructed in the laboratory. Three types of soil, with different gradings and hence different permeabilities, were used to make the more permeable layers, though only one type of permeable layer was used in each layered sample. The more permeable layers and the clay layers were placed in a 254mm diameter test cell alternately in order to form a layered sample. Before any test was carried out, the layered soil sample was consolidated vertically to an effective stress of 250kPa.

To investigate the effects of the sectional shape of a penetrating object on smear in layered soils, a mandrel carrying a vertical drain, either circular or rectangular in section, was vertically driven into the centre of the soil sample at a speed of 5mm/sec. After a sheath protecting the drain had been removed, pore water pressure probes were installed in the sample at various radii. The effects of smear due to the central drain installation were investigated by allowing water to flow inwards from the sample periphery to the drain. The permeability of the sample was determined from the measured flow rate, while the variation of pressure across the sample was measured by differential pressure transducers attached to the pore pressure probes. The effects of smear were evaluated by comparing the measured permeability with the theoretical permeability of the undisturbed sample and also by determining the head loss across the smear zone using the information from the pore pressure probes. The influence of the permeability of the more permeable layers on the degree of smear was observed by comparing tests on different layered samples.

After the flow tests, a mini-piezocone with pore water pressure measurement at either the tip or shoulder was driven into the layered sample at a rate of 20mm/sec. During the piezocone driving, the cone resistance and pore water pressures were recorded. At a predetermined driving distance, chosen so that the pore pressure was being measured in the middle of a clay layer, the piezocone was stopped and dissipation of the excess pore water pressure was monitored. A coefficient of consolidation was obtained from this dissipation test and compared with independently measured values for the clay. Performances of the piezocone in the various layered samples were compared.

After all the tests on a given sample had been performed, the sample was dissected. Deformations of the soil fabric due to drain installation were visually observed to assist the understanding of smear.

1.4 Thesis structure

The following chapter, Chapter 2, reviews literature relating to the permeability characteristics of sedimentary soils and some in-situ geotechnical devices, including vertical drains, whose efficiency could be affected by smear. In Chapter 3, sample building materials, experimental equipment, calibration of the instrumentation and calibration errors are described. Chapter 4 describes the methods and procedures used in the permeability tests in layered soil, the mini-piezocone tests and supplementary tests to determine soil properties. Experimental results obtained during the research are presented in Chapter 5. In Chapter 6, the experimental results are discussed and compared with previous experimental or theoretical work in order to draw conclusions. Chapter 7 summaries the main findings of the research. Recommendations for the further work are also given in this last chapter.

CHAPTER 2
LITERATURE REVIEW

2.1 Introduction

As described in the Chapter 1, one of the aims of the present research is to study effects of smear due to vertical penetration in layered soils. Sedimentary soils are generally layered and therefore, this chapter reviews literature relating to the formation and permeability characteristics of sedimentary soils, concentrating mainly on the anisotropy of permeability.

Also in the first chapter, piezocones, piezometers and vertical drains were indentified as in-situ geotechnical devices whose test results or working efficiency could possibly be affected by the disturbance of the penetrated soil. Literature relating to these devices is reviewed in this chapter.

In the last section of this chapter, an overview leading to the present research is presented.

2.2 Permeability Characteristics of Sedimentary Soil

A natural soil may be residual or sedimentary. A residual soil is formed in place by the weathering of rock. The rate of rock weathering, involving both physical

and chemical processes, is influenced by climate, time, type of source rock, vegetation, drainage, animal activity and bacterial activity.

In sedimentary soil, the individual particles originate in one place but are transported and deposited in another place by wind or water. Of course, particles can be transported by ice and gravity too, to form glacial soils and colluvium. Transportation may alter particle shape, size and texture by abrasion, grinding or impacting. Transportation may also sort the particles.

Lambe & Whitman (1979) described the degree of soil particle sorting occurring during transportation by air (very considerable sorting), water (considerable sorting), ice (very little sorting) and gravity (no sorting). The mode of transportation and deposition, especially in water and air, are obviously influenced by fluctuation of climatic conditions. For this reason, most sedimentary soils found extensively throughout the world consist of irregularly alternating layers of fine-grained soil and coarse-grained soil. The alternating soil layers have different engineering properties such as permeability, compressibility and shear strength and therefore the layered soil presents overall anisotropic behaviour.

The permeability anisotropy of the layered soil is normally expressed as the ratio (r_k) of the coefficient of permeability for flow in the direction parallel to the soil layers (k_h) to the coefficient of permeability for flow in the direction perpendicular to the soil layers (k_v). Holtz et al (1991) estimated r_k as 1 to 1.5 for clays with no macrofabric or only slightly developed macrofabric or homogeneous deposits, 2 to 4 for clays with fairly well to well-developed macrofabric, e.g. sedimentary clays with discontinuous lenses and layers of more permeable material, 2 to 3 for varved clays and 3 to 15 for other deposits containing embedded and more or less continuous permeable layers.

Kenney (1963) stated that in a repeatedly layered sediment, the materials in individual layers are not necessarily homogeneous and their properties will probably vary to some degree across each layer. The permeability ratio for the layered soil as a whole is dependent on the limits between which the permeability coefficients of the individual layers vary and the manner of the variation across the layers. It was

concluded that the average permeability ratio of the deposit could vary from 3 to 300 when the ratio of the two limiting permeability values is 1000.

Kenney & Chan (1973) conducted a laboratory investigation of the permeability ratio of New Liskeard varved soil. Cubic test specimens with dimensions of $64 \times 64 \times 64$ mm were cut from 114mm diameter tube samples by a vibrating-wire cutting tool. Then, for a given specimen, k_h and k_v were independently measured. The results indicated that the permeability ratio, r_k, was less than 4. The authors attributed the small value of r_k to the fact that the permeability of the constituent soils within the varves varied by a factor of less than 6. By making eight additional cut surfaces in some test specimens and evaluating their influence, the authors also reported that the decrease in k_h due to one cut surface at right angles to the layers was approximately 1.5 %. The authors also investigated r_k of the soil in the field by using a "pressure-pattern" method. In this method, the pressure pattern (pore pressure distribution) for a steady flow within the studied area was determined by using piezometers. Then, using the three dimensional steady state flow equation (Taylor, 1948), the measured pressure on the boundaries and an assumed value of r_k, the pore water pressure pattern within the boundaries was determined analytically. By trial and error, comparing the measured and computed water-pressure patterns, the most appropriate value of r_k was determined. It was reported that the maximum value of r_k was less than 5.

Little et al. (1992) performed some laboratory measurements of the permeability of Bothkennar clay. In a first set of tests, the vertical and horizontal permeabilities of the soil were determined indirectly using results from consolidation tests. The samples used for the consolidation tests were collected by a 100mm diameter piston sampler. Then they were extruded and oriented before specimens were recovered in stainless steel oedometer rings so that vertical and horizontal drainage during consolidation could be achieved. Furthermore, a remoulded sample was also tested to find its permeability. By using an X-ray densimeter (Edge & Sills,1989) to investigate the fabric of the soil, silt laminations with a thickness of 0.8-2mm and a spacing of 4.5-25mm were observed. By using the consolidation test results and making the assumption that the silt and clay layers were isotropic in terms

of permeability, the individual permeabilities of the silt and clay were calculated as $2.36x10^{-8}$ m/s and $2.25x10^{-9}$ m/s respectively. For the overall permeabilities, it was found that k_v was $2.47x10^{-9}$ m/s and k_h was $3.99x10^{-9}$ m/s ($r_k = 1.62$).

In a second set of tests, Rowe cells of 75mm and 150mm diameter were used. The soil samples were consolidated with vertical or horizontal drainage. For vertical consolidation, drainage was allowed at the top and bottom of the sample and, for horizontal consolidation, drainage was allowed at the periphery and at a central drain made of a porous plastic tube with a perforated brass rod as a core. Vertical flow tests and horizontal flow tests were then performed on the samples. It was found that at shallow depths, where the clay was described as rather homogeneous (Paul et al., 1992), there was a small degree of anisotropy of permeability (r_k=2.5). At 8m depth, where the clay was recorded as laminated with significant silt and fine sand laminae, there was a much higher degree of permeability anisotropy (r_k=8). The clay described as mottled at 10-15m depth showed a modest degree of anisotropy (r_k=3).

Rowe (1972) intensively reported the relevance of soil fabric to site investigation practice. Influences of soil fabric on test data and the performance of several sites were reviewed. It was reported, for example, that permeable fabric increases the rate of swelling of "unloaded" soil, e.g. slope cuts, and allows rapid softening of the soils leading to failure and that fabric causes uncertainties of results obtained from determination of soil properties e.g. the coefficient of consolidation in laboratory especially when small samples are used. Minimum sizes of undisturbed samples of non-fissured, fissured and jointed clay were suggested for the determination in the laboratory of the coefficient of consolidation, coefficient of compressibility and shear strength. Concerning fabric description, Rowe recommended that a comprehensive soils report should contain photographs (including x30 magnifications) of the fabric of the principal strata.

2.3 The Piezocone

Cone penetrometers have been widely used in soil investigation and cone penetration tests (CPT) have been performed since 1934 (Meigh, 1987). In the CPT, as the penetrometer is pushed into the ground, the resistance at the penetrometer apex and the drag on the side of the penetrometer body (friction sleeve) are measured and used for soil identification. Early measurements were made by mechanical methods but electrical transducers were later introduced.

After Janbu & Senneset (1974), Schmertmann (1974), Tortensson (1975) and Wissa et al. (1975) had reported pore water pressure responses as piezometer probes were driven into soil, Baligh et al. (1980) suggested that a combination of pore water pressure data and cone penetration (CPT) data could provide a promising method for soil identification and an estimate of overconsolidation in clay deposits. Roy et al. (1980) showed the first combination of pore water pressure and cone resistance results from the same probe during driving.

A present day electric piezocone (CPTU) is composed of the cone body incorporating the friction sleeve, the tip with a resistance sensor, and the pore water pressure transducers which are connected to one or several filters located either at the cone tip or along the cone body. Now, due to several advantages such as time and cost effectiveness, good repeatability, suitability for use on a large range of sites (including offshore), the piezocone is widely used in soil investigation.

The cone resistance (q_c) is gained by dividing the total force acting on the conical part of the instrument during driving by the projected area of the cone (A_c), while dividing the force acting on the friction sleeve by the sleeve surface area gives the sleeve friction (f_s). Several types of piezocone with different pore water pressure filter positions have been developed and used in soil investigation (Figure 2.1).

2.3.1 Piezocone calibration

Before the piezocone can be used the cone resistance, sleeve friction, and pore water pressure transducers must be calibrated

In ISSMGE (1999), it was recommended that, during cone resistance calibration, the cone should be subjected to loading and unloading axially and the calibration should be carried out for loading ranges which are relevant to the forthcoming tests. For a new probe, the sensors should be subjected to 15-20 repeated loading cycles up to the maximum load before the calibration. For the calibration of the pore water pressure measuring system, it was recommended that the cone should be calibrated in a pressure chamber in which an incrementally increasing pressure could be applied to the enclosed part of the probe.

Schaap & Zuidberg (1982) stated that during penetration testing the calibration factors can change either due to ingress of soil into the penetrometer grooves or due to a change of the modulus of the penetrometer material with time. The authors also stated that, in the load cell calibration, the accuracy of a penetrometer tip cannot simply be expressed by a single number or percentage. Several terms relating to accuracy were presented, (Figure 2.2). From inspection of penetrometers used in regular soil investigation, it was shown that the soil ingress contributes the major part of the calibration error, which could be limited to 0.4% if a standard procedure of maintenance is followed. Furthermore, it was suggested that hysteresis (the maximum difference between load cell output readings for the same load) and non-linearity (the maximum deviation of the calibration curve from a straight line drawn between no-load and full scale outputs) will be important when a load cell is to be used in a practical loading range which is different from the calibration range. Outputs at zero load before and after a test were recommended to be compared. The zero load error may have several causes such as output instability, temperature induced apparent load, soil ingress, internal friction and hidden loading during zero setting. The authors suggested that the zero load error should not exceed 1 to 2% of the full scale output of the penetrometer.

Lunne et al. (1997) suggested that the piezocone should be regularly calibrated, by using high quality reference load cells and pressure transducers, under exactly the same environment as applies in the real situation (i.e. when measurements are made). All the same cables and data acquisition systems used in the real test should be used during calibration and all the transducers should be calibrated accurately over the real test load range.

2.3.2 Piezocone saturation

De-airing the piezocone is a critical step of the necessary preparation before driving. When the piezocone is driven into the ground, changes in pore water pressure will be transmitted by the incompressible fluid saturating the transducer inside the cone. Effects of poor saturation have been reported by a number of researchers (e.g. Lunne et al,1997; Campanella & Robertson,1988). Lack of saturation could seriously affect the measured maximum pore water pressure pressures during penetration tests and the dissipation times which are normally used to determine the consolidation properties of the soils.

Several saturation fluids have been used in previous research and practice.

(i) Glycerol Due to its high viscosity, glycerol can develop a high air entry tension which can prevent loss of saturation when the piezocone is driven through the soil above ground water table or unsaturated soils. Nevertheless, Campanella & Robertson (1988) suggested that penetration through unsaturated clays can generate very large suctions and saturation of porous element may not be maintained.

(ii) De-aired water Kurup (1993) used de-aired water to saturate the filter and the transducer cavity. However, Lunne et al. (1997) suggested two difficulties of using de-aired water as the saturation fluid, namely that saturation could not be maintained while the cone is above the ground water table and that the water has too high a freezing point to be used as a saturation fluid for a piezocone test in cold climates.

(iii) Silicon oil With a viscosity higher than water, silicon oil can provide a high air entry value. Lunne et al. (1997) stated that if silicon oil is used as a saturation fluid, because it is immiscible with water, surface tension between the oil and the water in the soil could yield small errors in measuring the pore water pressure.

(iv) Alcohol With a freezing point well below $-100^{\circ}C$, alcohol is used for filter saturation when tests are performed in very cold conditions, e.g. Wissa et al. (1982) used alcohol as a saturation fluid for a test at a temperature of $-34^{\circ}C$.

Procedures to assemble the cone have been reported by Robertson and Campanella (1988), Larsson (1992), Kurup (1993) and Lunne et al. (1997). As reported, the best results are obtained by assembling the piezocone under the saturation fluid. The saturated filters are kept in airtight containers filled with saturation fluid at all times before being assembled. During assembly, a plastic syringe and hypodermic needle are used to flush the cavities between the filters and the pressure transducers. Before testing, the piezocone filters are sealed with a protective rubber membrane so that saturation is maintained.

2.3.3 Interpretation of cone load and pore water pressure responses

According to ISSMFE (1989) the rate of penetration for a CPT should be 20 ± 5 mm/s. While the piezocone is driven into the ground, all the transducer readings are recorded by the data acquisition system. The resistances, at the cone tip and the cone sleeve, and the excess pore water pressure depend on characteristics of the soils such as their type, state of stress and stress history.

Different locations of pore water pressure filter produce different excess pore water pressure results during piezocone penetration. Effects of pore water pressure element location have been studied and reported by many researchers as follows.

Lunne et al. (1997) described how, when the piezocone is driven into the ground, the zone beneath the cone is subjected to a maximum compressive stress

which always yields a positive pore pressure in saturated soils. They also described that the pore water pressure response immediately behind the cone on the cone shaft is dominated by large shear stresses which may induce either positive or negative pore pressure changes depending on the dilatancy properties and stress history of the soil.

Due to the geometry of a cone penetrometer the pore water pressure can act on the shoulder area behind the cone. The pore water pressure measured behind the cone can be used to correct the total cone resistance, q_c, which is influenced by the "unequal area effect". The corrected total cone resistance is given by the equation

$$q_t = q_c + u_2(1-a) \text{ ---------- } (2.1)$$

where q_t = corrected cone resistance

q_c = measured cone resistance

u_2 = pore pressure measured at cone shoulder

a = cone area ratio

The cone area ratio can be determined by geometry or by calibration. By geometry, it is the ratio of the area of the central stem of the cone probe to the overall cross-section area (Figure 2.3). By calibration, as described by Nyirenda & Sills (1988) and Lunne at al. (1997), when the cone is put in a calibration chamber filled with saturating fluid and subjected to a uniform pressure, the value (1-a) is the correction factor that makes the tip load cell response equal to the pressure in the chamber. Nyirenda & Sills (1988) described that, when the cone is subjected to a fluid pressure, an upward force will be transmitted to the cone stem by the o-ring seal between the cone stem and the friction sleeve so the downward force acting on the cone shoulder is reduced by the upward force on the cone stem. This reduction is ignored in the geometric calculation of the correction factor. For this reason, it was suggested that the cone area calibration factor should be obtained by the calibration method and not by the geometric calculation method.

For clays, theoretical studies of the excess pore water pressure distribution around the tip and shaft of the piezocone have been carried out by Lavadoux &

Baligh (1980), Teh (1987) and Whittle & Aubeny (1991). Figure 2.4 illustrates some theoretical pore water pressure distributions.

Sills et al. (1988) used a $5cm^2$ piezocone with four filter elements (at the cone face, at the cone shoulder and at 92mm and 157mm from the cone tip) to investigate the excess pore water pressure distribution while the cone was driven into soft clay with different over consolidation ratios (OCR) of 1, 1.3, 1.9 and 5. The test results were plotted against the theoretical excess pore water distributions proposed by Lavadoux & Baligh (1980) and Teh (1987), Figure 2.4 (a). It was shown that the experimental values fell closer to Teh's prediction on the shoulder but to Levadoux & Baligh's prediction on the friction sleeve. It was recommended that the pore water pressure used for cone load correction should be directly measured by positioning a pore water pressure filter element at the cone shoulder. Determination of the initial excess pore water pressure distribution could be improved by using a piezocone with pore pressure elements at three or four different positions but the interpretation could be difficult if the tested soil is not uniform.

Jacobs & Coutts (1992) studied the effects of filter locations and materials on the test results at Bothkennar, Scotland. Standard Fugro-McClelland piezocones with cross section areas of $10cm^2$ and $15cm^2$ were used. The location of the filter was either on the cone face or the cone shoulder. The types of filter material used were high density polyethylene plastic (HDPE), ceramic, sintered stainless steel and sintered bronze. The thickness of the shoulder filter was either 6mm or 3mm. The filter on the cone face was either sandwiched as an annulus between two metal sections of the cone tip or embedded in holes on the cone face. It was reported that, at both the cone face and cone shoulder, the different filter materials had little or no influence on the measured pore water pressure. It was stated that, for the clay with more detailed fabric, the thickness of the filter element in relation to the thickness of the soil bedding may be significant. Furthermore, pore water pressures measured at the cone face with the sandwiched filter were higher than those at the cone face with embedded filters. It was postulated that the difference may be because of compression of the sandwich type filter.

Senneset & Janbu (1985) defined a factor B_q which relates cone resistance and pore water pressure. The proposed factor is used in soil classification.

$$B_q = \frac{u_2 - u_0}{q_t - \sigma_{vo}} \quad \text{----------} (2.2)$$

where B_q = pore pressure coefficient

u_0 = hydro static pore pressure

σ_{vo} = total overburden stress

Sills et al. (1989) carried a comprehensive investigation of the correlation of three parameters with OCR. These parameters were B_q, β (May, 1987) and Q (Wroth, 1988)

where $\beta = \frac{u_2 - u_0}{u_{cf} - u_0}$ ----------(2.3) and

u_{cf} = pore water pressure measured at cone face

$$Q = \frac{q_t - \sigma_{vo}}{\sigma_{vo} - u_0} \quad \text{----------}(2.4)$$

The cone penetration tests were performed at three different sites by using a $5cm^2$ piezocone with four filter elements, as mentioned before. The results showed that the variation of β with OCR was more consistent than the variation of B_q and Q with OCR. It was considered that the inconsistency of B_q and Q occurred because the term q_t in these two parameters tends to be dependent on σ_{ho} which could vary up to 50% for a given OCR and σ_{vo}. However, it was suggested that consistent correlation of β with OCR could be achieved only when the two pore water pressure values used in the calculation (u_2 and u_{cf}) are gained by direct measurement.

Robertson (1990) proposed soil classification charts, Figure 2.5, gained by combining three parameters: the pore water pressure coefficient (B_q) the normalised cone resistance (Q) and the ratio of resistance at friction sleeve to cone resistance (Fr)

When a piezocone is driven into the ground, the reaction at the cone tip directly indicates the bearing capacity of the penetrated soil. For clay soils, the undrained shear strength, s_u, can be calculated as

$$s_u = \frac{(q_t - \sigma_{vo})}{N_{kt}} \quad \text{---------- (2.5)}$$

where N_{kt} is an empirical cone factor. As reported by Lunne (1997), ranges of N_{kt} have been proposed as, for example, 8-16 (Aas et al., 1986), 11-18 (La Rochelle et al., 1988) or 6-15 (Karlsrud et al., 1996).

Lacasse & Lunne (1982) performed piezocone tests in two soft Norwegian marine clays, Onsϕy clay and Drammen clay. Using the steady penetration theory of Baligh (1975), the undrained shear strength (s_u) of the clay was predicted and compared the earlier field vane test results. It was reported that the predicted s_u values fell within 10% of the field vane results.

Meigh (1987) stated that, for a conventional CPT, a thin layer of sand within a clay stratum may not be detected if it is less than about 100mm thick while the CPTU can detect a sand layer as thin as 30 to 50mm. By continuous monitoring of pore pressure during cone penetration, Lunne et al. (1997) reported that the response time of a fully saturated piezocone is usually sufficiently fast to observe pore pressure change for very thin layers (<5mm) and that the pore pressure measured on the face of the cone provides the best stratigraphic detail.

Moseley (1998) drove a mini-piezocone with a cross section area of $1cm^2$ into layered soil samples which were made by combining layers of consolidated Speswhite kaolin clay and silty sand in the laboratory. The permeability ratio of the constituent soils and the consolidation stress were controlled. The rate of the data logging during the piezocone penetration was at least 350 data/second or one reading every 0.057mm of penetration. With this fast logging rate, better layer detection could be achieved. By varying the constituent soil layer thicknesses, the capability of the piezocone to detect the soil layers could be systematically investigated. It was shown that, using the pore water pressure response, the piezocone could detect sand

layers as thin as 2mm. The filter element used in the research was made from porous steel and was located at the cone tip.

Van den Berg (1994) , by using a 30mm diameter piezocone (area = 7.1cm^2) with a pore water pressure element at the cone shoulder, performed tests with a driving rate of 20mm/s in a two layer sample made from 500mm of consolidated kaolin and 500mm of sand. In order to visually investigate the penetration behaviour, a cone cut in half lengthwise was pushed downwards alongside a flat clear wall of the sample container. Two test series were carried out. In the first series a clay layer was placed on top of a sand layer (clay on sand) while the opposite order (sand on clay) was employed for the second series. For the test in the clay on sand sample, in terms of the cone resistance, the cone started to sense the stiff sand layer when the junction was about 15mm ahead of the cone tip. As the cone penetrated the sand, the pore water pressure sharply reduced from a steady state value of 80kPa to –50kPa over a distance of 20mm. It was discussed that, when the piezocone started penetrating the sand, a stress relief occurred just above the cone shoulder. Due to dilatancy effects, a small negative pore water pressure was observed as the cone was penetrating the sand layer. For the test in sand on clay sample, it was found that, as the cone approached the junction, the cone sensed the soft clay layer at a distance of about 150mm from the junction. In terms of pore water pressure, a steady state response of about 100-120kPa was reached when the cone tip had penetrated into the clay layer a distance of 100-150mm.

2.3.4 Interpretation of dissipation tests

As described in Section 1.3, a dissipation test can be performed immediately after the piezocone penetration is stopped. A number of researchers have developed solutions to determine the coefficient of consolidation of the soil from dissipation test data (e.g. Torstensson, 1975; Senneset et al., 1982; Levadoux & Baligh, 1985; Teh & Houlsby, 1991).

Based on cylindrical and spherical cavity expansion theory, Torstensson (1975) suggested that the horizontal coefficient of consolidation, c_h, could be computed by using the equation

$$c_h = \frac{T_{50}}{t_{50}} r_c^2 \quad \text{---------- (2.6)}$$

where T_{50} is the theoretical time factor at 50% dissipation, t_{50} is the time at 50% dissipation and r_c is the piezocone radius. T_{50} is theoretically predicted based on the E_u/s_u value where E_u is the undrained Young`s modulus of the clay.

Levadoux & Baligh (1986), based on the strain path method (Baligh, 1985) and Terzaghi-Rendulic uncoupled consolidation theory, proposed excess pore water pressure dissipation curves for cones with tip angles of 18° and 60°. The predicted normalized excess pore water pressure distributions were compared with extensive field measurements in Boston Blue Clay (BBC). It was reported that excellent agreement between the theoretical predictions and the measurements for both the 18° and 60° cones was achieved in BBC with OCR≤ 3. Furthermore, it was concluded that the cone tip angle had a minor effect on the prediction, while coupling between total stresses and pore water pressures could have significant effects at the cone tip especially during the early consolidation stages. The coefficient of consolidation obtained from the dissipation tests were compared with those obtained from laboratory measurements and field performance data. It was found that the c_h (piezocone) of BBC below 18m was virtually identical to the field vertical coefficient of consolidation, c_v, during unloading and slightly higher (by a factor of 2) than the c_v obtained from laboratory consolidation tests during the unloading stages.

A more recent theoretical solution, again based on the strain path method, was proposed by Teh & Houlsby (1991). In this method the size of the zone in which the excess pore water pressure develops due to the cone penetration is dependent on the rigidity index of the soil, $I_r = G/s_u$, where G is shear modulus of the soil. They proposed a modified time factor, T^*, as

$$T^* = \frac{c_h t}{r_c^2 \sqrt{I_r}} \quad \text{----------(2.7)}$$

Teh & Houlsby (1991) also showed that the modified time factor can unify the dissipation curves for all values of I_r from 25 to 500, Figure 2.6. Lacasse & Lunne (1982) performed CPTU dissipation tests in Onsϕy clay and Drammen clay and reported that the horizontal coefficient of consolidation values (c_h) estimated by using Baligh & Levadoux (1980) agreed very well with those obtained from the re-consolidation stages of oedometer tests.

Robertson et al. (1992) presented a summary of comparisons between the experimental reference values of coefficient of consolidation with the values estimated from CPTU dissipation tests. In making the comparisons, for a particular test site, c_v values obtained from the oedometer tests were converted to c_h values by using the vertical and horizontal permeability ratio given by Baligh & Levadoux (1980). The obtained c_h and the corresponding t_{50} for a piezocone test performed at the site were then plotted on the chart for evaluation of c_h provided by Teh & Houlsby (1991). It was concluded that the theoretical solution given by Teh & Houlsby (1991) provided a reasonable estimate of c_h and that the pore pressure measured using the filter element at the cone shoulder gave the most consistent dissipation test results. The estimated c_h value fell within plus or minus half an order of magnitude of the directly measured value, whereas for the tip position this increased to a full order of magnitude.

Schnaid et al. (1997) conducted comprehensive piezocone dissipation tests to evaluate the Houlsby & Teh (1988) solutions. In the research a $5cm^2$ piezocone, with four filter elements at the cone face, the cone shoulder, and at 92mm and 157mm from the cone tip and a $10cm^2$ cone with a filter element at the cone shoulder were used. To quantify the similarity between a given experimental curve and the theoretical one, assuming that the rigidity index (I_r) was constant, c_h values obtained by matching at different degrees of dissipation were compared with the c_h value at 50% dissipation in terms of the ratio $c_{h(U\%)}/c_{h(50\%)}$. It was concluded that the c_h values derived from the pore water pressure element located at the cone shoulder were almost insensitive to the degree of dissipation. For the pore water pressure element at cone tip, the c_h values at initial stages of dissipation were significantly higher than those at 50% dissipation. A continuous reduction of the ratio

$c_{h(U\%)}/c_{h(50\%)}$ was found for values derived from the pore water pressure elements located on the cone shaft.

Some authors (Teh, 1987; Powell & Quatermann, 1997 and Lunne et al., 1997) have discussed the interpretation of consolidation data from short dissipation tests or from tests in which the initial excess pore pressure is not clearly defined. This may be due to the local redistribution of excess pore water pressure or a lack of saturation of the filter elements causing a delayed response.

2.4 Piezometers

A piezometer is a device that is sealed within the ground so that it responds only to the ground water pressure around itself and not to groundwater pressure at other elevations (Dunnicliff, 1988). Applications of piezometers include, for example, monitoring subsurface water pressure during well-pumping permeability tests, monitoring up lift pressures below concrete dams and investigating pore water pressure along a potential failure plane behind a cut slope. They may be also be used for the determination of the permeability of soil in the field by performing constant head or falling head permeability tests.

Based on the installation method, the two main types of piezometer are the pre-drilled piezometer (non-displacement installation method) and the push-in piezometer (full displacement installation method). For the first type, to install the piezometer, a hole is drilled to the depth at which the pore water pressure measurement needs to be performed. The piezometer is then embedded in a sand pocket and the top of the sand pocket is sealed with a low permeability material such as bentonite. For the second type, the piezometer is simply pushed into the ground, from the ground surface or from the bottom of a pre-drilled hole, to the required depth.

For certain types of measurement, such as monitoring of effective stress gains during stage-construction of embankment or fluctuations of pore pressure in the ground near tidal water, the response time of the piezometer is very important. The approximate response times for various types of piezometer have been presented by Terzaghi & Peck (1967). It was shown that pre-drilled piezometers have much shorter response times than those of push-in piezometers. This could mainly be attributed to the effect of the smear zone surrounding the piezometer, caused by installation.

For in situ permeability testing in piezometers, due to the simplicity of the equipment required, falling head tests are commonly used. A major difficulty in performing permeability tests in a pre-drilled piezometer is the definition and control of the shape of the cavity from which the permeant is injected into the soil, since the cavity shape depends on details of the borehole preparation and the installation of the piezometer (Tavenas et al., 1986). This problem is eliminated by using a push-in piezometer (permeameter) where the geometry of the porous element is known. However, this installation method leads to displacement and remoulding of the soil surrounding the piezometer. To minimise the soil disturbance during installation, a self-boring permeameter (Baguelin et al., 1974) was developed.

Tavenas et al. (1986) compared permeability test results gained from falling head and constant head tests using both a push-in permeameter (piezometer) and a self-boring permeameter on various test sites. It was found that the permeability values gained from the push-in permeameter were always lower than those from the self-boring permeameter. The ratio of the permeabilities measured by these two methods was 1.1 at Saint-Polycarpe, where the soil was described as "very homogeneous", and 9.1 at Saint-Alban, where the soil was more stratified. The authors concluded that the driven permeameter was subject to clogging and caused remoulding and a reduction in permeability of the soils tested. The self-boring permeameter was recommended.

DeGroot & Lutenegger (1994) compared field and laboratory measurements of permeability in a varved clay by using a flexible-wall laboratory permeameter and four types of in-situ testing device: a drilled piezometer, a push-in piezometer, a

piezocone and a dilatometer, Figure 2.7. It was shown that the pre-drilled piezometer gave the highest k_h values while the push-in piezometer gave the lowest values. The cone peneteration test and the dilatometer gave values in between those of the pre-drilled and push-in piezometers. In order to evaluate the scale effect on the piezometer test results, the variation of the k value with the ratio of the slot screen length to the diameter of the piezometer (L/D) was investigated. A piezometer with a larger L/D provided larger k values due to the influence of soil fabric until a limit was reached. It was concluded that the push-in piezometer gave very low values of hydraulic conductivity because of remoulding of the surrounding clay.

Leroueil et al. (1992) compared in-situ permeability test results with those obtained from laboratory tests on the estuarine silty clay at Bothkennar. The in-situ permeability test devices used were : (a) a push-in Geonor M-206 open standpipe piezometer with a porous element of 32mm diameter and 277mm length, (b) a self-boring permeameter with a perforated porous element of 73mm diameter and 146 and 292mm length, and (c) a push-in BAT permeameter (Torstensson,1984; Torstensson & Petsonk,1986) which can perform either outflow or inflow in-situ permeability tests. The laboratory equipment used was: (a) a 51mm diameter oedometer cell in which the samples were trimmed and oriented so that consolidation with vertical or horizontal drainage could be performed, (b) a triaxial cell used for constant head permeability tests on specimens with 101mm diameter and 116mm height and (c) a radial flow cell (Leroueil et al., 1990) with a 50mm diameter central injection hole. In terms of vertical permeability, the values obtained from triaxial tests were slightly higher than those obtained from oedometer tests because the larger triaxial specimens contained more silt and sand laminae or lenses than the oedometer specimens. In terms of horizontal permeability, again, the values obtained from oedometer tests were smaller than those obtained from radial flow cell tests, by one-third on average. Comparing all the results gained from the field and laboratory showed that the results from the self-boring permeameter and radial flow cell agreed very well and gave the most representative profiles of horizontal permeability of the soil. However, it was found that the in situ values were smaller than the laboratory values by 30% on average. It was explained that in the radial flow cell the sand or silt lenses are often

connected either to the central injection hole or to the peripheral drain or to both, but in situ the lenses may be discontinuous and have less influence on the measured permeability. It was also explained that the oedometer tests underestimated the horizontal permeability because the specimens were small and did not have silt or fine sand inclusions as existed in the field. Due to effects of their installation, the push-in piezometer, as well as the BAT system, also underestimated the permeability. It was finally concluded that the permeability anisotropy (r_k) was about 1.5-2 .

2.5 Vertical Drains

As described in Section 1.1, for construction on thick deposits of soft soils, consolidation time is an important design issue. To speed up the consolidation of the soil, vertical drains are used to reduce the drainage path length.

The first use of vertical drains, so-called sand drains, was proposed by Moran (1925). Later, Kjellman (1948) published the details of the ' Kjellman wick drain' which was the first prototype of a prefabricated drain and was made entirely of cardboard. Over the years since then, properties and installation techniques of vertical drains have been improved and they have been used in many ground improvement projects throughout the world. It is accepted that, in practice, vertical drain installation disturbs and changes the properties of the surrounding soil to a degree, depending on the soil sensitivity and macrofabric (Rowe, 1968). The soil in the smear zone normally has a lower coefficient of permeability than that of the undisturbed soil and this leads to lower efficiency of vertical drains in accelerating the consolidation of the ground. A number of researchers have been investigating, theoretically and experimentally, the effects of smear around vertical drains due to installation in both layered and homogeneous soils.

2.5.1 Studies of vertical drains in homogeneous soils

a) Analytical and numerical studies

Figure 2.8 shows the general configuration of a circular unit soil model (unit cell) used in several analytical and numerical studies of a vertical drain in homogeneous soil. This is composed of a circular drain with a radius r_w at the centre, a smear zone with a radius r_s surrounding the drain and an outer undisturbed zone with a radius r_e.

A theoretical solution for the consolidation of soft soil around a vertical drain was first derived by Kjellman (1937) by assuming pure radial drainage and equal vertical strain boundary conditions (the surface displacement is assumed to be uniform and the resulting vertical stresses are not uniform).

Barron (1948) presented theoretical solutions for both free vertical strain boundary conditions (the stress at the surface is assumed to be uniform and the resulting vertical displacement at the surface is non-uniform) and equal vertical strain boundary conditions with only radial flow in the soil and showed that the average consolidation obtained from the two solutions is nearly the same. For the case of equal strain analysis, Barron also presented solutions including the effects of smear caused by drain installation and the well-resistance of the drain.

Hansbo (1981) proposed a simplified solution as an alternative to Barron's solution. The equal strain boundary condition was assumed and the effects of smear and well resistance were taken into consideration. He also gave a solution for consolidation around a band shaped drain by transforming the drain into an equivalent circular one with equivalent diameter, d_w, given by

$$d_w = 2(b+t)/\pi \quad \text{----------(2.8)}$$

where b and t are the width and thickness of the drain respectively.

The simplified solution for equal strain boundary conditions without considering the smear effect is

$$\Delta u = \frac{u_i}{r_e^{\,2} \cdot F(n)}\left[r_e^{\,2} \ln\left(\frac{r}{r_w}\right) - \frac{(r^2 - r^2{}_w)}{2} \right] \exp \lambda \text{ ----------(2.9)}$$

where Δu = excess pore pressure

u_i = initial excess pore pressure

r_e = radius of equivalent soil cylinder

= 0.565 x drain spacing (square pattern)

= 0.525 x drain spacing (triangular pattern)

$\lambda = -8T_h/F(n)$, $T_h = \frac{c_h\, t}{4r_e^{\,2}}$

n = the drain spacing ratio= (r_e / r_w)

t = consolidation time

$$F(n) = \frac{n^2}{(n^2 - 1)} \ln(n) - \frac{(3n^2 - 1)}{4n^2} \text{ ----------(2.10)}$$

The average degree of consolidation with respect to radial flow is

$$\bar{U}_h = 1 - \exp\left[\frac{-8T_h}{F(n)} \right] \text{ ----------(2.11)}$$

For the case in which the effect of smear was considered, by assuming an annulus of smeared soil with radius r_s and horizontal permeability k_s around the drain, Hansbo (1981) proposed a simplified factor F(n) as

$$F_s(n) = \ln\left[\frac{n}{S}\right] - 0.75 + \left[\frac{k_h}{k_s}\right] \ln(S) \text{ ----------(2.12)}$$

where S = normalised smear zone diameter (r_s/r_w) and k_h = horizontal permeability of the undisturbed zone

Lancellotta et al. (1981) theoretically investigated the effects on the rate of consolidation of smear zones with different ratios of the horizontal permeability of the undisturbed zone to that of the smeared zone, $\eta = k_h/k_s$, and normalised smear zone diameters, Figure 2.9.

Onoue (1988) derived a rigorous solution for equal strain consolidation by vertical drains taking well resistance and smear into consideration. Two soil types considered in the solution were soil whose compressibility increases due to disturbance and soil whose permeability decreases due to disturbance. For the first soil type, it was concluded that the influence of smear caused by installation of a vertical drain on the consolidation rate is small. For the later type of soil, Onoue showed that Barron's and Hansbo's approximate solutions give a sufficiently high degree of accuracy for practical applications.

Madhav et al. (1993) used a finite difference method to model and study smear zones around band shaped drains. Three distinct zones, an inner smear zone, a transition zone and an undisturbed zone were considered in the analysis. The permeability of the transition zone was an average of the permeability values of the smear and undisturbed zones. Various sizes of rectangular and square smear zone were considered in the analysis. It was found that even a very small smear zone of low permeability can significantly delay the consolidation process and the permeability of the soil close to the drain strongly influences the overall consolidation process. It was also suggested that, with the degree of disturbance being the same, the installation of drains at closer spacing may not necessarily lead to more efficient consolidation of the soil. Changing the shape of the drain from a strip to a circle or an ellipse and reducing the mandrel size were recommended.

Hird et al. (1992) developed an equivalent plane-strain analysis considering a unit cell by matching the average degree of consolidation under axisymmetric and plane strain conditions. The developed methodology was introduced for use in finite element analysis of embankment construction on ground which incorporates vertical drains. They also pointed out that, with the proposed matching procedure, the excess pore pressure variation in the horizontal direction for plane-strain conditions was quite different from that in the axisymmetric case.

Chai et al. (1997) proposed a new solution derived by considering the permeability in the smear zone varying linearly or bi-linearly with radial distance. It was shown that the solution can yield a smooth excess pore pressure distribution in

the smear zone and a more uniform settlement within a unit cell, and that using the average value of permeability in the smear zone will under-estimate the smear effect.

b) Laboratory experimental studies

Singh & Hattab (1979) conducted a laboratory study of the efficiency of sand drains in relation to methods of installation. The ratio of the soil sample diameter to the diameter of the drains used in the research was approximately 10. They reported the ranking (starting with the most successful) of the methods of installation according to the rate of consolidation as (i) closed mandrel (cross-shape), (ii) jetted drains (Dutch method), (iii) jetted mandrel, (iv) auger, (v) closed mandrel (circular), (vi) closed mandrel (star-shape) and (vii) open mandrel.

Ali (1990) investigated the effects of vertical drain deformation caused by settlement of the surrounding soil on the longitudinal flow behaviour of the drains. It was found that the decrease in discharge capacity due to the drain deformation is related to the bending rigidity and the geometrical structure of the drain core and also the stiffness of the filter jacket. The discharge capacity of a vertical drain cannot be based only on results of tests on straight drain samples, especially for sites where a large settlement is expected.

Ali (1991) reported the influence of the filter jacket and core geometry on the longitudinal permeability of a prefabricated drain. In the research, the performances of three types of drain core wrapped by five types of geotextile were investigated. It was found that the discharge capacity of a band-shaped drain depends on the duration of loading as a result of creep deformation of the plastic core and creep of the filter fabric into the flow channels. The tensile strength of the filter must be high enough to overcome the tensile stress induced in the filter and to prevent blocking of flow channels in the core.

Onoue et al (1991) investigated the permeability of the disturbed zone around circular vertical drains. The drains were driven into Boston Blue Clay samples, 305 mm in diameter and 140 mm in height, with OCR=4. Then horizontal flow tests with

measurements of pore water pressure across the sample were performed. The test results were compared with theoretical curves computed using a two-zone model (e.g. Barron, 1948; Hansbo, 1981). It was reported that, using values of S = 1.6 and $\eta = 3$ provided satisfactory predictions for the pore water pressure distribution.

Long & Covo (1995) used an electrical analogue field plotter to determine the equivalent diameter of oblong drains and reported that

$$d_w = 0.5b + 0.7t \text{ ----------(2.13)}$$

The results were then compared with a list (Rixner et al., 1986) of equations that might be used in computing the equivalent diameter of a prefabricated vertical drain. The results were comparable to those obtained using the following similar equation.

$$d_w = (b + t)/2 \text{ ----------(2.14)}$$

However, the values were smaller than those calculated by Eq. 2.8 (Hansbo, 1979;1981) by 30% on average.

2.5.2 Studies of vertical drains in layered and laminated soils

a) Analytical and numerical studies

Horne (1964) introduced an approximate solution for the problem of consolidation of a regularly layered soil surrounding a vertical drain. The soil comprised two different layer types with thicknesses H_1 and H_2, vertical permeabilities k_{v1} and k_{v2} and horizontal permeabilities k_{h1} and k_{h2} where $H_2 << H_1$, $k_{v1} << k_{v2}$ and $k_{h1} << k_{h2}$. The solution becomes more involved when the soil exists in a series of horizontal strata because, during the consolidation, drainage first tends to follow vertical routes to the more permeable layers and then drainage takes place preferentially towards the vertical drains.

Onoue (1988) predicted the consolidation of multi-layered anisotropic soils served by vertical drains with well resistance by using a finite difference method. He

also proposed two simple calculation procedures for the consolidation of multi-layered soils. The first procedure is to assume the multi-layered soil to be homogeneous, by averaging the soil constants using layer thickness weighting. It was concluded that this method yields reasonable results only when the degree of heterogeneity of the soil is small. In the second procedure, for a multi-layered soil where the total thickness is H, it is assumed that each single layer has a homogeneous thickness of H. Then, for a certain load and time, the degree of consolidation of each layer is calculated separately. The water pressure distribution of the layered soil is determined by extracting the excess pore water pressure of the homogeneous soil at the same depth. The layer thickness weighted mean of each consolidation degree was taken as the overall average degree of consolidation.

b) Laboratory experimental studies

Kim et al. (1997) used model mandrels of various shapes (circular, diamond, rectangular and cross shape) to study effect of shape on smear caused by installation. The clay samples used in the experiment were obtained from Busan in Korea and were preconsolidated under a pressure of 49 kPa in a cylindrical mould with an inner diameter of 250mm. Then the soil sample was horizontally cut at 30mm intervals. As the soil sample was reassembled, strips of soup noodles were laid horizontally on the surface of every layer. After sample preparation, a model mandrel was driven into the sample with a speed of 1.5 mm/sec. Then the soil sample was carefully cut vertically and the deformed shapes of the lines of noodles were sketched. It was found that rectangular and diamond shape mandrels are more efficient for reducing the smear effect.

Bergado et al. (1991) studied smear effects due to the installation of prefabricated vertical drains in the laboratory using a large specially designed consolidation test cell with 45.5cm diameter and 92cm height. Remoulded soft Bangkok clay was placed inside the cylinder and consolidated by a vertical pressure of 10.2kPa. At about 90% consolidation, an Alidrain with plan dimensions of 40x6mm was installed using a 60x60mm mandrel. Soil specimens for permeability tests were taken from the undisturbed zone near the periphery and from the smear

zone near the center of the test cell. Then the soil specimens were consolidated under a vertical confining pressure of 48kPa. Permeability tests on the soil specimens showed that ratio between the vertical permeability of the undisturbed zone and horizontal permeability of the smeared zone (k_v/k_s) was close to unity. Furthermore, the ratio of the horizontal permeability of the undisturbed zone to that of the smeared zone (η) ranged between 1.5 and 2.0 with an average value of 1.75. From the large-scale consolidation test, the horizontal coefficient of consolidation (c_h) was back-calculated by using Asaoka's (1978) solution and compared to the value of c_h obtained from oedometer tests. It was found that, with the assumption that η= 1.75 and S = 3, the c_h values obtained from back-calculation were comparable to those obtained from the oedometer tests. With the hypothesis that the friction between the soil and the consolidation cell possibly delayed the consolidation and caused a higher value of S to be inferred, the authors suggested that S = 2 was more realistic.

Moseley (1998) and Hird & Moseley (2000) investigated the effects of smear during vertical penetration of laminated soils. The layered soil model was achieved by combining layers of consolidated Speswhite kaolin clay and silty sand in a model. The sheathed circular vertical drain with diameter of 25mm was driven into the soil model to form the central vertical drain. After drain installation, radial flow permeability tests were performed. Pore water pressure distributions across the sample during the flow tests were investigated by using pore water pressure probes installed at various radii. The influence of lamination geometry, penetrator geometry and penetration rate on smear was investigated by performing parametric variations of clay layer thickness (10, 20, 40mm), sand layer thickness (1, 2, 4mm), mandrel tip angle (20^0, 60^0, 180^0) and mandrel driving rate (0.5, 5, 15mm/sec). It was found that the smear increased as the clay layer thickness, the sand layer thickness, or the driving rate reduced. The mandrel tip angle did not appear to be an influential factor.

2.5.3 Field study of vertical drains

Davies & Humpheson (1981) compared the performance of two types of vertical drain, sand drains and Alidrains, beneath a trial embankment in Belfast. The Alidrains were installed to the depth of about 10m with an Alimak drain stitcher assembly mounted on a Hy-mac Excavator, while the sand drains were installed using traditional shell and auger techniques. It was found that the sand drains appeared to be more efficient than the Alidrains. It was thought that since the sand drains were installed by a non-displacement method the effect of smear due to remoulding was not as great as for the Alidrains, which were installed by a displacement method.

Bergado et al. (1991) studied smear effects due to the installation of prefabricated vertical drains using a full-scale load test. A test embankment was constructed on soft Bangkok clay at the Asian Institute of Technology test site. Alidrains with cross-sectional dimensions of 100x6mm were installed to a depth of 8m in a square pattern with 1.2m centre to centre spacing by using two different sizes of mandrel (45x150mm and 150x150mm). Pore water pressure changes under the embankment and settlement of the ground were investigated by using piezometers and subsurface settlement plates. After construction of the embankment, a faster settlement rate and higher compression were observed in the small mandrel area than in the large mandrel area. It was concluded that, during vertical drain installation, the smear zone caused by the small mandrel was smaller that that caused by the large mandrel.

2.6 Overview

2.6.1 Piezocone

In the studies concerning the piezocone test (CPTU), much attention has been devoted to: (a) the pore water pressure distribution around the cone body and cone tip during penetration, (b) variation of cone resistance and pore water pressure during penetration with soil type and stress history and (c) relationships between dissipation behaviour of excess pore water pressure after penetration and the coefficient of consolidation of the soil.

Several theoretical solutions, in which homogeneity of the soil is one of the most important assumptions, have been developed to predict the pore water pressure distribution around the cone during penetration and during dissipation for a particular filter position on the cone. Many CPTU tests have been performed in the laboratory and the field to evaluate the proposed solutions.

In practice, the piezocone is not only used for soil classification and determination of soil properties but also for profiling the soil fabric (layering) which has been highlighted as essential information for soil engineering works. The performance of the piezocone in determining soil layering has been investigated by some researchers. It was reported that, compared to the cone resistance, the pore water pressure response during penetration is a better indicator of layered fabric in the soil. However, more intensive investigation is needed of the influence of soil layer permeabilities, cone filter locations and smear due to penetration on the layer detection ability and dissipation behaviour of the piezocone. Such investigation forms part of the present research.

2.6.2 Smear during vertical penetration

For in-situ permeability tests, it has been shown by past research that the degree of smear affecting the test results depends on the method of installation (displacement or non-displacement) and the physical properties of the soil, e.g. permeability anisotropy, and its fabric.

For vertical drains, the size and shape of the mandrel used for the drain installation have been reported as important factors affecting the degree of smear. The size of the smear zone and permeability in the smear zone have been predicted and reported by many researchers. Furthermore, some analytical studies have been carried out to investigate the effects of smear on the rate of consolidation of the soil around vertical drains.

Although it has been recognised that installation by a push-in method for permeameters or vertical drains can disturb the soil to a high degree, due to its convenience and economy, this method of installation is still commonly used.

The effects of smear due to installing a push-in permeameter have been generally investigated by comparing the associated permeability values with those obtained by laboratory tests on undisturbed samples collected from the field or from pre-drilled or self-boring permeameters. The soil fabric was investigated but could not be controlled. Moseley (1998), for the first time, systematically investigated the correlation between the degree of smear caused by vertical penetration of a circular object and layer configuration (thickness and spacing) in layered soil samples constructed in laboratory. Influences of penetrating object sectional shape and the permeabilities of the layering materials on the degree of smear are investigated in the present research.

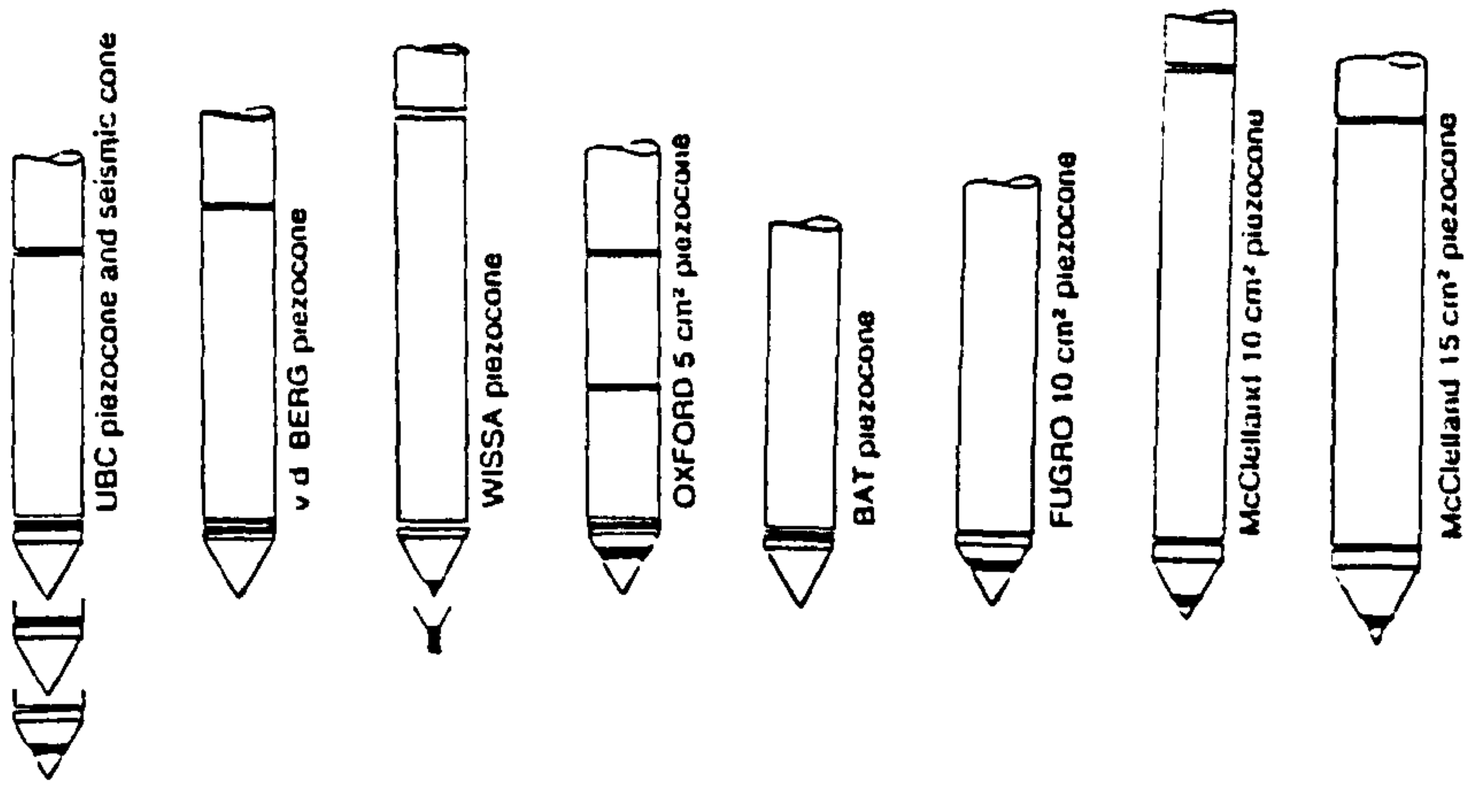

Figure 2.1 Various types of piezocone (Lunne et al..1989)

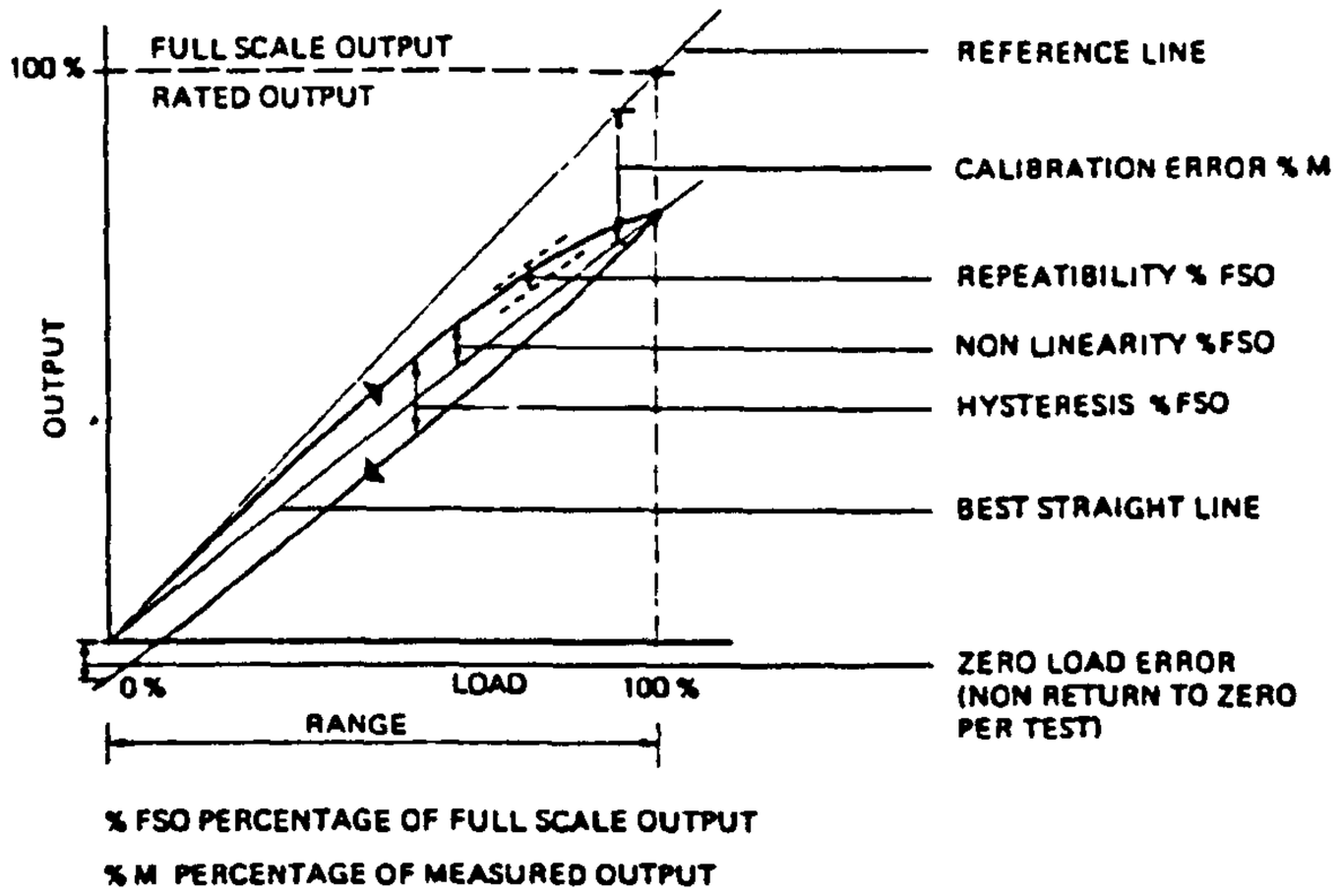

Figure 2.2 Terms relate to accuracy of piezocone during calibration (Schaap & Zuidberg, 1982)

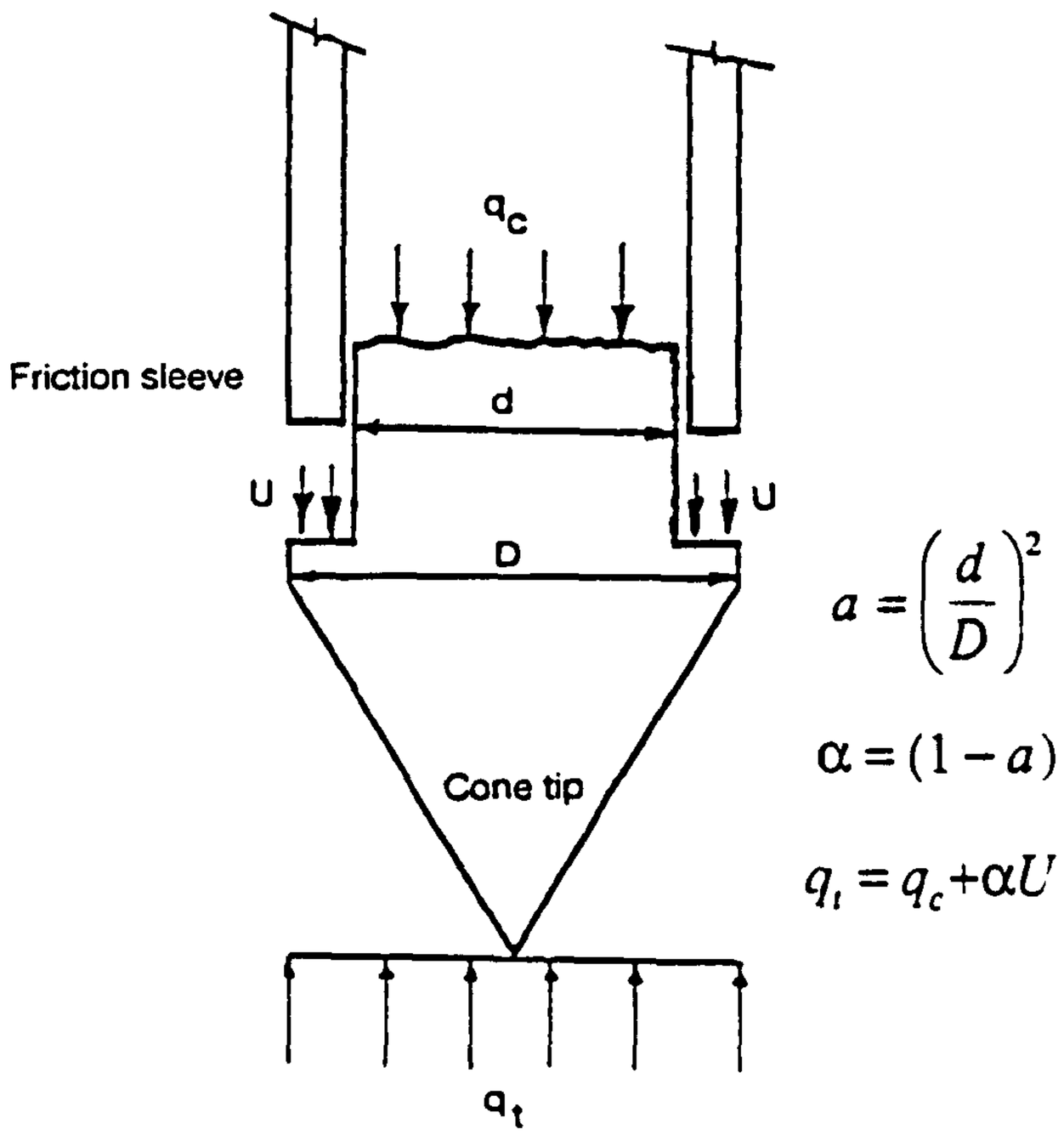

Figure 2.3 The correction of tip resistance (q_t) (Nyirenda, 1989)

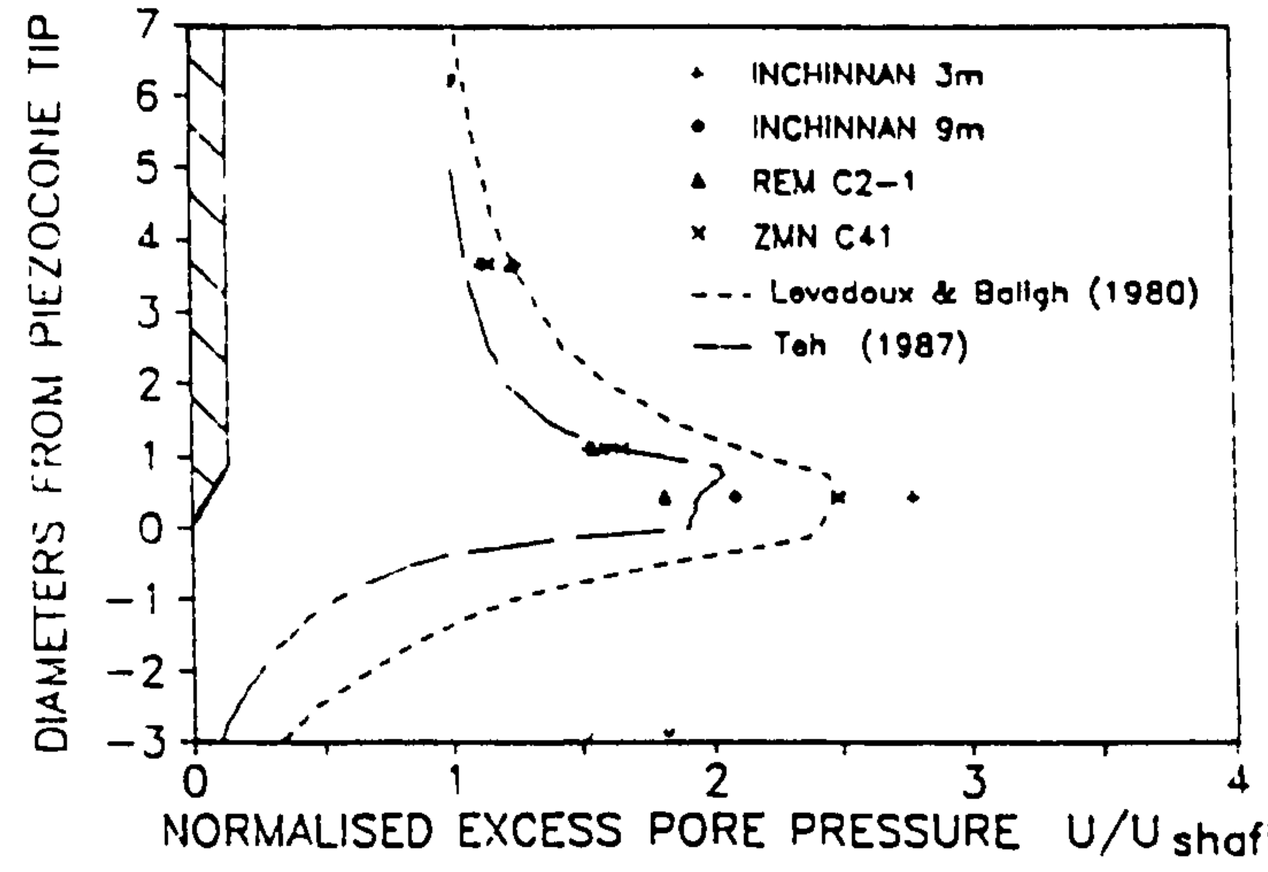

a) Theoretical and experimental plots of normalised excess pore pressure during piezocone driving (after Sills et al., 1988)

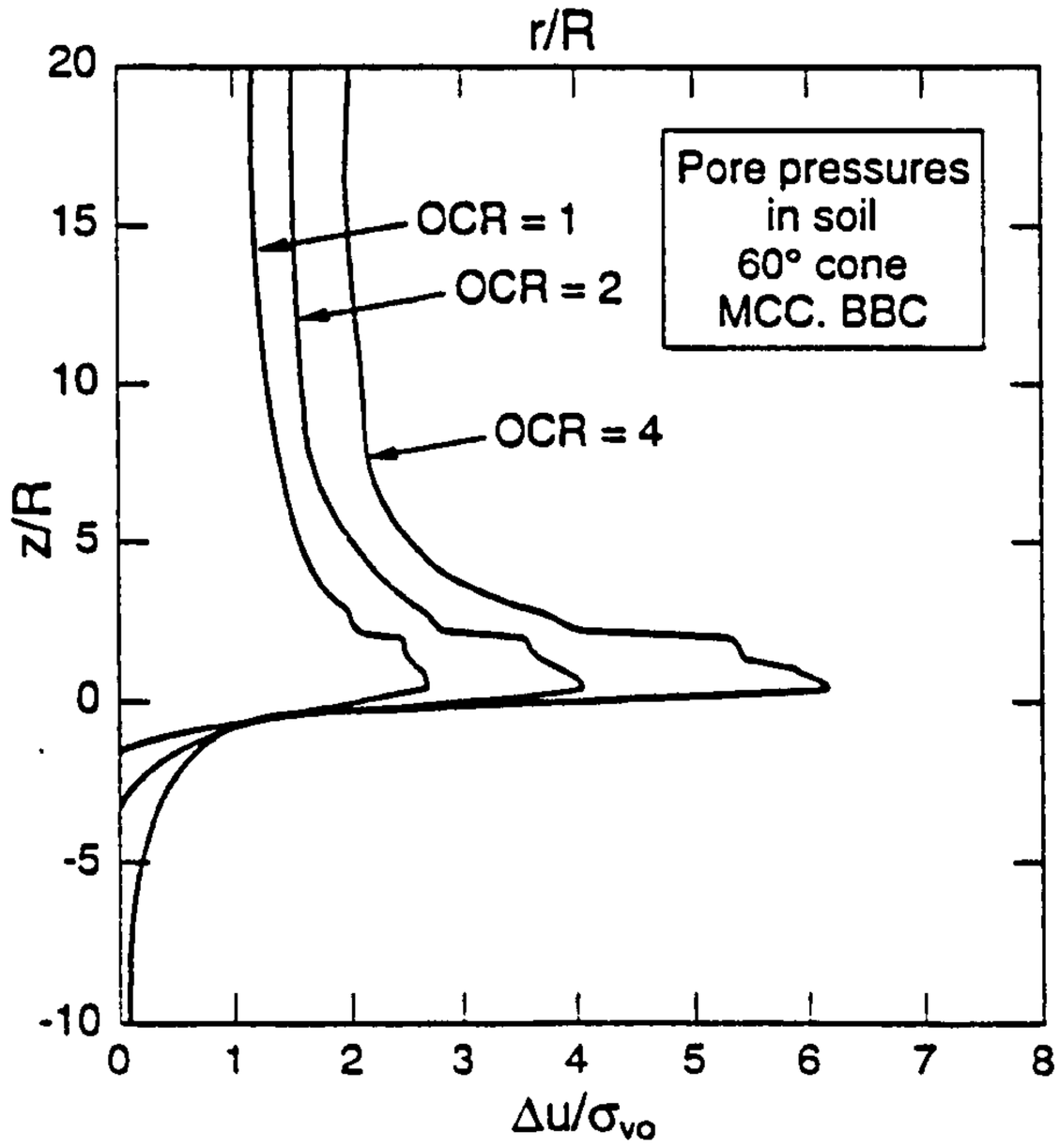

b) Prediction of pore water pressure distribution (Whittle and Aubeny, 1991)

Figure 2.4

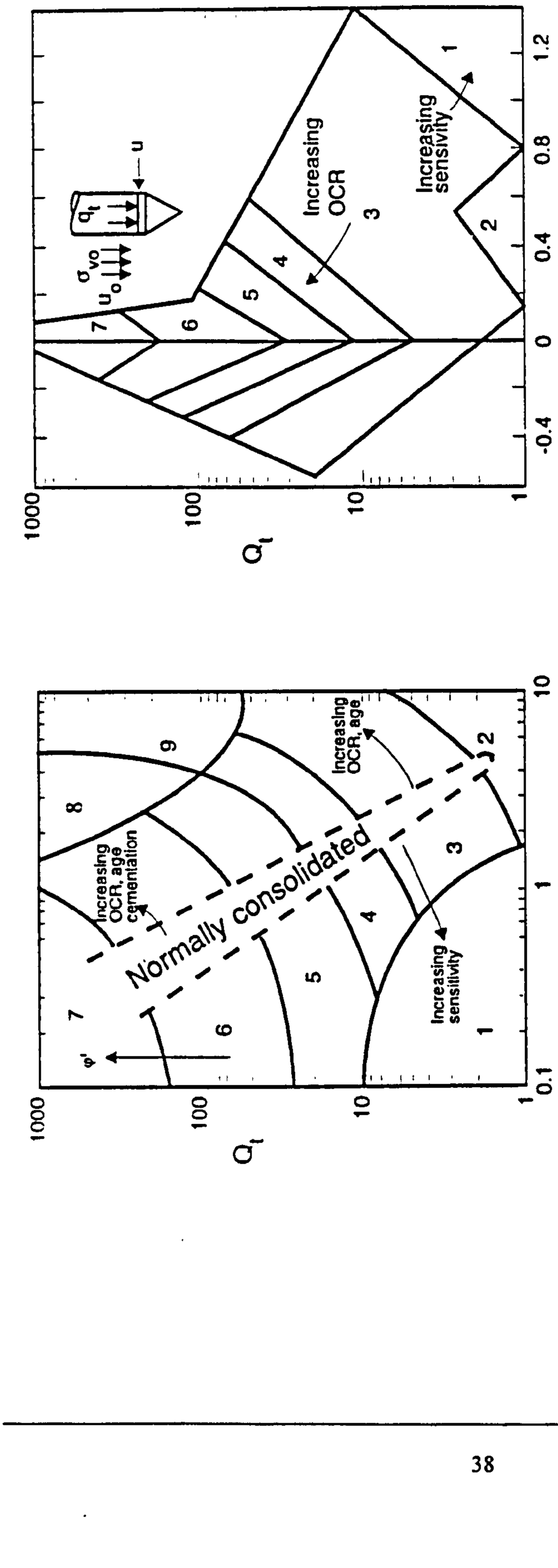

Figure 2.5 Soil classification chart base on Q_t (Robertson, 1990)

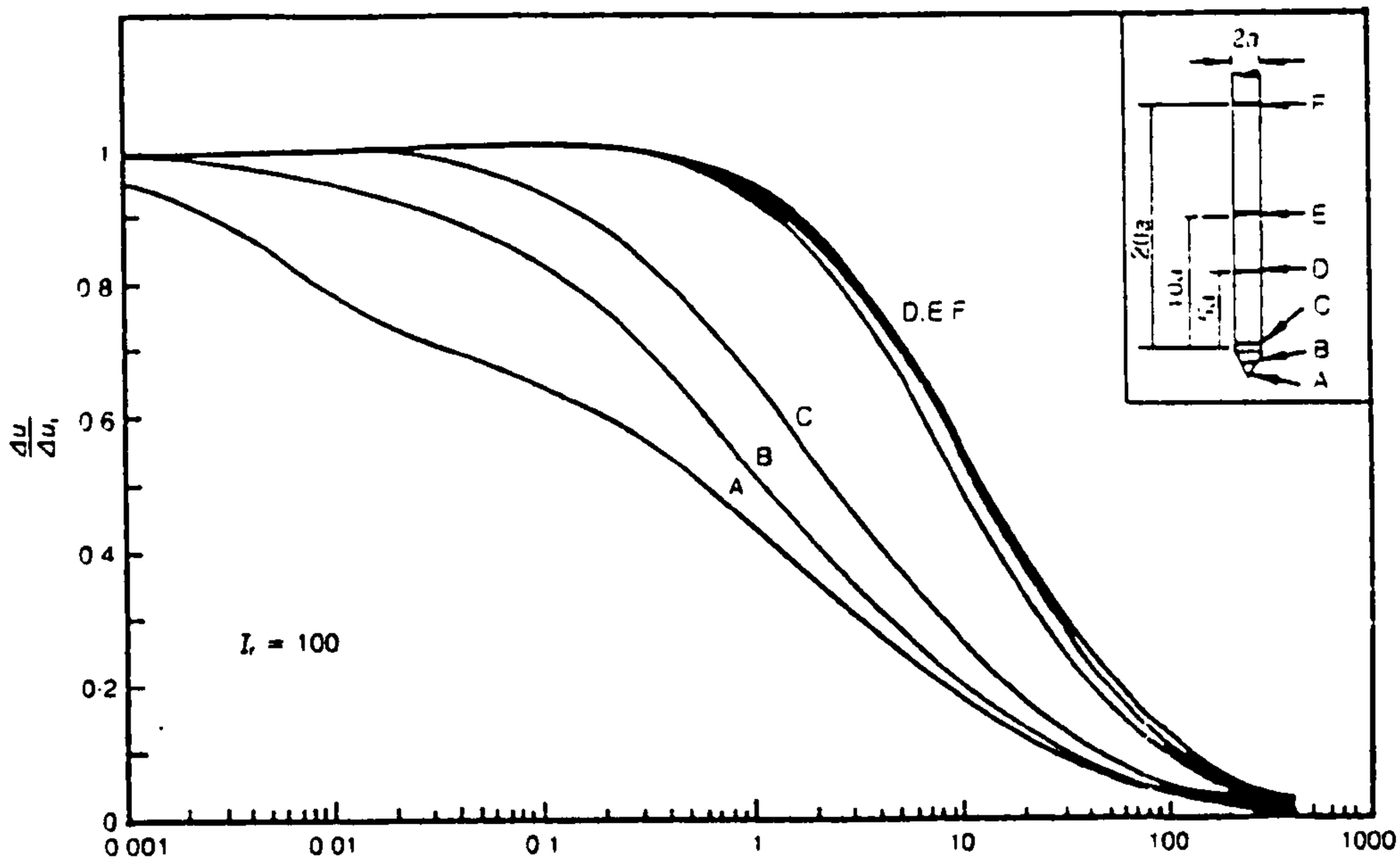

a) Dissipation curves for a 60° cone penetrometer based on T

(Teh and Houlsby, 1991)

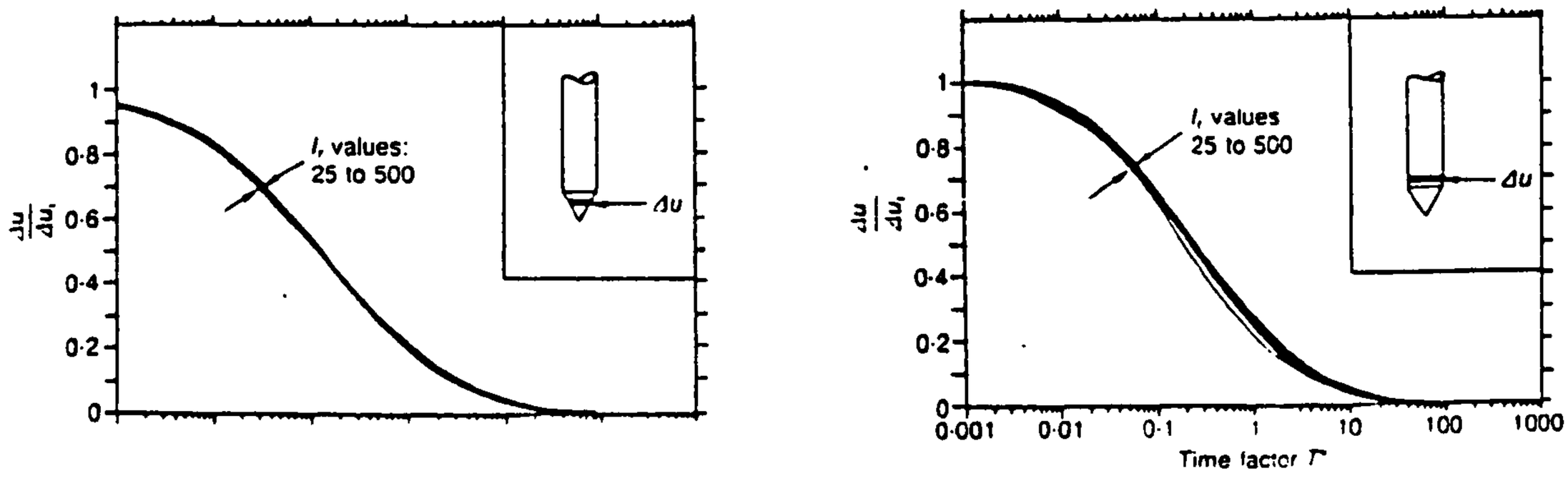

b) Dissipation curves for a 60° cone penetrometer based on T*

(Teh and Houlsby, 1991)

Figure 2.6

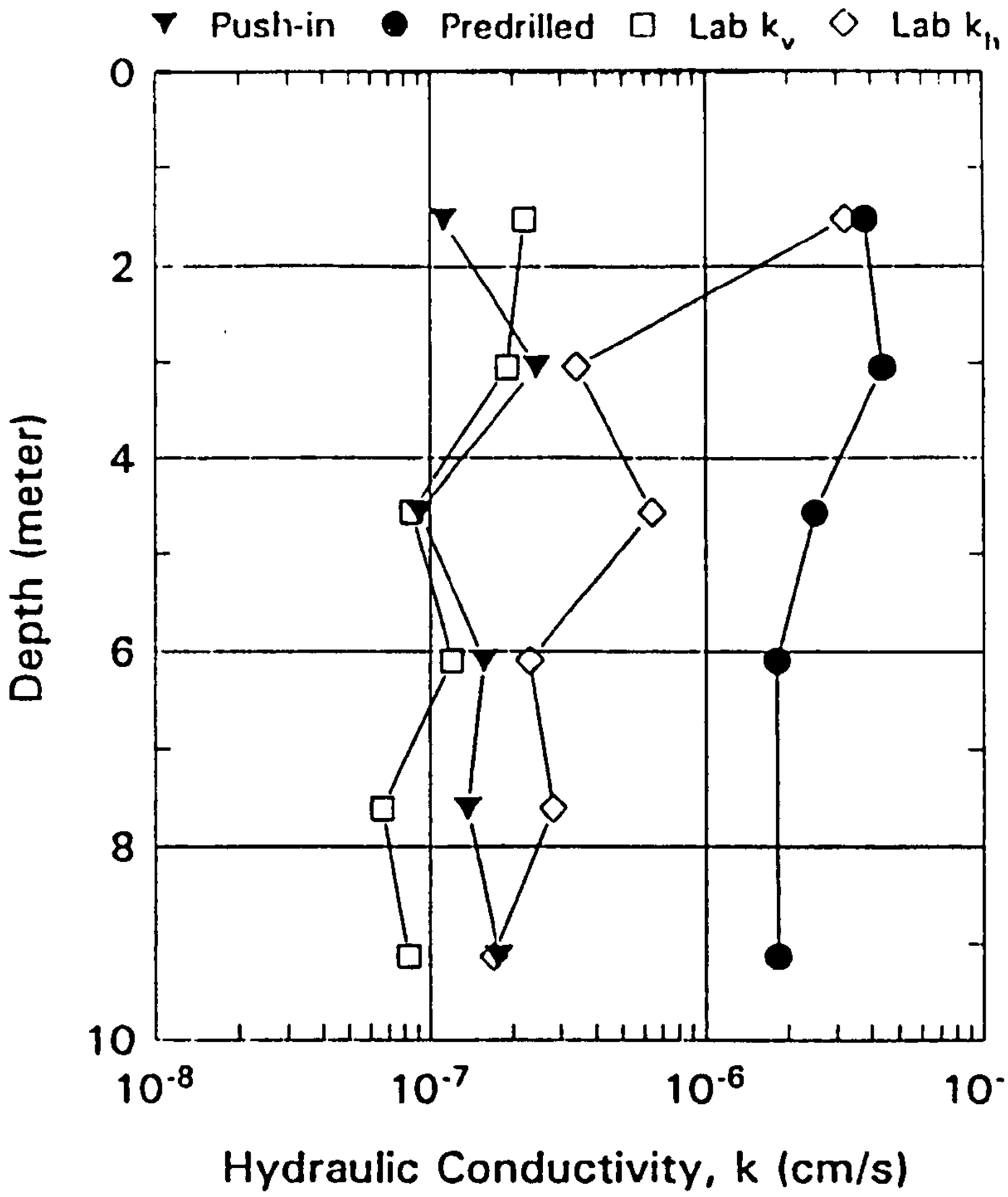

Figure 2.7 Comparisons between laboratory and field measurements of the permeability of varved clay (DeGroot and Lutenegger, 1994)

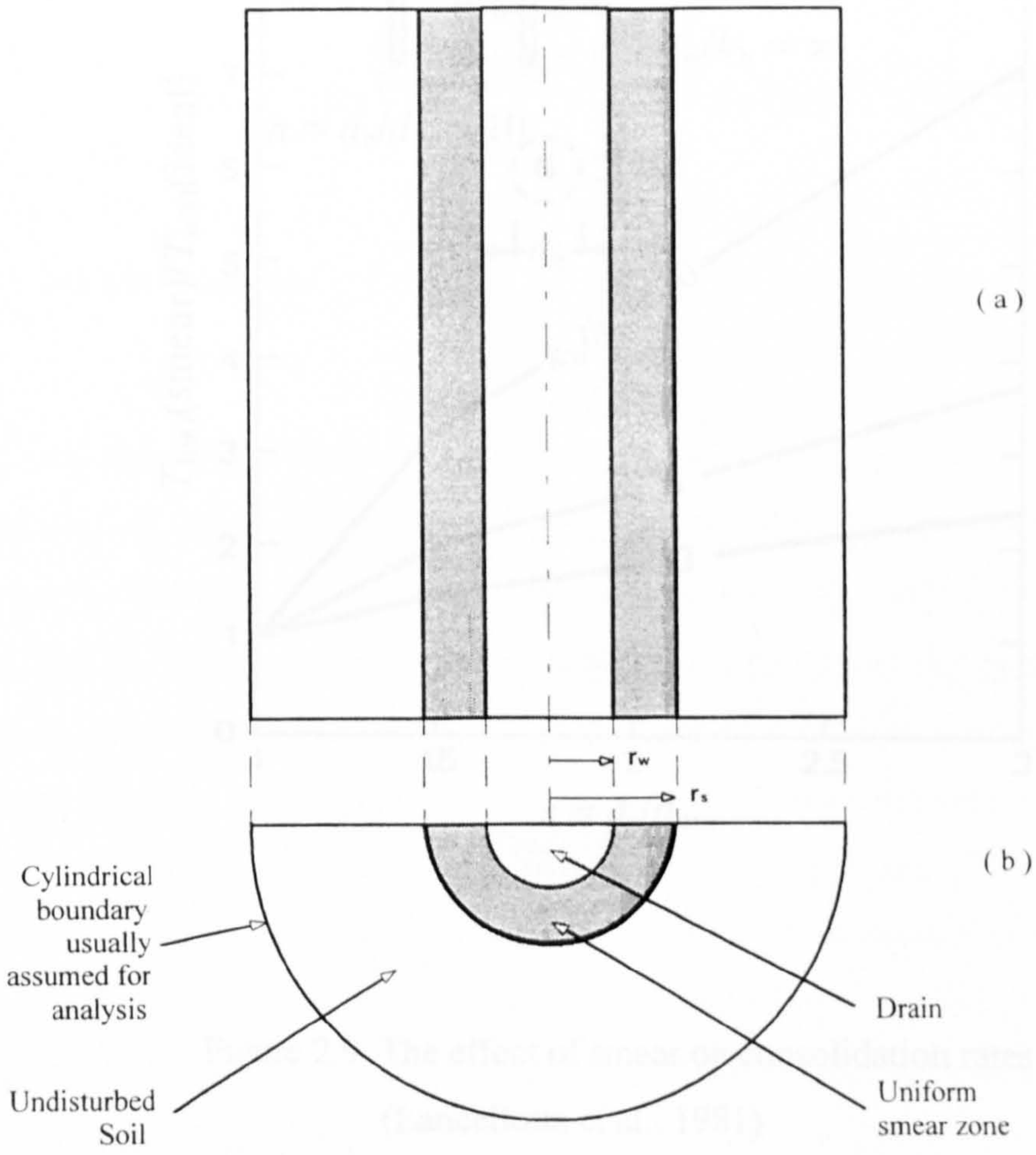

Figure 2.8 Geometry of idealised uniform smear zone

a) section b) plan

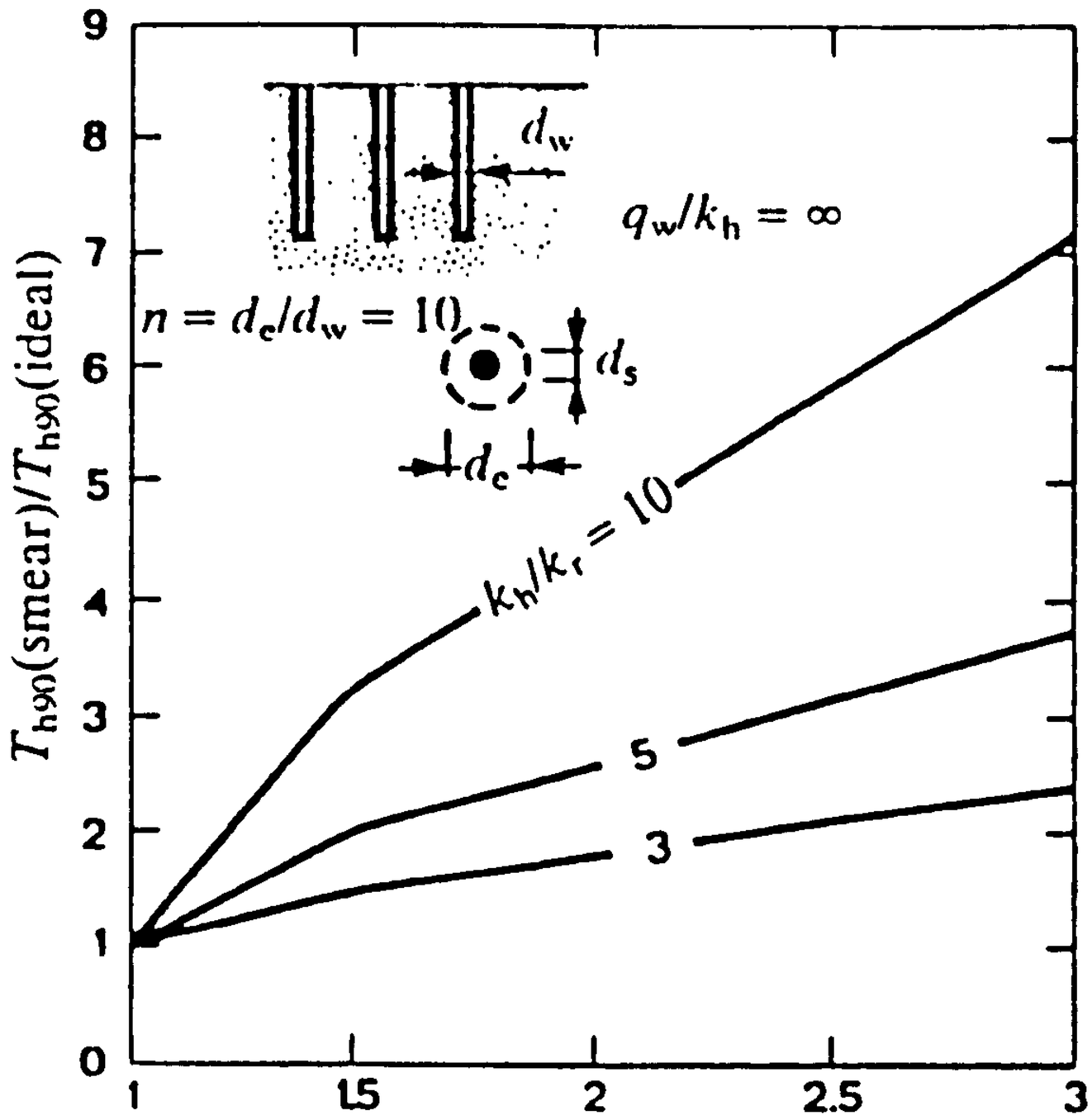

Figure 2.9 The effect of smear on consolidation rates
(Lancellotta et al., 1981)

CHAPTER 3

EXPERIMENTAL MATERIALS AND EQUIPMENT

3.1 Introduction

As reported in Chapter 2, previous research concerning the effects of smear during vertical penetration of layered soil was carried at the University of Sheffield by Moseley (1998). To construct the soil sample, clay layers were prepared by consolidating Speswhite kaolin slurry one-dimensionally and the consolidated cake was then extruded and wire cut horizontally. Sand layers were prepared by freezing saturated fine silty sand in moulds. Alternate layers of sand and clay were placed in a test cell to form a layered sample. The layered soil sample was then consolidated to an effective stress of 250kPa before the circular vertical drain was driven into the sample and the horizontal permeability of the sample was measured. The sample was further consolidated to an effective stress of 450kPa and the piezocone was then driven into the sample.

In the present research, in order to obtain comparable results and investigate the effects of smear caused by mandrels with different shapes, the same materials as used by Moseley (1998) were used for making the clay and sand layers. In order to quantify the effect of the permeability ratio of the layers on the degree of disturbance caused by mandrel installation, the permeability ratio of the layers was varied, test by test, by adding ground flint (a silt size material) to the sand or replacing all the sand with flint.

The testing equipment was originally designed by Moseley (1998) to investigate smear effects when a circular drain was used as the penetrating object. The circular drains used in the previous research were sheathed and unsheathed drains with diameter of 23.5mm. In the present research some parts of the equipment such as the cell base were redesigned to permit tests on a band drain with plan dimensions of 50x6.5mm.

The first part of this chapter describes the sample building materials used in the research, namely Speswhite kaolin powder, sand and flint. The second part describes the experimental equipment and calibration of the instrumentation. The third part deals with calibration errors and their effect on measurements.

3.2 Experimental Materials

3.2.1 Speswhite kaolin

The speswhite kaolin powder used in the research was supplied by ECC International Ltd. The manufacturers of the clay quote a value of 2.60 for the particle density of the clay which is the same as that reported by Moseley (1998). Moseley (1998) also reported that the liquid limit of the kaolin was 61% using the cone penetrometer method (BS 1377:Part2:1990). Plastic limit (PL) and liquid limit (LL) of kaolin have been reported by many researchers e.g. Al-Tabbaa (1994) LL=69%, PL=38%, Anderson et al. (1991) LL=72%, PL=36%, Rossato et al. (1992) LL=63%, PL=33%, Brown (personal communication) LL=61%, PL=31%. Figure 3.1 illustrates the particle size distribution of the kaolin obtained from the manufacturers (ECC International Ltd, 1991). The coefficient of volume compressibility, m_v, of the kaolin was determined in the course of the present research during the slurry consolidation in two 152mm diameter Rowe cells (Section 4.2.3) and layered sample consolidation (Section 4.3.7). The values varied with effective vertical stress and are

listed in Tables 5.2 and 5.3. The vertical and horizontal permeability of the kaolin were indirectly determined from consolidation data obtained from the 152mm diameter Rowe cells. The test results were compared with those predicted by correlations (Al-Tabbaa & Wood;1987) between void ratio and both horizontal permeability (k_h) and vertical permeability (k_v) and these comparisons are presented in Chapter 5.

3.2.2 Sand

Moseley (1998) performed two sieve analysis tests, two sedimentation tests (hydrometer method B. S. 1377, part 2, (1990)) and an oedometer test on samples of the fine silty sand. The oedometer test was carried out to investigate the compressibility of the sand under various effective stresses. From the test, the coefficient of volume compressibility, m_v, was found to be below 0.05 m^2/MN. A value of 2.65 was used for the particle density of the (silica) sand. Figure 3.1 presents the sieve analysis and sedimentation test results.

Before conducting any tests, the sand from two large bags was oven-dried and mixed together in a large rotary mixer for about 20 minutes in order to ensure uniformity. In order to determine the permeability of the sand, which was critical for quantifying the effects of smear, falling head permeability tests (Section 4.2.1) and horizontal permeability tests (Section 4.2.4) were performed.

3.2.3 Flint

The flint used in the research was supplied by Potterycrafts Ltd. (London). The material was composed of 100% silica flour and, therefore, the specific gravity of the flint was assumed to be 2.65. Using the consolidation data obtained during the horizontal permeability test in a 254mm Rowe cell (Section 4.2.4), it was found that, for an effective stress change from 200kPa to 250kPa, the m_v value of the flint was

0.043 m^2/MN. To determine the permeability of the flint, falling head permeability tests (Section 4.2.1) and horizontal permeability tests (Section 4.2.4) were performed.

3.3 Experimental Equipment and Calibrations

The following sections describe the various items of testing equipment, their functions and, where appropriate their calibrations. The accuracy of the calibration equipment is also reported. The following general points regarding calibration should be noted.

a) Most transducers were calibrated twice during the research. However, the piezocone transducers were calibrated more often.

b) Relationships between the applied loads, pressures or displacements and the output voltages from the transducers were assumed to be linear.

c) To check repeatability, at least two cycles were performed during calibration of any transducer. The calibration factors were generally calculated from a linear regression analysis performed on all the calibration data. For the piezocone load cell, calibration factors were determined from the regression analysis of the data points from the first half cycle.

d) The power sources and data logging system used in the calibrations were the same as those used in the experiments.

3.3.1 Slurry consolidation cell

Two slurry consolidation cells were used to consolidate kaolin slurry to an effective stress of 200kPa before the kaolin cakes were extruded and wire-cut to form a layered sample. Each slurry consolidation cell consisted of two Rowe cell bodies bolted together to form a single cell with 252mm internal height and 254mm internal diameter. The inside walls of the Rowe cells were lined with 1 mm thick PTFE sheet to reduce friction during consolidation. Acrylic discs were used as the loading plates during the consolidation process. Consolidation pressure was applied to the consolidation cells using two large air-water interfaces and controlled using Moore Model 40-100 Nullmatic pressure regulators. Two 1200kPa pressure gauges manufactured by Budenberg Co. Ltd. (Altrincham) were used to measure the consolidation pressures. During consolidation, drainage was allowed at top and bottom of the cells. Slurry consolidation procedures will be described in Section 4.3.2.

3.3.2 Layered sample test cell

A cell with the same dimensions as the slurry consolidation cells, again formed by bolting together two Rowe cells, was used for the layered sample consolidation (Section 4.3.7), "head" and permeability tests (Section 4.3.10) and mini-piezocone tests (Section 4.3.11). In the cell wall near the base two drainage valves were located diagonally opposite each other. A 1mm square peripheral groove was cut in the cell wall to connect these two valves. The inside wall of the cell was lined with a 1mm thick porous plastic sheet to allow radial drainage during the consolidation and permeability tests. Before use, the porous plastic was grooved vertically with a spacing of about 10mm (shown schematically in Figure 3.2 a). To make these grooves, the porous plastic sheet was placed on a table and a steel ruler was used as a guide while a screw driver was gently dragged along the plastic sheet.

The grooves on the porous plastic were intended to ensure that excessive head losses did not occur in the peripheral drain during permeability tests.

The cell base used in the previous research was designed by Moseley (1998) for circular vertical drain tests and there were three positions for piezocone testing. For the present research, the cell base, Figures 3.2 (a) and (b), was redesigned so that a vertical drain with either a band shape or a circular shape and pore water pressure probes could be inserted into the soil sample in the cell. Adapters for a circular drain and a rectangular drain were designed so that they could be alternatively mounted on the cell base. Four inclined holes and eight vertical holes were drilled in the cell base for the pore pressure probe installation. All the pore water pressure probe connections on the cell base were redesigned to avoid any leaking of water, as reported by Moseley (1998), when a high back pressure was applied.

Two aluminium circular discs with a thickness of 25mm were used as loading plates for layered sample consolidation. The loading plates, one with a 30mm diameter circular recess and the other with a 20x66mm rectangular recess, were used for tests with the circular drain and band drain respectively. Before use, the recesses on the loading plates were filled with Plasticene. After the drain installation (Section 4.3.8), the tip of the vertical drain was embedded in the recess (Figure 3.10).

3.3.3 Sand and flint layer mould

Four acrylic moulds were used to make sand or flint layers. Each mould consisted of a base plate, a body and a lid, Figure 3.3. The base of the mould was lined with a 1mm thick PTFE sheet. An acrylic ring was greased and bolted to the base plate to form the mould body. The underside of the mould lid was also lined with 1mm thick PTFE sheet. The moulds were originally designed by Moseley(1998) for sand layer preparation (Section 4.3.3). With the original design, after sand was sprinkled through deaired deionised water and levelled in the mould, the mould lid was placed into the mould until it touched the top of the sand inside the mould. The mould was then placed in a freezer. During layered sample preparation

(Section 4.3.6) in which layers of sand and clay were alternately placed in the test cell, it was found that the sand layers prepared by this method, having been frozen, melted very quickly in the test cell while the next clay layer was placed. Hence placing the clay layers could easily disturb the melted sand layers.

In the present research, it was considered that a protective ice layer could slow down the melting rate of the sand or flint layers and so reduce the degree of disturbance caused by placing the clay layers. To make the protective ice layer, the mould lids were redesigned by placing four adjustable screws on the rim of each lid, which could then be adjusted up or down by turning the screws against the mould body. By this method, the distance from the underside of the mould lid to the top of the material inside the mould could be controlled and an approximately 3mm thick ice layer could be formed on top of the material.

3.3.4 Volume change units

Two Imperial College 100ml volume change units were used to monitor flows into and out of the layered sample during various stages of the tests. The volume change units operate by measuring the movement of a piston within a cylinder caused by the flow of water. The movement of the piston was monitored by a 25mm linear variable displacement transducer, manufactured by MPE Transducers Ltd. and mounted on the outside of the cylinder.

Figure 3.4 shows volume change unit calibration set up. The volume change units were calibrated under the same back pressure as used in the samples. To calibrate the volume change units, a 10ml graduated glass burette, readable to 0.02 ml and mounted in an acrylic outer tube, was used. By alternately filling and then bleeding the burette, the full range of the transducers was calibrated in about 10ml increments.

3.3.5 Displacement transducer

To monitor the height of the layered sample, a 10mm linear variable displacement transducer (Model No.HS10/7042) manufactured by Apex Ltd. (Wimborne) was used. To calibrate the transducer, a Mitutoyo digital output micrometer, readable to 0.001mm was used. The full range of the transducer was calibrated in 0.5mm increments.

3.3.6 Pressure transducers and pressure gauges

One 500kPa and one 800kPa standard test gauge manufactured by Budenberg Gauge Co. Ltd. (Altrincham) and two 700kPa diaphragm type pressure transducers manufactured by Druck Ltd. (Leicester) were used to monitor and record back pressure and confining pressure (Section 3.3.12) during the layered sample tests. The pressure transducers and the standard test gauges were calibrated by using a Budenberg oil dead weight tester. Calibrations of these transducers and gauges were performed with 100kPa increments.

3.3.7 Differential pressure transducers

A total of eight 35kPa differential pressure transducers (Model No.PDCR 2110) manufactured by Druck Ltd. were used to measure the pore water pressure at various points in the soil sample as well as the pressure difference applied across the sample.

To calibrate the differential pressure transducers, all the transducers were fixed vertically on a wooden board and placed on a table, as shown in Figure 3.5. Two 10 ml graduated glass burettes were used as pressure sources to the transducers. One of the burettes was attached to the high pressure side and another burette was

attached to the low pressure side of the transducers. An air-water interface tank was filled with de-aired water and connected to the burettes by using plastic tubes. Zero readings of the transducers were recorded while the pressure from only one burette was applied to the high and low pressure sides of the transducers at the same time. To apply a differential pressure to the transducers, a rack system was used to mount the burettes at various heights and by controlling pressure in the air-water interface tank, the water levels in the burettes could be adjusted. By attaching a tape measure, readable to 1mm, to the outside of the burettes, the difference in head applied to the transducers could be recorded. The differential pressure applied to the transducers was varied between 0 and 20kPa and the output voltages were recorded.

3.3.8 Pore water pressure probes

The needle-type probes, Figure 3.6, used for pore water pressure measurement inside the sample were made from stainless steel hypodermic tubes with an outside diameter of 2.5mm and an inside diameter of 1.7mm. A piece of porous plastic was placed in the end of the hypodermic tube to prevent soil particle migration into the probe. To reduce the volume of water within the probe, a 1.5mm diameter piece of brass wire was placed inside the hypodermic tube.

At the other end of the stainless steel tube, a plastic tube was fitted over the stainless steel tube and then a brass olive was tightly fitted at the middle of the plastic tube. A screw fitting bearing on the olive was used to make a sealed connection between the probe and the connector to the differential pressure transducers. The seal ensured that pore water pressure around the porous plastic tip was transferred directly to the differential pressure transducer.

The pore water pressure probe arrangement and installation procedures will be described in Section 4.3.9.

3.3.9 Draw wire transducer

The displacement of the drain mandrel and the mini-piezocone during insertion into the soil sample was monitored by a 600mm draw wire transducer (Model No. 0.2VD) manufactured by RDP Ltd.(Wolverhampton). The transducer body was fixed at a static point on the test frame. The end of the draw wire was attached to a metal plate which, in turn, was attached to the central drive rod of the driving system (Section 3.3.10). A Mitutoyo 300mm digital calliper, readable to 0.01 mm, was used to calibrate the draw wire transducer. In the calibration, the draw wire transducer and the calliper were fixed horizontally on a wooden board. The wire of the transducer was attached to the moveable arm of the calliper. Over the driving range of the vertical drain and the piezocone, the calliper was adjusted to produce a displacement increment of 25mm and the output voltage from the transducer was recorded.

3.3.10 Driving system

An existing driving system designed by Moseley (1998) was used for drain installation and mini-piezocone driving. The system included a 600mm long, 35mm diameter central threaded drive rod with a 15mm diameter hole drilled through its entire length and two vertical movement limit switches. This was connected to a permanent magnet DC electric motor controlled by a potentiometer. Power from the motor was transferred to the drive rod by two pulleys that were connected by a timing belt. A maximum motor speed of 1200 RPM was used for the piezocone driving. This rotating speed produced a 20mm/sec vertical movement of the central drive rod. A digital meter was connected to the drive motor so that its rotational speed could be visually monitored.

3.3.11 Circular and band drains

Circular shape drains with an diameter of 23.5mm and rectangular shape drains with plan dimensions of 50x6.5 mm, Figure 3.7, were used in the research to quantify the effects of smear caused by installation.

The circular drain, which was designed by Moseley (1998) had a core (mandrel), a filter tube and a sheath, Figure 3.8. The circular drain core was a brass column with longitudinal grooves of 1 mm width and 0.5mm depth cut on the sides at roughly 5mm centres. The drain core was surrounded by a 1mm thick porous plastic tube supplied by Porvair Technology Ltd. and a thin brass sleeve. An O-ring seal was placed at the end of the core to provide a seal with the sleeve so that saturation could be retained during handling and driving (Section 4.3.8). A new porous plastic tube was used for every test. A 2mm hole was drilled through the centre of the core and two diagonal 1 mm holes were drilled near the base in order to connect the outer porous plastic tube hydraulically to the central hole and reduce any head loss within the mandrel.

The band drain was composed of an acrylic core, 3 x 48mm, wrapped by a porous plastic filter and a protective brass sheath, Figure 3.9. The acrylic core had 20 parallel rectangular grooves 3mm wide and 1mm deep. To make the porous plastic filter, a 1mm thick porous plastic sheet was cut to dimensions which would allow it to fit closely around the drain core. At the position of the core corners, the porous plastic was scored by a knife and then folded. At the last corner the end of the plastic sheet was carefully melted in order to fuse it to the other end. Then two screws (2.1mm diameter) were used to fix the bottom end of the porous plastic sheath to the drain core. This was to ensure that the porous plastic was kept in place during removal of the brass sheath. Then another pair of screws were used to fix the plastic core to the brass drain base. Deairing and installation of the band drain will be described in Section 4.3.8.

To make a comparison between the results gained from the circular drain and band drain tests, the equivalent diameter (Section 2.5.1) of the band drain used in the

research was kept reasonably similar to the diameter of the circular drain. Many equivalent diameter calculations were considered during the preliminary design of the band drain. The internal dimensions of the manufactured sheath for the band drain were 50.0 x 6.5 mm. The sheath fitted the band drain closely so that the collapse of soil surrounding the drain was minimised. With the size of 50.0mm x 6.5mm, the equivalent diameters of the prefabricated band drain computed by Equations 2.8, 2.13 and 2.14 were 36mm, 29.6mm and 28.3mm respectively.

3.3.12 Test system configuration

Figure 3.10 shows a schematic diagram of the test system. A vertical confining pressure and a back pressure were applied to the sample. The back pressure was applied from two air-water interface tanks. The first tank, referred to as the "high" tank, was connected to a volume change unit and then to two valves at the side of the cell. The second tank, the "low" tank, was connected to the top of the drain cover, a second volume change unit and the low pressure side of the differential pressure transducers.

A head difference between these two tanks permitted a flow from the high air-water interface tank to the first volume change unit and then to the test cell via the valves connected to the peripheral drain near the cell base. The water pressure could distribute all around the sample via the square groove on the cell wall (Section 3.3.2) and the peripheral porous plastic. The water then flowed through the soil sample, in which the pore water pressure probes were installed (Section 4.3.9), to the drain at the centre of the sample, along the drain to the drain cover, through the second volume change unit and finally into the low air-water interface tank. The differences between the pressure at the drain and at various positions across the sample were recorded by the differential pressure transducers. The total applied pressure difference was measured by a separate differential pressure transducer.

To control the pressure in the two air-water interface tanks, two Moore Nullmatic Pressure Regulators (Model 40-100 and 40-30), connected together in

series, were used. As suggested by Moseley (1998), using two regulators in series minimised the pressure fluctuations in the main air pressure supply. The pressures in each tank were visually monitored by using a 500kPa standard pressure gauge (Section 3.3.6) and a pressure transducer was used to record the back pressure at the peripheral drain inside the test cell. This transducer was connected to the cell at the mid-height of the sample.

The vertical confining pressure was applied to the test cell membrane from a large air-water interface. Again, two Moore Nullmatic Pressure Regulators (Model 40-100), connected together in series, and a 800kPa standard pressure gauge were used to control and visually monitor the supplied pressure. A pressure transducer was connected to the cell pressure pipe to record the applied pressure.

3.3.13 Miniature piezocone

A mini-piezocone provided by Fugro Engineers B. V. of Holland was used in the research. The mini-piezocone has a cross sectional area of 1cm^2 and contains a pore water pressure transducer, a cone load cell, a sleeve load cell and a slope sensor, Figure 3.11. However, only the cone resistance and pore water pressure were monitored during the experiments.

a) Filters

The two filter locations used in the research were the tip and the shoulder of the cone, Figure 3.12 . The tip filter originally provided by Fugro Engineers was a sintered stainless steel filter with a 60^o tip and this had been used by Moseley (1998). Moseley reported that, after some tests had been performed, the porous tip became clogged with clay. To remove any clay that had been trapped in the filter, it was placed in an ultra-sonic bath filled with deaired and deionised water. Then the ultra-sonic bath was operated for at least one and a half hours.

In the early stages of the present research, after a test had been performed, the same tip filter cleaning procedures were adopted. However, a satisfactory response to changes of pressure during deairing (Section 4.3.11) was not generally achieved. It was considered that the ultra-sonic bath could not remove all the trapped clay, so every time the tip filter was used clay was present in the filter. To solve this clogging problem, sintered glass tip filters with roughly 30% effective porosity were manufactured and used, instead of the sintered stainless steel filter.

To make the sintered glass filter, the required amount of glass beads, with diameters of 46-90 μm, was placed in a ceramic mould with dimensions of 25x90mm. To make the surface of the glass beads flat, the mould was gently tapped and then it was placed in a high temperature oven. The temperature in the oven was increased at a rate of 2 °C per minute and kept constant (dwelling) at 680 °C. Then the temperature was decreased at a rate of 1 °C per minute until room temperature was achieved. The dwelling time was varied, as summarised in Table 5.1, to achieve a material that was machinable and not too brittle to make tip filters. It was found that a dwelling time of 20 minutes was suitable. After removal from the mould, the filter material was machined to form a small circular rod with a diameter of 2.1mm and a length of approximately 15mm. Then the circular filter rod was glued into the metal cone body. Finally, it was shaped to form a 60° tip. The glass filter was changed for every piezocone drive to make sure that the best response to changes of excess pore water pressure could be gained.

The shoulder filter was made of porous plastic and, again, a fresh filter was used for every drive. These filters were provided by Fugro Engineers.

b) <u>Assembly and de-airing</u>

The cone tip, with the filter either at the tip or the shoulder, was assembled to the cone body in a funnel of silicone oil to make sure that the pore pressure measuring system was fully saturated (Figure 3.13a). First, the cone body was turned over and clamped to a support. A funnel was fixed on the cone body with a rubber seal at the bottom. The cone tip was taken apart and all the components were cleaned

with cotton wool. Silicone oil was poured into the funnel and a syringe was used to flush the cone body. One of two brass spacers was pushed into the cone body. When the filter was at the cone tip, the oil flushed through the center of the brass spacer(item no. 2, Figure 3.11a) but, when the filter was at the cone shoulder, the oil flushed through two holes at the side of the spacer (item no.5, Figure 3.11b). The spacer was moved up and down a few times to make sure that the oil properly flowed through the spacer holes and all entrapped air was flushed out.

The filter was deaired under silicon oil with a vacuum of –100 kPa for at least 3 hours and transferred into the funnel. The o-ring (item no.10, Figure 3.11a and b) and the filter were put into position under the silicon oil. Then the cone body was clamped and the cone tip was screwed onto the body. After assembly of the piezocone, the oil in the funnel was transferred to a container. Then the cone was turned upside down and quickly put into a vacuum bottle filled with silicon oil (Figure 3.13b). The level of the silicon oil in the bottle was above the cone filter. Then a rubber seal was applied between the cone body and the bottle neck, the vacuum pump was operated and vacuum of about –90 kPa was applied to the bottle. The piezocone was deaired in the vacuum bottle for at least 6 hours and its response was recorded by the computer logging system. The vacuum was then released and the cone was left under atmospheric pressure for at least 6 hours before testing or calibration. Checking of the piezocone response to pressure change will be described in Section 4.3.11.

c) Calibration

To calibrate the cone resistance, firstly the piezocone was clamped to a stand without any load applied to the cone tip. At this stage the zero reading was recorded and the clamps on the stand were released to loosely hold the piezocone in a vertical direction. Then the tip of the cone was rested on a balance readable to 0.1g which was placed underneath. Next, weights were applied to the clamp on the cone body as shown in Figure 3.14. The increment of load applied to the cone was roughly 190kPa. For each loading increment, at least 10 output voltage values were logged

within 20 seconds. The load applied to the cone was varied from about 190kPa to 1200kPa.

To calibrate the piezocone pore water pressure transducer, a special pressure tank with a hole in the middle of the top plate was manufactured. Before calibration, the pressure tank was filled with deaired and deionised water and connected to an air-water interface tank. A 700kPa pressure transducer was attached to the pressure tank to measure the water pressure in the tank. The piezocone was prepared for calibration using the assembly and de-airing procedures described above and the zero reading was recorded. After that, the piezocone was slowly inserted into the pressure tank until the tip of the piezocone was roughly at the middle of the tank. During insertion, the top valve of the pressure tank was open to allow some water to drain out. Calibration was started by increasing the pressure in the air-water interface tank from 100kPa to 600kPa in increments of 100kPa. For each increment, the output voltages from the pore water pressure transducer and the cone resistance transducer were recorded by the computer logging system. Calibration factors for the pore water pressure transducer and the cone area ratio (Section 2.3.3) were calculated from the data gained. The average area ratio value was 0.63. Moseley (1998) reported the same area ratio value.

3.3.14 Computerised logging system

During the various stages of the layered sample tests (sample consolidation, vertical drain installation, pore water pressure probe installation, permeability testing and mini-piezocone testing, Sections 4.3.7-4.3.11) all test data were collected by a computerised logging system. The computer used for data acquisition was a Viglen 486 PCI operating with MS-DOS version 6.22. The software used was Quick LogPC Version 1.0.5 by Strawberry Tree Incorporated.

A total of fifteen channels on two interface boxes manufactured by RS Components Ltd. were used to transfer the output voltages from the transducers to the computer logging system. 10 volts of DC power were supplied to every channel,

except those for the draw wire transducer and the piezocone, by using a 18V5C voltage regulator manufactured by Kingshill Electronic Products Ltd. 15 volts of DC power were separately supplied from an identical source to the channels for the draw wire transducer and the piezocone. The software was able to convert the voltages from the transducers to engineering units using the known calibration factors.

The data logging rate was varied to suit the type of testing. For example, in the sample consolidation tests, the logging interval was set to 2 seconds for the first minute, then to 5 seconds for the next five minutes, then to 20 seconds for the next half hour and finally to 500 seconds until the consolidation finished. During piezocone driving, logging occurred every 2msec (205 readings/sec) and this was the fastest rate which gave acceptable data. It was found that logging at a faster rate introduced errors and resulted in scattering of the data.

3.4 Calibration Errors

3.4.1 Transducers

For each data set from a transducer calibration (except the piezocone), a trend line produced by linear regression was drawn on a graph of the calibration quantity (e.g. displacement, pressure) versus the output voltage of the transducer. The scatter of the calibration data around the trend line was expressed in terms of a standard deviation calculated by the following equation.

$$SD = \sqrt{\frac{\sum(x - x_{est})^2}{n}} \quad \text{---------- (3.1)}$$

where SD = standard deviation in engineering units

x = calibration quantity in engineering units for a given transducer output voltage

x_{est} = an estimated value on the trend line at the same output voltage

n = number of calibration data points

Each transducer was calibrated two times. Dates and standard deviations of the calibrations are presented in Table 3.1. Results from the first and second calibrations were compared in terms of zero reading drifts and calibration factor changes, Table 3.2. The zero reading drifts (only calculated for pressure transducers) were the differences of the output voltages of the transducers at "no load" stages of the first and the second calibrations. The zero drifts in terms of engineering units were then calculated by substituting the output voltage at the "no load" stage of the second calibration into the first calibration equation. The slopes of the lines obtained by linear regression from the first and second calibrations were compared and these are presented as calibration factor changes.

3.4.2 Piezocone

Errors in the piezocone calibrations were evaluated in terms of hystersis and non-linearity, Schaap & Zuidberg (1982). During the load cell calibrations, Figure 3.15, the maximum hystersis and non-linearity were recorded in calibration no.3. The values were 7% and 4.3% respectively. These errors were equivalent to 80kPa and 50kPa. It should be noted that these values were obtained from a full load-reload cycle. From the piezocone test results (Figure 5.21-5.30), it can be seen that large variations of cone resistance were not observed after a drive had been started, i.e. the load acting on the piezocone during driving was principally a monotonic loading. Therefore, with a calibration factor obtained from the regression analysis of the data points from only the first half cycle during calibration (see Section 3.3), smaller errors than those mentioned above were expected in a test.

Zero drifts between each load cell calibration are presented in Table 3.3 (a) (column 2). Comparing all the load cell calibration results shows that the zero drift of the piezocone varied over a wide range. On the other hand, it was found that the

calibration factors were reasonably consistent. During the testing period, the maximum change of the calibration factor between calibrations was 6.4%, Table 3.3 (a) (column 4).

Pore water pressure transducer calibrations are shown in Figure 3.16, for the two pore water pressure transducers that were used in the piezocone. The first transducer was calibrated under a maximum pressure of 200kPa. The second transducer was calibrated under higher pressures that were approximately the same as those in the tests. Comparing all the calibrations showed that the calibration factors were very consistent with a maximum change of 2.9%, Table 3.3 (b) (column 4). For every calibration, hystersis and non-linearity were negligible. Therefore, although the first pore water pressure transducer was calibrated with pressures lower than those in the tests, the calibration factor gained was considered to be reliable. The maximum zero drift between calibrations was 37kPa, Table 3.3 (b) (column3).

In the piezocone data analysis, Section 5.4.1, an independent datum for the excess pore water pressure and cone resistance was recorded before each penetration test. The datum readings at the beginning of a test were investigated for at least four hours to ensure that they were constant. Therefore, zero drifting of the cone load and pore water pressure transducers between calibrations should have been automatically taken into account. Only the calibration factors were used in the data analysis.

Transducer	Dates		Standard deviation from Eq. 3.1		units
	cal no.1	cal no.2	cal no.1	cal no.2	
Displacement transducer (DS)	01-Jun-98	01-Mar-01	0.003	0.025	mm
Consolidation pressure transducer (CP)	20-May-98	29-Sep-00	0.117	0.367	kPa
Back pressure transducer (BP)	20-May-98	29-Sep-00	0.059	0.254	kPa
Draw wire transducer (DW)	12-Dec-98	27-Sep-00	0.231	0.141	mm
Volume change unit (high) (Vh)	28-May-98	11-Apr-01	0.063	0.062	ml
Volume change unit (low) (Vl)	29-May-98	12-Apr-01	0.051	0.052	ml
differential pressure transducers 1 (DT1)	11-Jun-98	13-Jun-99	0.068	0.047	kPa
DT2	12-Jun-98	14-Jun-99	0.090	0.046	kPa
DT3	13-Jun-98	15-Jun-99	0.087	0.046	kPa
DT4	14-Jun-98	16-Jun-99	0.074	0.045	kPa
DT5	15-Jun-98	17-Jun-99	0.082	0.046	kPa
DT6	16-Jun-98	18-Jun-99	0.080	0.046	kPa
DT7	17-Jun-98	19-Jun-99	0.075	0.046	kPa
DT8	18-Jun-98	20-Jun-99	0 085	0.046	kPa

Table 3.1 Calibration errors of the transducers

Transducer	Zero reading drift (V)	Equivalent zero drift (kPa)	Calibration factor change (%)
DS	-	-	0.34
CP	5.40E-04	3.69	0.60
BP	-1.52E-03	10.66	-0.01
DW	-	-	-0.50
Vh	-	-	0.83
Vl	-	-	1.06
DT1	3.57E-05	-0.131	1.00
DT2	2.65E-05	-0.010	0.16
DT3	5.51E-05	-0.070	0.29
DT4	2.64E-05	-0.036	0.60
DT5	1.32E-04	-0.172	0.54
DT6	2.77E-05	-0.018	0.60
DT7	2.88E-05	-0.022	0.07
DT8	9.29E-05	-0.080	-0.09

Table 3.2 Zero reading drifts and calibration factor changes of transducers

a) Cone load calibration

Calibration number	Zero reading drift (V)	Equivalent zero drift (kPa)	Calibration factor change (%)
Fugro* cal no.1	1.99E-04	-4.62	1.73
cal no.1 to cal no.2	-2.29E-03	155.44	-0.23
cal no.2 to cal no.3	-5.83E-03	400.55	-0.38
cal no.3 to cal no.4	-3.64E-03	270.86	3.53
cal no.4 to cal no 5	8.13E-03	-518.21	-6.36

b) Cone pore water pressure calibration

Calibration number	Zero reading drift (V)	Equivalent zero drift (kPa)	Calibration factor change (%)
Fugro* cal no.1	5.29E-03	-33.53	2.93
cal no.1 to cal no.2	pore pressure transducer change		
cal no.2 to cal no.3	-1.85E-03	4.57	0.43
cal no.3 to cal no.4	-1.33E-02	37.42	-0.19

* Calibration at Fugro laboratory

Table 3.3 Zero reading drifts and calibration factor changes of piezocone

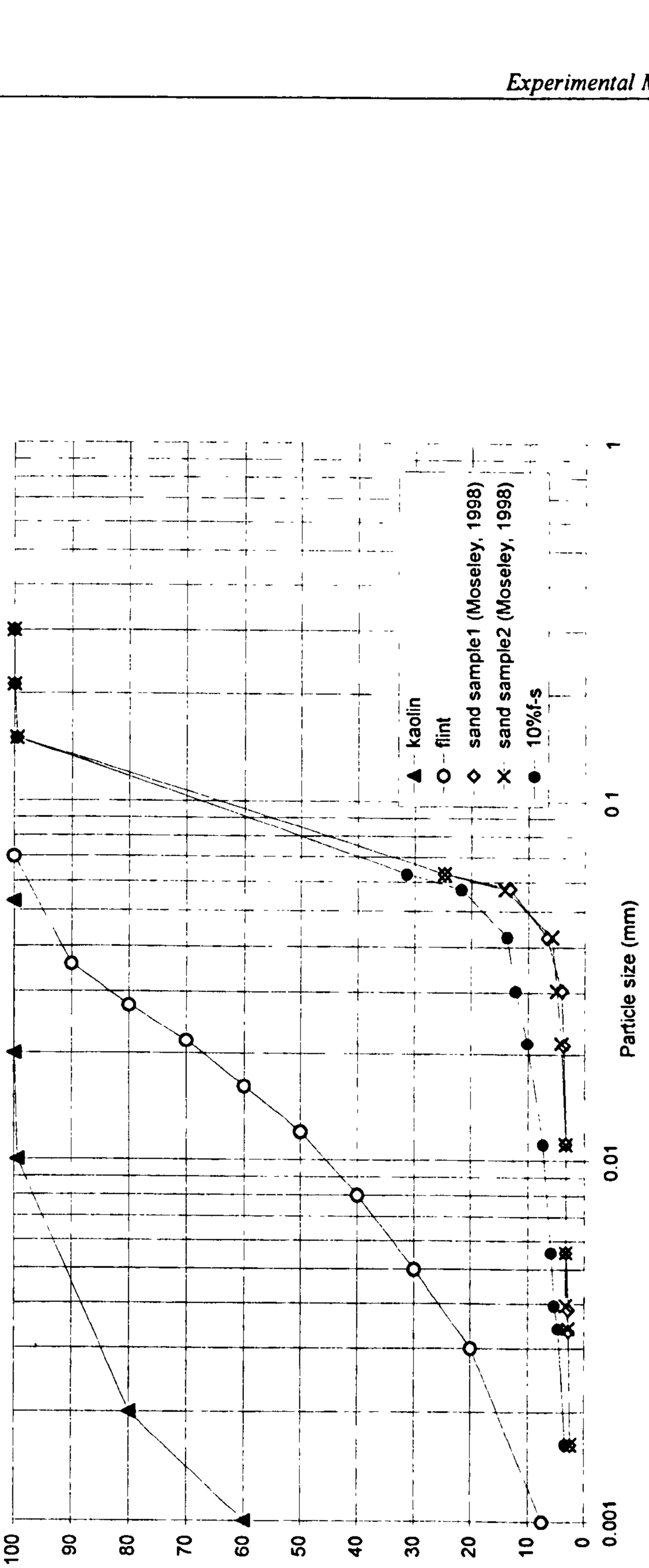

Figure 3.1 Material particle size distributions

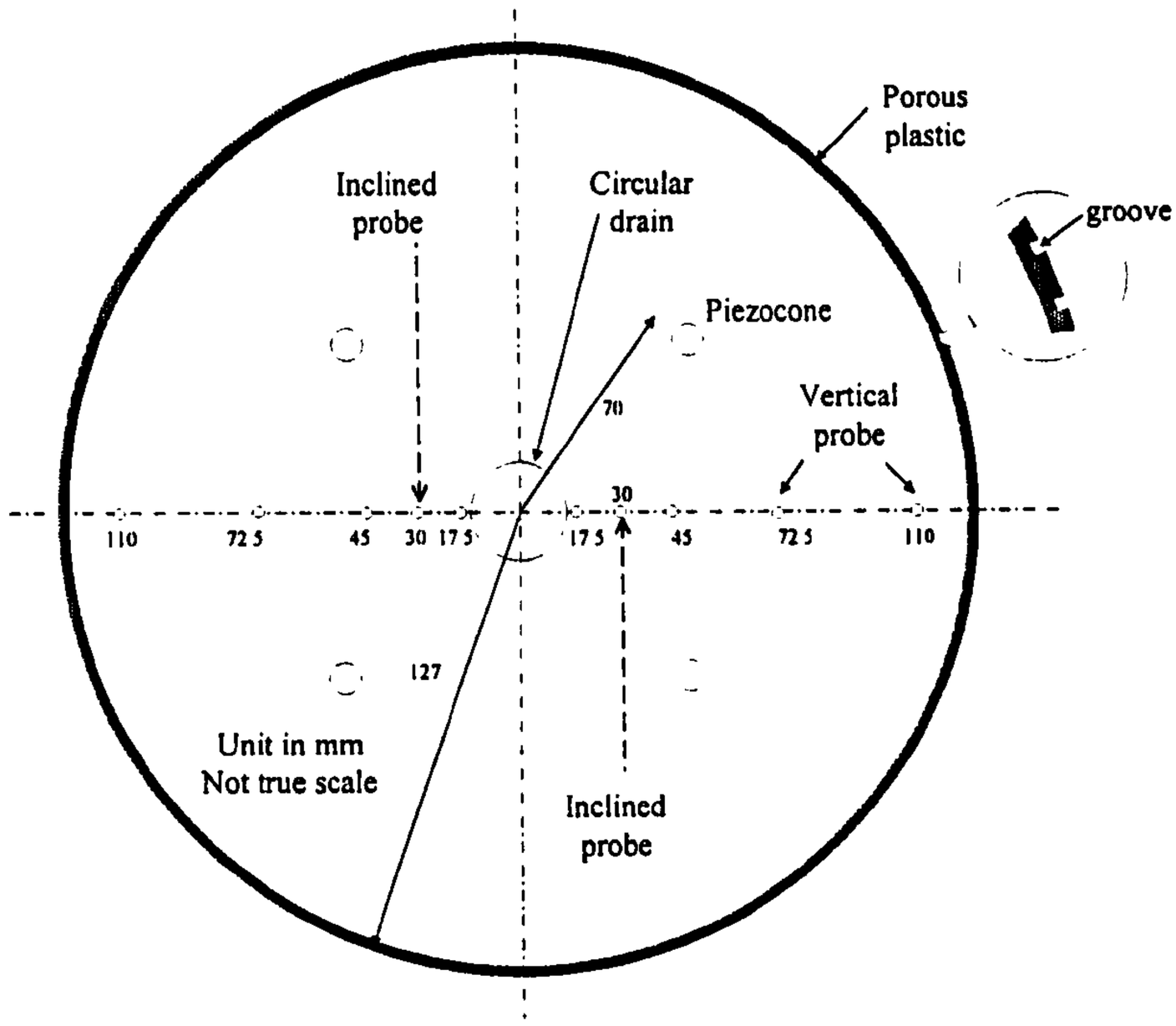

a) Cell base for circular drain

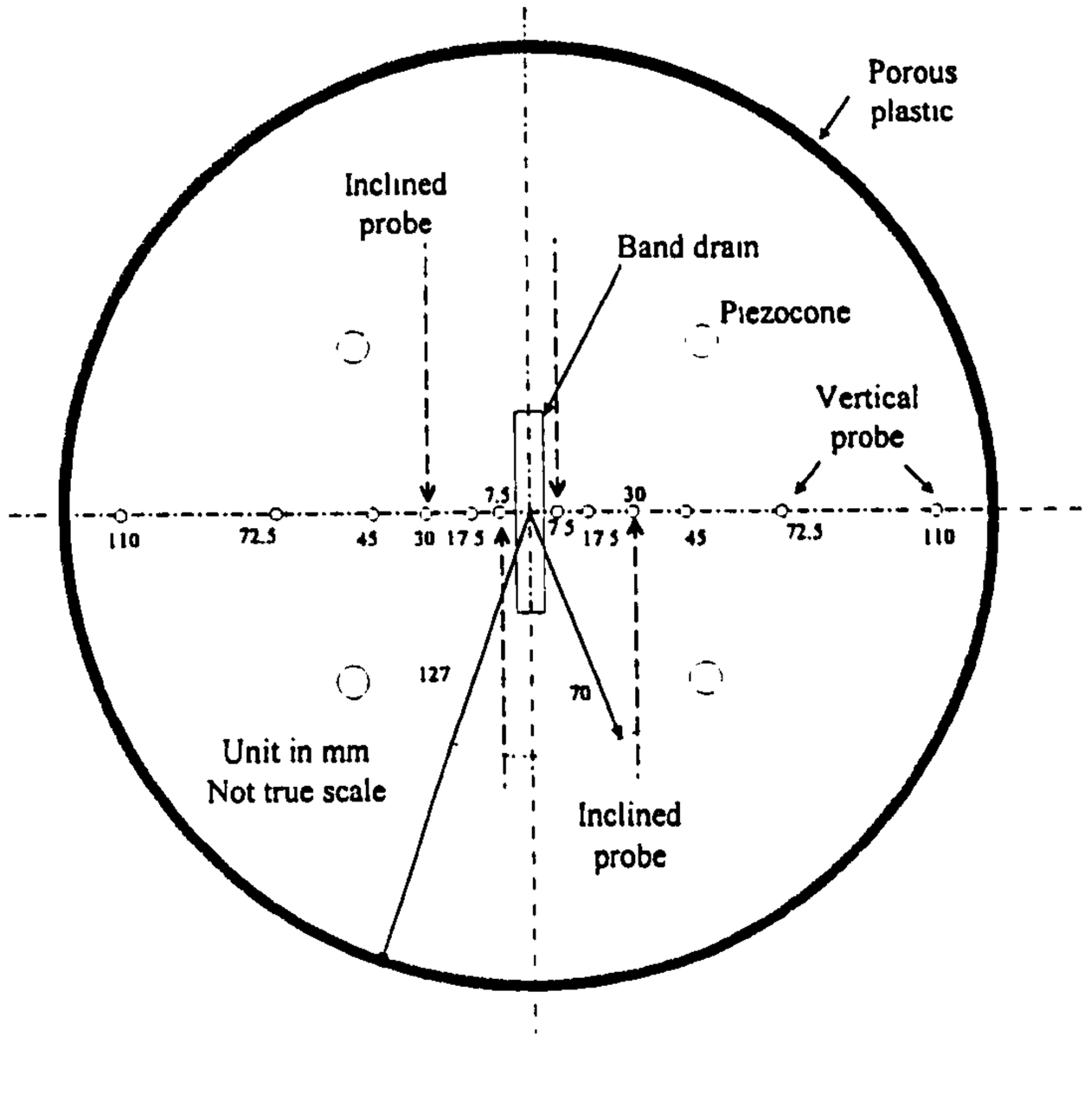

b) Cell base for band drain

Figure 3.2 Cell bases

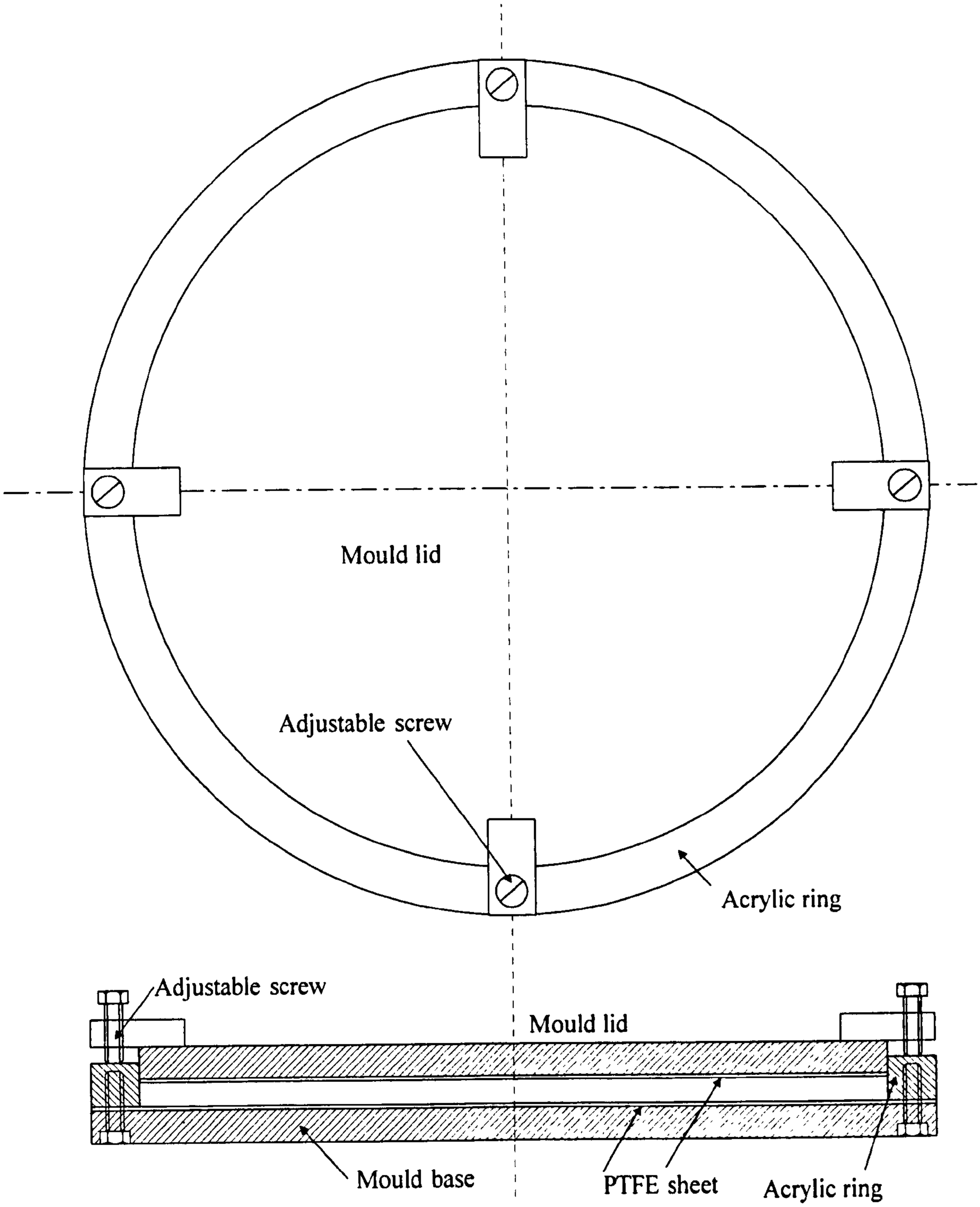

Figure 3.3 Mould for forming permeable layers

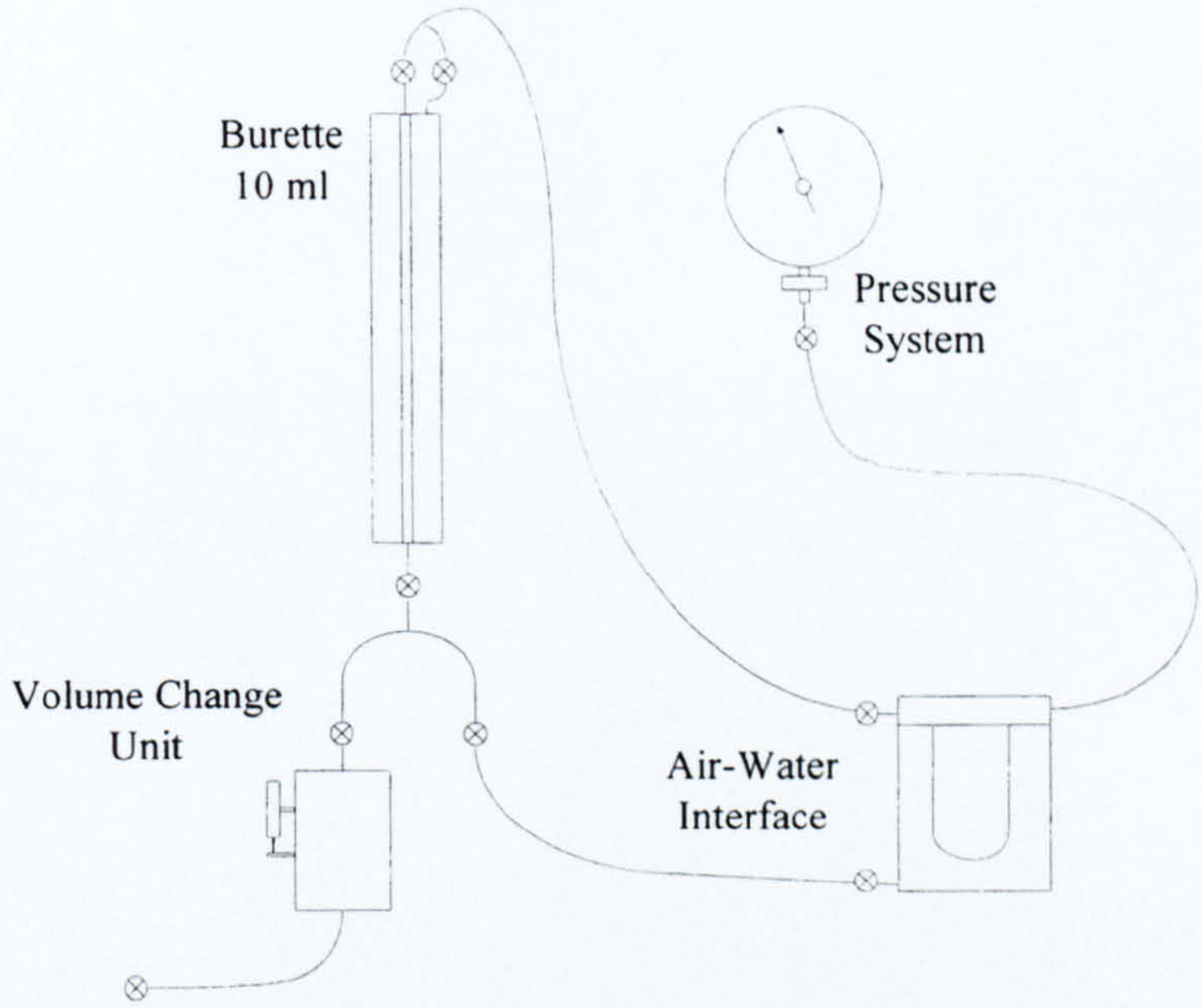

Figure 3.4 Volume change unit calibration

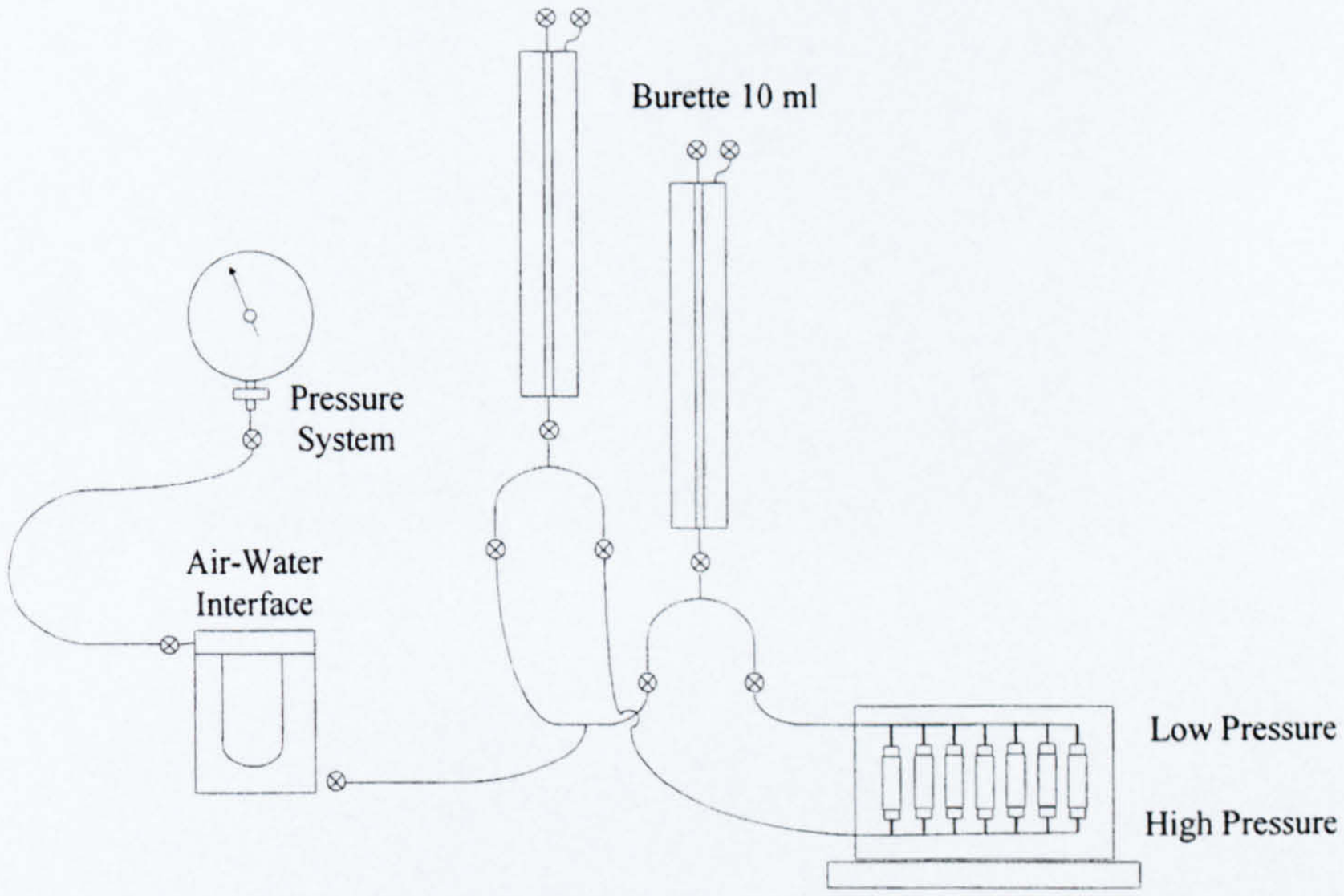

Figure 3.5 Differential pressure transducers calibration

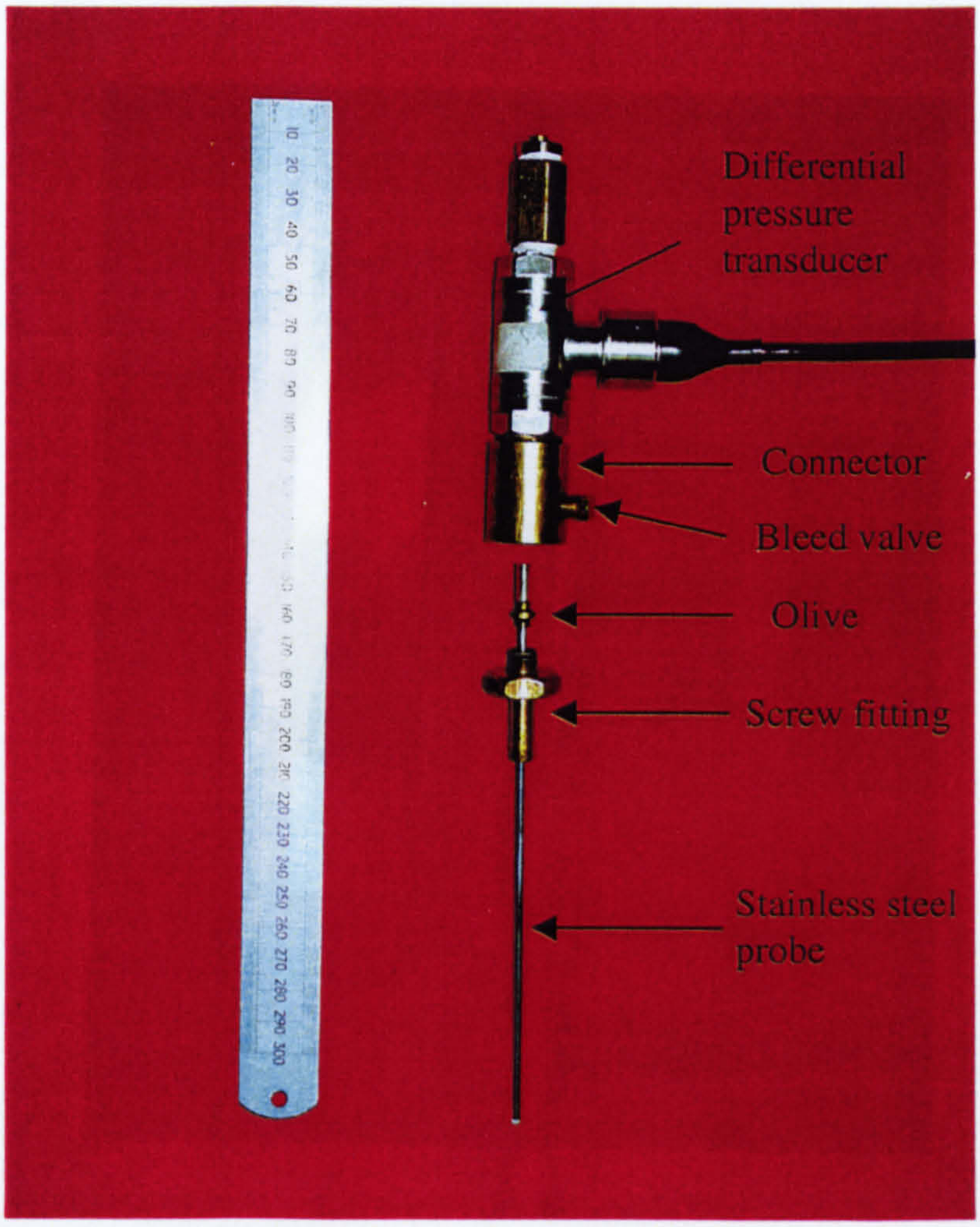

Figure 3.6 Differential pressure transducer and pore water pressure probe fittings

Figure 3.7 Band and Circular drains

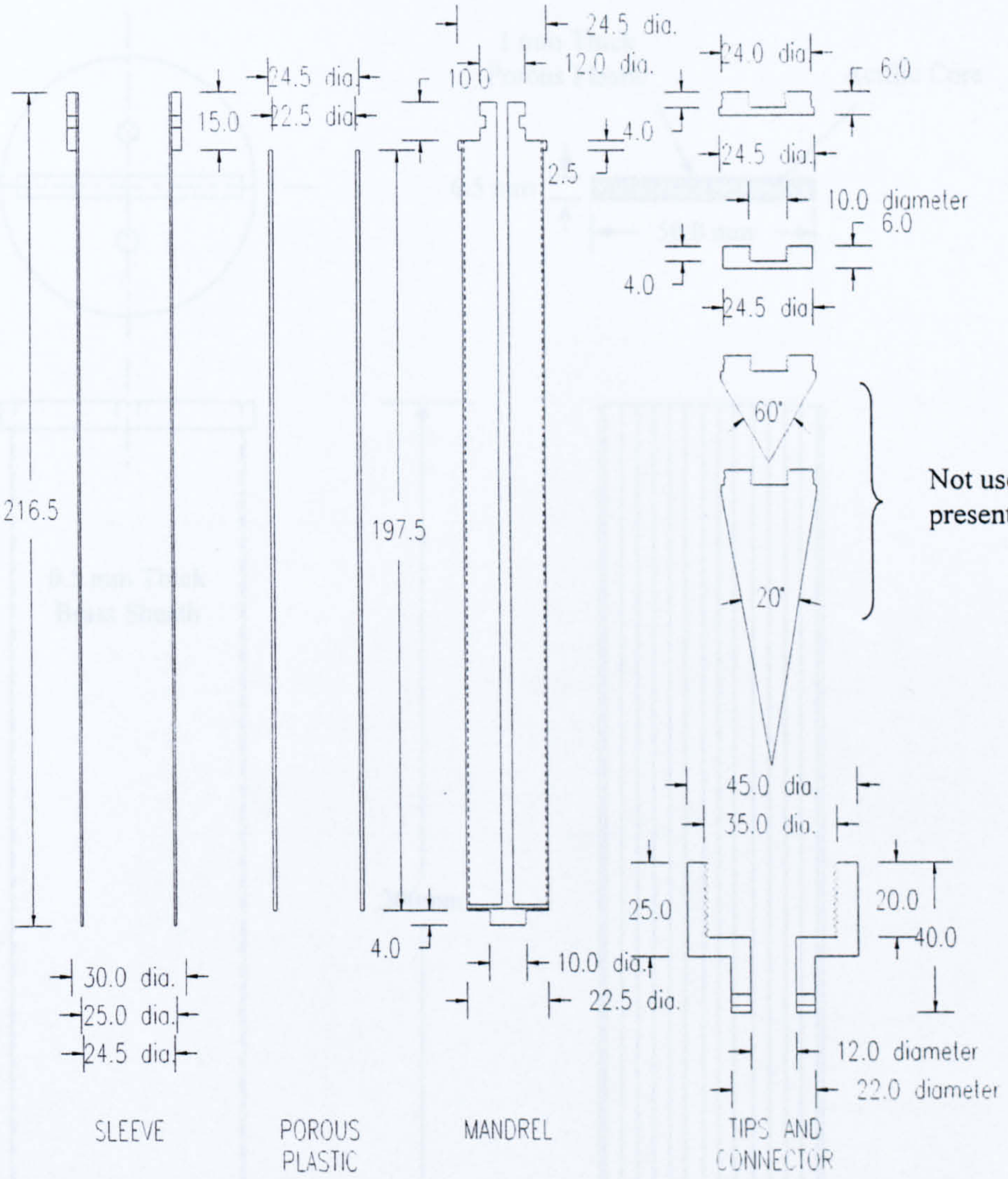

Figure 3.8 Circular drain (Moseley, 1998)

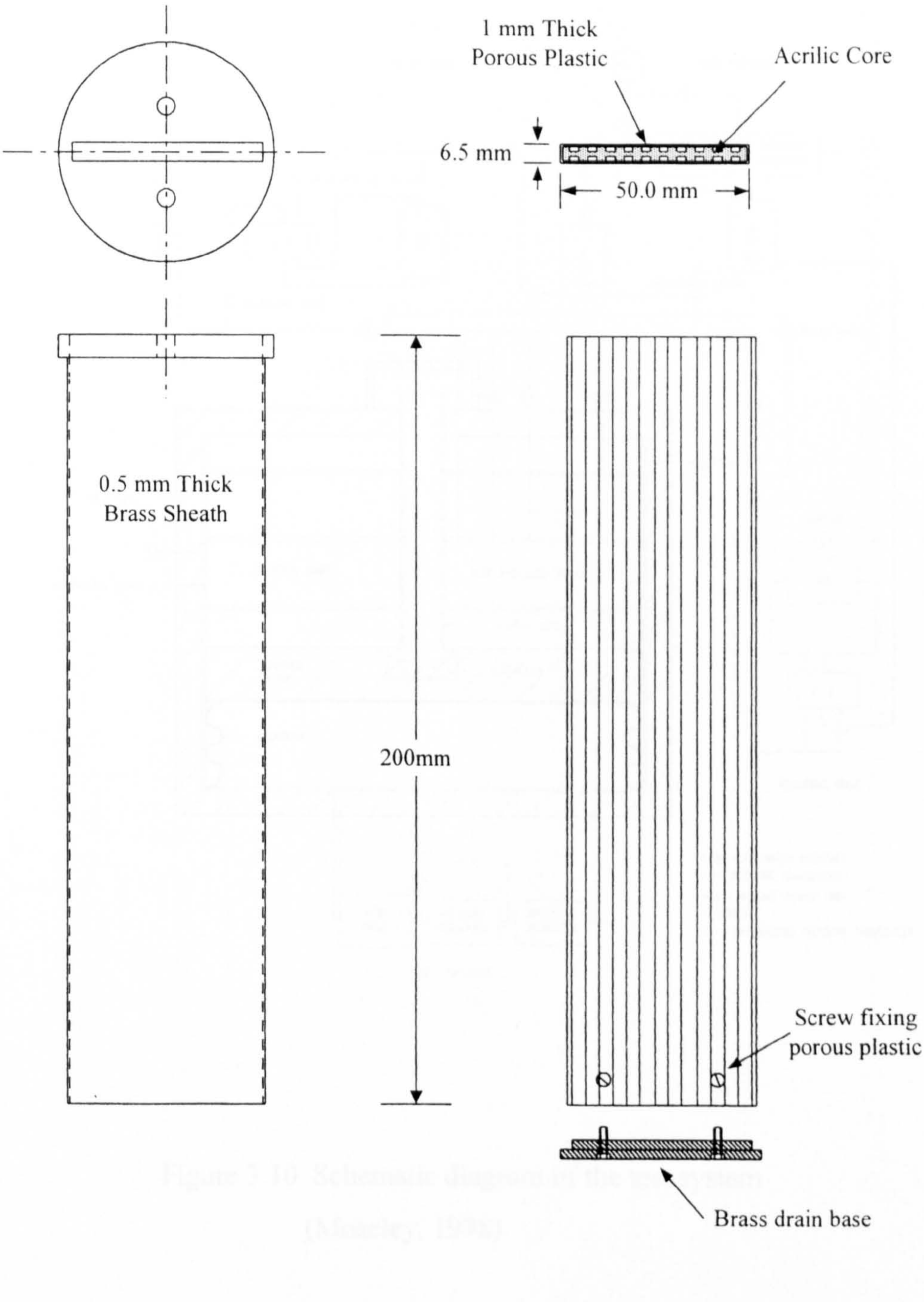

Figure 3.9 Band drain

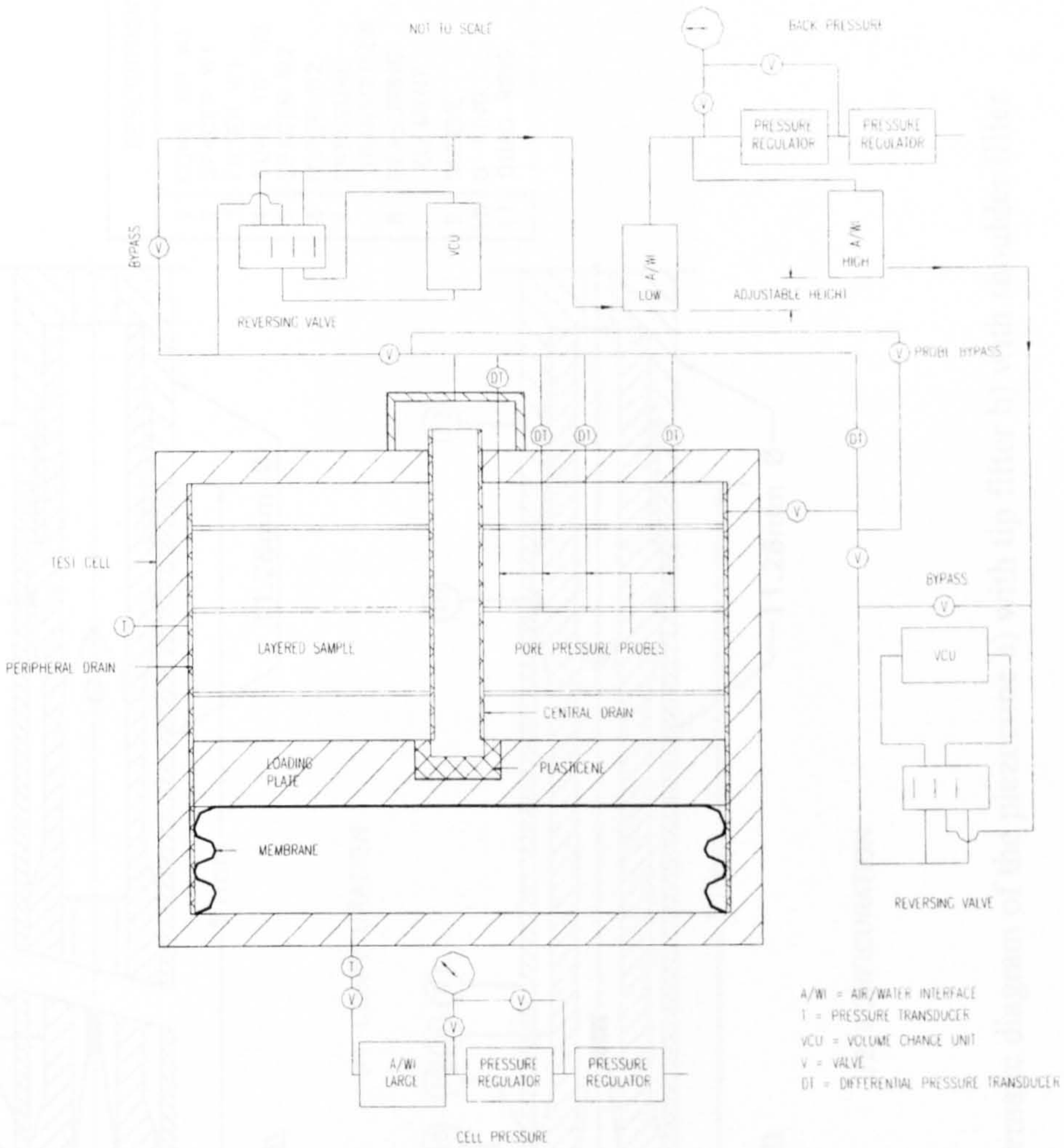

Figure 3.10 Schematic diagram of the test system

(Moseley, 1998)

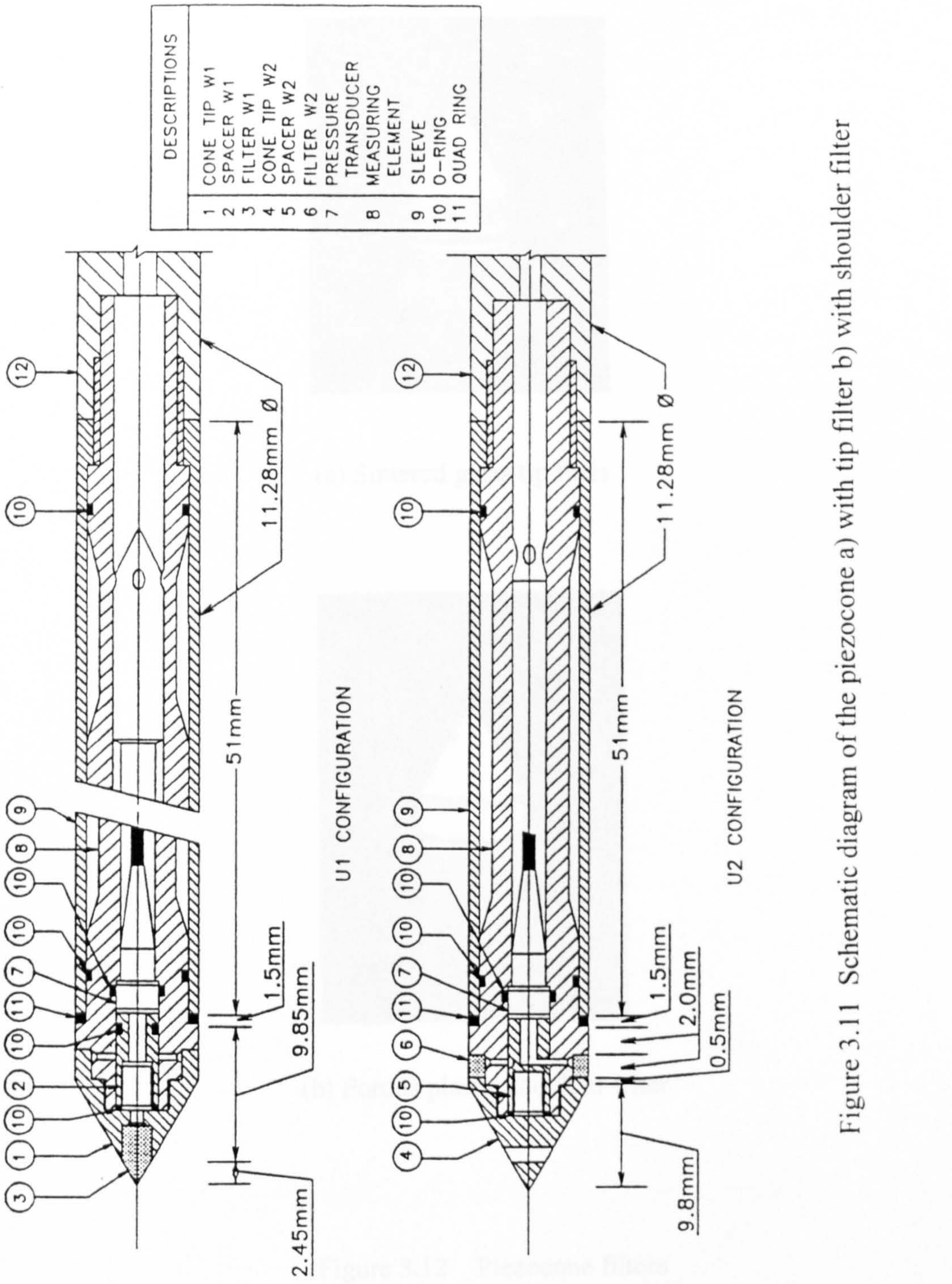

Figure 3.11 Schematic diagram of the piezocone a) with tip filter b) with shoulder filter

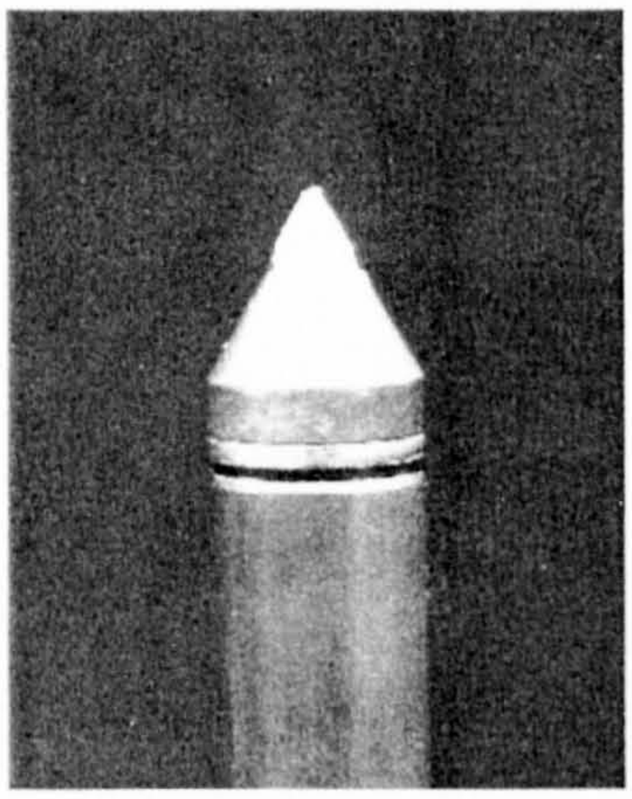

(a) Sintered glass tip filter

(b) Porous plastic shoulder filter

Figure 3.12 Piezocone filters

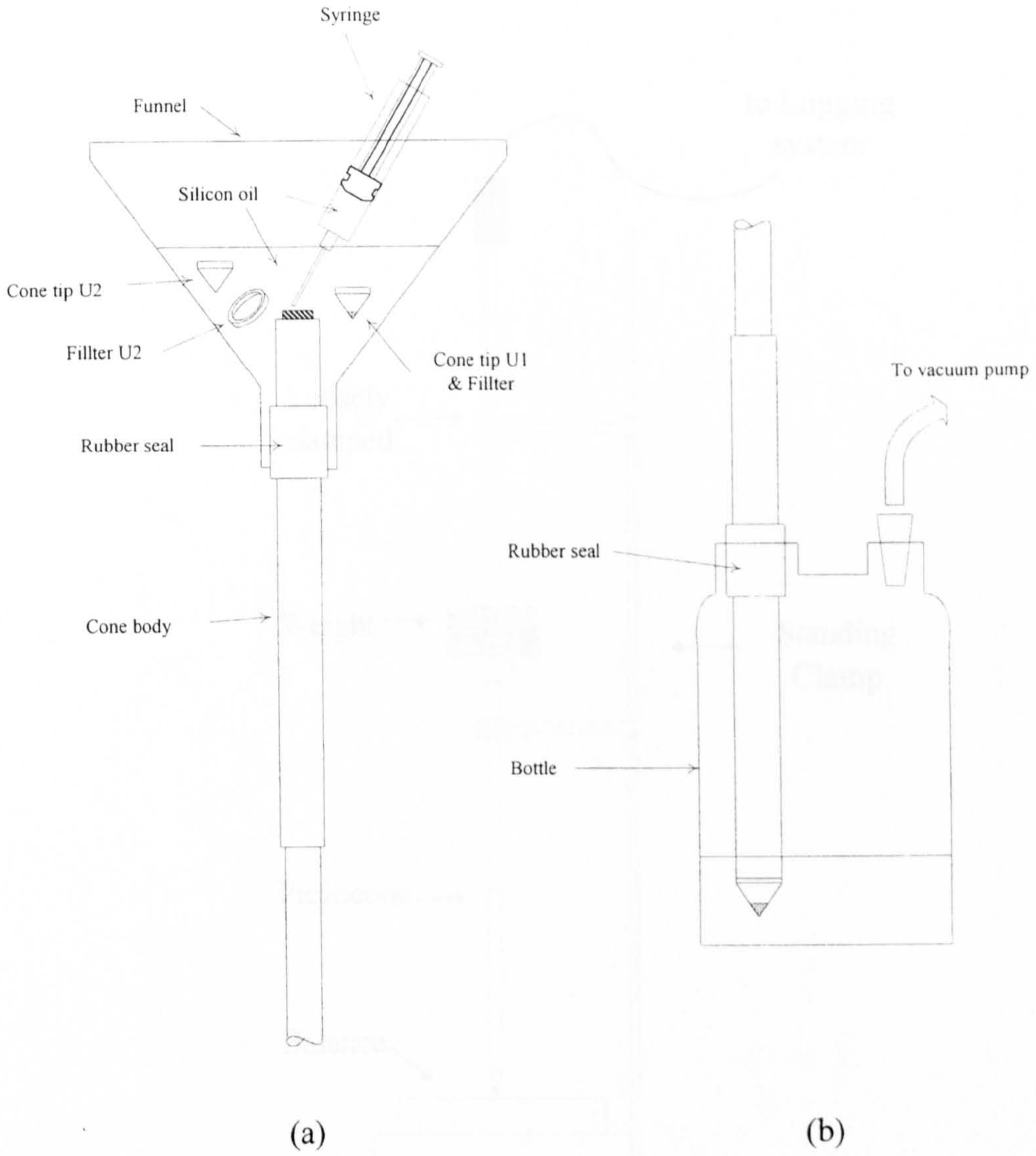

Figure 3.13 Piezocone assembling and de-airing

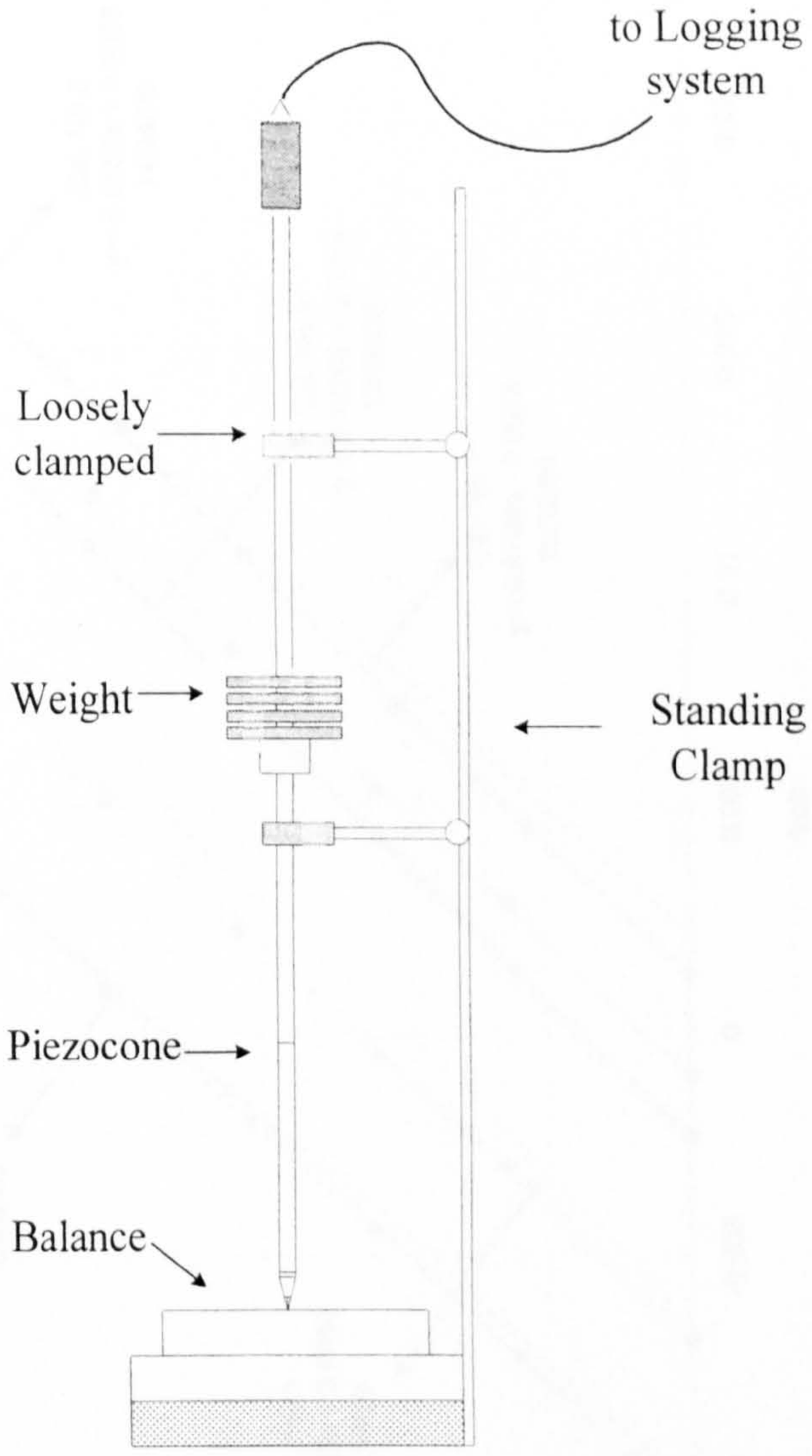

Figure 3.14 Cone resistance calibration

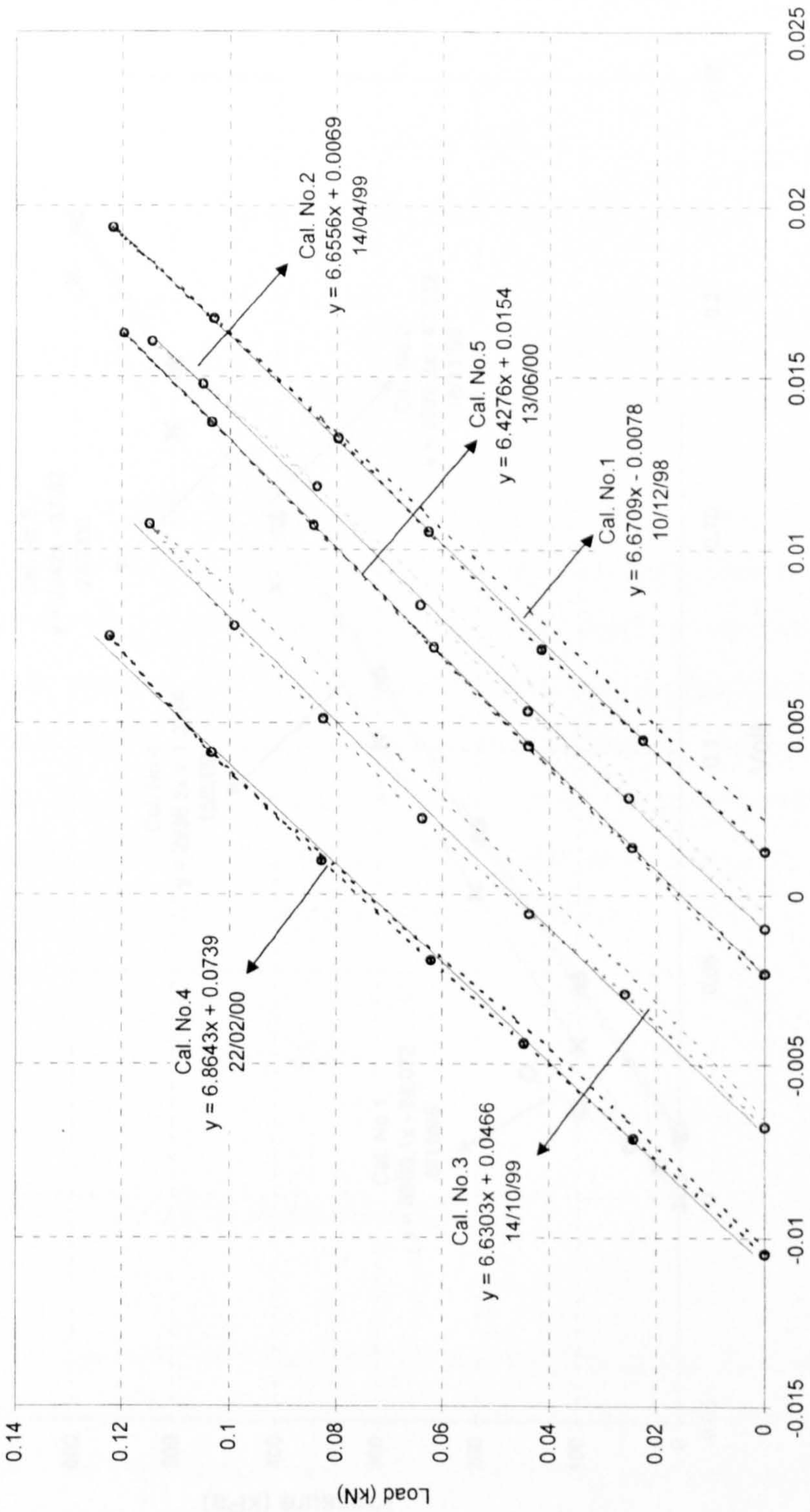

Figure 3.15 Cone load calibration for piezocone

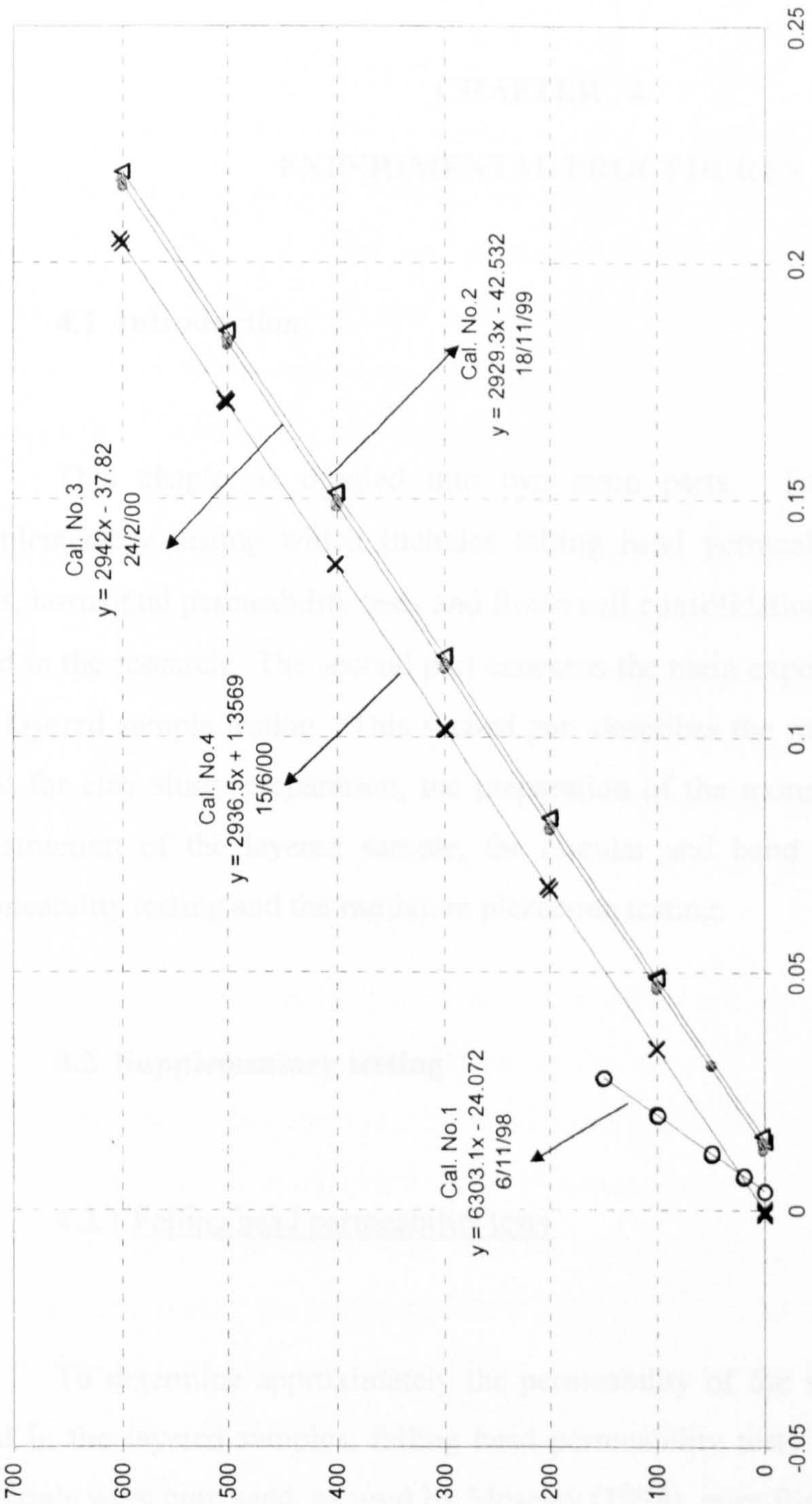

Figure 3.16 Pore water pressure transducer calibration results for piezocone

CHAPTER 4

EXPERIMENTAL PROCEDURES

4.1 Introduction

This chapter is divided into two main parts. The first part concerns supplementary testing which includes falling head permeability tests, oedometer tests, horizontal permeability tests and Rowe cell consolidation tests on the materials used in the research. The second part concerns the main experimental work, namely the layered sample testing. This second part describes the methods and procedures used for clay slurry preparation, the preparation of the more permeable layers, the construction of the layered sample, the circular and band drain installation, the permeability testing and the miniature piezocone testing.

4.2 Supplementary testing

4.2.1 Falling head permeability tests

To determine approximately the permeability of the sand and silt materials used in the layered samples, falling head permeability tests were conducted. The materials were pure sand, as used by Moseley (1998), pure flint and mixtures of flint and sand. The mixtures had ratios by weight of flint to sand of 5%, 10%, 17%, 30%, and 50%.

Samples for the falling head permeability tests were taken from the prepared batch of oven dried silty sand (Section 3.2.2). The flint was also oven-dried for at least 24 hours and sieved to break up the clods before use. Then the required amount of sand and flint was placed in a small rotary mixer which was operated continuously for at least 20 minutes.

To prepare the falling head test sample, about 500ml of deaired and deionised water was placed in the outer container of the falling head permeability apparatus. The perforated base was first placed in the container, then a saturated porous plastic disc and an O-ring seal were put on top of the perforated base. After that, the cylindrical permeameter body was placed on top of the O-ring seal. The water level was kept about 10 mm above the porous plastic disc. Then a teaspoon was used to sprinkle the test material into the permeameter. The water level was kept about 10mm above the sample surface all the time by syphoning. These processes were continued until the permeameter was full of material. By using a vernier calliper, the heights of the material were determined at three different positions around the mould and at the centre of the mould. The top of the permeameter was assembled and tightly clamped before the permeability tests. Then a large amount of deaired and deionised water was placed into the header tank which was approximately 2m above the permeameter. All the connecting tubes were attached between the header tank, the stand-pipe and the permeameter.

Falling head permeability tests were conducted on each material at three different dry densities. The dry density of the material was varied by tapping the mould and compacting the initially loose material in the mould. The falling head tests were performed by allowing water in a stand pipe with a diameter of 5mm to flow down through the sample and, for each test, the flowing time for a given change of level in the stand pipe was recorded. A total of three tests was performed for each dry density. The sample heights were then averaged and used to calculate the volume of the material. By assuming the material was fully saturated and knowing the volume and the mass of the material in the mould, the dry density and void ratio could be calculated.

4.2.2 Oedometer tests

Two oedometer tests were performed to determine the mass of the flint required to make layers of a given thickness under the effective stress applied to the layered samples. The flint was oven-dried, mixed to a slurry with de-aired and de-ionised water and put into the oedometer cell. A spirit level was used to level the cell and then a porous plastic disc was placed on top of the flint slurry. The height of the slurry in the cell was carefully measured with a vernier calliper. The cell loading plate was very gently placed on top of the slurry. Then the oedometer cell was placed in the standard test frame.

The pressures applied to the cell were 12.5, 25, 50, 100 and 250kPa. The whole test process was repeated using another cell. The final height of the material at 250kPa effective stress and the dry weight of the material in the cell were used to calculate the mass of flint required for a flint layer (Section 4.3.4) with a nominal thickness of 2mm.

4.2.3 Rowe cell consolidation tests

In order to determine the vertical and horizontal coefficients of consolidation of the kaolin, four Rowe cell consolidation tests were performed. The kaolin slurry was prepared by mixing the kaolin powder with de-aired and de-ionised water at twice the liquid limit in a rotary mixer. The slurry was then subjected to a vacuum of –100kPa for three hours before use.

Two Rowe cells with 152mm internal diameter were used for the consolidation tests. The inside walls of the Rowe cells were lined with 1mm thick PTFE sheet to reduce friction during consolidation. After being vacuumed, the required amount of slurry was scooped into the cells. A previously saturated circular porous plastic sheet, a perforated metal loading plate and another porous plastic sheet were placed on top of the slurry respectively. The cell lids, each with a pressure

membrane, were then assembled to the cells. For the first two tests, the consolidation pressures were 12.5, 25, 50, 100, 200, 400, 200 and 100kPa, each being applied for at least 24 hours. Drainage during consolidation was allowed from the top of the sample only. The results from these two first consolidation tests were used to determine the vertical coefficient of consolidation of the kaolin during consolidation and swelling stages. For the other two tests, after the pressures of 12.5, 25, 50 and 100kPa were applied, the cell pressure was reduced to zero and a peripheral porous plastic drain was installed around the sample. To do this, the cell lid was removed and the cell body was also removed by sliding it upwards. The PTFE at the side of the sample and the porous plastic disc at the top were then gently removed. Porous plastic, previously saturated, was then installed at the periphery of the sample and the cell was re-assembled. Consolidation pressures of 50, 100, 200, 400, 200, 100, 200, 400, 200, 100, 200, 400, 200 and 100kPa were applied to the sample. With data from these loading and unloading cycles, the horizontal coefficient of consolidation of the kaolin was determined. It should be noted that all the interpretation for the coefficient of consolidation was based on changes in the height of the samples.

4.2.4 Horizontal permeability tests

In order to determine the horizontal permeability of the sand and silt materials horizontal permeability tests were performed on three types of material: pure sand, pure flint and a mixture of flint (10% by weight of sand) with sand or "10%f-s". These were performed in a 254mm diameter Rowe cell with a circular vertical drain at the centre, under an effective stress of 250kPa, and so conditions were similar to those in the layered sample tests. Preparation of the materials was exactly the same as for the layered sample testing (Sections 4.3.3-4.3.5). For three separate tests, eight sand layers, twelve flint layers and twelve 10%f-s layers, all with 2mm nominal thickness, were prepared. However a different technique was used for the vertical drain installation.

To install the drain, after the sample had been saturated and consolidated as described in Section 4.3.7, the back pressure was removed, the Rowe cell was turned over and the central cell base plug was removed. A thin-walled circular brass tube was driven into the soil sample. The end of the sheath was embedded in Plasticine in the circular recess on the loading plate. Then the material inside the tube was removed using a syringe and de-aired water to flush out the soil particles, Figure 4.1 (a). A porous plastic tube was inserted into the brass tube, Figure 4.1 (b). Two pieces of thick rubber were pushed down inside the plastic tube to seal its bottom end. The plastic tube was then filled with medium size gravel to form the drain. The brass tube was removed and a circular aluminium ring was placed in the gap between the drain and the cell base to seal the gap and prevent piping failure during the permeability test, Figure 4.1 (c). The drain cover was placed in position. The pore water pressure probes were installed and then permeability measurements were performed as described in Sections 4.3.9 and 4.3.10.

4.3 Layered Sample Tests

4.3.1 Slurry preparation

Clay slurry was prepared by mixing kaolin powder with de-aired and de-ionised water at twice its liquid limit in a rotary drum mixer. Before mixing, the kaolin powder was placed in an oven at 105 °C for 2 days to avoid the effects of biological activity as recommended by Moseley(1998). The drum mixer was carefully cleaned before use and then a total mass of 20kg of deaired and deionised water was transferred into the mixer. After that, the kaolin powder (16.66kg in total) was slowly scooped into the water and the mixer was operated continuously for 1 hour. After mixing, the slurry was transferred into two air tight buckets. Then the weight of the two buckets was recorded so that the total amount of kaolin slurry used

could be determined later. Before the slurry was transferred into the consolidation cells (Section 3.3.1) samples were taken from the top of both buckets to find the water content of the slurry. Samples of slurry were also taken from the bottom of the two buckets after most of the slurry had been scooped into the consolidation cells.

4.3.2 Clay slurry consolidation

Before slurry was placed in the consolidation cells, the cells were lined with 1 mm thick PTFE sheets to reduce friction between the side of the cell and the slurry during consolidation and extrusion. Then a saturated 2mm thick circular porous plastic disc was put into each cell to allow drainage from the bottom during slurry consolidation. Although the porous plastic discs were re-used, they were properly cleaned every time by flushing water through them and boiling them. If any porous disc was noticed to be partially blocked by kaolin, it was replaced by a new disc. Kaolin slurry was scooped into the two consolidation cells in four layers of about 50mm thickness. After each layer was placed, the vacuum lids were assembled and a vacuum of about –100kPa was applied for 30 minutes to remove any air entrapped in the slurry.

Once the required amount of slurry was in the consolidation cells, the buckets were weighed again so that the weight of slurry scooped into the cells could be determined. A porous plastic disc was placed on top of the slurry in each cell followed by a 12mm thick circular perforated acrylic disc to encourage an equal strain consolidation condition. Then another porous plastic disc was placed on the top of the acrylic disc. To get rid of any air in the consolidation cells, about 500ml of deaired and deionised water was put into the cell before the cell lid was assembled and the piston length measured so that the height of the slurry in the cell could be determined. Knowledge of the height of the slurry in the cell, the water content of the slurry and the weight of slurry in the cell permitted the initial void ratio and degree of saturation of the slurry to be calculated.

To initiate consolidation, a cell pressure of 12.5kPa was applied to the slurry and consolidation allowed to take place for 36 hours. For the next two pressures of 25 and 50kPa, consolidation took at least 48 hours to complete. To avoid over stretching of the Rowe cell membranes, once the slurry had been consolidated to 50kPa, two more acrylic discs, 15mm thick, and another porous plastic disc were placed on top of the other discs above the clay by reducing the cell pressure to zero and opening the cell lid. During this process, swelling of the clay was allowed. For the continuation of consolidation, cell pressures of 50,100 and 200kPa were applied, each for at least 48 hours. Settlement readings were taken until the end of primary consolidation for every loading stage.

4.3.3 Sand layer preparation

The sand layers were formed by sprinkling dry sand through deaired and deionised water in a circular mould (Section 3.3.3) and then freezing the sand layer in the mould. To prepare a sand layer, silicon grease was placed on the outside part of the rim of the mould and then the mould was assembled. The mould was placed on a flat table and a spirit level was used to check the levelling. About 500ml of deaired and deionised water were then placed into the mould. The mould was divided into four quadrants by placing two pieces of wire on top of the mould. The required weight of sand, 165g for a nominal 2mm thick layer, was divided into four parts and put in four glass dishes. A sand layer was made by sprinkling sand from each glass dish into one of the four quadrants of the mould. Then a wide toothed comb was used to level the top of the sand. Two central cross dragging operations were performed first, followed by two full circular dragging operations. The details of this procedure were reported by Moseley (1998). After that, the side of mould was tapped gently so that the ridges formed by combing the sand were levelled. Then the mould lid was placed on the top of the mould. Initially, during placement, the lid was slightly inclined so that any entrapped air could be removed. A spirit level was

placed on top of the lid while the lid was finally being pushed down to contact the sand. Then the mould was placed in a freezer for 24 hours.

A total of four sand layers was prepared at one time. If more than four layers of sand were required, the moulds were removed from the freezer, the sand layers were removed from the moulds and wrapped in cling film before being put back into the freezer. After that, the moulds were cleaned and used again.

4.3.4 Flint layer preparation

To vary the permeability of the more permeable layers (Section 3.1), flint was used in some layered samples instead of sand. It was found that, under zero effective stress conditions, the flint was more easily disturbed than the sand. To prevent disturbance, especially during model building, a protective ice layer was formed on top of each flint layer.

Firstly, after 24 hours of oven drying, 150g of flint was weighed out. This amount eventually produced a layer of 2mm nominal thickness. The flint was put into a 500ml beaker and mixed with 85g of de-aired and de-ionised water. A magnetic spinner was put into the beaker and the beaker was put into a glass vessel. Then the vessel was placed on a spinning magnetic field generator while a vacuum was applied. In this way, the flint slurry was mixed by the spinning magnet in the beaker and de-aired by the applied vacuum at the same time. The de-airing process was carried out until no more air came out from the flint slurry. Then the flint slurry was slowly poured into the mould on a flat table. Once the slurry was in the mould, a spirit level and comb were used to level it with the same procedures as used for sand layer preparation. By using adjustable screws on the rim of the lid, Figure 3.3, the mould lid was placed so as to just about touch the surface but not to put load on the flint. After that, the slurry was left in the mould and the flint was allowed to settle and form a stiffer layer before the next stage. After about 3 hours, the lid was removed and 500ml of de-aired and de-ionised water was slowly added into the

mould and the lid was placed on top of the mould leaving a gap which gave a depth of free water above the flint surface of about 3mm. Then the mould was placed in a freezer for 24 hours. By this method, an ice layer about 3mm thick was formed on top of the flint.

4.3.5 Mixed flint and sand layer preparation

A mixture of flint and sand was used to form higher permeability layers in some layered samples. It was expected that the mixture would give a permeability value in between those of pure flint and pure sand. In the falling head permeability tests (Section 4.2.1) the percentage of flint mixed with the sand was varied in order to identify a suitable mixture with the desired permeability. Finally, a mixture with 10% flint by weight of sand (referred to as 10%f-s) was selected.

The flint and sand were oven-dried for 24 hours before mixing. The required amounts of the materials were put in a small rotary mixer. The mixer was operated for 20 minutes. For such a mixture, sprinkling through water could have caused segregation and non-uniformity of the permeability in the layers. To avoid this problem, the mixture of dry materials was mixed with an amount of de-aired and de-ionised water, 176g of dry material with 94g of water, using the same method as for the pure flint layers. The amount of water was seen from trials to be the minimum amount that allowed the spinning magnet to work properly. After mixing and de-airing, the mixture was carefully transferred into the mould and levelled before the top cap was immediately placed on top. Then the mould was placed in a freezer for 24 hours.

4.3.6 Layered sample preparation

Layered samples were constructed by combining relatively thick layers of consolidated Speswhite kaolin clay and relatively thin more permeable layers.

The layered sample test cell (Section 3.3.2) was carefully assembled. All the joints and connections were cleaned and properly reconnected to avoid leakage. The 1mm thick porous plastic peripheral drain was grooved and de-aired before being placed in the cell. Some de-aired and de-ionized water was put in the cell prior to sample formation. The water was kept about 5mm above the cell base.

The Speswhite kaolin slurry, which had been pre-consolidated in the two consolidation cells, was extruded from one consolidation cell to obtain an extruded thickness of kaolin cake of 20mm. A vernier calliper was used to measure the exact thickness of the clay layer. The cake was then wire-cut and put in the test cell using a suction pad to carry it, Figure 4.2. The kaolin layer was slightly inclined when it was placed into the cell so that any entrapped air could be flushed out from the underside. After all the air had been expelled, the suction pad was detached from the top of the clay layer by blowing down the plastic tube and gently rocking the handle of the suction pad. After putting the first clay layer into the cell, tissue paper was used to remove any kaolin smeared on the porous plastic lining. The next clay layer was extruded from the cell, wire cut and lifted up by the suction pad so that it could be placed into the cell immediately after placing the first more permeable layer.

Before the first sand layer (or flint, or 10%f-s) was placed, water on top of the clay layer which had became contaminated with suspended clay particles was siphoned out in order to prevent entrapping of the clay particles in the next sand layer. Then fresh cool water was added to the cell and a sand layer was carefully taken out from a mould and placed on top of the first clay layer. The sand layer was slightly inclined while it was put into the cell to expel the air bubbles from between the base of the sand layer and the top of the clay layer, Figure 4.3. During this stage, a hard pushing force could break the fragile sand layer and damage the sample so it had to be ensured that the rim of the frozen sand layer was smooth without excessive ice crystals that could produce high friction between the layer and the porous plastic. Once the sand had been properly placed on top of the clay, the next clay layer was put into the cell. By performing this process quickly, the sand was still frozen while the next clay layer was pushed into contact.

By repeating all the above processes and placing frozen sand layers alternately between clay layers, a layered sample was constructed.

4.3.7 Layered sample consolidation and saturation

Once the layered sample had been prepared, the cell was lifted up to the test frame and the loading plate (Section 3.3.2) was placed on top of the sample. For tests with a vertical band drain, placement of the loading plate had to be done with the correct orientation of the recess.

After the cell lid was assembled, the piston position was measured so that the height of the layered sample in the cell could be determined. Cell pressures of 12.5, 25, 50 and 100kPa were successively applied to the sample. The volume of water flowing out of the sample under each pressure was measured. Once water stopped flowing from the sample at the cell pressure of 100kPa, the peripheral drain was flushed with a large amount of de-aired and de-ionised water in order to expel any trapped air. The differential pressure used to flush the drain was about 5-10kPa. Flushing continued until no more visible air came out.

After flushing, a back pressure of 200kPa was applied to the layered sample in two steps. First, the cell pressure was increased from 100 to 200kPa and the back pressure was increased from zero to 100kPa. Second, the cell pressure was increased from 200 to 300 kPa and the back pressure was increased from 100 to 200kPa. Then the sample was left at least 6 hours to allow any trapped air to dissolve into the pore water.

After saturation, the layered soil sample was consolidated to an effective vertical stress of 250kPa in two increments, 100 to 200kPa and 200 to 250kPa, before the vertical drain was driven into the model. For each increment, the sample was left for at least 36 hours. The height of the layered sample in the cell was calculated by measuring the position of the piston before consolidation and recording the change of

the height (piston movement) using a displacement transducer with the computer logging system.

4.3.8 Vertical drain installation

After the layered sample had been consolidated, a mandrel carrying a sheathed vertical drain was driven into the model. In order to quantify the effects of smear caused by different shapes of vertical drain, a circular drain and a rectangular drain (Section 3.3.11) were used in the research.

To saturate the vertical drain, it was deaired under water for about eight hours in a vacuum chamber with a pressure of about –100kPa. Before driving, the 200kPa back pressure was removed from the sample. The effective stress of 250kPa was kept constant while the back pressure was removed. Then the test cell was inverted, the cell base plug was removed and the sheathed drain was attached to the driving system (Section 3.3.10). It had to be ensured that the water level was always kept above the drain inside the sheath. For the circular drain, an O-ring seal at the bottom prevented leakage. For the band drain, instead of using an O-ring seal, Plasticine was applied to the joint between the sheath and the drain bottom to keep the water inside the drain. When attaching the drain to the driving system, Figure 4.4 (a), positioning was very important to ensure that the drain was driven exactly at the centre of the sample. Otherwise, it could touch the side of the access hole in the cell base. This could generate high friction and lead to strong vibration during the driving.

The vertical drains were driven into the sample at a rate of 5mm/sec. During driving, drainage from the sample was allowed. The flow due to driving, the change of sample height, the water pressure in the peripheral drain and the driving distance were recorded by the data logging computer. After the vertical drain was driven into the sample, a steel reaction rod was inserted into the hole at the centre of the central drive rod (Section 3.3.10). The end of the reaction rod was placed inside the sheath,

Figure 4.4 (b), to hold the vertical drain in place when the sheath was removed vertically at a rate of 5mm/s. Then the drain cover was assembled on the cell base.

4.3.9 Pore water pressure probe installation

The pore water pressure probes were prepared shortly prior to placing them in the layered sample. As described in Section 3.3.8, the probes were made from hypodermic steel tube. A 5mm thick porous plastic sheet was boiled and vacuumed before being used for the probe tip filters by embedding the sharpened end of the hypodermic tube 4 mm into the plastic sheet. The tube was then pushed through the sheet leaving 1 mm of rough sided porous plastic protruding from the end of the tube. The protruding porous plastic was trimmed with a knife to a smooth shape. The brass wires were placed inside the hypodermic tubes to reduce the volume of the water in the tube and decrease the response time. Then the probes were left overnight under de-aired and de-ionised water in a vacuum chamber with a pressure of −100kPa.

Once the drain had been driven into the sample, a large container was filled with de-aired and de-ionised water and a measuring cylinder was used to transfer the probes to the large container. A differential pressure transducer and a connector were placed into the large container. The water level in the container was kept just above the transducer so that the electric cable was still dry. The bleed valve screw, Figure 3.6, was removed from the connector and air was flushed from the high pressure end of the transducer using a hypodermic syringe and needle. Then the pore water pressure probe was connected to the transducer under water and the bleed valve screw replaced. The assembly was then moved to the layered sample cell. During this time, the probe tip was kept under water in a small beaker. Before insertion of a probe, the access hole plug was removed from the cell base and the syringe, filled with de-aired and de-ionised water, was used to flush the hole. Then the probe was slowly inserted through the hole into the cell. During insertion, the pore water pressure was recorded by the computer logging system and kept under 100kPa so that

the transducer would not be damaged. Seven differential pore water pressure probes were inserted into the soil sample at various radii so that the variation of pressure head due to water flowing across the sample could be investigated (see Section 4.3.10). Figure 3.2 shows the general arrangement of the probes for the tests with a circular drain and a band drain.

After all the probes had been inserted into the soil model, plastic tubes were attached to the low pressure side of the transducers and to the drain cover (Section 3.3.12). After that, a pressure of about 5kPa was applied to the low pressure air-water interface tank. All the plastic tubes and connections connected to the low pressure supply were flushed with water from the tank by temporarily disconnecting the tubes from the low pressure side of the transducers one by one. Before reconnecting the tubes to the transducers, the syringe filled with de-aired and de-ionised water was used to flush the low pressure side of each transducer. A flushing process was also carried out for the high pressure connection to the sample so that all tubes in the system were flushed out and saturated with water.

After all the plastic tubes and transducers had been flushed and connected, Figure 4.5, the soil sample was saturated by increasing the back pressure to 200kPa while keeping the effective vertical stress at 100kPa. The back pressure was raised in four 50kPa increments so that the differential pressure transducers would not be damaged. Increments of pressure were applied through the high pressure air-water interface tank. The probe bypass, Figure 3.10, valve and the valve to the low pressure air-water interface tank were closed. For each increment of cell pressure, initially drainage was not allowed so that the pore pressure response to the increase of cell pressure could be recorded. Then the pressure in the high pressure air-water interface tank was raised by 50kPa and the drainage valve was opened. The whole process was repeated until the back pressure reached 200kPa. The sample was left for at least 8 hours to ensure full saturation of the system before the tests described in the following section.

4.3.10 Head distribution test and permeability test

The head distribution test, or "head test", and permeability test were performed by applying differential water pressure across the soil sample. The head test was performed by allowing water to flow across the sample without measuring the rate of flow. However, the pressure head distribution was measured throughout the test. The purpose of head test was to avoid the effect of head losses in the volume change units on the head readings and to create a reasonably constant head difference across the sample. As reported by Moseley (1998), the deflections of the rolling membranes (belloframs) within the volume change units produced a variation in the pressure across the sample during permeability tests.

Before starting the head test, the air-water interface tanks were placed on the adjustable rack on the wall. The levels of the two tanks were arranged to produce about 10kPa of pressure difference across the sample. The probe bypass, Figure 3.10, valve and the valve to the low pressure air-water interface tank were closed. Only the valve to the high pressure air-water interface tank was opened. Thus the pressure differences read by all the differential pressure transducers were expected to be very close to zero. If the reading was not close to zero at this stage, it was possible that the flushing process had not been done properly so that some air bubbles were still in the system. Before the head test started, the "zero readings" were recorded by the computer logging system until all the values were constant over a period of about 20 minutes. It should be noted that if any transducer gave a zero reading higher than 0.5kPa or lower than –0.5kPa, its data were neglected during the subsequent test. After the zero readings were taken, the head test was started by closing all the valves in the system and then opening the two volume change unit by-passes, opening the valve to the high pressure air-water interface tank and opening the valve to the low pressure air-water interface tank. The head test took several hours. After the test had finished, zero readings of the differential pressure transducers were taken again.

The permeability test was conducted in the same way as the head test but the volume change units were used to measure the inflow and outflow rates. To start the

permeability test, the same procedures described above for the head test were used except that, instead of opening the volume change unit by-passes, the reversing valves of the volume change units were opened. It was found that turning the reversing valve of the volume change units could produce a very high pressure in the system. To avoid damage to the differential pressure transducers, the reversing valves had to be turned while the connections to the high pressure air-water interface tank and to low pressure air-water interface tank were closed. In the permeability test, about 60ml of water was allowed to flow through the sample.

4.3.11 Miniature piezocone penetration testing

After the permeability test had been carried, the mini-piezocone (Section 3.3.13) was driven into the layered sample at a rate of 20mm/sec.

As described in Section 3.3.13, after the de-airing processes had been completed, the cone was left under atmospheric pressure for at least 6 hours. This gave time for the silicon oil to flow into the cone and fill any voids caused by deairing (discussed in Section 6.3.4). After that, the vacuum was applied to the cone again and then it was released immediately to check the cone response. This was done 2-3 times and the response of the cone was visually observed on the monitor of the computer logging system (Section 3.3.14). If a sharp response was not shown, the filter was removed and replaced by a new one. Then all the de-airing processes were repeated.

The piezocone was taken out from the de-airing apparatus and a medical fingercot filled with silicon oil was immediately placed on the end of the piezocone. The level of the silicon oil in the fingercot had to be kept higher than the cone filter so that the filter was kept saturated. Then the piezocone was transferred to the driving frame, Figure 4.6. The upper clamp was fastened first. The lower clamp was clamped loosely and then a plumb line was used to ensure that the piezocone axis was vertical.

Before the piezocone was driven into the soil sample, the "zero readings" of cone resistance and pore pressure were recorded by the computer logging system for approximately ten minutes. The back pressure in the cell was reduced from 200kPa to zero in the same way as it had been increased (Section 4.3.9) while the effective stress was kept constant at 250kPa. Then one of the access holes in the cell base, Figure 3.2, was opened and the cone was slowly driven into the sample to a depth of about 10mm. During driving of the cone tip into the sample, the lower clamp remained loose so that the cone position was slightly adjustable.

Once the cone tip was in the right position in the soil sample, the lower clamp was tightened up properly. The cell pressure was increased to 350kPa, but drainage was not allowed. This was so the cone pore water pressure response to the increase of cell pressure could be investigated. Then the valve connecting the cell to the high pressure air-water interface tank with a back pressure of 100kPa was opened. This process was repeated for a cell pressure of 450kPa and a back pressure of 200kPa. After that, the cone was left for at least 6 hours. This gave time for any entrapped air in the model to be dissolved in the pore water. During this time, the volume of water flowing into the sample was recorded by the logging system.

After six hours, the data logging routine was switched to the routine used for piezocone driving. This logging routine was set to the fast logging mode to collect data every 0.005 second. The driving distance was measured in order that the cone could be stopped at a planned position. Normally, it was intended that the cone filter should stop approximately at the middle of a clay layer towards the lower end of sample. Once everything was ready, the logging system was operated and immediately the driving system was operated to drive the cone into the sample at the desired speed of 20 mm/sec. During the driving, drainage was allowed from the sample. The driving was stopped manually by switching off the power to the driving system once the required distance was reached, the cone was left in the soil sample and the dissipation of the excess pore water pressure was monitored. Approximately 10 seconds after the cone stopped, the logging rate was reduced to collect data every 1 second for a minute, every 5 seconds for 5 minutes and every 50 seconds for 1 hour. After about 1 hour of the dissipation test, the cone response to a cell pressure increment was investigated again and then the back pressure was reduced to zero in two steps while the effective stress

was kept at 250kPa. The piezocone was then withdrawn from the sample at a rate of about 1mm/sec.

After the cone had been taken out of the sample, the data logging computer was still operated for few hours in order to ensure that the load cell and pore pressure transducers were working properly. Then the cone was transferred to the support for replacing the filter.

4.3.12 Sample dissection and photography

After the tests on the sample had been completed, the cell pressure and back pressure were removed from the sample. Swelling was not allowed during this stage. The cell lid, the drain cover and the bolts at the cell base were removed. The cell body was then vertically lifted from the soil sample sitting on the cell base and the peripheral porous plastic was removed from the sides of the sample. To take clay specimens for moisture content determination, stiff spatulas were used to cut from the periphery to the central drain and remove a wedge shaped portion of the sample. The remaining part of the sample was then wrapped with cling film and stored for photography. Using a knife, two sets of small clay specimens were then taken from the wedge shaped portion. The first set of specimens was taken across the sample at distances of 5, 25, 50, 75 and 100mm from the drain. The second set was taken 52mm from the central drain in every clay layer.

Prior to the photography, the wrapped samples were placed in a freezer for 48 hours. Each sample was then cut vertically by a mechanical band saw with the cut passing through the middle of the drain at the centre of the sample. For the samples with a band drain, the cutting surface was perpendicular to the long side of the drain. After the sample was cut, two pieces of wood were placed on top and under the sample and clamped by two G-clamps so that the sample could be transferred to a table prepared for photography. Before the photography, any clay smearing across more permeable layers due to cutting was scraped away with a knife and a scale readable to 1mm was placed on the sample. The sample photographs were then taken by using a digital camera (Olympus Camedia C-2500L).

a)

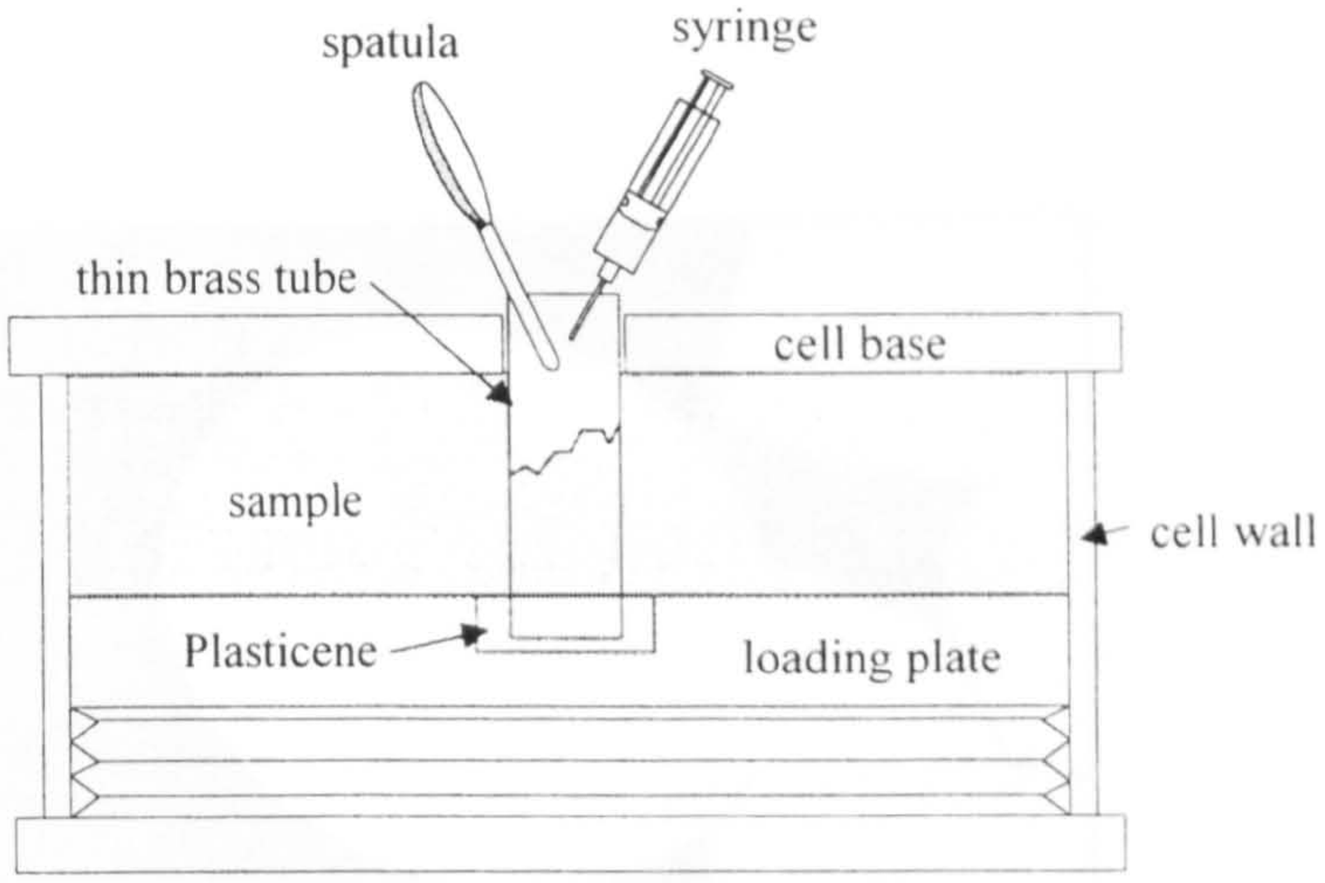

b)

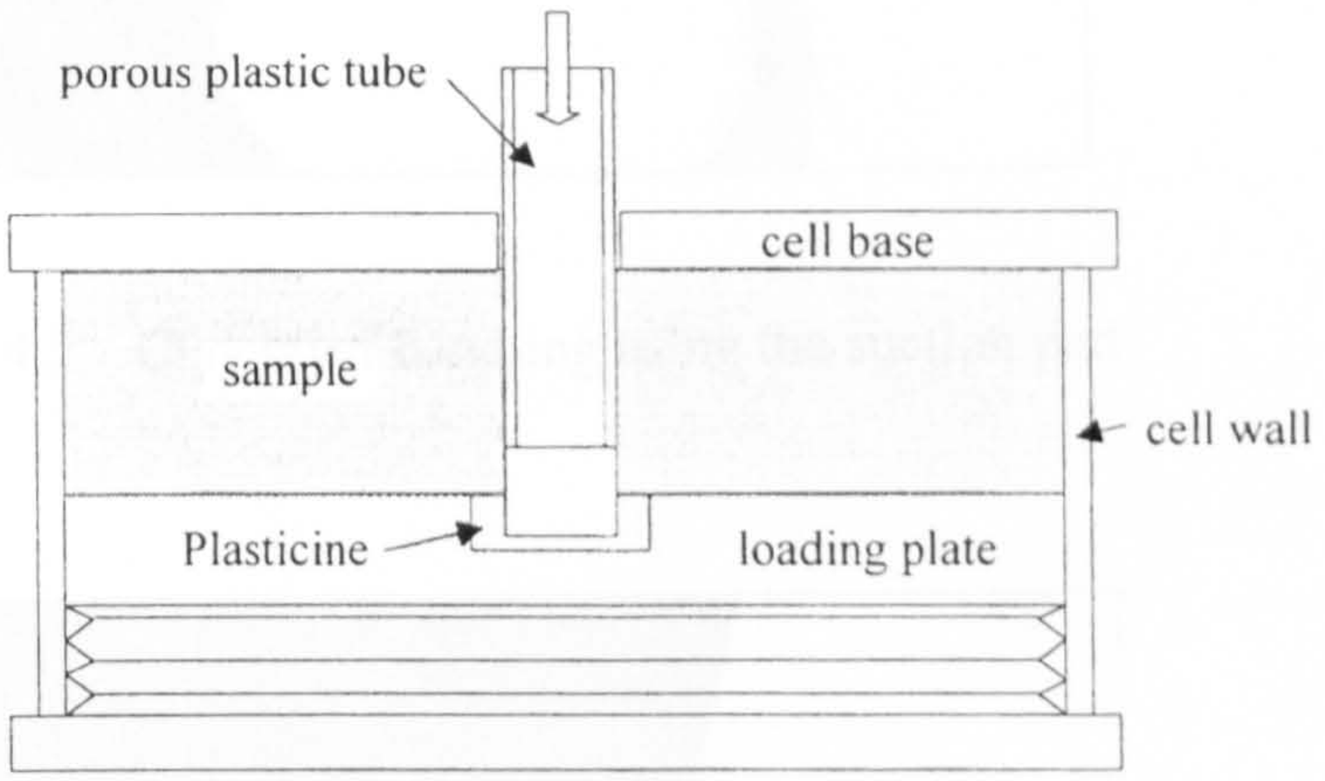

c)

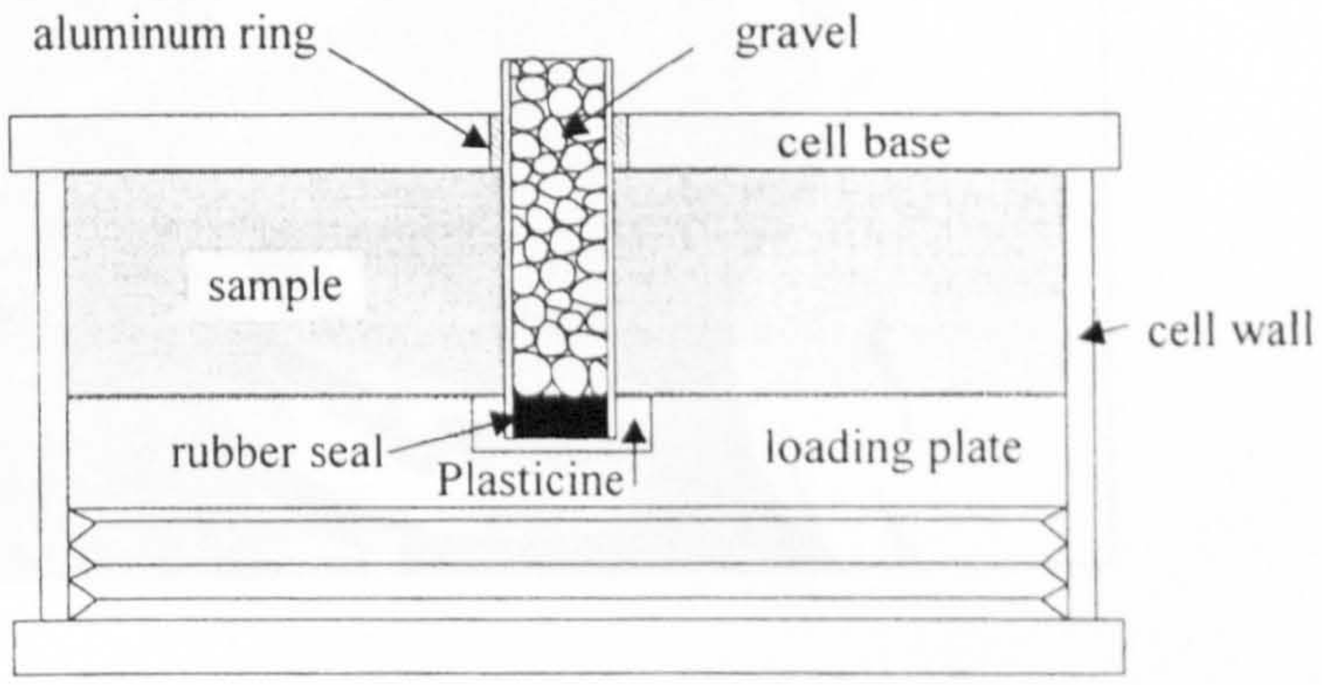

Figure 4.1 Vertical drain installation for horizontal permeability tests on pure sand, pure flint and pure 10 % f-s

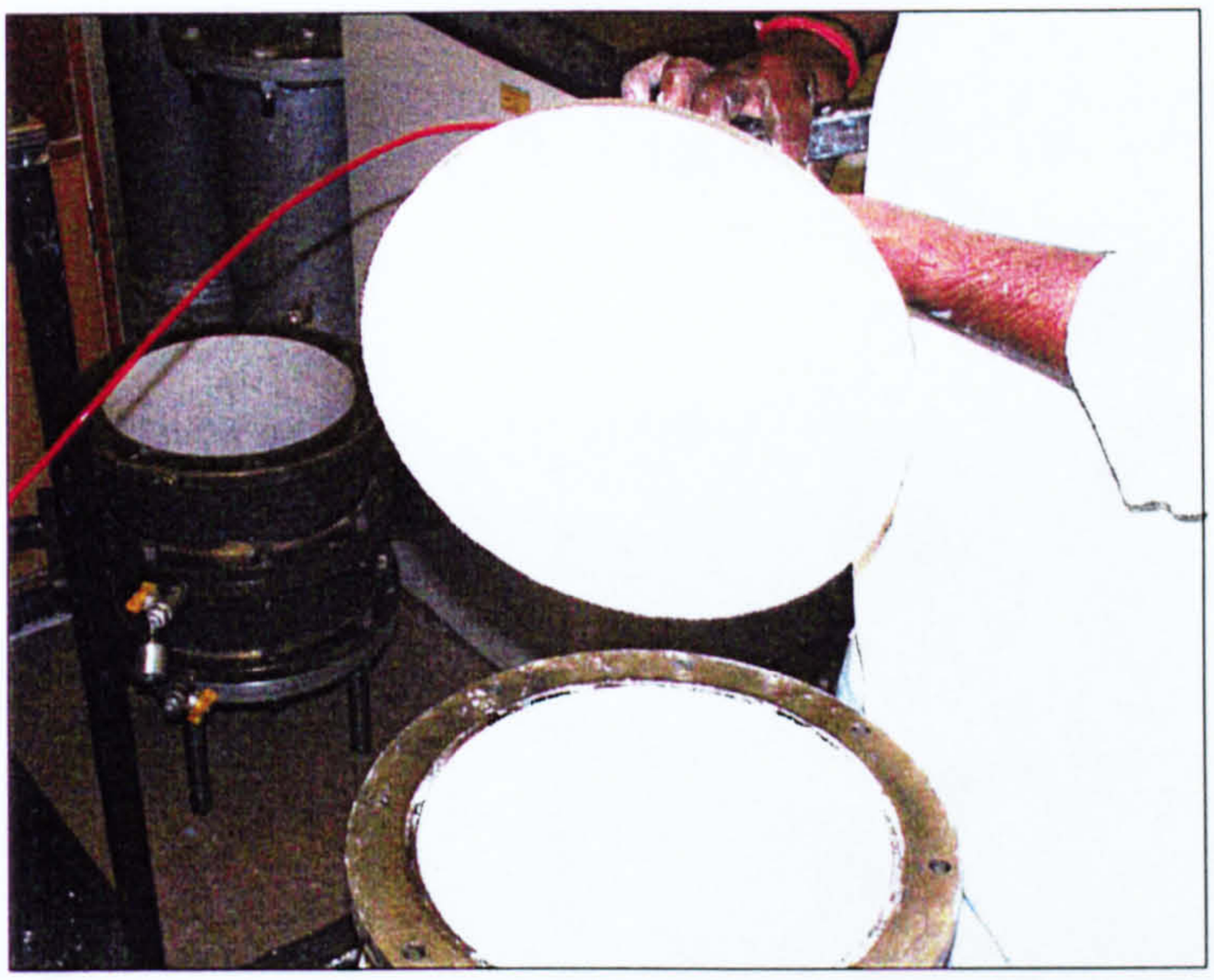

Figure 4.2 Clay layer handling using the suction pad

Figure 4.3 Permeable layer placement into the layered sample test cell

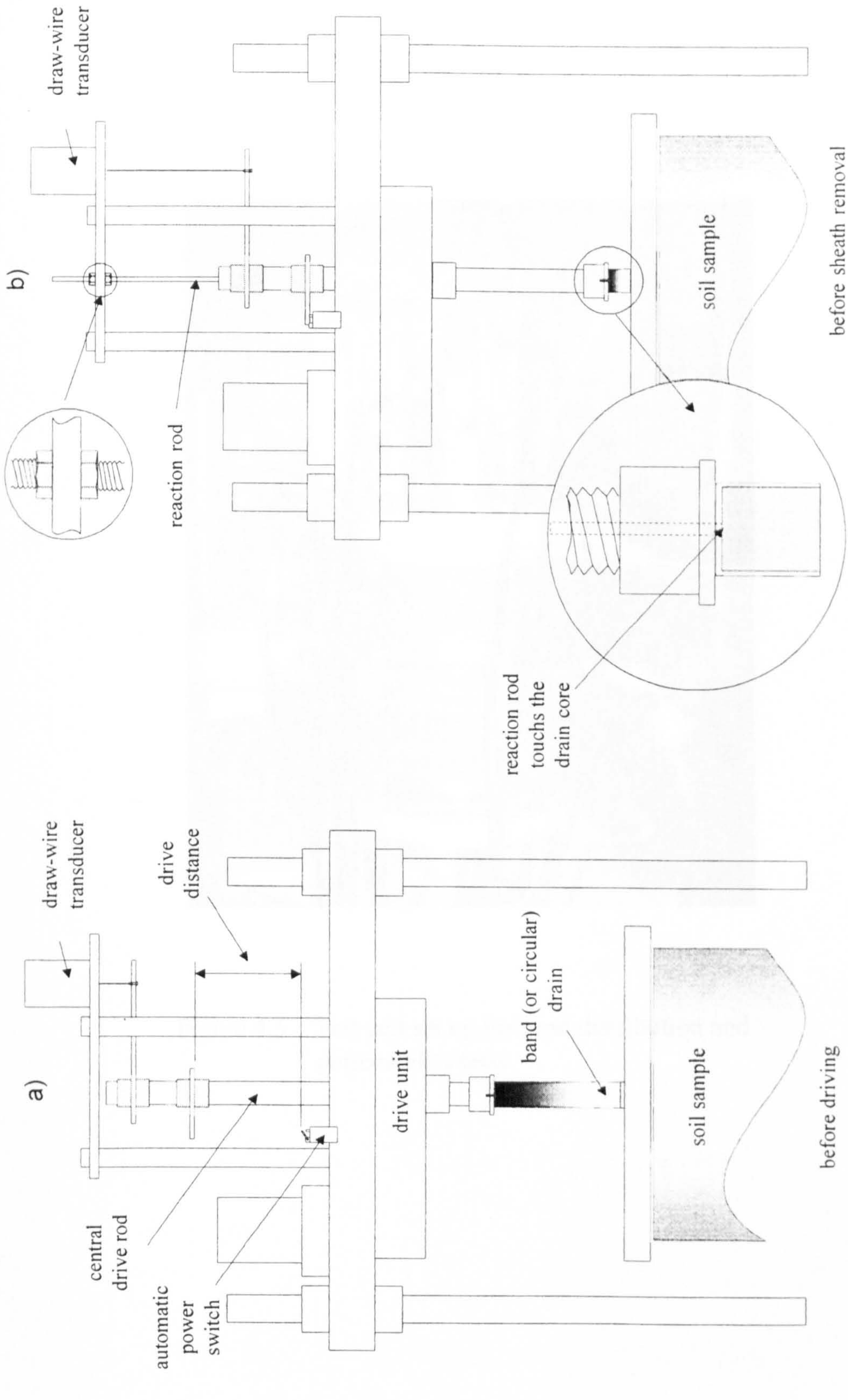

Figure 4.4 Set up of driving system for drain installation and sheath removal

Figure 4.5 Test cell set up for head distribution and permeability tests

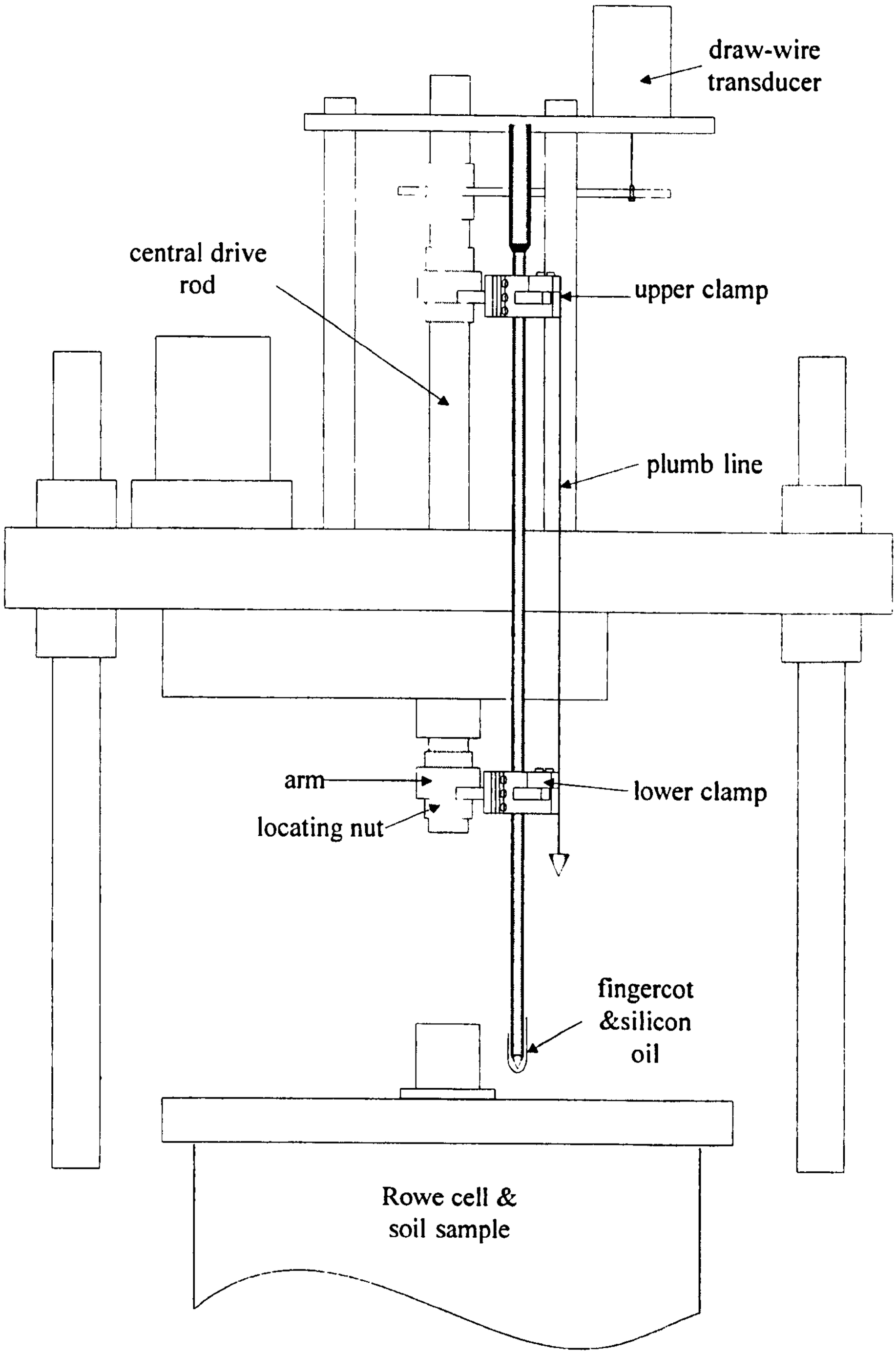

Figure 4.6 Set up of the piezocone prior to driving

CHAPTER 5

EXPERIMENTAL RESULTS AND ANALYSIS

5.1 Introduction

This chapter presents the experimental results gained during the research. Four main groups of test results are presented:

a) the results obtained from consolidation tests during pre-consolidation of the kaolin slurry and during layered sample consolidation,
b) the smear effect investigation results including the results obtained from instrumentation during both constant head distribution tests and permeability tests,
c) the piezocone test results gained during cone driving and during the dissipation tests,
d) the results from sample dissection.

For some classes of result, such as data from slurry consolidation, vertical drain installation and pore water pressure probe installation, only typical data will be presented. Typical test results were taken from Test 7 and Test 8. The main tests (Test 1-10) are summarised in Table 5.1.

5.2 Consolidation Results

5.2.1 Slurry consolidation

Consolidation of kaolin slurry was performed using two different sizes of consolidation cell. 254mm diameter cells were used for clay cake preparation to make layered samples (Section 4.3.2) and 152mm diameter cells were used for the determination of the coefficient of consolidation (Section 4.2.3).

During the consolidation process, the change in height of the sample and the consolidation time were recorded for each loading increment. The void ratio of the soil at each stage was calculated from the final water content and the height of the consolidated kaolin slurry by assuming that the mixed and de-aired slurry was fully saturated. Therefore

$$e_f = w\,G_s \text{ ---------- } (5.1)$$

where e_f = final void ratio of the kaolin,

w = the water content at the end of the test

G_s = the specific gravity of the kaolin particles (assumed to be 2.60, Section 3.2.1)

and

$$\Delta e = \frac{1+e_f}{H_f}\Delta H \text{ ———————— } (5.2)$$

where Δe = change of void ratio between a given test stage and the end of the test

H_f = final sample height

ΔH = change of sample height between a given test stage and the end of the test

Figures 5.1 and 5.2 present typical results of kaolin consolidation performed in 254mm Rowe cells. In Figure 5.3 the void ratio results are compared with the results reported by Eid (1978), Al-Tabbaa (1987) and Moseley (1998). Figure 5.4 presents the void ratio results obtained from slurry consolidation performed in 152mm Rowe cells. It was found that at stresses of more than 50kPa the results of the present research were comparable with those reported by Moseley (1998) and plotted in between those reported by Al-Tabbaa (1987) and Eid (1978). Comparison of Figures 5.3 and 5.4 shows that the average void ratio results from the 254mm Rowe cells were comparable with those from 152mm Rowe cells performing horizontal consolidation. Both void ratio results were slightly lower (at a given stress) than those obtained from 152mm Rowe cells performing only vertical consolidation. This reduction of void ratio is almost certainly due to unloading and reloading to put the additional loading plates into the 254mm Rowe cells (Section 4.3.2) and to install the peripheral drains in the 152mm Rowe cells (Section 4.2.3).

The results gained from the consolidation tests performed in the 152mm Rowe cells were used to determine the vertical coefficient of consolidation, c_v, and the horizontal coefficient of consolidation, c_h, of the kaolin. To determine the coefficient of consolidation, the sample deformation was plotted against the square root of time and the logarithm of time and the traditional graphical methods of Taylor (1942) and Casagrande & Fadum (1940) were applied. The averages of the c_v and c_h values gained from these two graphical methods are summarised in Tables 5.2 (a) and 5.2 (b) (columns 6 and 12).

The permeability of the kaolin was then calculated by using the conventional consolidation theory (Terzaghi, 1943) as follows:

$$k_{vi} = c_v \cdot m_v \cdot \gamma_w \quad \text{----------} \quad (5.3)$$

$$k_{hi} = c_h \cdot m_v \cdot \gamma_w \quad \text{----------} \quad (5.4)$$

where k_{vi} and k_{hi} = vertical and horizontal permeability from indirect measurement respectively

m_v = coefficient of one-dimensional volume compressibility

The results were then compared with permeabilities obtained from empirical relationships (Al-Tabbaa & Wood, 1987) based on direct measurement.

$$k_{vd} = 0.53e^{3.16} \times 10^{-6} \text{ mm/sec} \text{ ---------- (5.5)}$$

$$k_{hd} = 1.49e^{2.03} \times 10^{-6} \text{ mm/sec} \text{ ----------(5.6)}$$

where k_{vd} and k_{hd} = vertical and horizontal permeability based on direct measurement respectively

e = void ratio

Columns 7 and 13 in Tables 5.2(a) and 5.2(b) present the permeabilities calculated by using Equations 5.3 and 5.4 while, columns 9 and 15 in the same tables present the permeabilities estimated by using Equations 5.5 and 5.6. Graphical comparisons are made in Figures 5.5 and 5.6. It can be seen that some of the data obtained during swelling and re-consolidation stages are more scattered than those obtained during virgin compression stages. This could be because, during swelling and re-consolidation stages, changes of sample height were very small and happened in very short time. Therefore, larger errors could have been generated during the manual recording of these data. However, at a given void ratio, the vertical and horizontal permeability results obtained from Rowe cell consolidation were generally within ±25% of the values predicted using empirical method (Al-Tabbaa & Wood, 1987). It was considered that the empirical method gives reasonable accuracy in predicting the permeability of kaolin at a given void ratio.

The horizontal coefficient of consolidation, c_h, obtained from the tests was compared with that obtained from the piezocone tests as described in Section 5.4.2.

5.2.2 Layered sample consolidation

After the layered samples or pure clay samples had been made, they were consolidated to an effective vertical stress of 250kPa in two stages, 100 to 200kPa and 200 to 250kPa (Section 4.3.7). Figure 5.7 presents a typical layered sample consolidation result from one of these stages.

To determine the void ratio of the kaolin in the layered samples, the more permeable layering materials (flint, 10%f-s and sand) were assumed to be incompressible. The thickness of each more permeable layer was determined during the horizontal permeability tests, Section 4.2.4. At an effective stress of 250kPa, the layer thicknesses of the flint, 10%f-s and sand were 2.14mm (e = 0.85), 2.15mm (e = 0.61) and 2.10mm (e = 0.67) respectively. These were the constant values assumed to apply in the layered samples.

The initial void ratio, e_o, of the clay was calculated from the water content determined after slurry consolidation (Section 4.3.2). The initial clay thickness was measured during the layered sample preparation (Section 4.3.6). With knowledge of the subsequent changes in clay layer thickness, the void ratios at different effective stresses were then calculated. Figure 5.8 presents the void ratios of the clay layers in the layered samples plotted against consolidation stress.

For the layered samples with pure sand, it could be assumed that the sand layers acted as perfect drains. However, the difference of the drainage path length of the top and bottom clay layers (approximately 18mm) and the clay layers in between (approximately 9mm) caused some difficulties in determining the coefficient of consolidation. At a given consolidation time, the degrees of consolidation of the clay layers with different drainage path lengths were different. To determine the vertical coefficient of consolidation of the clay, c_v, the following procedure was applied.

a) With a trial c_v value and a given time 't', the time factors, T_{v1} and T_{v2} were calculated for the clay layers with total thicknesses of h_1 (top&bottom layers), and h_2 (other layers) respectively.

b) With the calculated time factors, T_{v1} and T_{v2} the degree of

consolidation of the layers, U_1 and U_2, were calculated.

c) The overall degree of consolidation, $\overline{U}$, was calculated as

$$\overline{U} = \frac{h_1 U_1 + h_2 U_2}{h_1 + h_2}$$

d) The overall degree of consolidation at time t, $\overline{U}$, was then compared with that observed from the testing, U_t.

e) The c_v value was then changed until $\overline{U}$ and U_t agreed.

Table 5.3 summarises the consolidation results for the kaolin in the layered samples.

5.3 Effects of Smear on Vertical Drain Performance

Effects of smear caused by vertical drain installation were investigated by performing constant head distribution tests and permeability tests (Section 4.3.10) on the soil samples with the vertical drain, of either a circular shape or a band shape, installed in the middle.

5.3.1 Results from instrumentation

After consolidation had finished, a mandrel carrying a vertical drain was driven into the layered sample (Section 4.3.8). Figure 5.9 illustrates typical data obtained during the vertical drain installation. In this drive, after the drain (with a volume of 71.6cm^3) had been completely installed and the drainage had stopped, the measured outflow and volume change of sample were 87.3cm^3 and 15.7cm^3 respectively. It can be seen that summation of the volume of the drain and sample volume change due to consolidation after drain installation (71.6+15.7 = 87.3) agreed well with the total outflow.

5.3.2 Zero readings prior to the head distribution test

Before the head distribution test, zero readings of the differential pressure transducers attached to the pore pressure probes (Section 4.3.9) were investigated. Because there was only one pressure source supplying pressure to the probes in the cell and the lines on the other side of the transducers, the differential pressures recorded should have been zero. In practice, it was found that the zero readings of the transducers were affected by the temperature fluctuation (± 0.5 degree) caused by the laboratory air conditioning system. In order to avoid the problem, the test cell was protected from the vigorous air currents by using a cardboard shield every time the head distribution test and the permeability test were performed. Figure 5.10 shows typical zero readings recorded continuously for approximately eight hours before the head distribution test. In this case, the readings of every transducer were within the range of ± 0.5 kPa, which was deemed acceptable. The differential of the pressures at this stage could exist because of surface tension of tiny air bubbles entrapped in the more permeable layers during the sample preparation (Section 4.3.3-4.3.6) or in the filters at the end of the pore pressure probes during the installation processes. The reading taken across the sample (DT1) was always very close to zero because both sides of the transducer were directly connected to only one pressure source (Section 4.3.10) and were not affected by the above factors.

5.3.3 Head distribution test

The head distribution tests (Section 4.3.10) were performed by applying differential water pressure across the soil sample without attempting to measure the flow rate. During the test, as the water flowed from the peripheral drain to the central drain, the responses of the differential pressure transducers at different radii were recorded. All data were plotted against time and then a "window" was taken at a time of approximately 30 minutes when the pressure responses were observed to be most constant. The pressure of each probe was determined by averaging the response of the probe during the snapshot. Figure 5.11 shows a typical snapshot of the pore

water pressure responses recorded during a constant head distribution test.

In considering the pressure distribution across the sample, there were two problems: the initial zero readings of particular transducers before the test and the head loss across the peripheral drain. In order to achieve consistency in the rejection of the data points for analysis, the following schemes were applied.

a) As mentioned in Section 4.3.10, a reading obtained from a differential pressure transducer with a zero reading higher than 0.5kPa or lower than –0.5kPa was ignored.
b) The measured pressure difference across the sample was ignored if it was found that the head loss across the peripheral drain was higher than 0.5kPa.
c) The reading obtained from a pressure probe within 6mm of the drain was ignored because the pressure at this point could have been affected by disturbance of the soil surrounding the drain.

This data rejection scheme was applied to the data from all the constant head distribution tests and also from all the permeability tests (Section 5.3.4).

For the samples with a circular drain, the differential pressures measured at different radii during the head distribution tests were plotted against the natural logarithm of the radius. Then a straight line was drawn through each set of points remaining after the rejection scheme. The differential pressure applied between the central and peripheral drains was determined by extrapolating this straight line to the radial distance at which the peripheral drain was located. The pressure at this distance was then used to normalise the measured differential pressures across the sample.

Figure 5.12 compares the normalised pore water pressure distributions obtained from the constant head tests which were performed on samples with different layering materials. In the figure, the normalised head loss due to smear, h_s, can be determined by extrapolating the straight line drawn through each set of outer points in the unsmeared zone to intercept the normalised pressure axis. The

magnitude of h_s can be used to indicate the effect of smear due to drain installation in each soil sample as discussed in Section 6.2.2.

For a constant head distribution test on a sample with a band drain installed in the middle, the pressure distribution across the unsmeared zone in the outer part of the sample is not linear on the logarithmic radius scale. In order to interpret the pressure distribution in the unsmeared zone, finite element computer modelling using OASYS SEEP (steady state seepage analysis) software was carried out. Because of symmetry, the finite element mesh, based on the work of Ong (1998), was prepared to analyse only one-quarter of the soil sample with the band drain in the middle, Figure 5.13. Due to a limitation of the software in dimensioning very small elements, the size of the soil model and the drain in the computer modelling was hundred times larger than that in the laboratory.

The flow in the computer modelling was simulated by setting the piezometric heads at the central and perimeter drains as 0m and 12.5m respectively. The pore pressure distribution across the model was then normalised by the pressure at the circumference of the model and plotted against the normalised distances obtained by dividing distances from the centre line by the radius of soil model, as shown in Figure 5.14. It should be noted that the effect of smear was not considered in the computer modelling. Fitting the curve shown in Figure 5.14 by using the trend line function in Microsoft Excel 97, provided a polynomial equation as follows.

$$y = -0.8296x^4 + 2.5689x^3 - 3.3407x^2 + 2.6664x - 0.0651 \text{------(5.7)}$$

where x and y are defined in Figure 5.14

Substituting x in the above equation by numbers (distance/r_{sample}) between 0.024 (at the drain side) and 1 provided a suitably transformed distance axis. When plotted against this axis the normalised pore water distribution was linear.

Figure 5.15 shows results gained from the computer modelling performed by Ong (1998) re-plotted against the transformed distance axis. In Ong's simulation, a smear zone with a horizontal permeability reduction factor of 50 was assumed. The width of the smear zone was assumed to be 1.5, 2 or 3 times the half-thickness of the

band drain. From this figure, a linear variation of the pore water pressure distribution outside the smear zone can again be seen.

The transformed axis was then used for plotting the normalised pore water pressure gained from the laboratory tests on samples with a band drain. Figure 5.16 compares the normalised pore water pressure distributions obtained from the head distribution tests which were performed on the samples with different layering materials. It should be noted that the procedures used to reject data and determine the normalising pressure were the same as those used for the tests with a circular drain.

After the data points were selected and plotted, a straight line was drawn through the outer points in the unsmeared zone and extrapolated to intercept the normalised head axis (see Figure 5.16). Then h_s was determined and used in evaluating the effects of smear caused by band drain installation.

5.3.4 Permeability test

a) Measured sample permeability

The procedures used to perform the permeability tests were described in Section 4.3.10. In the layered sample permeability determination, it was assumed that that the proportion of the flow taking place in the clay was negligible. Based on the known permeability ratio, k_r, of layering material (Section 5.3.5), the errors associated with this assumption would not have been more than 0.2%, 0.7% and 11.7% for samples with pure sand, 10%f-s and pure flint layers respectively. The measured horizontal permeability (k_m), including effects of smear, could be obtained from the following equation.

$$k_m = \frac{q \cdot \gamma_w \cdot \mathrm{Ln}(R/r_w)}{2\pi D \cdot \Delta p} \quad \text{---------- (5.8)}$$

where

q = the flow rate across the sample

R = radius of soil sample

r_w = radius of circular drain
or equivalent diameter of band drain

D = thickness of the more permeable layers
(or height of pure clay sample)

Δp = pressure applied across the sample

Using the computer modelling for a band drain mentioned in Section 5.3.3 and Equation 5.8, the equivalent diameter of the band drain was determined with k_m = the assumed permeability of clay, q = the flow rate calculated by OASYS SEEP (ignoring smear) and Δp = pressure difference across the model. The ratio of radius of the soil model (R) to the equivalent radius of the band drain (r_w) was 8.59. This value is slightly less than that of the circular drain (10.72).

As mentioned in Section 4.3.10, head losses in the volume change units produced variations in the pressure across the sample (Δp) with time (e.g. see Figure 5.17). However, during the permeability tests, the inflow and outflow were separately measured by two volume change units and were similar at all times. This implied that no significant consolidation or swelling of the sample occurred during the test and, therefore, pseudo steady state flow existed. As in the analysis of the head distribution data (Section 5.3.3), all the data gained during the permeability tests were plotted against time and then a window was taken when the pressure, Δp, was observed to be most constant. To calculate the permeability, the flow rates from the two volume change units and the pressure across the sample during the snapshot were averaged and substituted into Equation 5.8. Although the flow rate and pressure difference across the sample varied throughout the test, wherever the snapshot was taken the calculated permeability was almost constant, Figure 5.17.

b) Permeability of undisturbed materials based on probe readings

For the tests with a circular drain, with the knowledge of the flow rate and the pore water pressure distribution across the sample at a particular time, the

horizontal permeability (k_h) of the more permeable layers in the layered soil samples (or the permeability of kaolin in a pure clay sample) could be estimated by substituting the gradient, S, of the straight line drawn through the points of the pore water pressure distribution in the unsmeared zone, plotted on a logarithmic radius scale, into Equation 5.9.

$$k_h = \frac{q \cdot \gamma_w}{2 \cdot \pi \cdot D \cdot S} \quad \text{---------- (5.9)}$$

Again, for layered samples it was assumed that the proportion of the flow taking place in the clay was negligible.

The estimated permeability was then compared, Figure 5.18, with the values gained from direct measurement in horizontal permeability tests (Section 4.2.4) and falling head permeability tests (Section 4.2.1). Void ratios of the more permeable layers in the layered sample under 250kPa effective vertical stress were assumed to be equal to the values measured in the horizontal permeability test at the same effective stress.

5.3.5 Smear effect due to drain installation

Two independent parameters calculated to quantify the smear effect were the normalised head loss, h_s, determined from the pore water pressure readings in the head distribution tests (Section 5.3.3) and the reduction of permeability of the sample, r_s.

$$r_s = 1 - \frac{k_m}{k_h} \quad \text{---------- (5.10)}$$

where k_h = estimated material permeability of permeable layers (or pure clay)

To present the effects of smear in the flow tests, relationships between these

two parameters and the permeability ratio of the layering materials are presented in Figures 5.19 and 5.20 for the circular drain and band drain tests respectively. In these figures, the permeability ratio (k_r) is the ratio of estimated horizontal permeability of materials (pure clay, flint, 10%f-s and pure sand) to the estimated horizontal permeability of pure clay. For a pure clay sample the ratio is, of course, unity.

From test 9, the horizontal permeability of pure clay was estimated based on pore pressure probe readings (Section 5.3.4) as 1.91×10^{-9} m/sec. The horizontal permeability of the kaolin in every sample was estimated from the void ratio at an effective vertical stress of 250kPa, Table 5.3, using an empirical relationship (Al-Tabbaa and Wood, 1987). The average horizontal permeability estimated in this way was 1.83×10^{-9} m/sec. In calculating k_r, the average of these two numbers (i.e. average of 1.91×10^{-9} and $1.83 \times 10^{-9} = 1.87 \times 10^{-9}$ m/sec) was used as the horizontal permeability of the kaolin at 250kPa effective stress. Hird & Moseley (1999) reported a value of 1.90×10^{-9} m/sec for the horizontal permeability of the same kaolin under the same stress

Ranges of horizontal permeability of the more permeable layers were estimated by considering results, Figure 5.18, from falling head permeability tests (Section 4.2.1), horizontal permeability tests (Section 4.2.4) and pore pressure probes in layered samples (Section 5.3.4). For flint, 10%f-s and pure sand, the selected horizontal permeability ranges were 1.5×10^{-7} to 2.0×10^{-7} m/sec, 2.5×10^{-6} to 3.0×10^{-6} m/sec and 1.5×10^{-5} to 2.0×10^{-5} m/sec respectively. These ranges led to a range of k_r values being calculated for each layered sample test, as indicated in Figures 5.19 and 5.20. A summary of the test results for the effect of smear is presented in Table 5.4.

5.4 Piezocone Test Results

After the permeability tests had been carried out, a mini-piezocone (Section 3.3.13) was driven into the pure clay or layered samples. A pore pressure dissipation test was then performed with the cone stationary. The details of the piezocone test

procedures were described in Section 4.3.11.

As described in Section 4.3.11, before the piezocone was fully driven into the soil sample, the cone filter, either at the tip or shoulder position, was embedded a distance of 10mm into the sample and a back pressure of 200kPa was applied while the effective stress was kept constant. This procedure was to ensure that the sample was fully saturated before the testing.

5.4.1 Pore water pressure and cone resistance during cone driving

All the pore water pressure and cone load responses during piezocone driving were plotted against driving distance as shown in Figures 5.21 to 5.30. The cone resistances are presented by plotting the cone tip position on the vertical distance scale while the pore water pressure responses are presented by plotting the location of the filter, either at the cone tip or at the cone shoulder (12mm from the tip).

The pore water pressure responses are presented in terms of excess pore water pressure. The datum pressure (u_d) used to calculate excess pore water pressure was the pressure recorded immediately before the piezocone was fully driven into the soil sample.

For the cone resistances, before each test, the datum was taken while the piezocone was outside the sample. It is recommended (ISSMGE, 1999) that, due to the unequal area effect, the pore water pressure measured behind the cone should be used to correct the total cone resistance (Section 2.3.3). In the present research, the piezocone was mainly driven into layered soil samples and the pore pressure behind the cone was measured only in some tests (i.e. when a shoulder filter was used rather than a tip filter). Due to the difficulties of obtaining the proper cone resistance correction, it has been decided that all the cone resistance results gained from the cone driving should be presented in an uncorrected form. The uncorrected cone resistance was obtained by dividing the measured cone resistance force by the projected area of the cone. Nevertheless, in the next chapter (Section 6.3.3), a comparison of the corrected and uncorrected resistance will be made for discussion purposes.

5.4.2 Dissipation Tests

A dissipation test was performed in a clay layer once the cone penetration stopped. The dissipation test results were presented by plotting the normalised excess pore water pressure against the logarithm of time and square root of time. The normalised excess pore pressure, Δu_n, was calculated as.

$$\Delta u_n = \frac{u_t - u_o}{u_{max} - u_o} \text{ ---------- (5.11)}$$

where u_t = measured pore water pressure at time t

u_{max} = maximum measured pore water pressure at the start of the dissipation test

u_o = final measured pore water pressure at equilibrium

In practice, as described by Levadoux & Baligh (1986), the values u_o are normally estimated because allowing for full dissipation of excess pore water pressure can cause significant delays to the test program. Steps to estimate u_o were described by Rust & Clayton (1999). In the present research, the pore water pressure caused by cone penetration could be allowed to dissipate fully and u_o was measured. It should be noted that u_o and the datum pressure (u_d) generally agreed well and fell within approximately $\pm$10kPa of the back pressure.

To determine u_{max}, excess pore water pressures observed from just before the end of driving until dissipation had clearly started were inspected and the maximum excess pore water pressure was identified (Figure 6.7). It was assumed that dissipation started (t = 0) at this point.

Figures 5.31-5.34 show dissipation test results gained with the pore water pressure filter, either at the cone tip position or at the cone shoulder position, in samples with the three different permeable layer materials. Figures 5.35 and 5.36 shows corresponding results from pure clay samples. Values of the horizontal coefficient of consolidation, c_h, were determined from the above plots using

theoretical solutions.

For dissipation test results plotted against the logarithm of time $c_h / \sqrt{I_r}$ values were determined by substituting t_{50} (time for 50% dissipation), T^*_{50} (modified theoretical time factor at 50% dissipation = 0.069 for tip filter and 0.245 for shoulder filter) and the cone shaft radius (r_c) into Equation 2.7.

For the dissipation test results plotted against the square root of time the following equation (Teh, 1987) was applied.

$$\frac{c_h}{\sqrt{I_r}} = (m/M)^2 \cdot r_c^{\,2} \quad \text{---------- (5.12)}$$

where M = initial theoretical gradient of the dissipation curve
= 1.3 for cone with filter at tip
= 1.15 for cone with filter at shoulder
m = measured initial gradient of the dissipation curve

A further method of interpretation was developed in which experimental and theoretical curves plotted using the logarithm of time were compared by a least squares method over a range of the degree of consolidation (U) from 20% to 80%. A Visual Basic based program was developed for this purpose. In the analysis, the following procedures were applied.

a) A trial value of $c_h / \sqrt{I_r}$ was assumed.

b) From the dissipation test data, data points that were uniformly distributed on a logarithmic time scale were selected.

c) T^* was calculated for each selected time using Equation 2.7.

d) For each calculated T^*, the theoretical degree of consolidation, U_i, was determined by interpolation from the dissipation curve, Figure 2.6 (a), proposed by Teh and Houlsby (1991).

e) $(U_i - U_{lab})^2$ was calculated for each selected time where U_{lab} = degree of consolidation at that time from the piezocone test.

f) The values of $(U_i-U_{lab})^2$ for the assumed $c_h / \sqrt{I_r}$ value were summed.

g) $c_h / \sqrt{I_r}$ was varied and steps **a** to **f** were repeated.

h) The value of $c_h / \sqrt{I_r}$ was plotted against $\Sigma(U_i-U_{lab})^2$ and the value selected that gave the lowest value of $\Sigma(U_i-U_{lab})^2$.

A summary of the $c_h / \sqrt{I_r}$ values gained from all three determination methods described above is presented in Table 5.5. If the rigidity index (I_r) is known (or can be estimated), c_h can be determined by multiplying the values of $c_h / \sqrt{I_r}$ in Table 5.5 by $\sqrt{I_r}$.

The c_h value of the kaolin was also determined independently by performing horizontal consolidation tests in a 152mm Rowe cell (Sections 4.2.3). The results are presented in columns 6 and 12 of Table 5.2 (b). The results from these two columns were averaged and plotted on charts on which derived values of c_h (for a range of I_r between 50 and 500) based on the solution proposed by Teh & Houlsby (1991) were also shown. The comparisons were based on the measured times for 50% dissipation (summarised in Table 5.6). Separate charts were drawn for the two filter element positions and also for the pure clay and layered soils, Figures 5.37-5.40. For a given c_h from the Rowe cell tests, the spread of the plotted points (due to differences in t_{50}) during piezocone dissipation tests defines a range of kaolin rigidity index in the piezocone tests. It can be seen that different values of c_h, depending on the consolidation stress history (Section 4.2.3) gave different rigidity index ranges, as further discussion in the next chapter (Section 6.3.2)

5.5 Results from Sample Dissection

After all tests had been performed, the soil samples were dissected for the water content determination and photography (Section 4.3.12)

The water contents of the clay layers (i.e. a single layer from each sample)

were plotted against distance from the side of the central vertical drain as shown in Figures 5.41 and 5.42. By assuming that all the clay was fully saturated and knowing the clay particle density, the void ratios of the clay in the pure clay sample with a circular drain (Test 9) were compared with the test results reported by Onoue et al. (1991) who performed tests on Boston Blue Clay (BBC) and Moseley (1998), Figure 5.43.

Examples of the sample photographs are shown in Figures 5.44 and 5.45. The digital pictures were loaded onto a personal computer and analysed using the UTHSCSA Image Tool for Windows (version 2.0). This software provided tools to measure distance, angle and area in a picture with a known scale.

The geometry of the more permeable layers was measured using the following procedures.

a) Three permeable layers in the middle of the samples were selected as being representative in each layered sample.
b) For each of these layers, the intersection of the vertical centre line of the drain and a horizontal line drawn to pass through the undisturbed part of the layer was determined and used as a reference point.
c) Co-ordinates on the digital photograph were converted to distances based on the known distance of the scale with 1mm divisions in the photograph.
d) Within 5mm from the drain surface, co-ordinates of the more permeable layers were recorded at radial intervals of approximately 2mm. Further away from the drain the records were made at radial intervals of about 4mm.

To compare the permeable layer geometies after penetration with those predicted by the strain path method (Baligh, 1985), co-ordinates of the layers were normalised by the radius of the circular drain or the half-thickness of the band drain. The strain path solutions, provided by Hird (2001) predict the deformation of the soil penetrated by a "simple pile" (axisymmetric or two-dimensional) at a distance behind the tip of approximately three times the pile diameter (axisymmetric) or three times the pile thickness (two-dimensional). The experimental and predicted results are

presented in Figures 5.46-5.47.

Using the computer software, the thicknesses of the more permeable layers were measured on the digital photographs. Distances on the digital photographs were calibrated using a scale on each photograph while the picture was magnified on the computer screen to be about four times larger than the original object. Then the thickness of each layer was measured at six different positions on the straight (virtually undisturbed) portion of the layer while the photograph was magnified to be about twice the size of the original object. The results of layer thicknesses are presented in Figure 5.48.

Test No.	materials	vertical drain	clay layer thickness (mm)	permeable layer thickness (mm)	piezocone test; filter position (type) *see sketch and table below*				
					drive 1	drive 2	drive 3	drive 4	drive 5
1	clay/sand	circular	18.17	2.10	U1(s)	U2	U1(s)	U2	-
2	clay/sand	band	18.79	2.10	U2	U2	U2	U2	-
3	pure clay	band	18.90	-	U2	-	U2	U1(A)	-
4	clay/sand	-	18.84	2.10	U1(A)	U2	U1(A)	U1(A)	U2
5	clay/flint	circular	18.10	2.14	U2	U1(A)	U2	U1(A)	-
6	clay/flint	band	18.49	2.14	U1(B)	U2	U1(C)	U1(C)	-
7	clay/10%f-s	circular	18.77	2.15	U2	U1(D)	U2	U1(D)	-
8	clay/10%f-s	band	18.67	2.15	U2	U1(D)	U1(D)	U1(D)	-
9	pure clay	circular	18.43	-	U2	U1(D)	U1(D)	U1(D)	-
10	clay/flint	band	18.64	2.14	U2	U1(D)	U1(D)	U1(D)	-

Note: Piezocone access holes are shown in Figure 3.2. However, the holes were not used in any particular order.

Exceptionally Drive 1 of Test 4 was done in the centre of the sample which had no central drain.

Sintered glass tip filter	bead size	increase temp (c°/min)	Dwelling time at 680°c(min)	decrease temp (c°/min)	remarks
A	45-90μm	2	60	1	
B	45-90μm	2	10	1	very brittle, difficult to machine
C	45-90μm	2	30	1	very hard, difficult to machine
D	45-90μm	2	20	1	

S = sintered steel tip supplied by Fugro

filter position

U1 tip filter

U2 shoulder filter

Table 5.1 Test summary

(a)

σ' (kPa)	σ' (kPa)	stage	vertical consolidation											
			cell1						cell2					
			e	m_v (m^2/kN)	C_v (m^2/sec)	k (m/sec)	average e	k Al-Tabbaa	e	m_v (m^2/kN)	C_v (m^2/sec)	k (m/sec)	average e	k Al-Tabbaa
50-100	100	virgin c	1 493	1 20E-03	1 48E-07	1.73E-09	1 572	2.22E-09	1 505	1 28E-03	1 67E-07	2 10E-09	1 591	2 30E-09
100-200	200	virgin c	1 332	6.46E-04	2 57E-07	1.63E-09	1 412	1.58E-09	1 348	6 29E-04	2.66E-07	1 64E-09	1 427	1 63E-09
200-400	400	virgin c	1.181	3.23E-04	4 16E-07	1.32E-09	1 256	1 09E-09	1 197	3 20E-04	3 51E-07	1 10E-09	1 273	1 14E-09
400-200	200	swell	1 202	4.70E-05	2.97E-06	1.37E-09	1.191	9 22E-10	1.221	5.38E-05	2 22E-06	1 17E-09	1.209	9 66E-10
200-100	100	swell	1 227	1.17E-04	9 34E-07	1.07E-09	1 214	9 79E-10	1.251	1 36E-04	9 05E-07	1.21E-09	1 236	1 04E-09
column 1	**2**	**3**	**4**	**5**	**6**	**7**	**8**	**9**	**10**	**11**	**12**	**13**	**14**	**15**

(b)

σ' (kPa)	σ' (kPa)	stage	horizontal consolidation											
			cell1						cell2					
			e	m_v (m^2/kN)	C_h (m^2/sec)	k (m/sec)	average e	k Al-Tabbaa	e	m_v (m^2/kN)	C_h (m^2/sec)	k (m/sec)	average e	k Al-Tabbaa
50-100	100	virgin c	1 446	6 16E-04	6 01E-07	3 63E-09	1 485	3 33E-09	1 429	6 24E-04	4.63E-07	2 84E-09	1 468	3 25E-09
100-200	200	virgin c	1.305	5 79E-04	5 64E-07	3 20E-09	1.375	2 85E-09	1 289	5 78E-04	6 02E-07	3 41E-09	1 359	2 78E-09
200-400	400	virgin c	1 148	3 39E-04	8 39E-07	2.79E-09	1 226	2 26E-09	1 136	3 34E-04	8.22E-07	2 69E-09	1 212	2 20E-09
400-200	200	swell 1	1 178	6 93E-05	3 25E-06	2.21E-09	1 163	2 03E-09	1 173	8 73E-05	2 77E-06	2 37E-09	1 155	1 99E-09
200-100	100	swell 2	1 199	9 77E-05	1 51E-06	1 44E-09	1 189	2.12E-09	1 191	8 00E-05	1 29E-06	1 01E-09	1 182	2 09E-09
100-200	200	recom 1	1.196	1 45E-05			1.198	2 15E-09	1 176	6 81E-05			1 183	2 10E-09
200-400	400	recom 2	1 137	1.36E-04	2 31E-06	3 07E-09	1 166	2 04E-09	1 123	1 20E-04	2.19E-06	2 58E-09	1.150	1 98E-09
400-200	200	swell 3	1 159	5 23E-05	3.12E-06	1.60E-09	1.148	1 97E-09	1 150	6 14E-05	2.06E-06	1 24E-09	1 136	1 93E-09
200-100	100	swell 4	1 188	1 33E-04	1.40E-06	1 83E-09	1 173	2 06E-09	1 178	1 33E-04	1.12E-06	1 47E-09	1 164	2 03E-09
100-200	200	recom 3	1.165	1.02E-04			1.176	2 07E-09	1 162	7 42E-05			1 170	2 05E-09
200-400	400	recom 4	1 125	9.34E-05	2.47E-06	2 26E-09	1 145	1 96E-09	1 107	1 26E-04	2 33E-06	2 89E-09	1.135	1 93E-09
400-200	200	swell 5	1 149	5 76E-05	3.44E-06	1.94E-09	1.137	1 93E-09	1.138	7 37E-05	2 58E-06	1 86E-09	1 123	1 89E-09
200-100	100	swell 6	1 176	1 24E-04	1.38E-06	1 68E-09	1 163	2 02E-09	1 164	1 22E-04	1.21E-06	1 45E-09	1 151	1 98E-09
column 1	**2**	**3**	**4**	**5**	**6**	**7**	**8**	**9**	**10**	**11**	**12**	**13**	**14**	**15**

Table 5.2 Summary of (a) vertical consolidation and (b) horizontal consolidation (b) test results and comparisons with Al-Tabbaa & Wood (1987)

Test No	consolidation pressure (kPa)	e	m_v (m^2/kN)	k_h (m/sec) (Al-Tabbaa & Wood, 1987)	c_v (cm^2/sec)	
					t_{50}	t_{90}
1	100	1.156		2.00E-09		
	100-200	1.100	2.60E-04	1.81E-09	2.80E-03	2.85E-03
	200-250	1.074	2.51E-04	1 72E-09	1.10E-03	1.30E-03
2	100	1.178		2.08E-09		
	100-200	1.137	1.85E-04	1.94E-09	2.87E-03	2.39E-03
	200-250	1.116	2.04E-04	1.86E-09	1.94E-03	1.47E-03
3	100	1.272		2.43E-09		
	100-200	1.196	3.33E-04	2.14E-09		
	200-250	1.161	3.23E-04	2.02E-09		
4	100	1.211		2.20E-09		
	100-200	1.145	3.01E-04	1.96E-09		
	200-250	1.121	2.24E-04	1.88E-09		
5	100	1.156		2.00E-09		
	100-200	1.083	3.35E-04	1.75E-09		
	200-250	1.056	2.59E-04	1.67E-09		
6	100	1.172		2.06E-09		
	100-200	1.109	2.93E-04	1.84E-09		
	200-250	1.075	3.15E-04	1.73E-09		
7	100	1.204		2.17E-09		
	100-200	1.147	2.57E-04	1.97E-09		
	200-250	1.123	2.28E-04	1.89E-09		
8	100	1.194		2.14E-09		
	100-200	1.135	2.69E-04	1.93E-09		
	200-250	1.109	2.49E-04	1.84E-09		
9	100	1.202		2.17E-09		
	100-200	1.127	3.43E-04	1.90E-09		
	200-250	1.099	2.57E-04	1.81E-09		
10	100	1.203		2.17E-09		
	100-200	1.137	2.98E-04	1.93E-09		
	200-250	1.113	2.27E-04	1.85E-09		

Table 5.3 Summary of layered sample consolidation results

Test	Drain type	Estimated permeability of more permeable layers (k_t)		Permeability ratio (k_r)		Measured permeability (m/sec)	Permeability reduction (r_s)			head loss due to smear (h_s)
		minimum (m/sec)	maximum (m/sec)	minimum	maximum		minimum	maximum	average	
1	circular	1.50E-05	2.00E-05	8021.39	10695.19	1.47E-06	0.902	0.927	0.915	0.950
2	band	1.50E-05	2.00E-05	8021.39	10695.19	7.97E-06	0.469	0.602	0.535	0.561
3	band	1.87E-09	1.87E-09	1.00	1.00	1.67E-09	0.109	0.109	0.109	0.197
4	-	1.50E-05	2.00E-05	8021.39	10695.19	-	-	-	-	-
5	circular	1.50E-07	2.00E-07	80.21	106.95	8.82E-08	0.412	0.559	0.485	0.220
6	band	1.50E-07	2.00E-07	80.21	106.95	1.30E-07	0.136	0.352	0.244	0.166
7	circular	2.50E-06	3.00E-06	1336.90	1604.28	4.31E-07	0.828	0.856	0.842	0.610
8	band	2.50E-06	3.00E-06	1336.90	1604.28	1.90E-06	0.241	0.367	0.304	0.367
9	circular	1.87E-09	1.87E-09	1.00	1.00	1.16E-09	0.379	0.379	0.379	0.340
10	band	1.50E-07	2.00E-07	80.21	106.95	1.24E-07	0.174	0.380	0.277	0.310

Table 5.4 Summary of smear effects due to vertical drain installation

sample	Tip filter				Shoulder filter			
	test No.	$c_h/\sqrt{I_r}$ (cm^2/sec)			test No.	$c_h/\sqrt{I_r}$ (cm^2/sec)		
		Eq 2.7	Eq 5.12	least sq		Eq 2.7	Eq 5.12	least sq
pure sand	test4 drive1	2.87E-03	7.24E-03	2.79E-03	test1 drive2	8 63E-03	6.16E-03	8 14E-03
	test4 drive3	2.97E-03	7.24E-03	3.18E-03	test1 drive3	7.32E-03	6.07E-03	8 00E-03
					test2 drive1	5.55E-03	4.91E-03	6 38E-03
					test2 drive2	5.55E-03	5.13E-03	6.46E-03
					test2 drive3	5.99E-03	5 22E-03	6 75E-03
					test2 drive4	6.02E-03	5.70E-03	6.47E-03
					test4 drive2	7.41E-03	7.50E-03	7 87E-03
10% flint	test7 drive2	3.42E-03	6.22E-03	3 27E-03	test7 drive3	5 35E-03	5 09E-03	5 29E-03
	test7 drive4	3.91E-03	8 90E-03	3 39E-03	test8 drive1	5.01E-03	5.00E-03	5.04E-03
	test8 drive4	3.45E-03	-	3.55E-03				
pure flint	test5 drive2	3.01E-03	6 94E-03	3.18E-03	test5 drive1	5.70E-03	5.28E-03	6 45E-03
	test5 drive4	2.93E-03	5.23E-03	2.81E-03	test5 drive3	3.88E-03	3.22E-03	4.19E-03
	test6 drive1	2.37E-03	5.60E-03	2 39E-03	test6 drive2	4.92E-03	4 35E-03	4.78E-03
					test10 drive3	5.33E-03	-	-
pure clay	test3 drive4	3.99E-03	-	3.47E-03	test3 drive1	1 81E-03	1.82E-03	1 85E-03
	test9 drive3	2 31E-03	-	1 76E-03	test3 drive3	3.30E-03	2.84E-03	3 60E-03
	test9 drive4	1.69E-03	-	1 60E-03	test9 drive1	1.95E-03	2.21E-03	2 08E-03

Table 5.5 Summary of $c_h/\sqrt{I_r}$ from piezocone dissipation tests

sample	Tip filter		Shoulder filter	
	test No.	t_{50} (sec)	test No.	t_{50} (sec)
pure sand	test4 drive1	7.63	test1 drive2	9.03
	test4 drive3	7.40	test1 drive3	10.65
			test2 drive1	14.06
			test2 drive2	14 04
			test2 drive3	13.02
			test2 drive4	12.94
			test4 drive2	10.52
10% flint	test7 drive2	6.43	test7 drive3	14.57
	test7 drive4	5.62	test8 drive1	15.57
	test8 drive4	6.37		
pure flint	test5 drive2	7.29	test5 drive1	13.67
	test5 drive4	7.50	test5 drive3	20.10
	test6 drive1	9.23	test6 drive2	15.86
			test10 drive3	14.63
pure clay	test3 drive4	5.50	test3 drive1	43.15
	test9 drive3	9.50	test3 drive3	23.60
	test9 drive4	12.96	test9 drive1	39.97

Table 5.6 Summary of t_{50} obtained from piezocone dissipation test

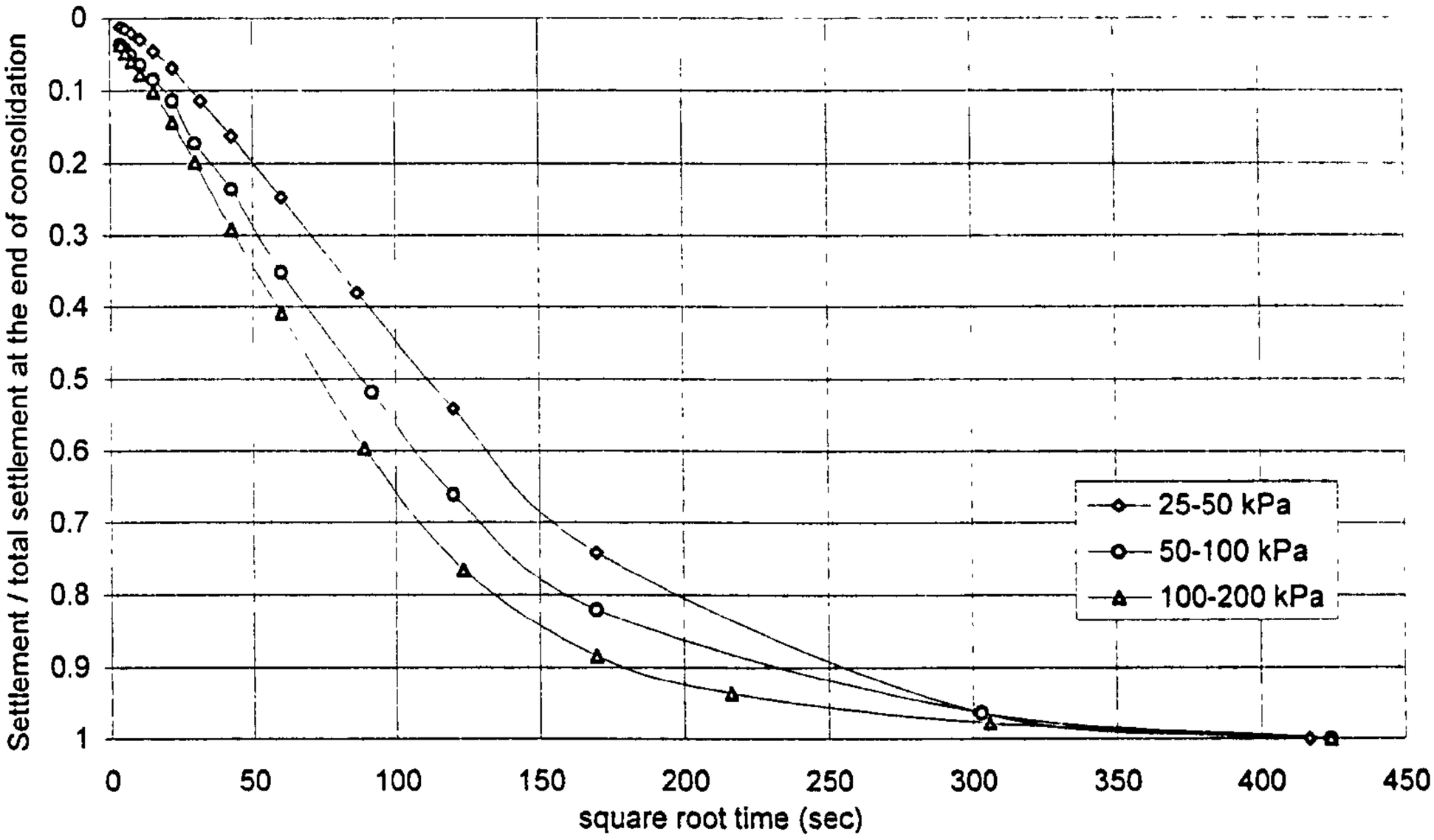

Figure 5.1 Typical slurry consolidation results from 254mm Rowe cell (Test7)

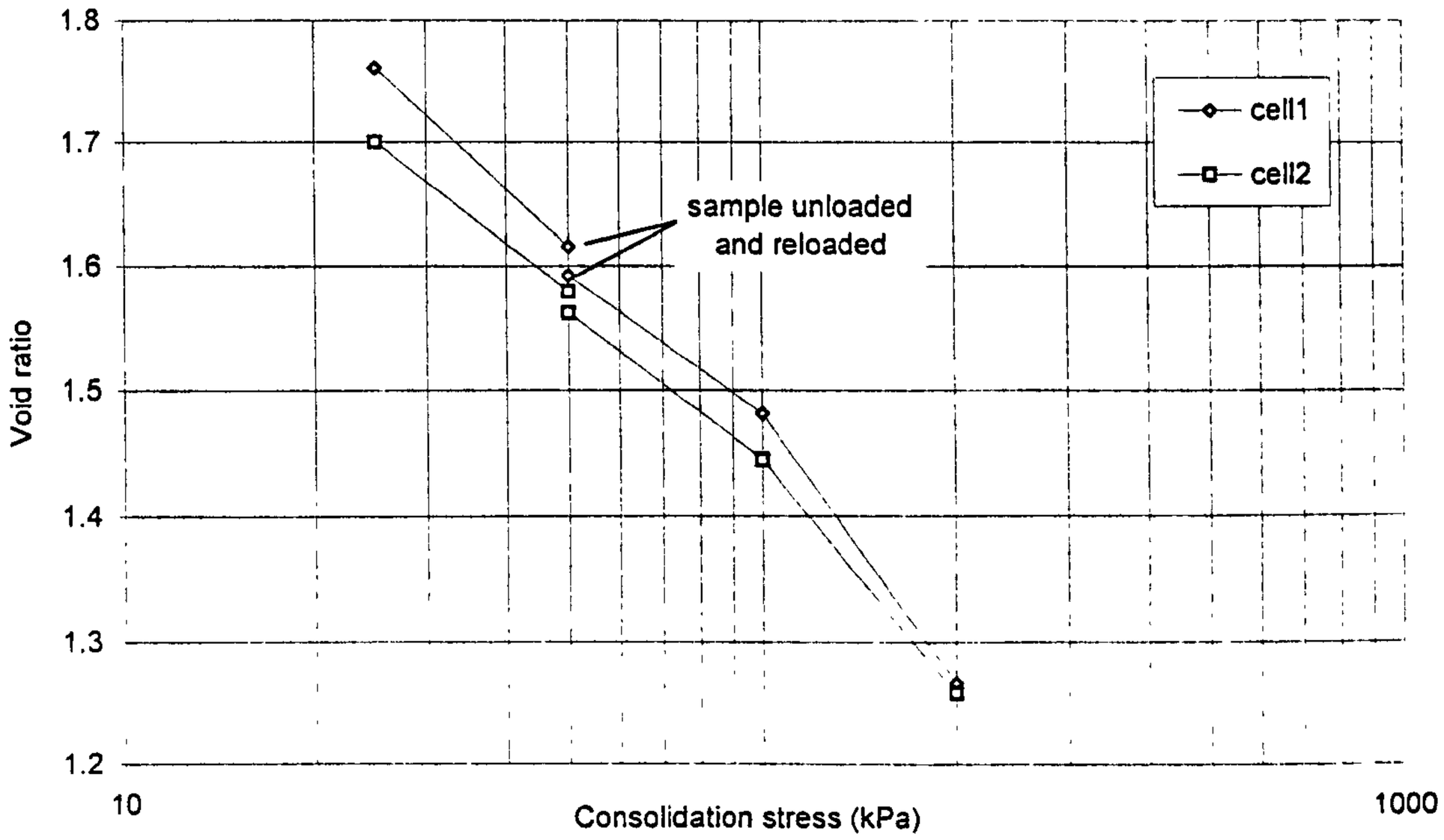

Figure 5.2 Typical void ratio against consolidation stress in slurry consolidation from 254mm Rowe cells (Test 7)

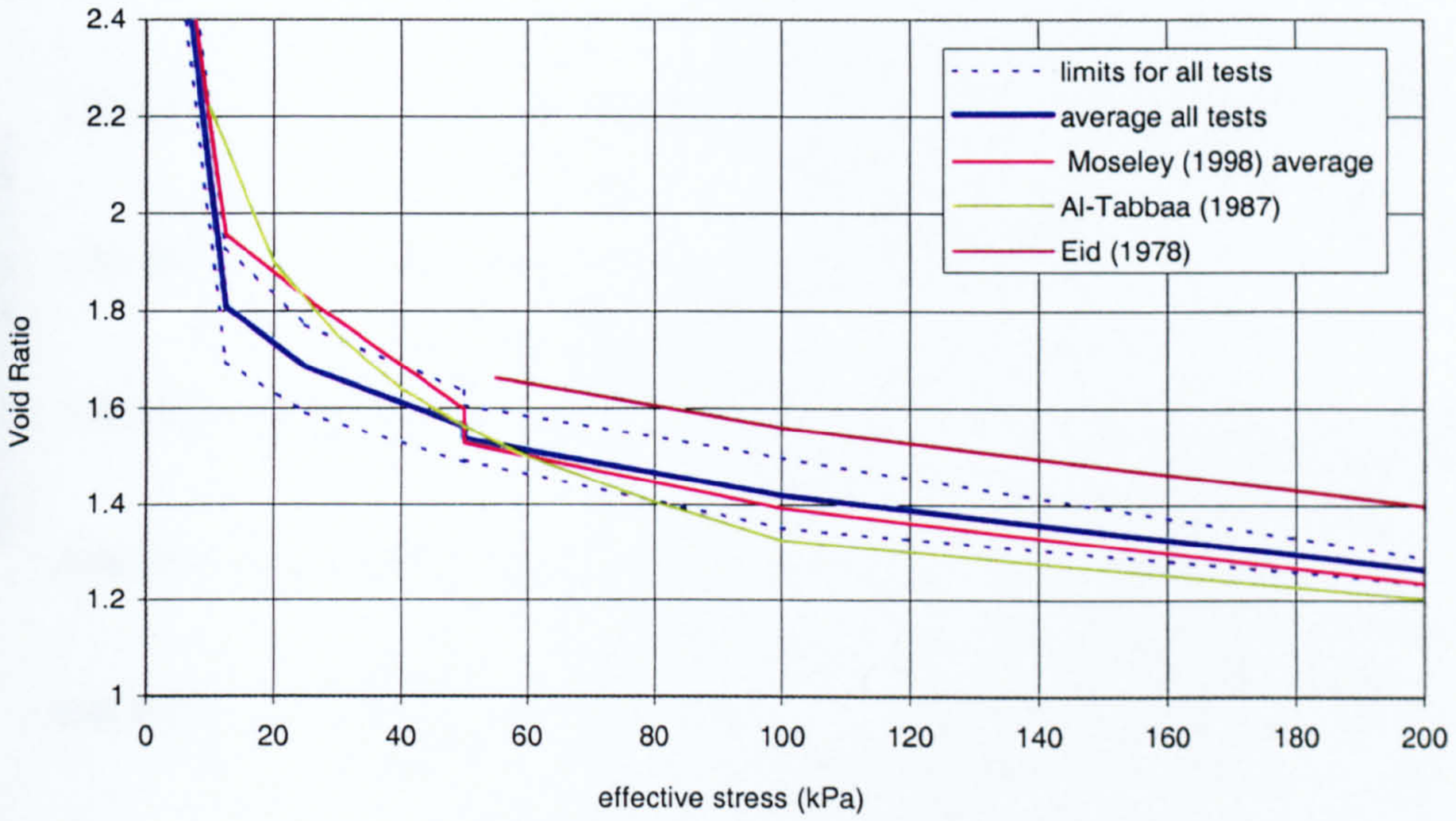

Figure 5.3 Slurry consolidation void ratio against consolidation stress (254mm cells) comparison with Moseley (1998), Al-Tabbaa(1987) and Eid (1978)

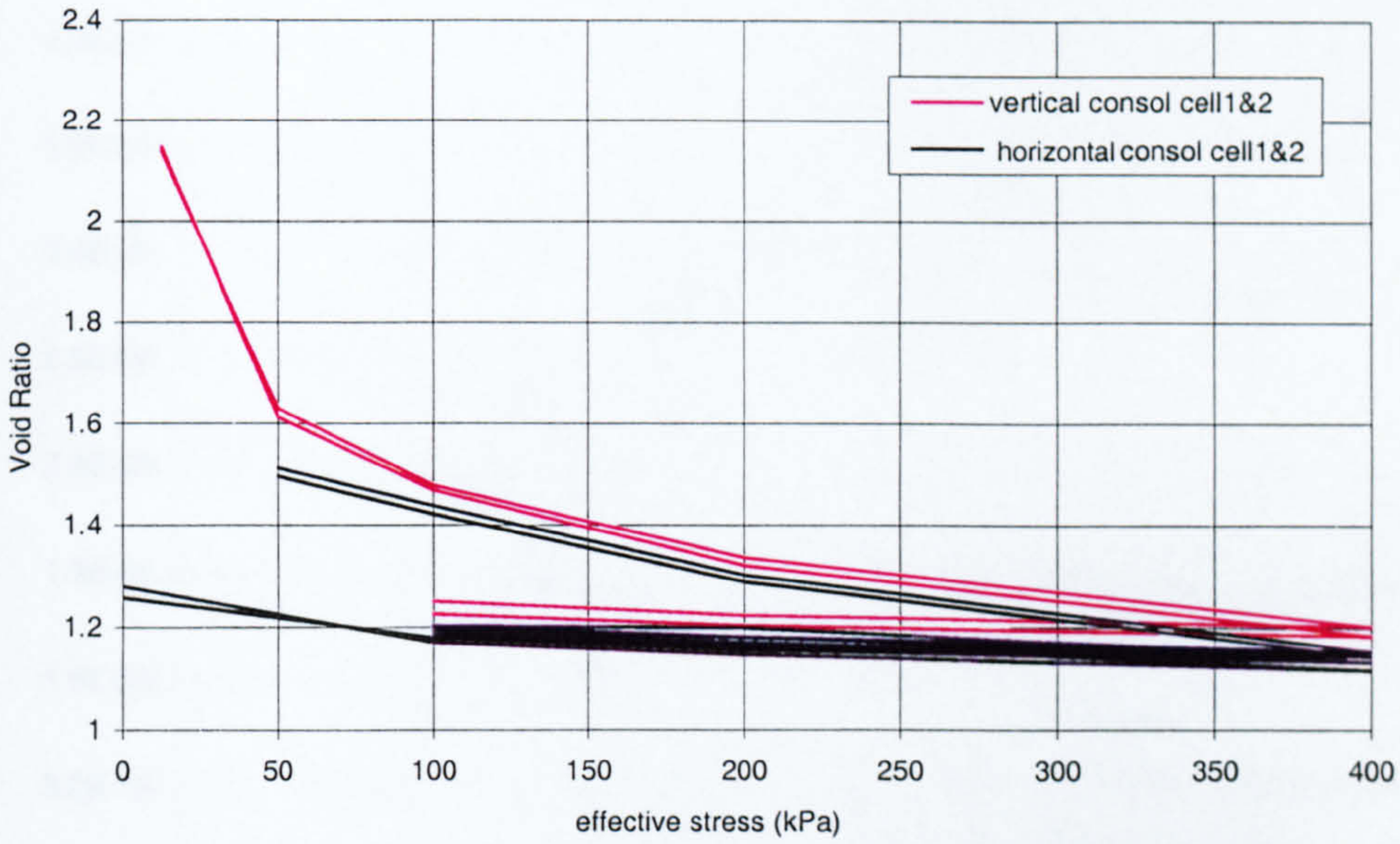

Figure 5.4 Slurry consolidation void ratio against consolidation stress (152mm cells) for kaolin

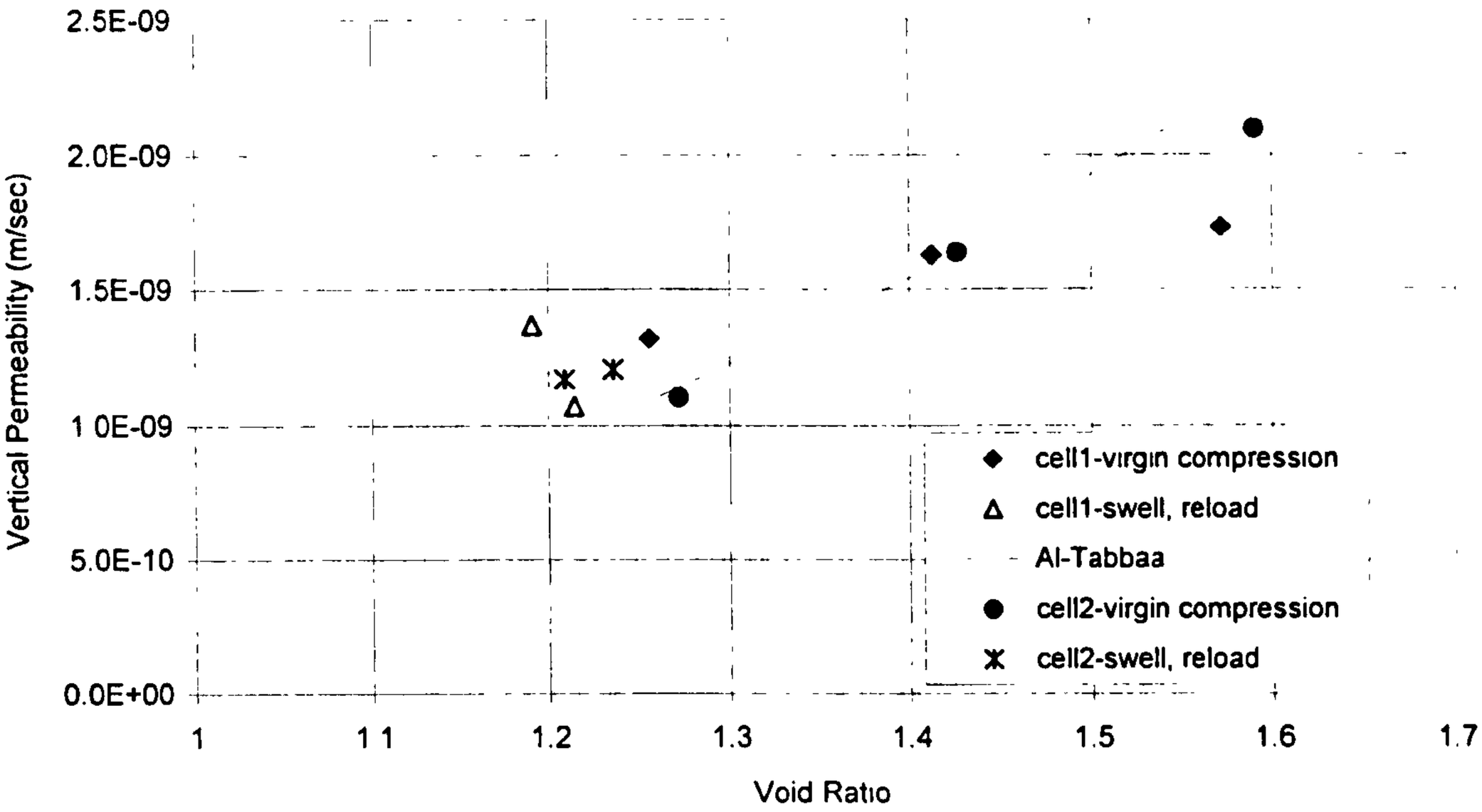

Figure 5.5 Comparison of kaolin vertical permeability gained from indirect measurement (Rowe cell consolidation) and empirical relationship (Al-Tabbaa&Wood, 1987)

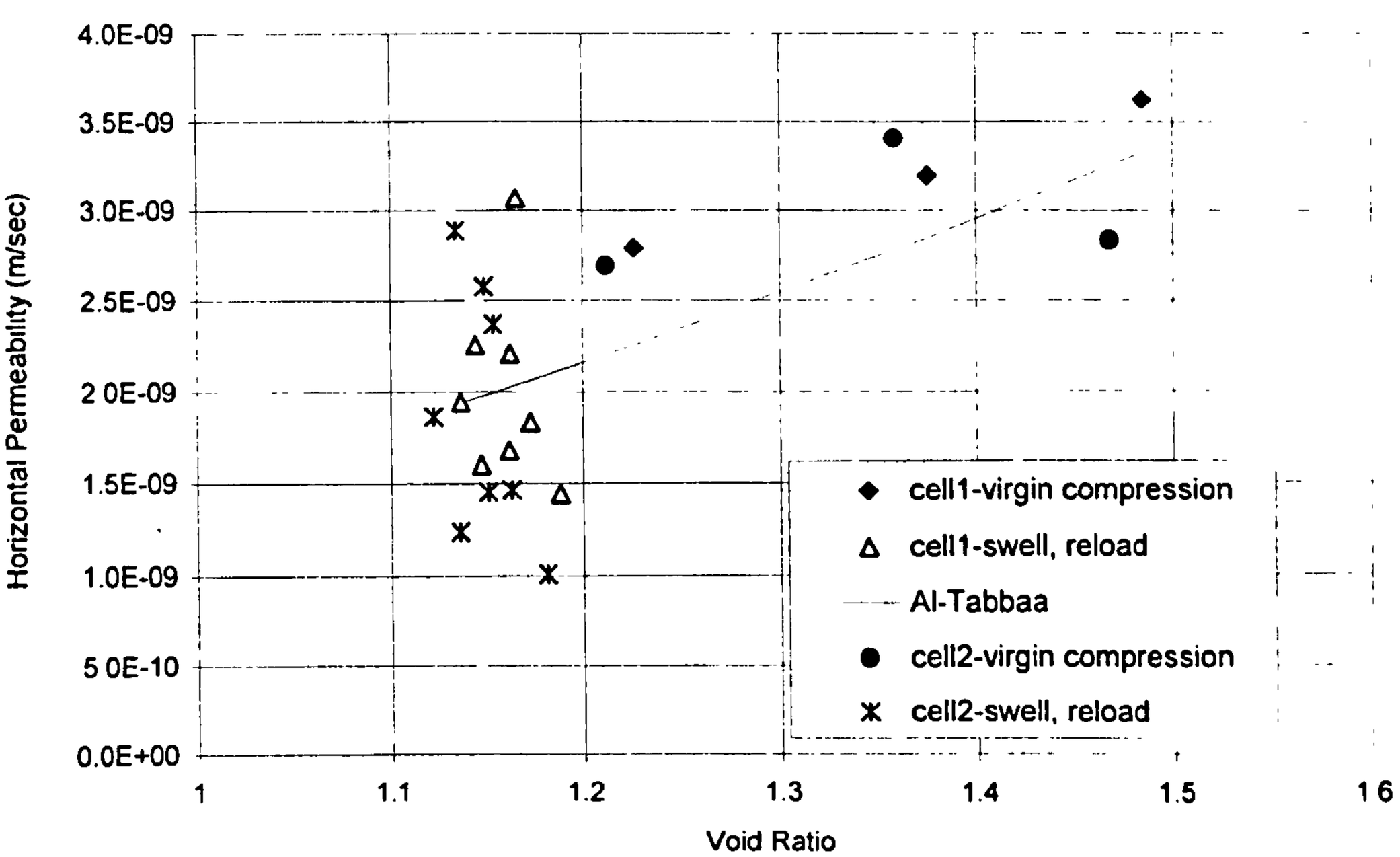

Figure 5.6 Comparison of kaolin horizontal permeability gained from indirect measurement (Rowe cell consolidation) and empirical relationship (Al-Tabbaa&Wood, 1987)

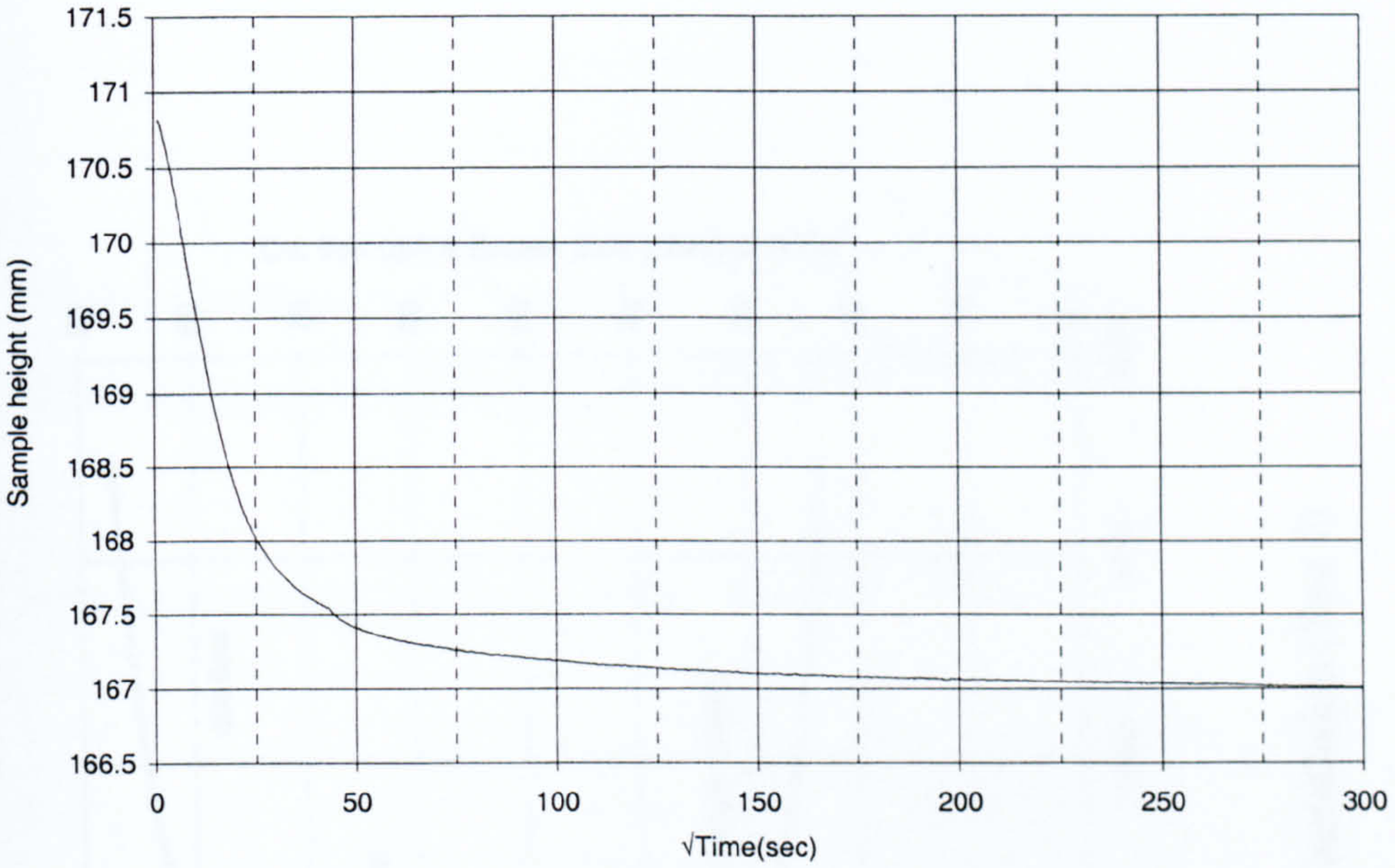

Figure 5.7 Typical layered sample consolidation result (Test 7)

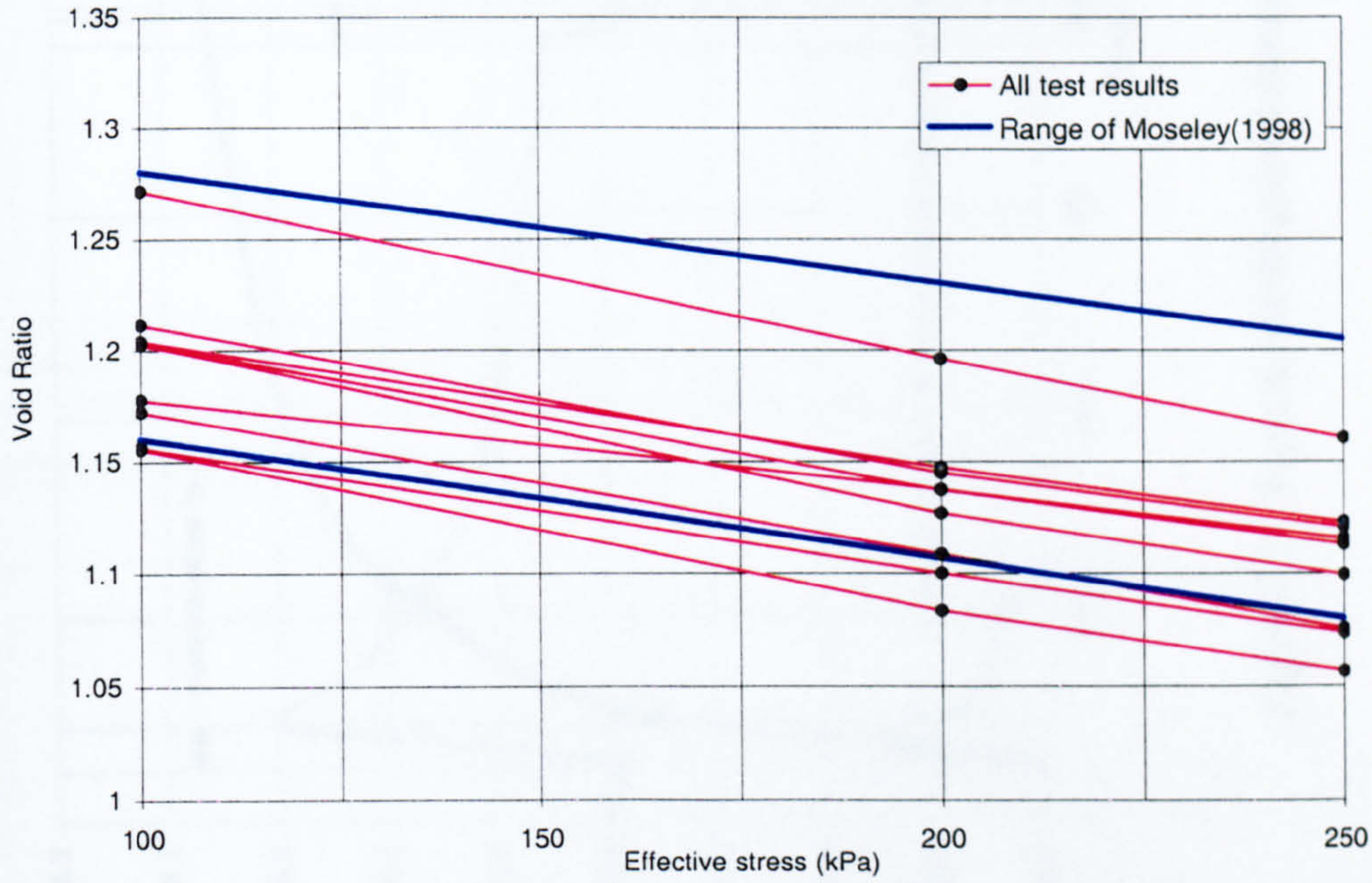

Figure 5.8 Void ratio of kaolin in layered samples against consolidation stress and comparison with Moseley (1998)

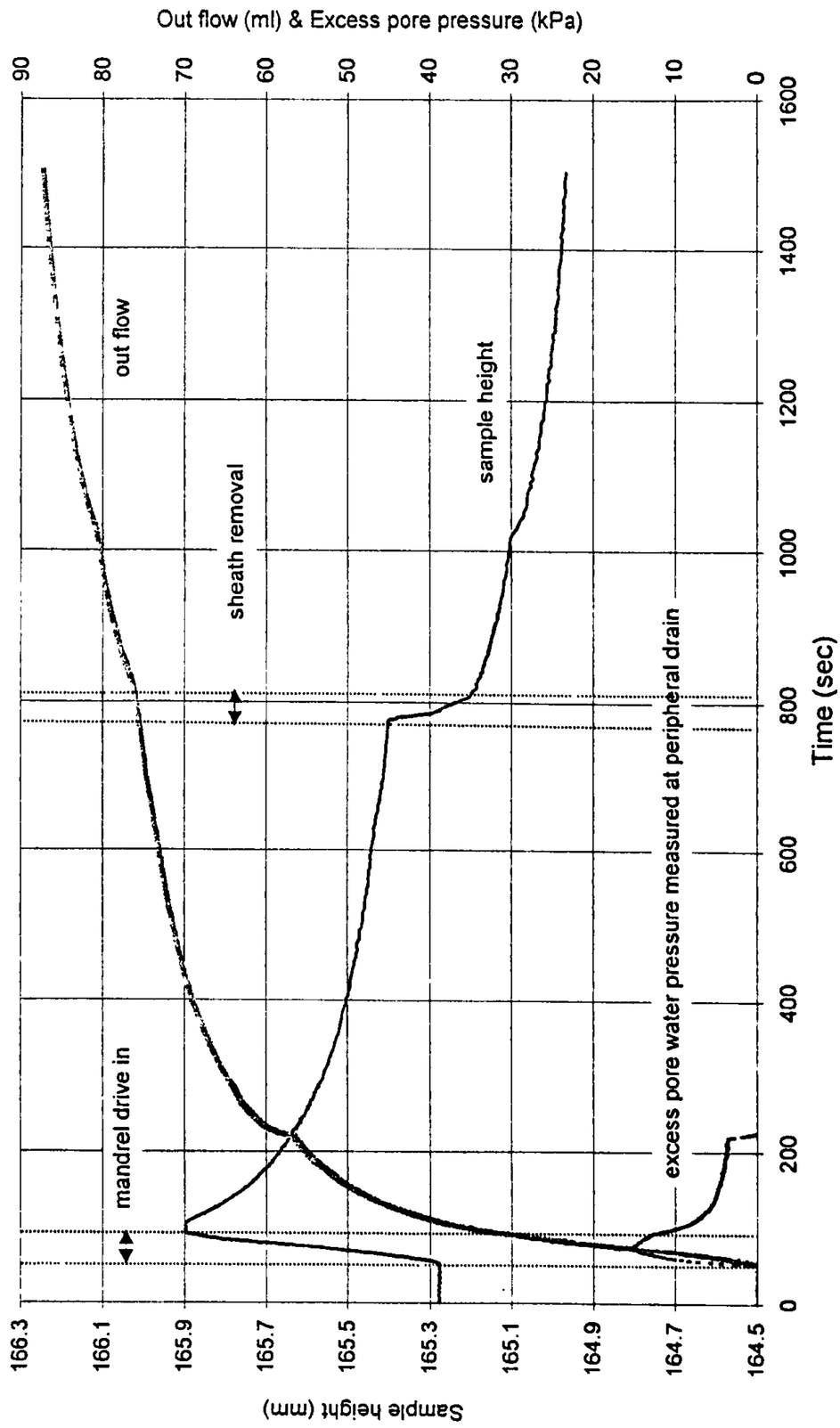

Figure 5.9 Typical results gained during vertical drain installation (Test 7)

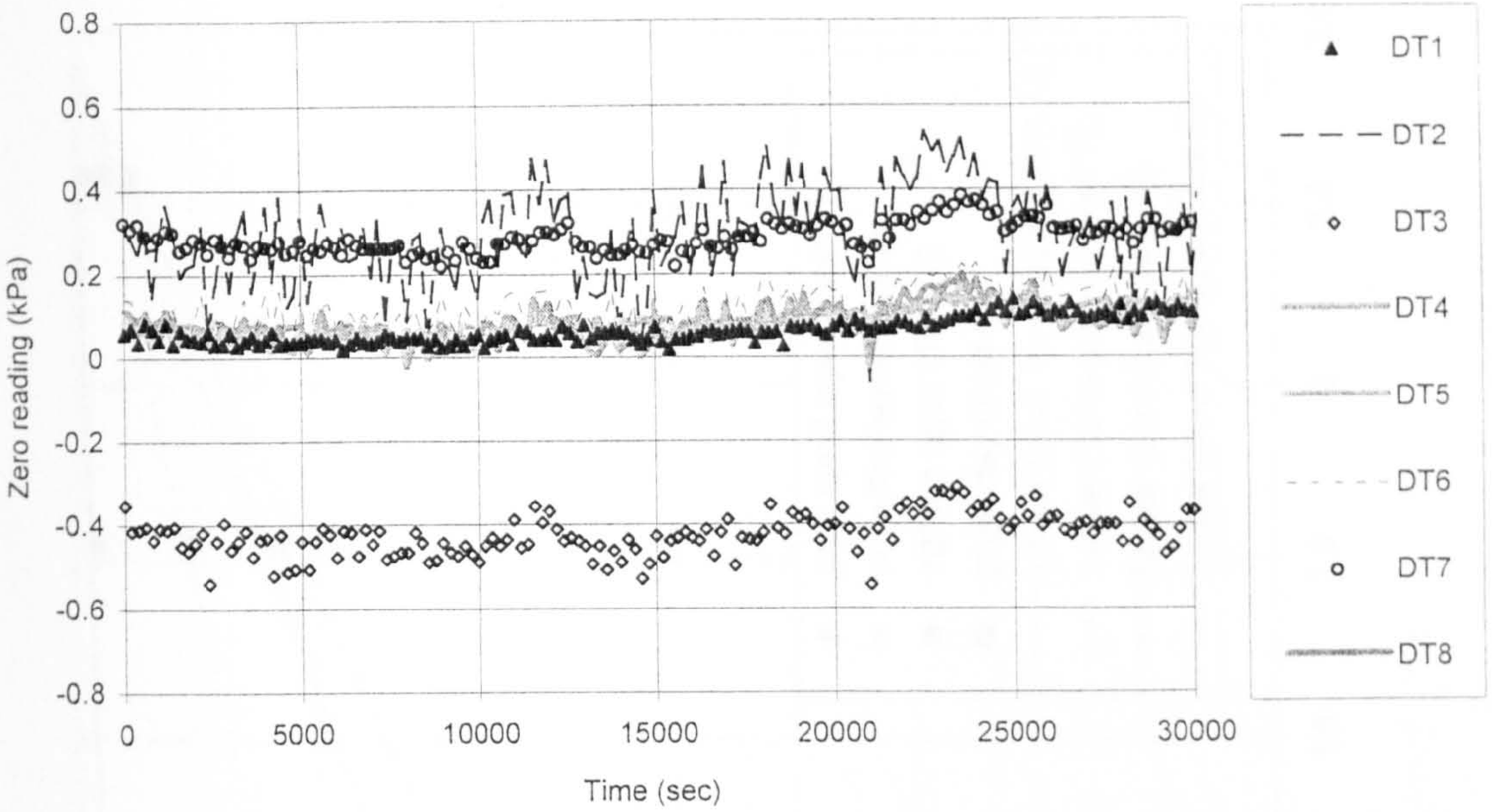

Figure 5.10 Typical zero readings before a constant head distribution test (Test 7)

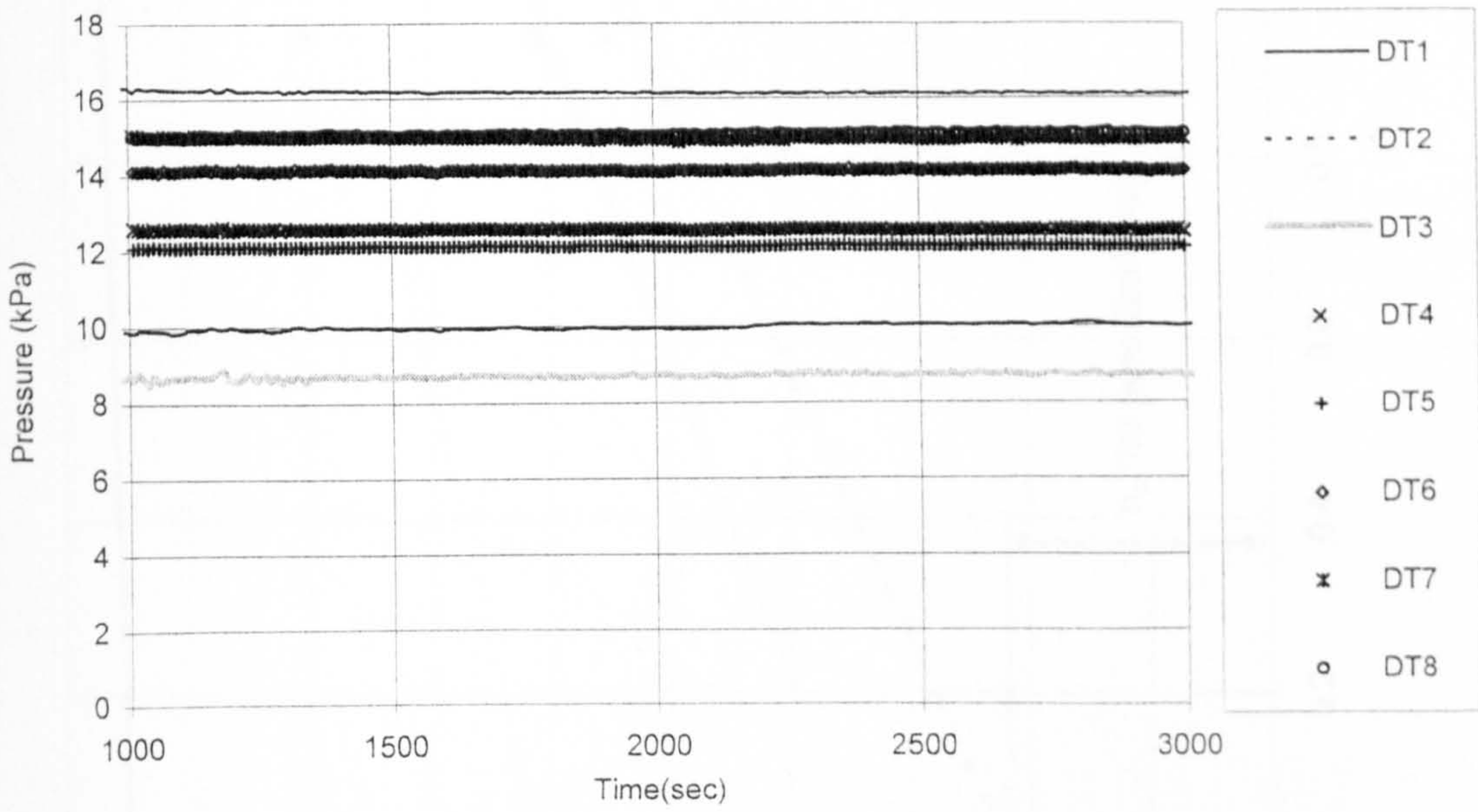

Figure 5.11 Typical window of pore pressure reading during a constant head distribution test (Test 7)

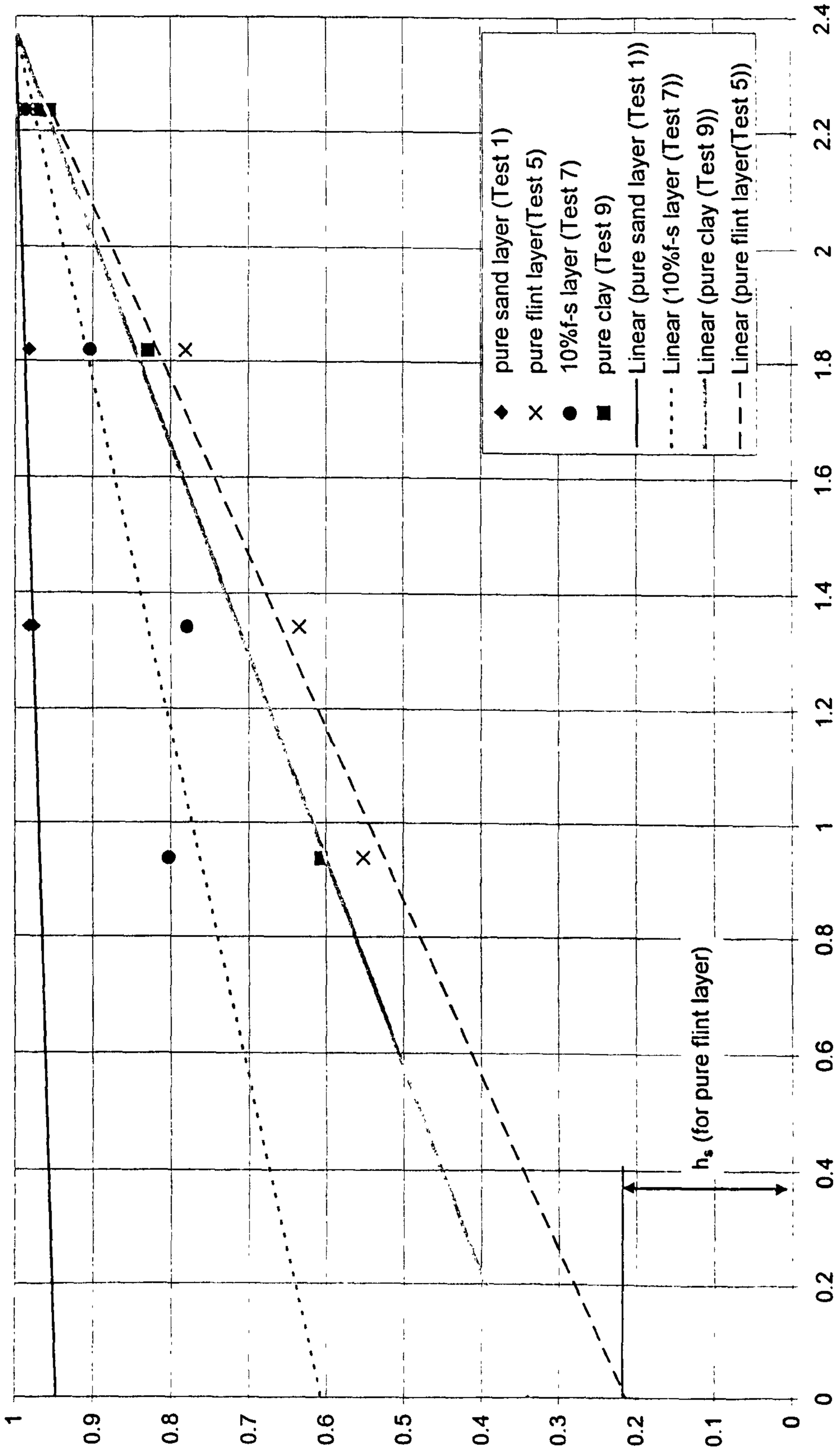

Figure 5.12 Head distributions in samples with a circular drain

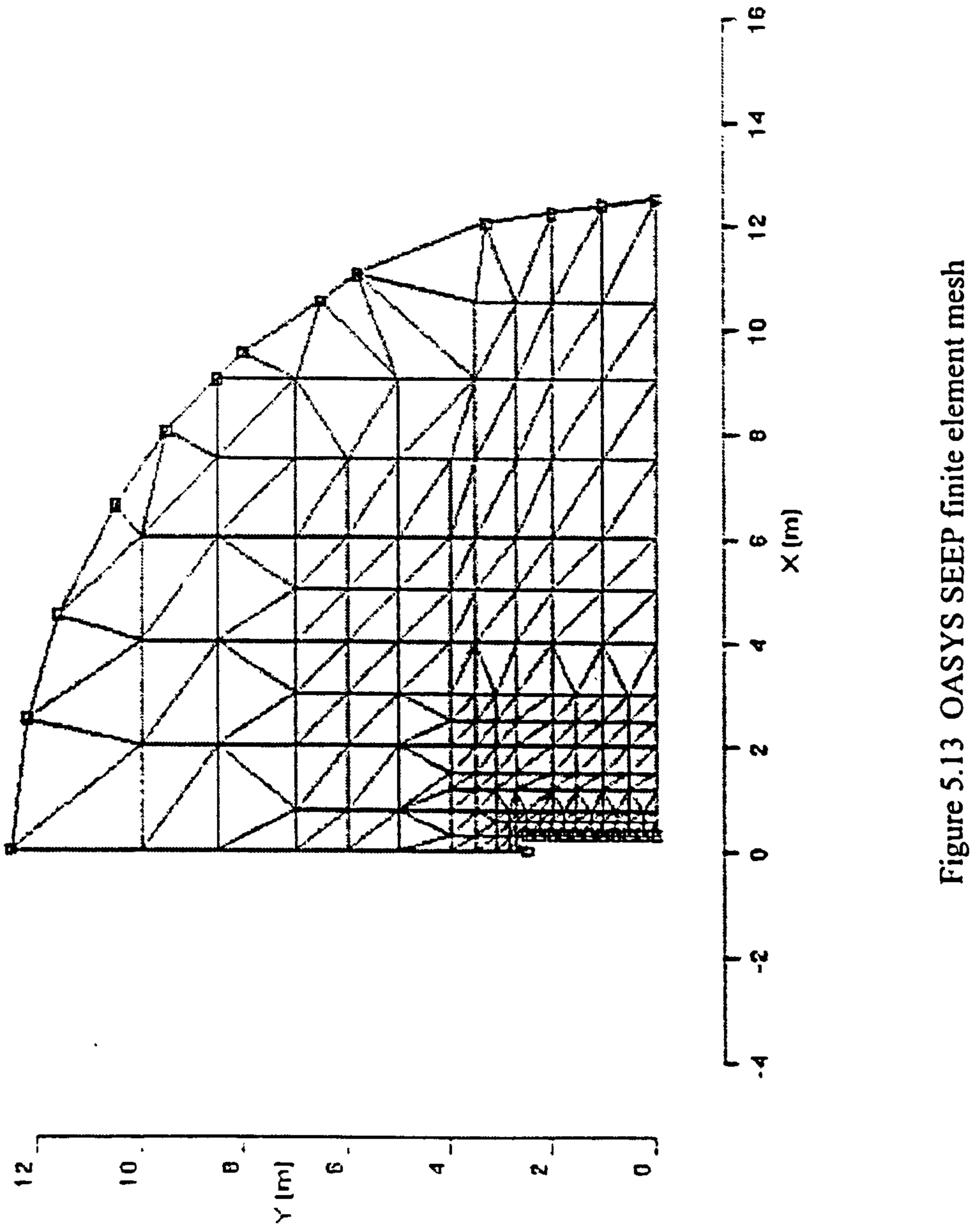

Figure 5.13 OASYS SEEP finite element mesh

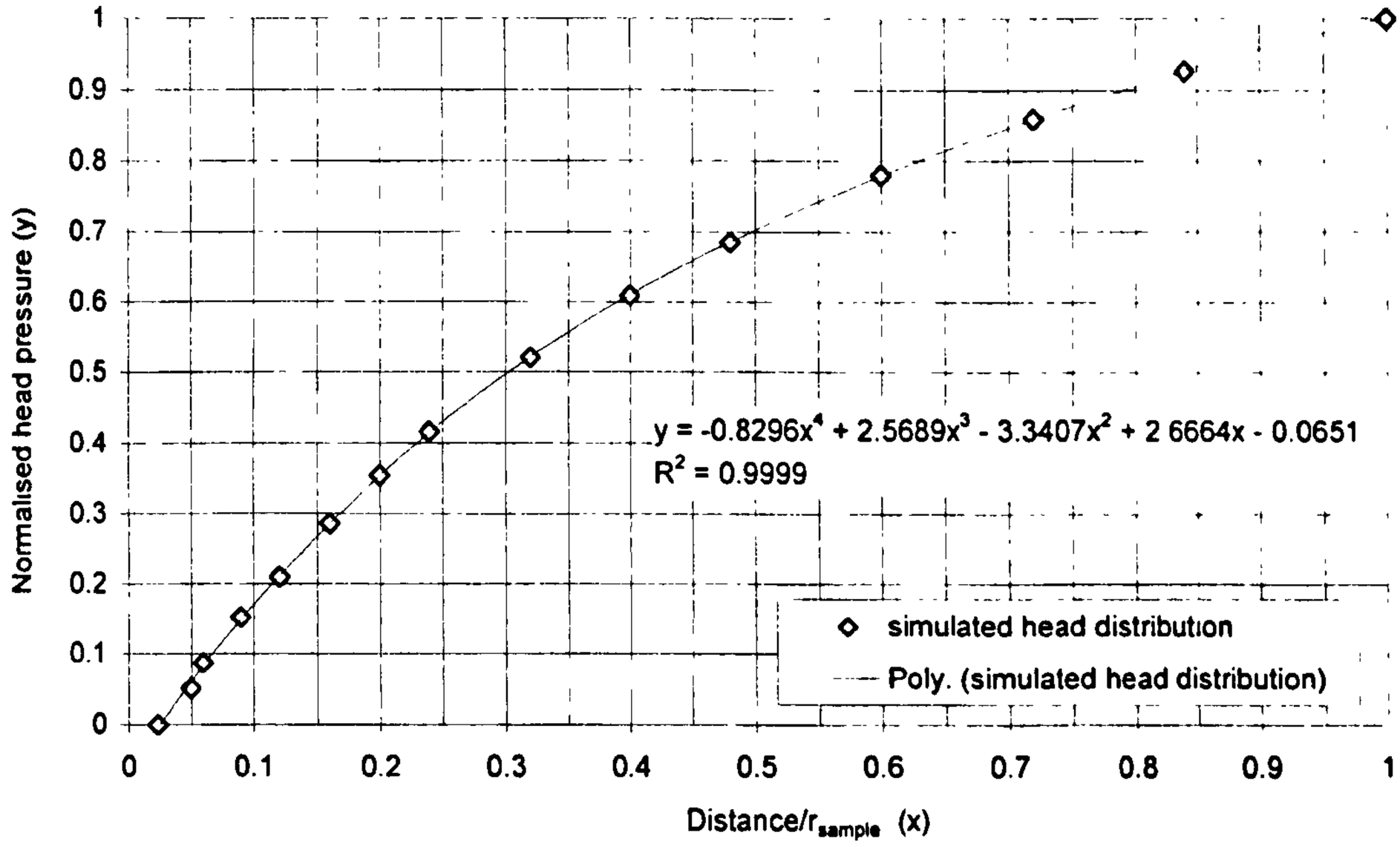

Figure 5.14 Computer simulation of head distribution across a sample with a band drain (no smear effects)

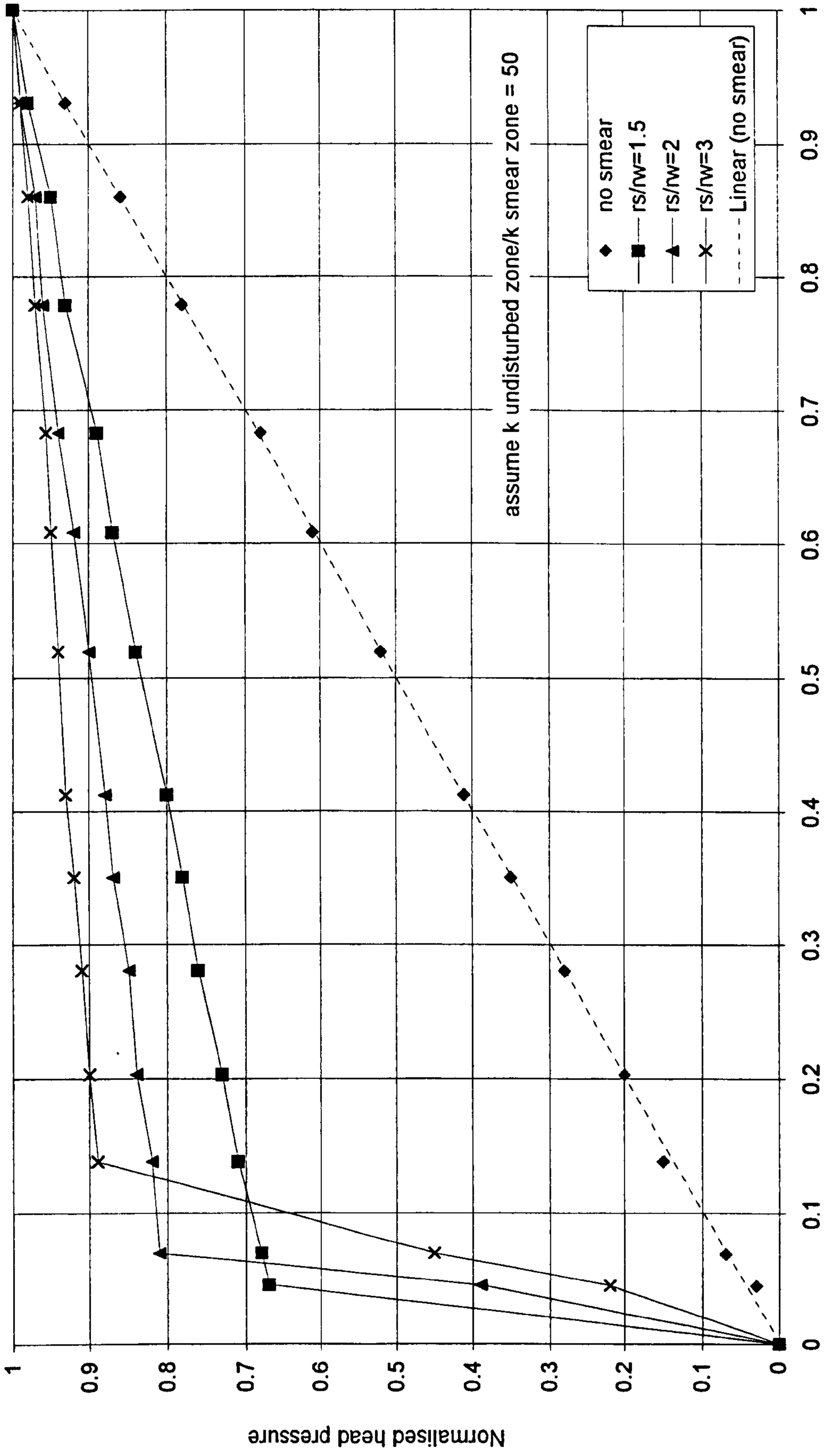

Figure 5.15 Plot of computer modelling results (Ong, 1998) on transformed distance axis

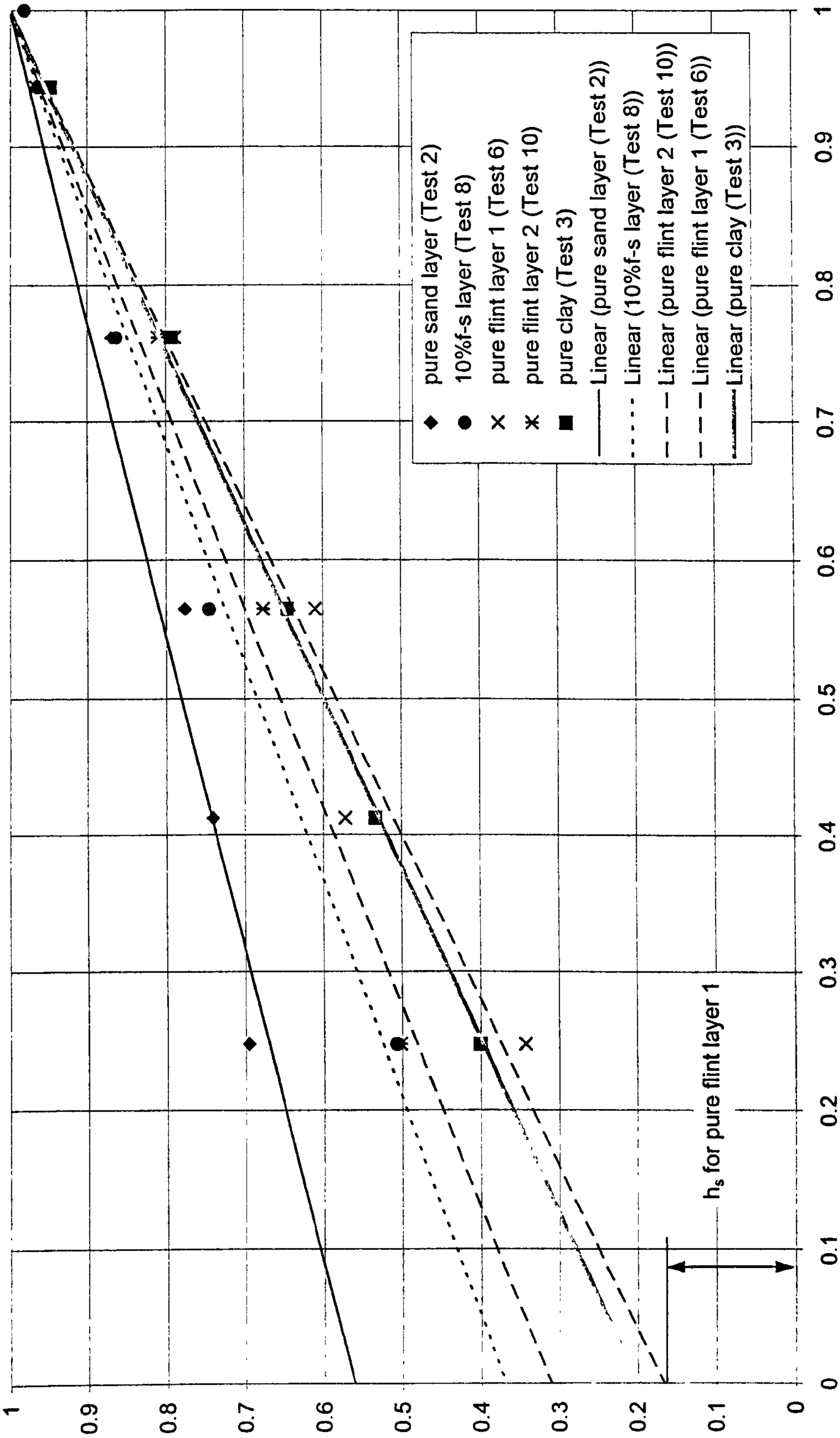

Figure 5.16 Head distributions in a samples with a band drain

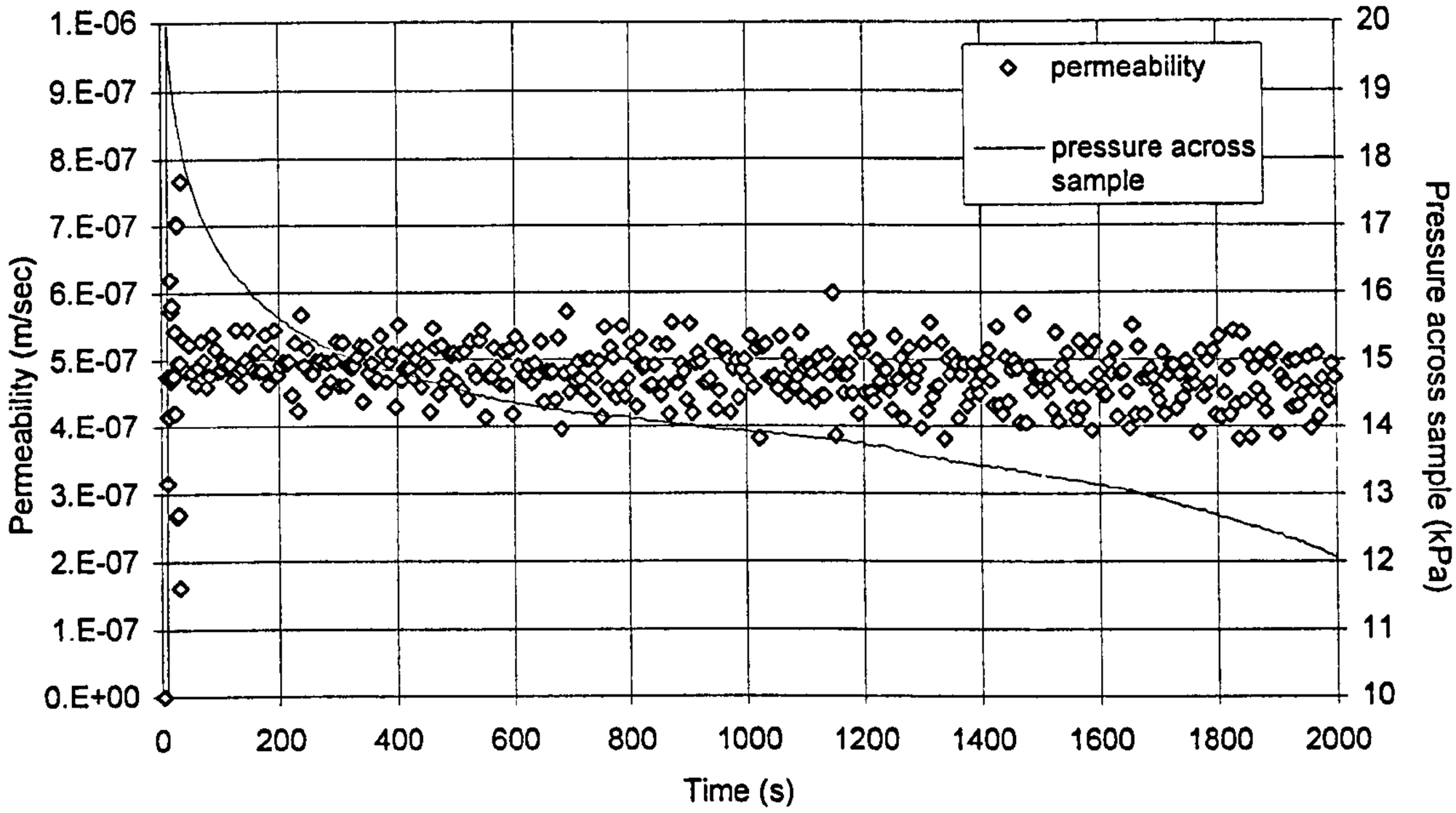

Figure 5.17 Typical layered sample permeability variation with time (Test 7)

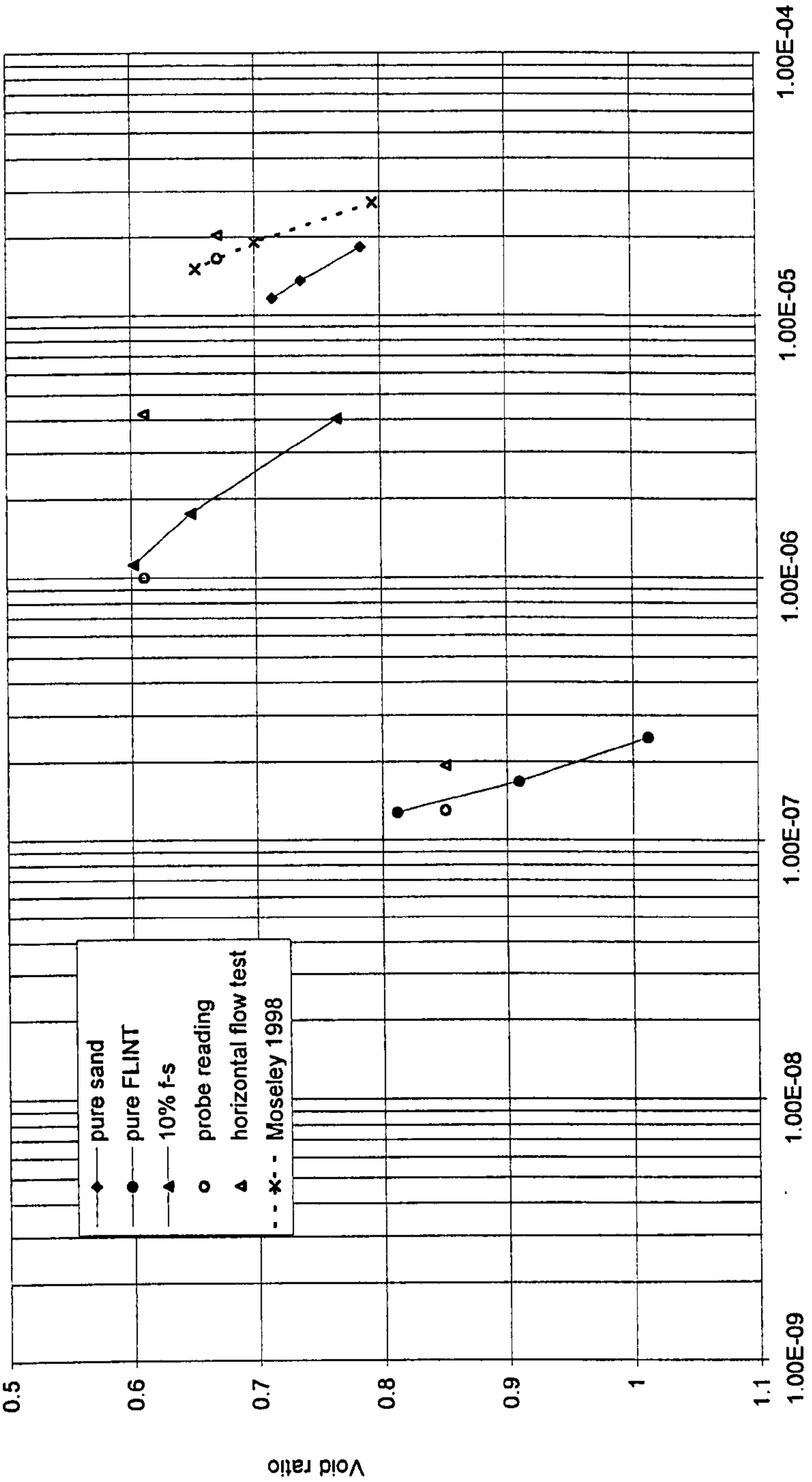

Figure 5.18 Comparison of the k_h values obtained from different measurement methods

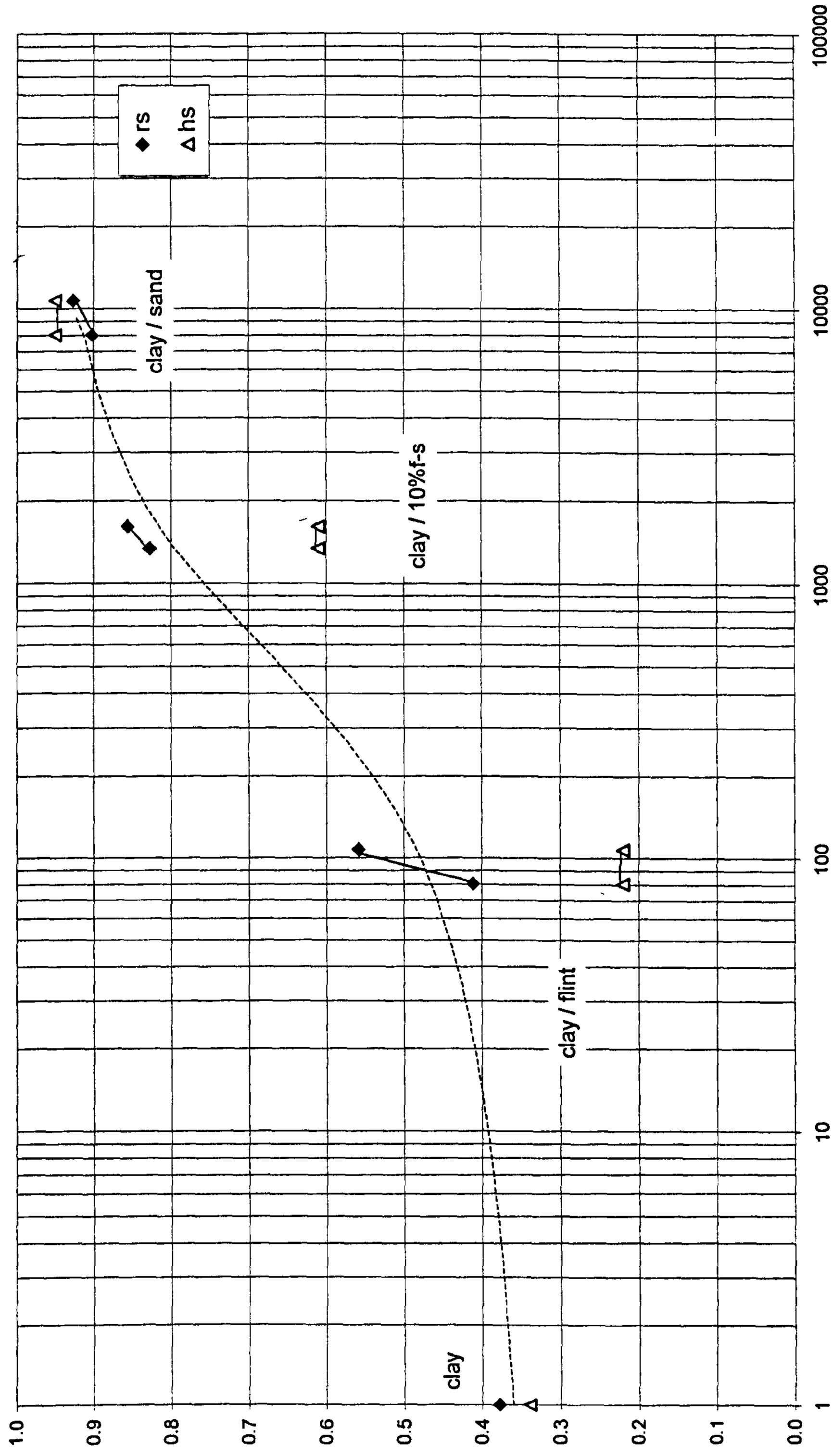

Figure 5.19 Effect of smear due to circular drain installation

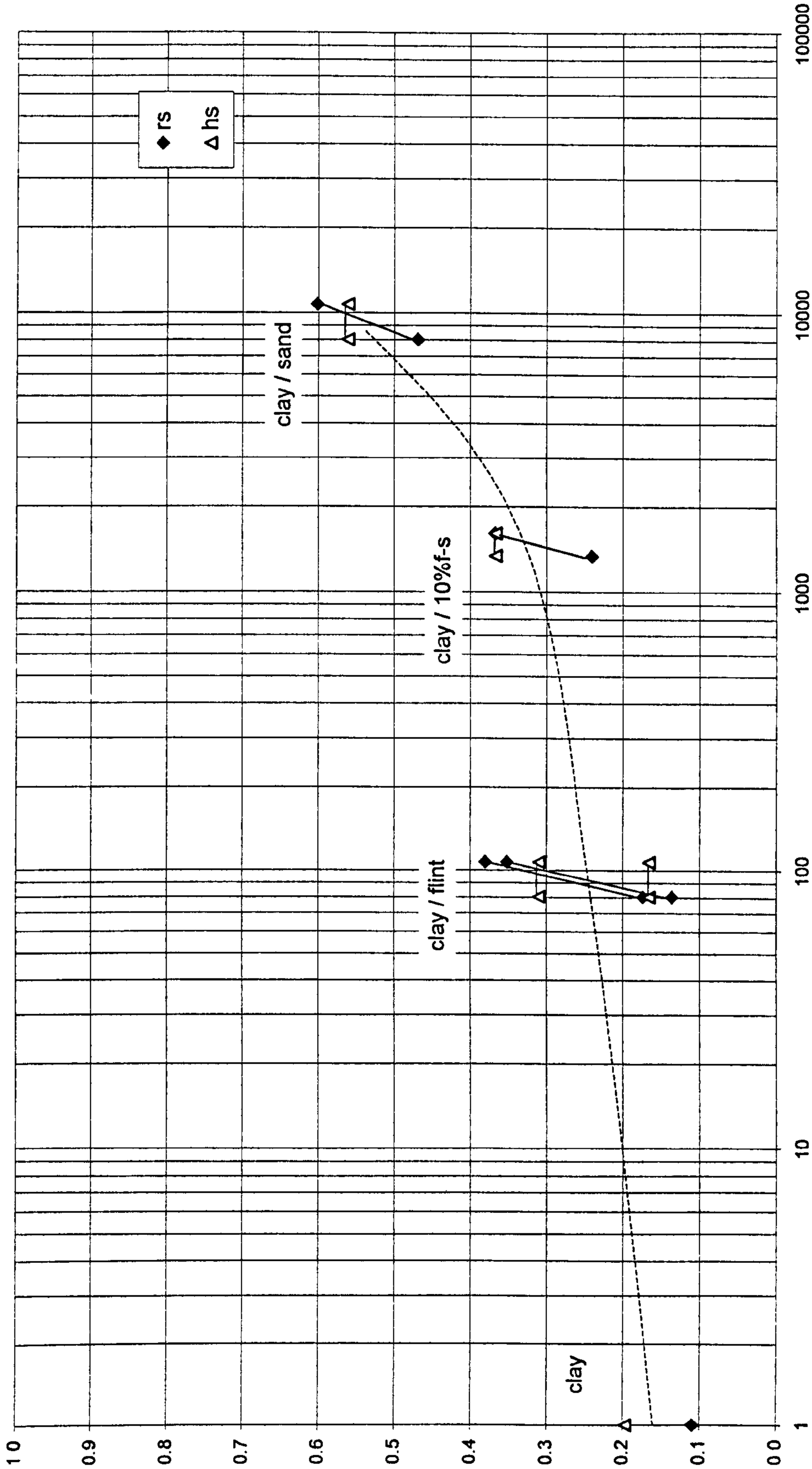

Figure 5.20 Effect of smear due to band drain installation

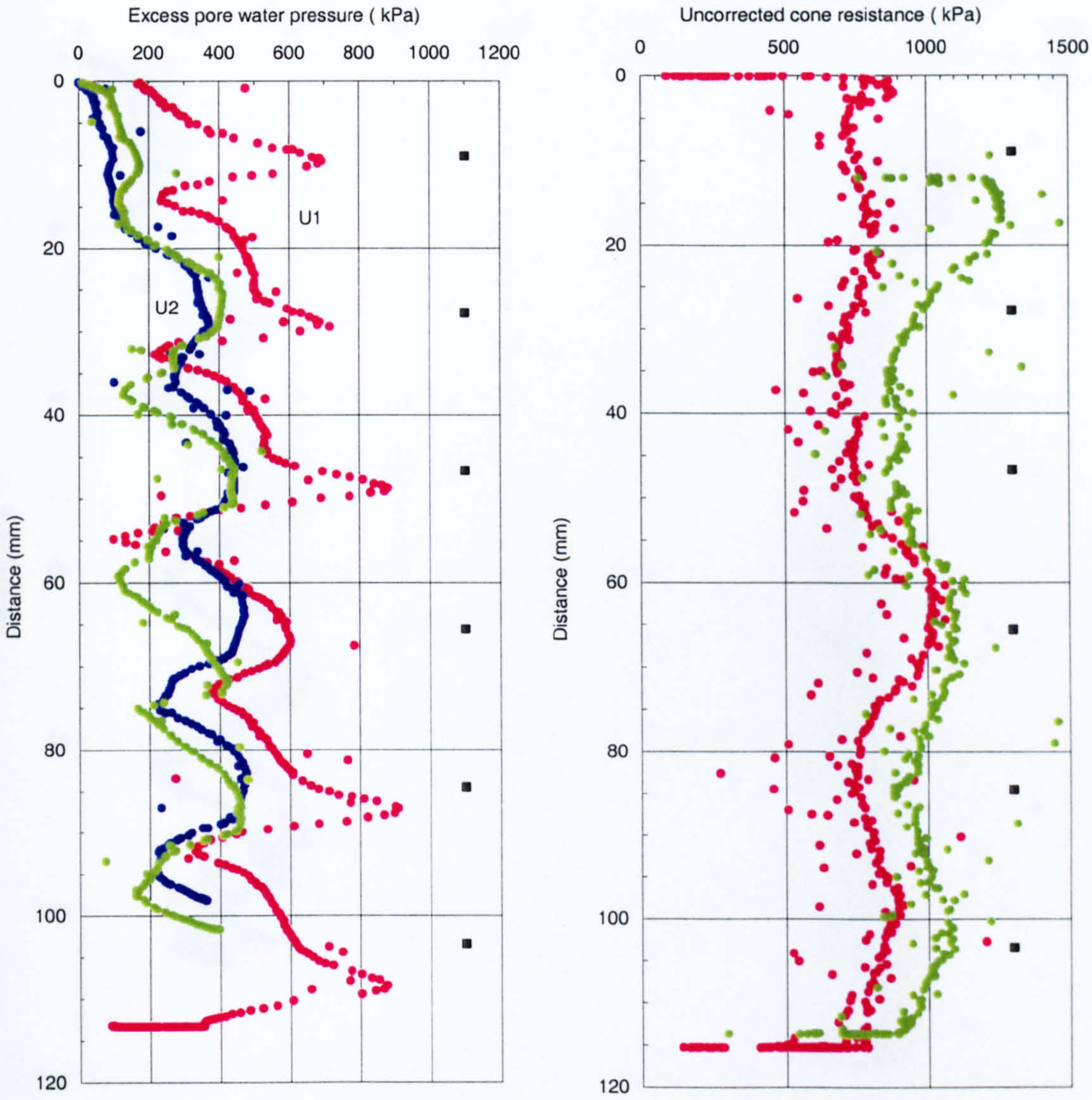

Back pressure (kPa)

drive1	200
drive2	200
drive3	200

higher logging speed (350 data/sec) led to scattering of data points (see section 3.3.14 of text) and, therefore, results can not sensibly be presented using continuous lines.

Figure 5.21 Piezocone test results of sample No. 1 (clay & pure sand)

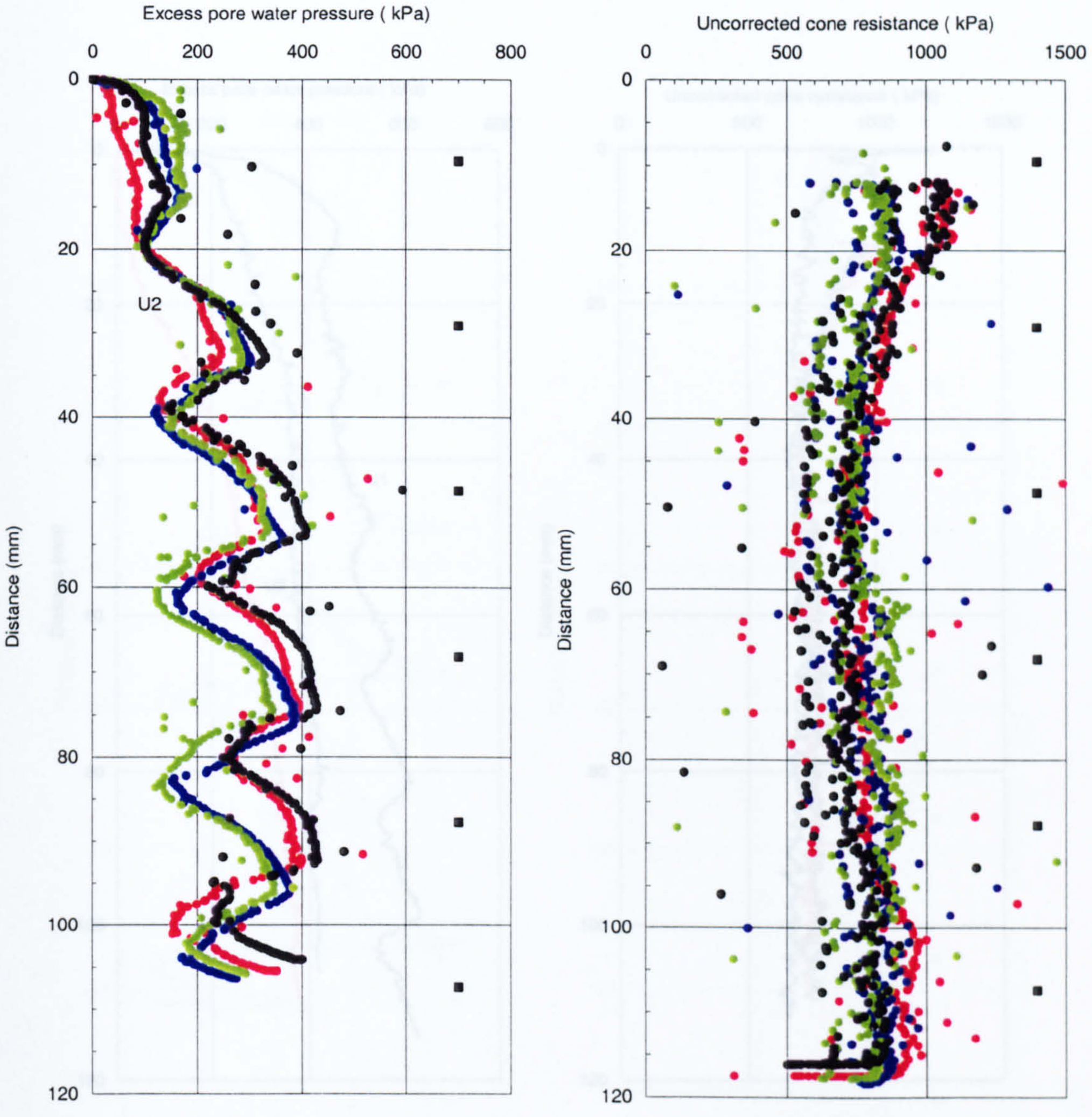

Back pressure (kPa)

drive1	200
drive2	200
drive3	200
drive4	200

higher logging speed (350 data/sec) led to scattering of data points (see section 3.3.14 of text) and, therefore, results can not sensibly be presented using continuous lines.

Figure 5.22 Piezocone test results of sample No.2 (clay & pure sand)

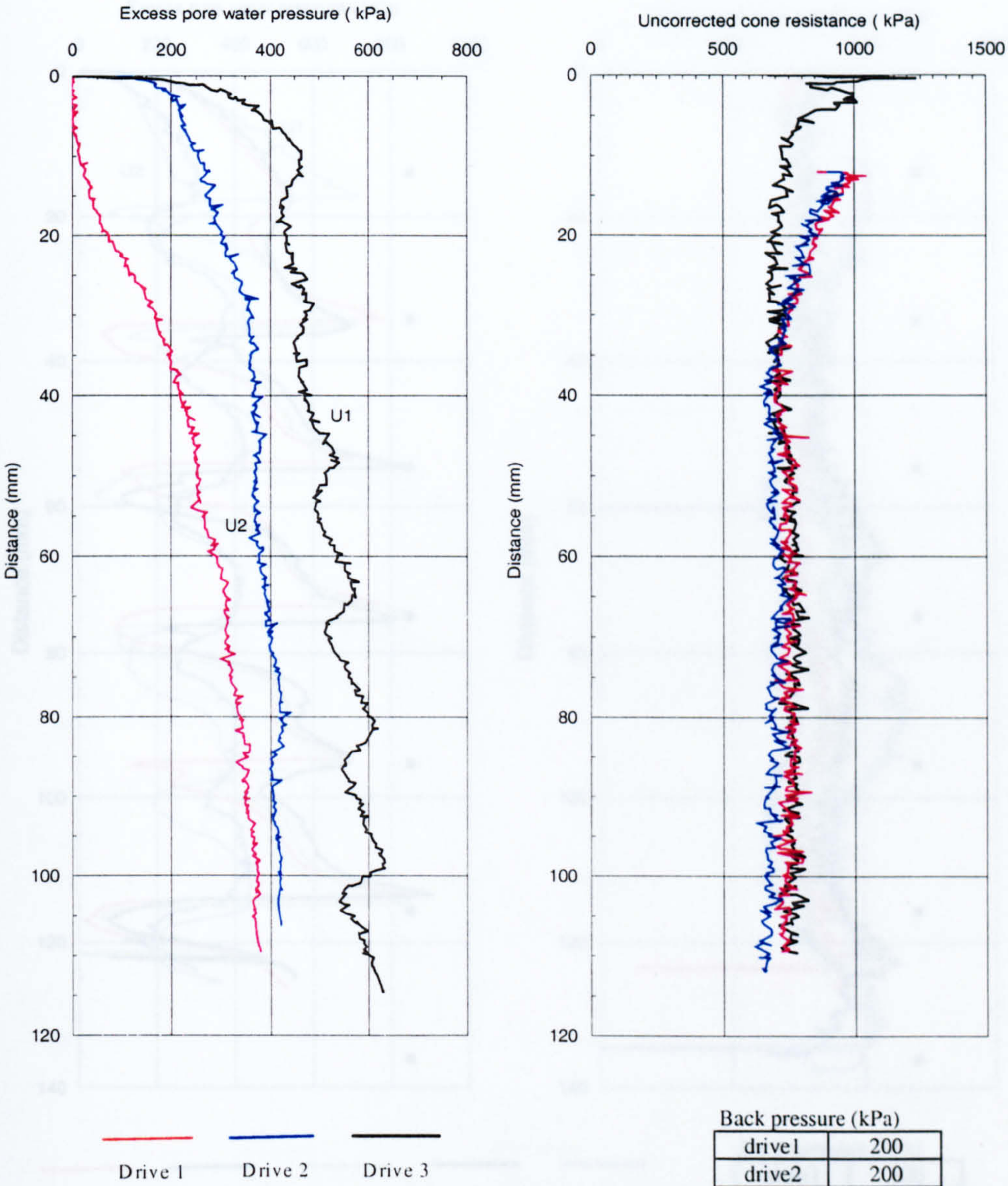

Back pressure (kPa)

drive1	200
drive2	200
drive3	200

Figure 5.23 Piezocone test results of sample No.3 (pure clay)

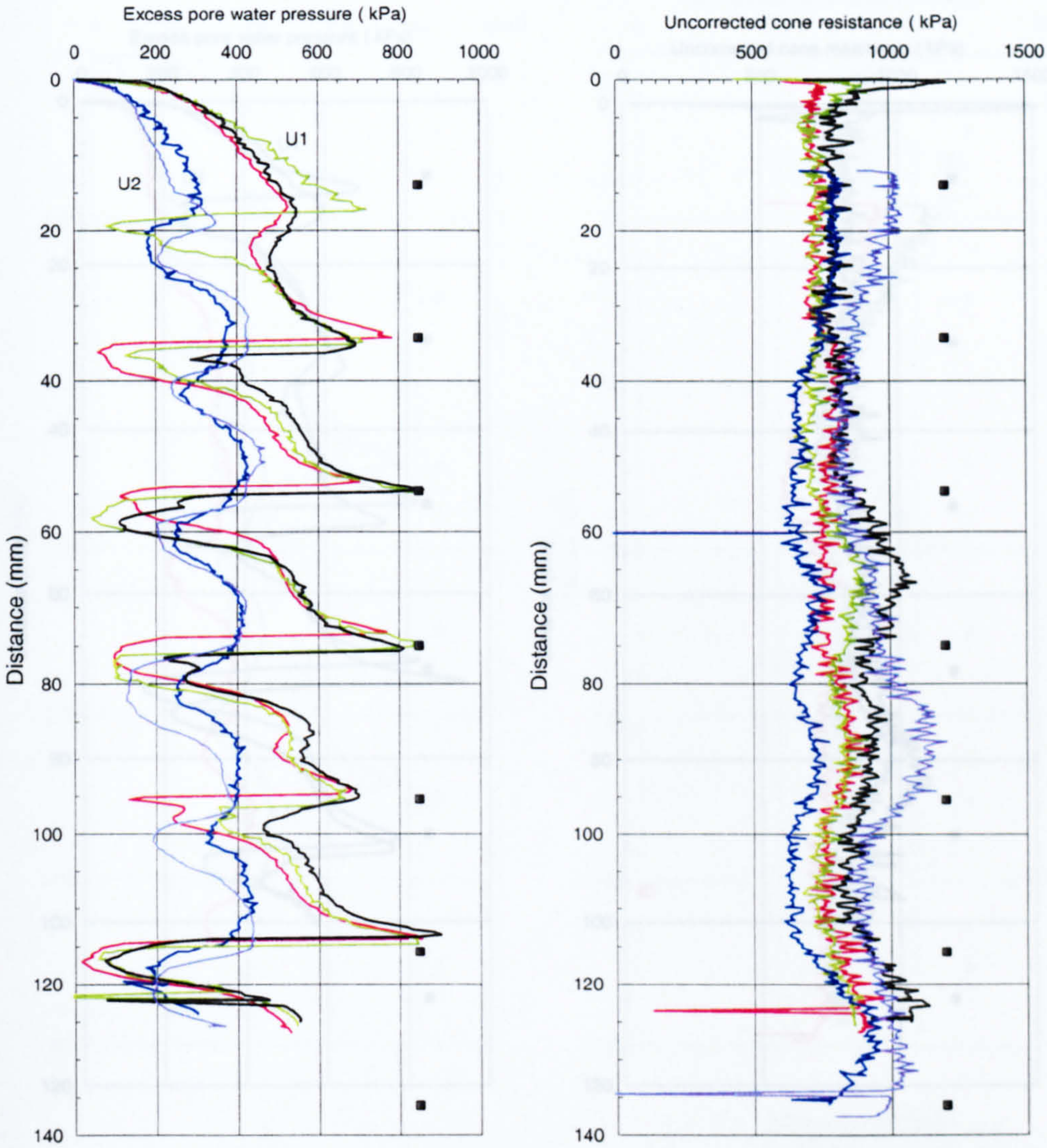

Back pressure (kPa)

drive1	200
drive2	200
drive3	200
drive4	400
drive5	400

Figure 5.24 Piezocone test results of sample No.4 (clay & pure sand)

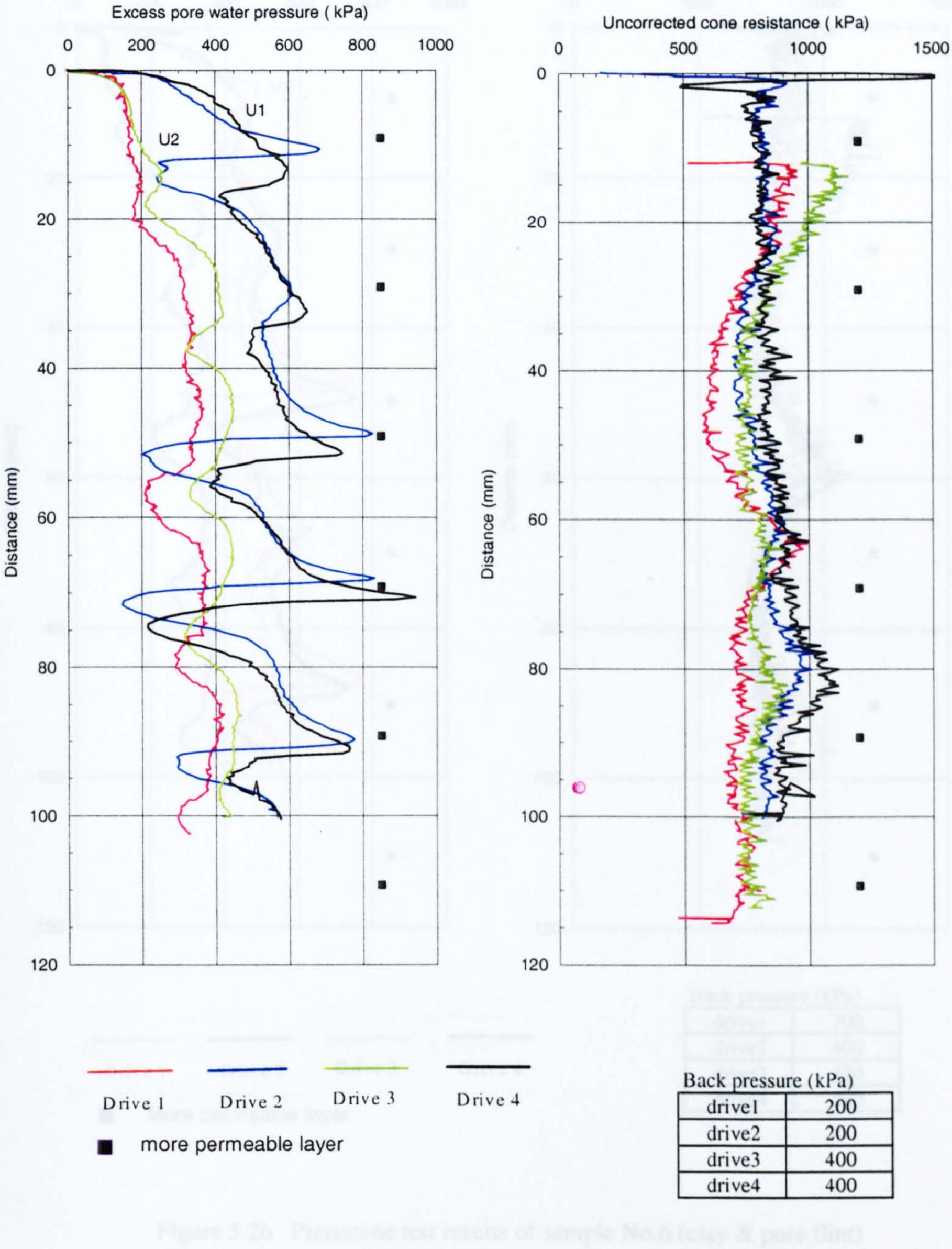

Back pressure (kPa)

drive1	200
drive2	200
drive3	400
drive4	400

Figure 5.25 Piezocone test results of sample No.5 (clay & pure flint)

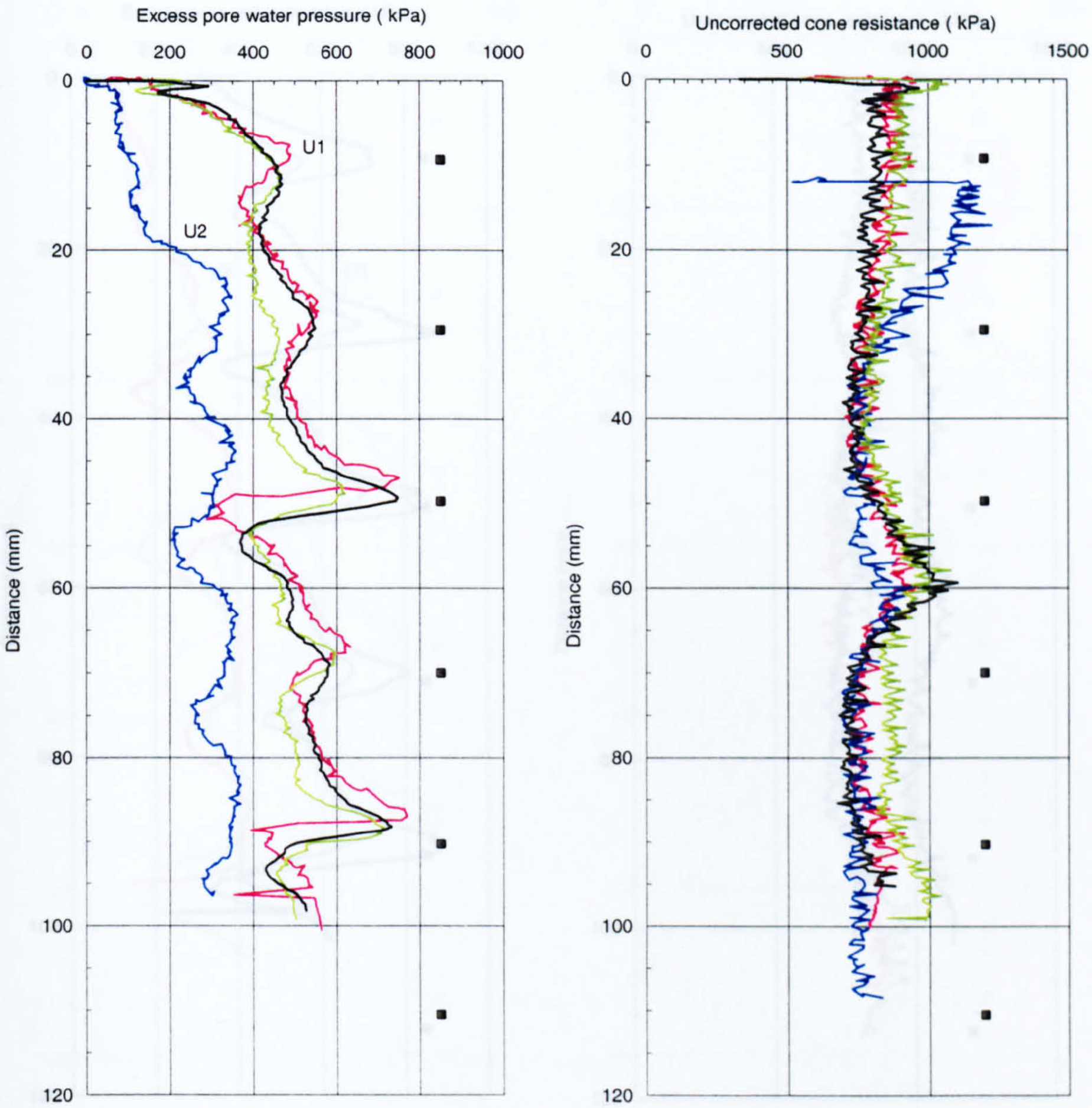

Back pressure (kPa)

drive1	200
drive2	400
drive3	400
drive4	200

Figure 5.26 Piezocone test results of sample No.6 (clay & pure flint)

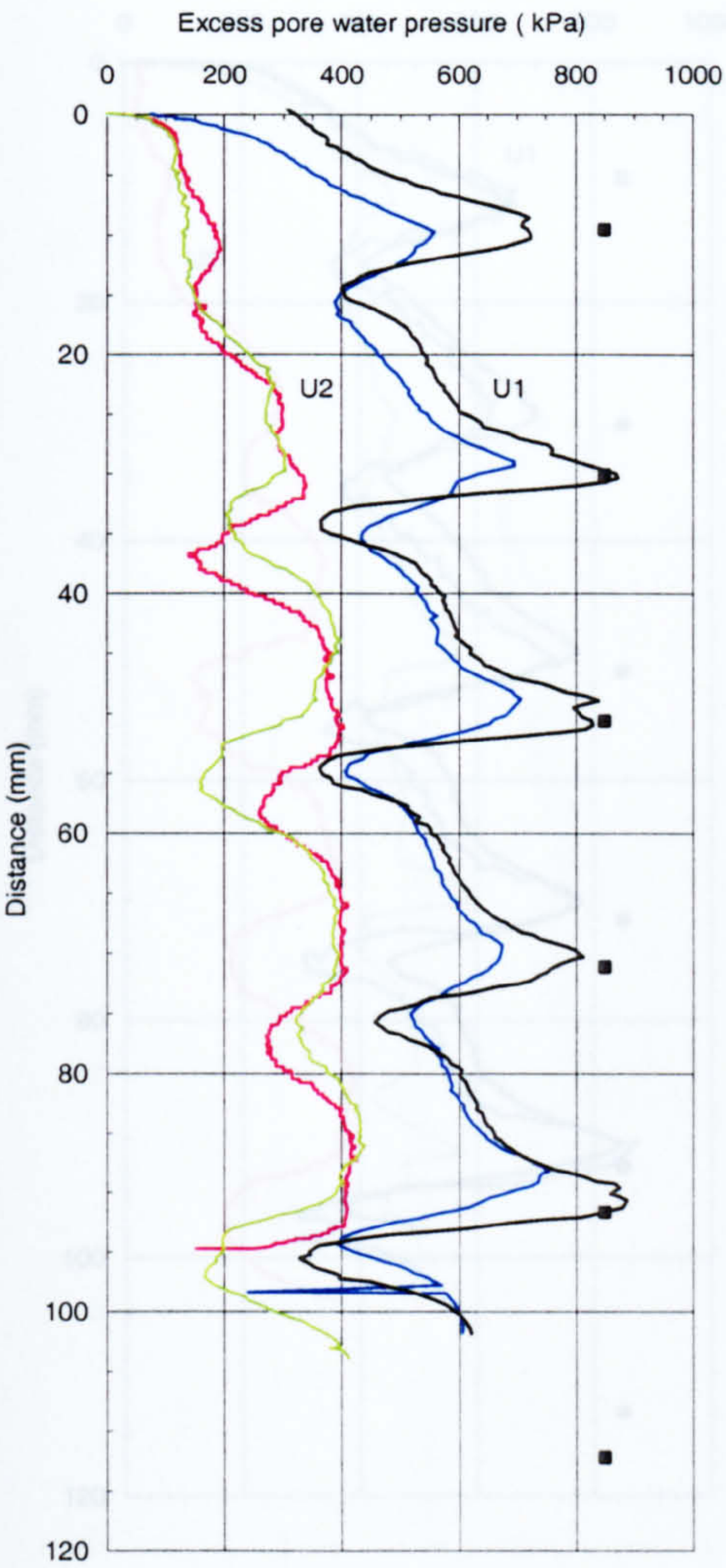

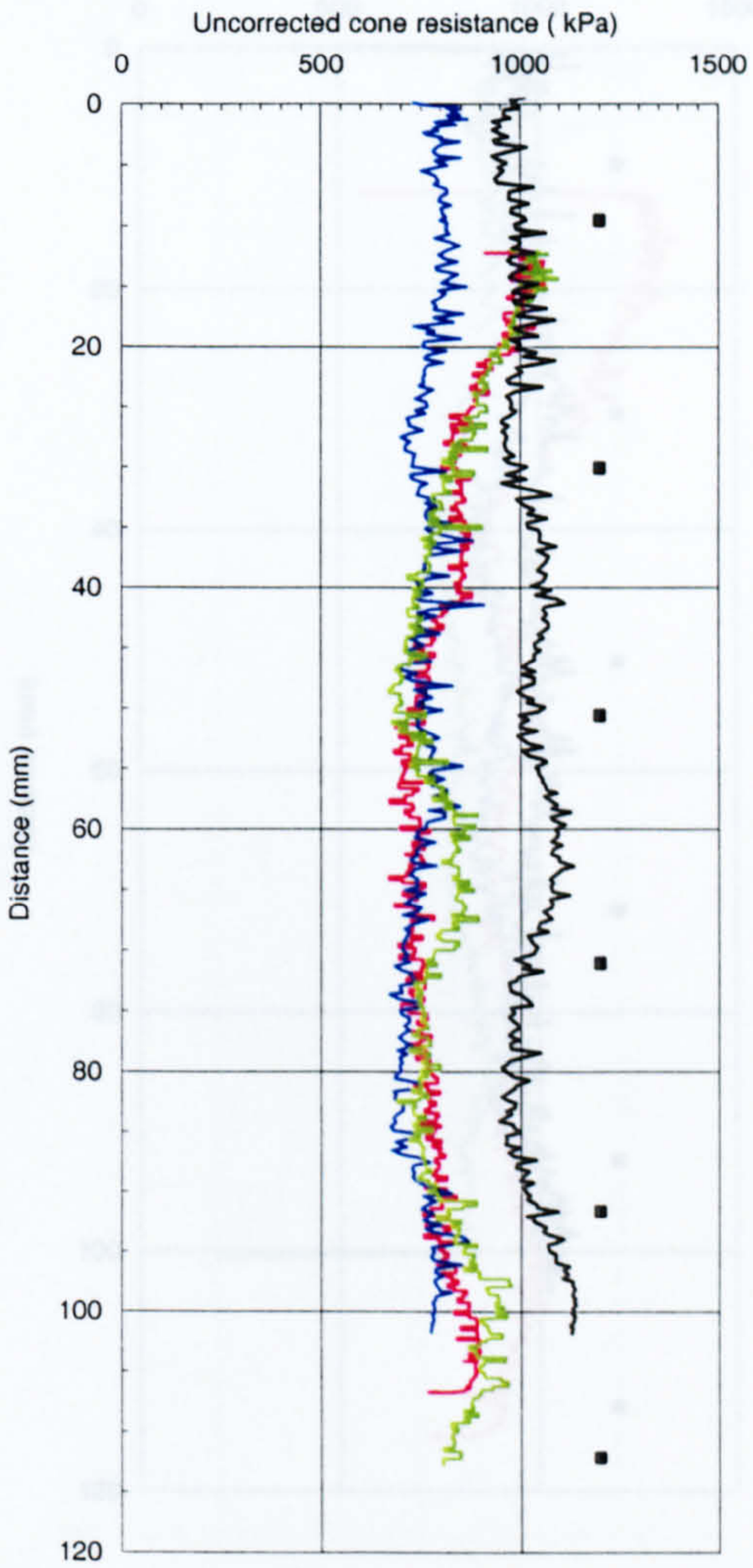

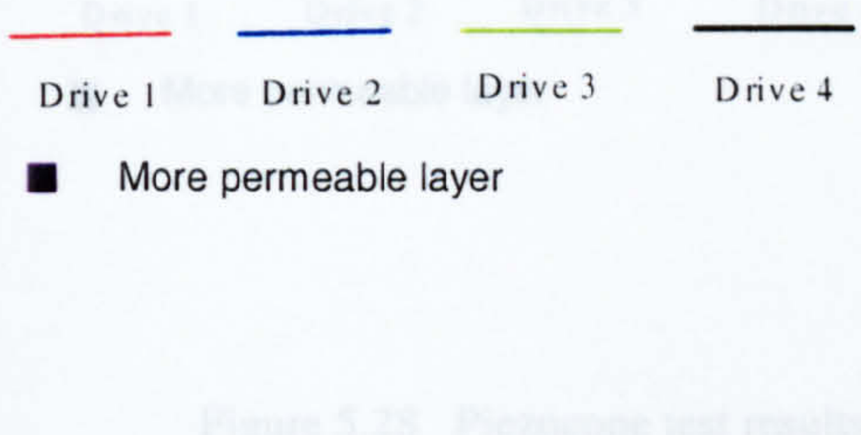

Back pressure (kPa)

drive1	200
drive2	200
drive3	200
drive4	400

Figure 5.27 Piezocone test results of sample No.7 (clay & 10%f-s)

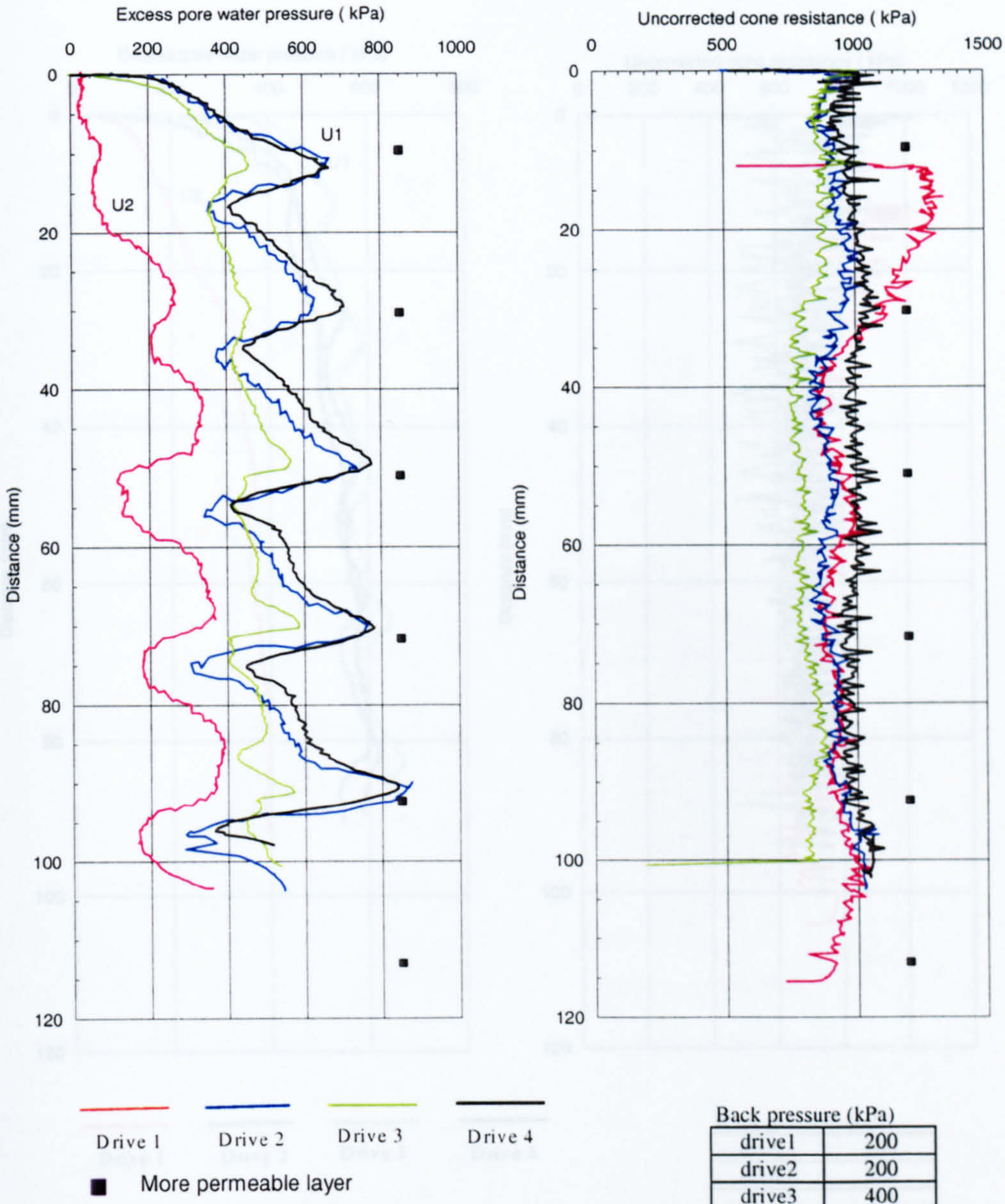

Back pressure (kPa)

drive1	200
drive2	200
drive3	400
drive4	400

Figure 5.28 Piezocone test results of sample No.8 (clay & 10%f-s)

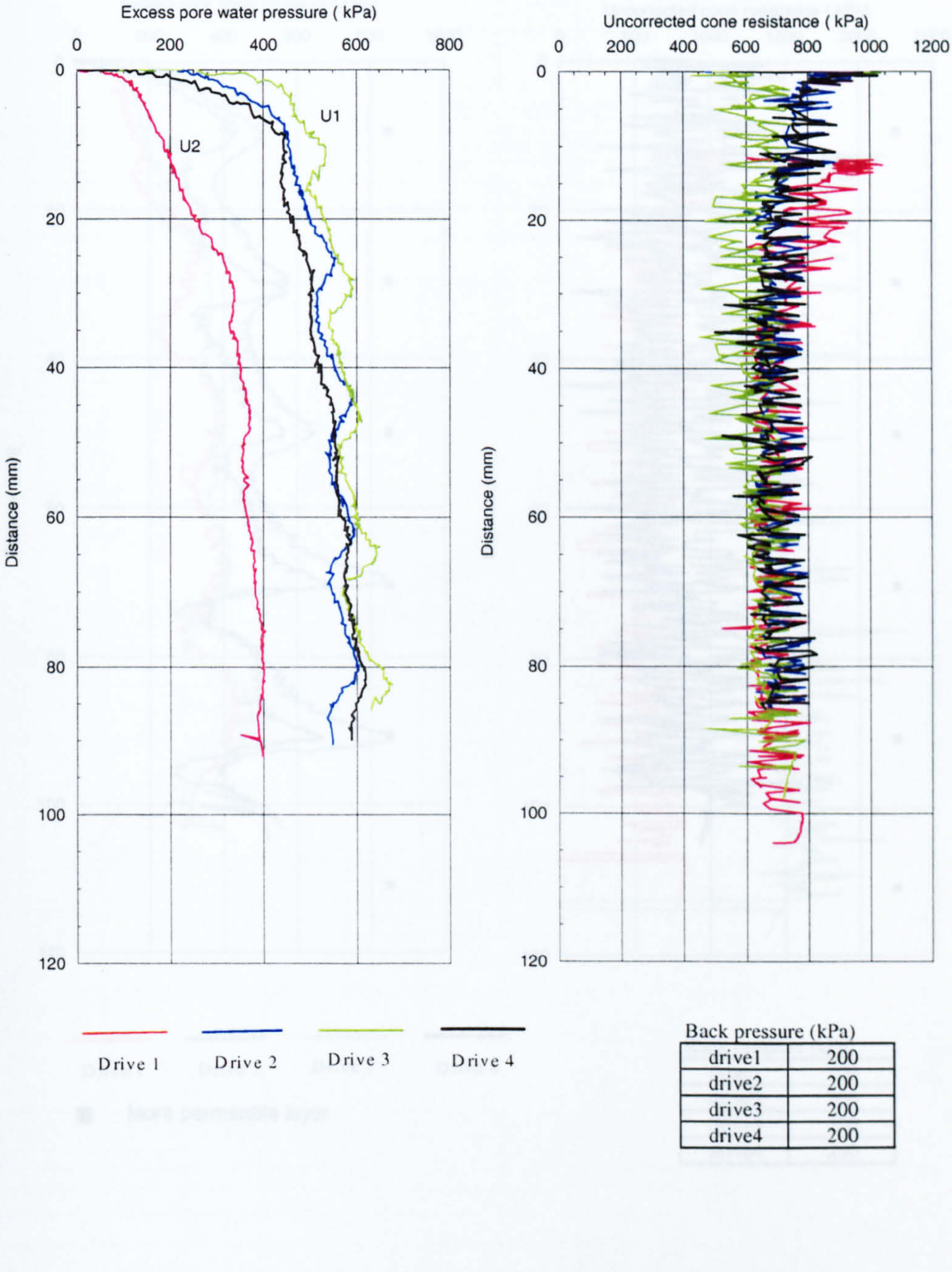

Back pressure (kPa)

drive1	200
drive2	200
drive3	200
drive4	200

Figure 5.29 Piezocone test results of sample No.9 (pure clay)

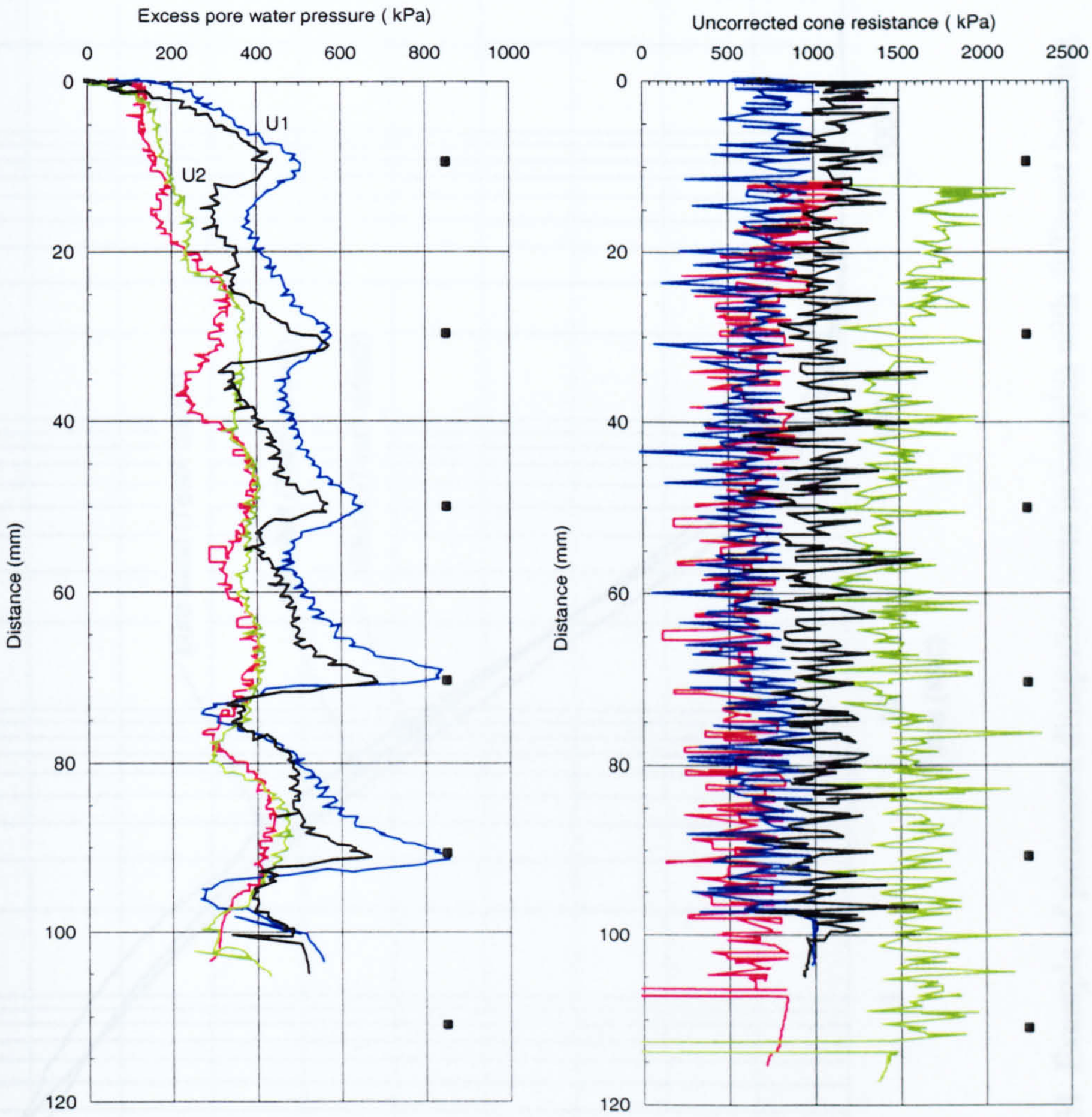

Back pressure (kPa)

drive1	200
drive2	200
drive3	200
drive4	200

Figure 5.30 Piezocone test results of sample No.10 (clay & pure flint)

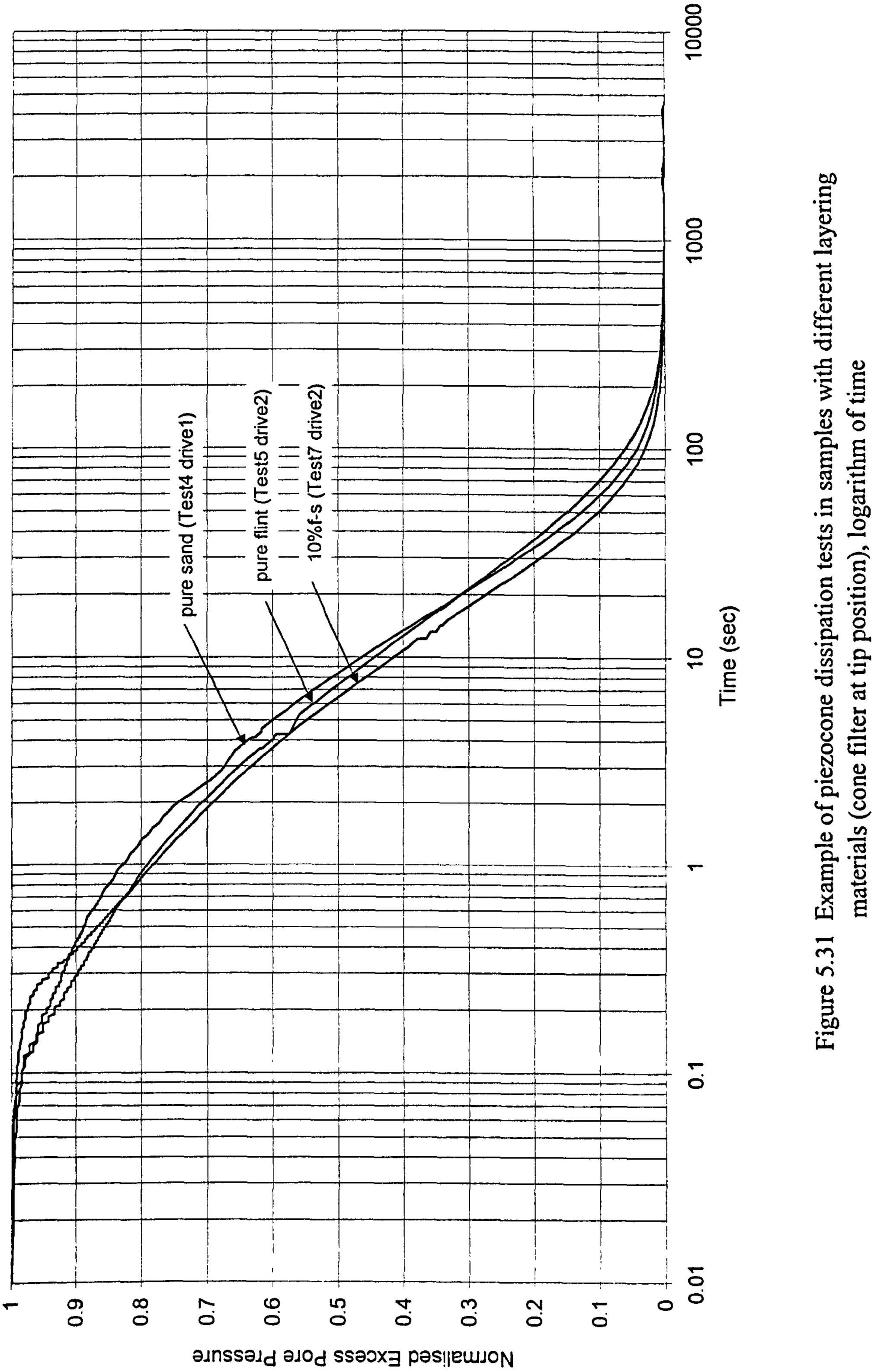

Figure 5.31 Example of piezocone dissipation tests in samples with different layering materials (cone filter at tip position), logarithm of time

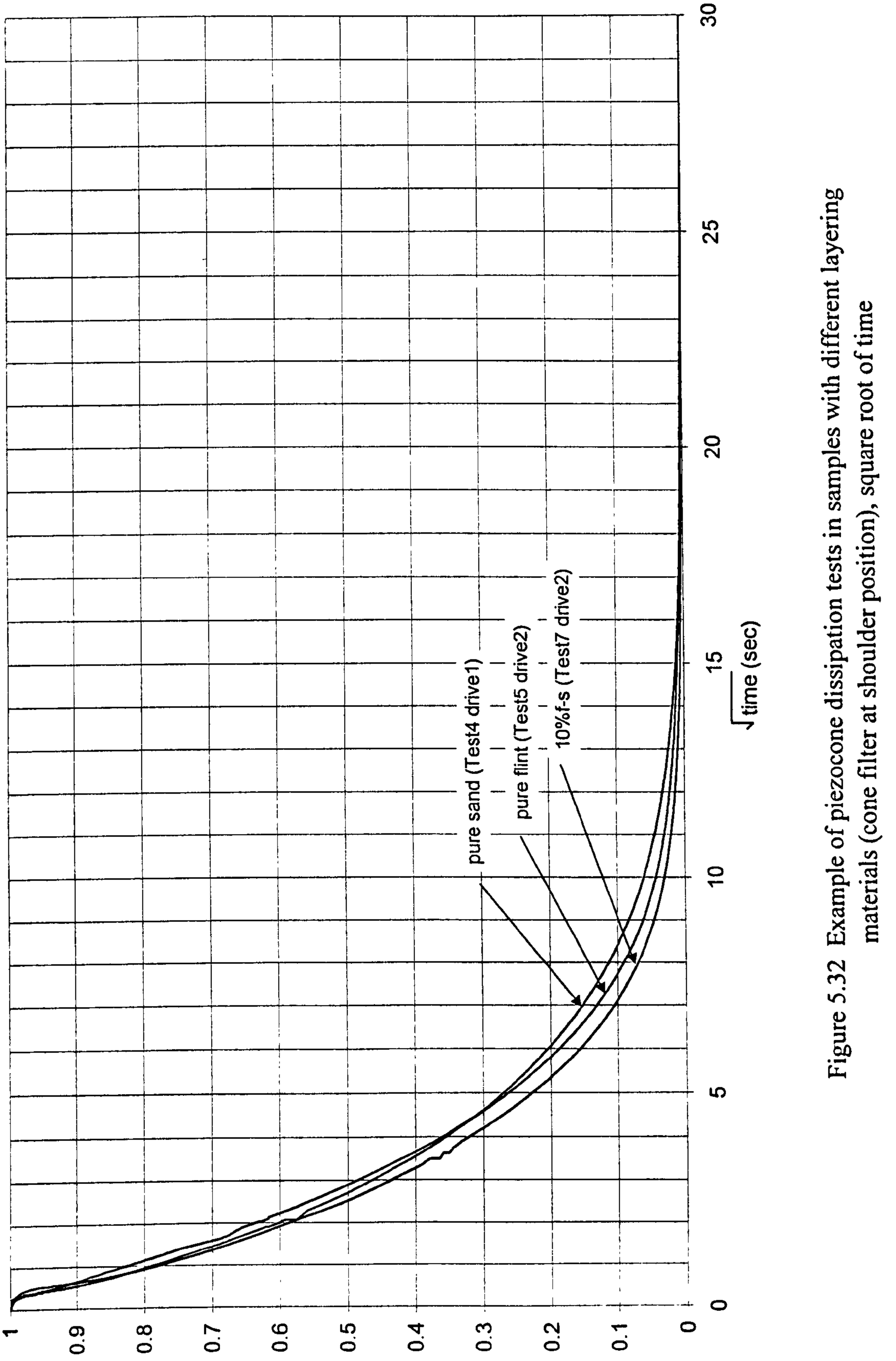

Figure 5.32 Example of piezocone dissipation tests in samples with different layering materials (cone filter at shoulder position), square root of time

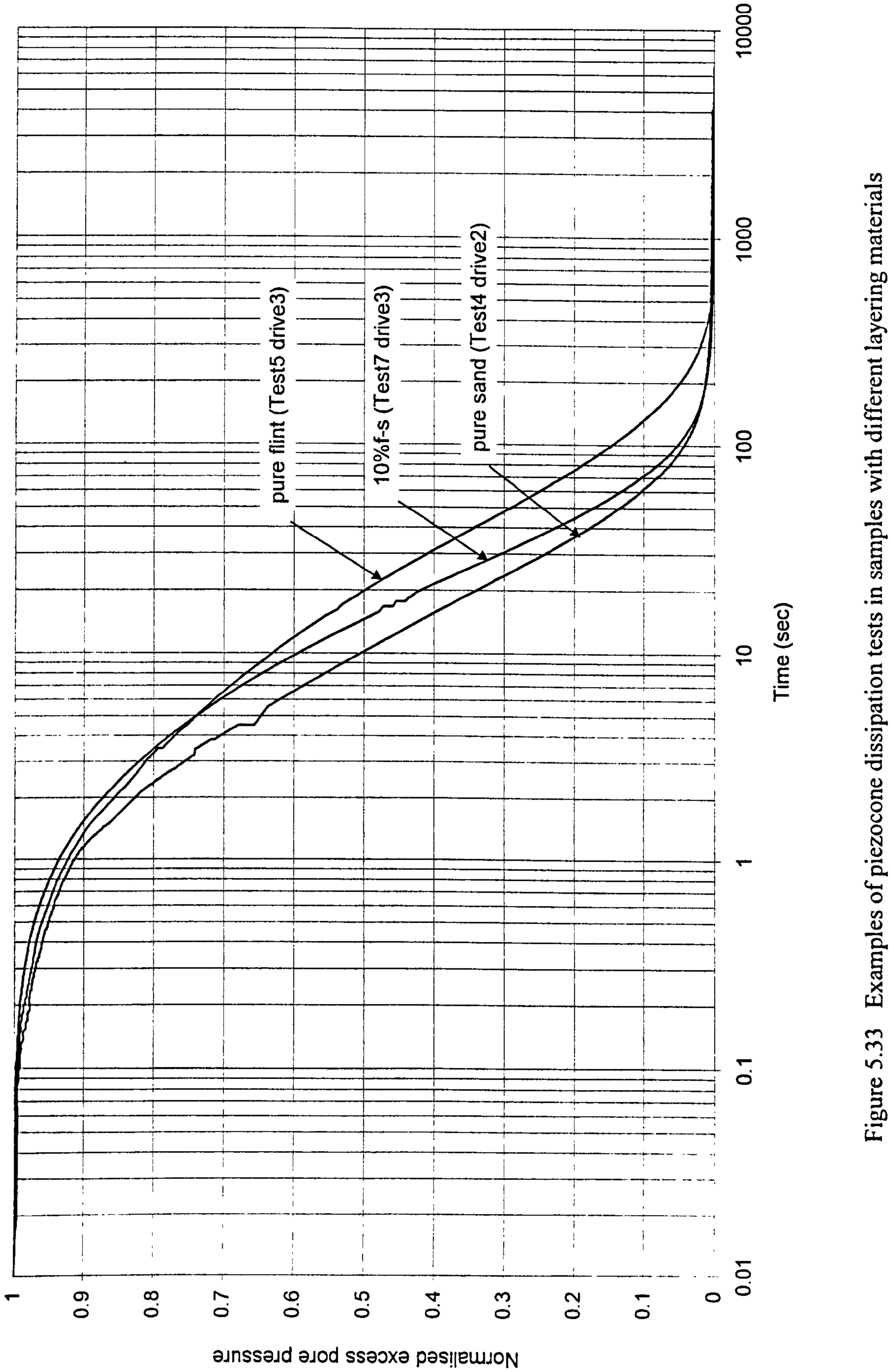

Figure 5.33 Examples of piezocone dissipation tests in samples with different layering materials (cone filter at shoulder position), logarithm of time

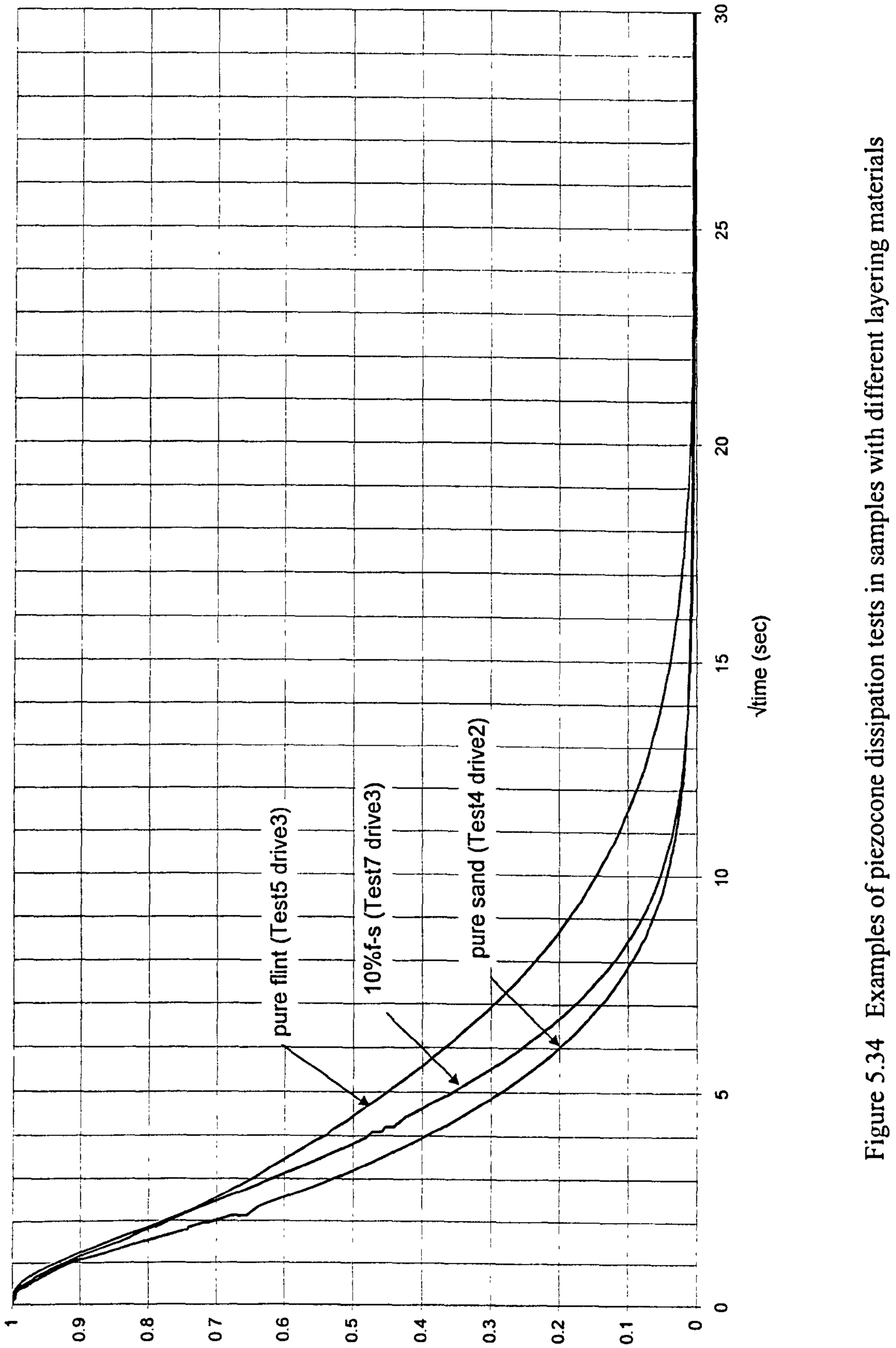

Figure 5.34 Examples of piezocone dissipation tests in samples with different layering materials (cone filter at shoulder position), square root of time

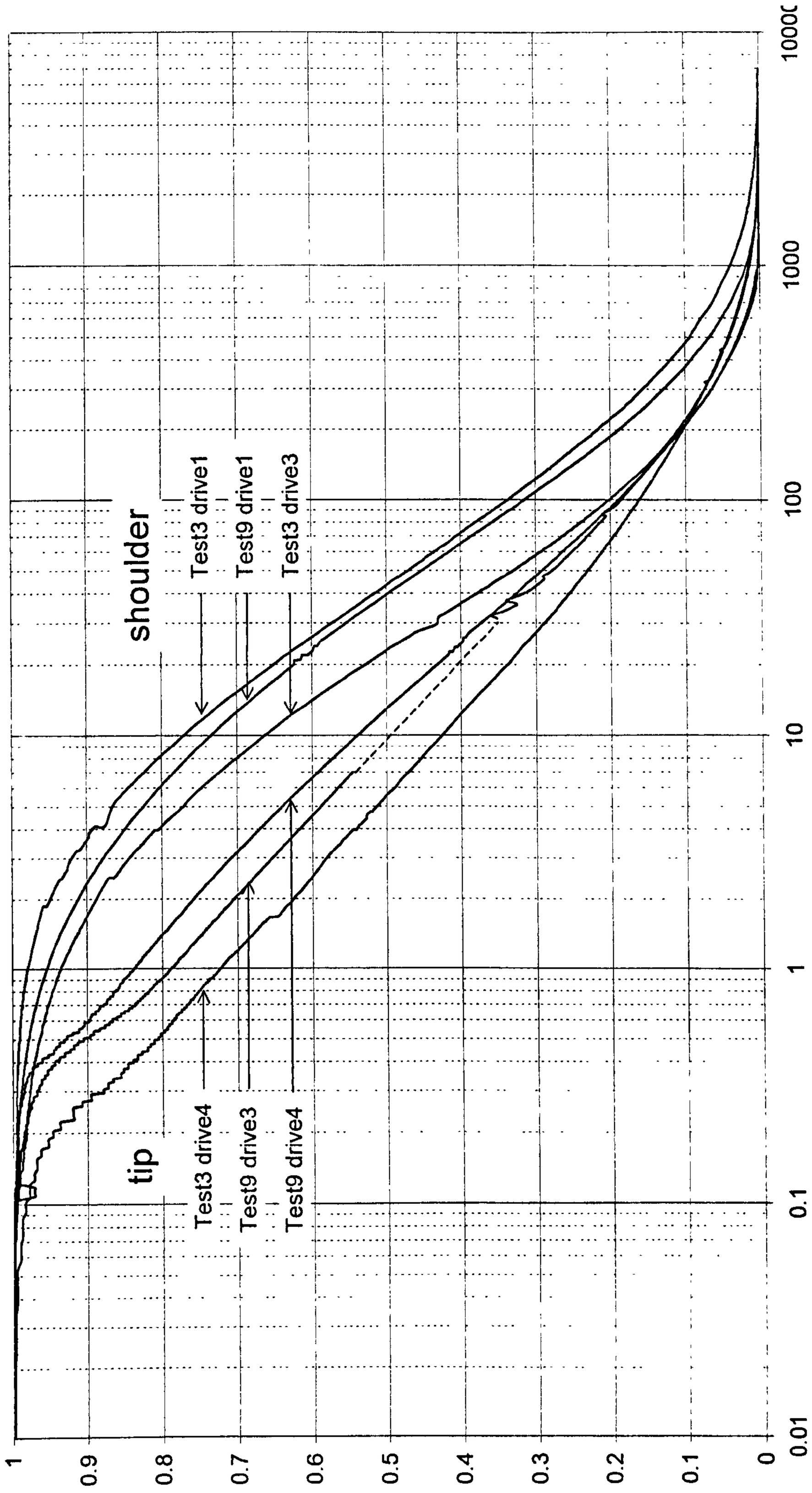

Figure 5.35 Piezocone dissipation tests in pure clay, logarithm of time

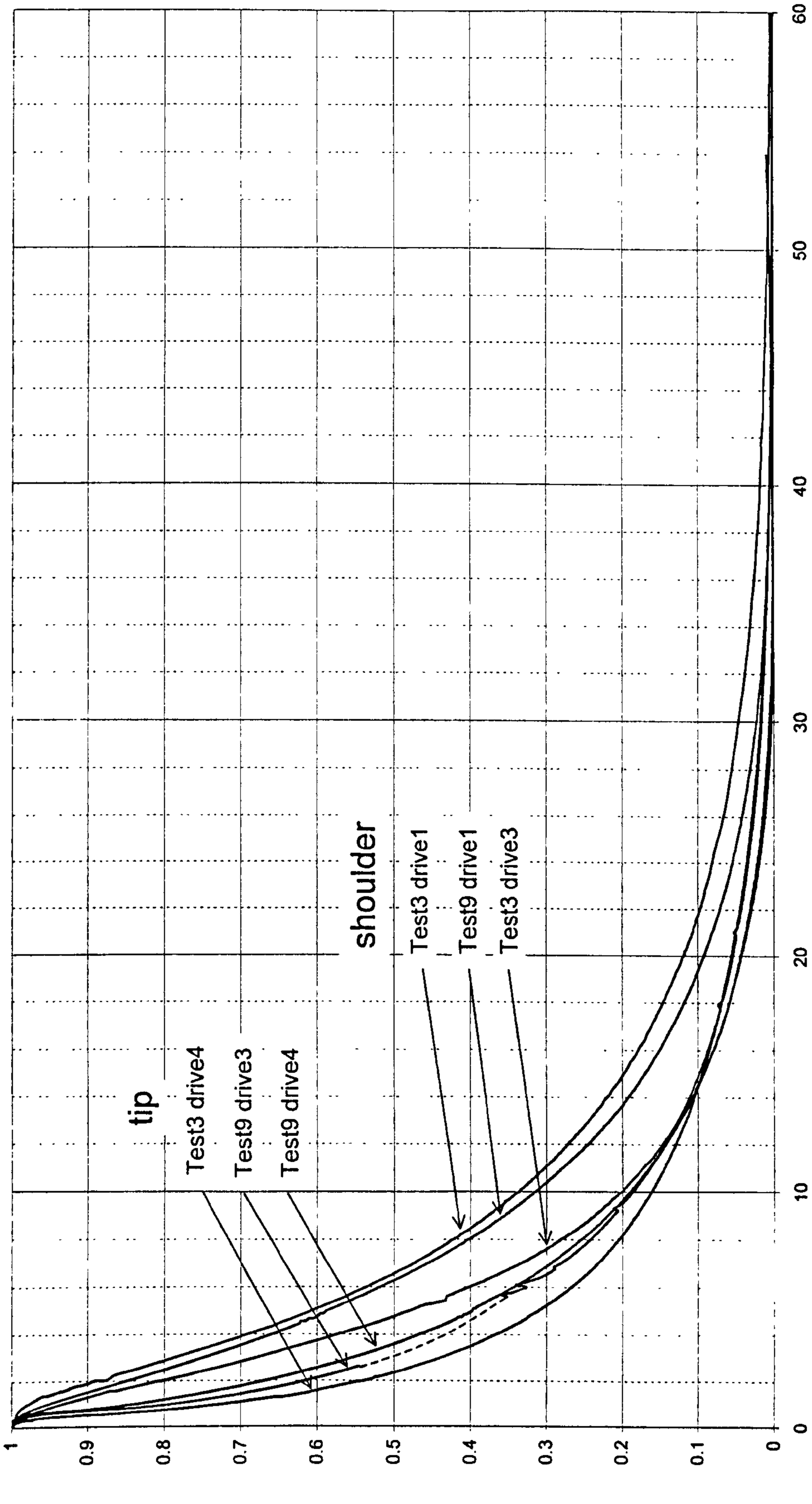

Figure 5.36 Piezocone dissipation tests in pure clay, square root of time

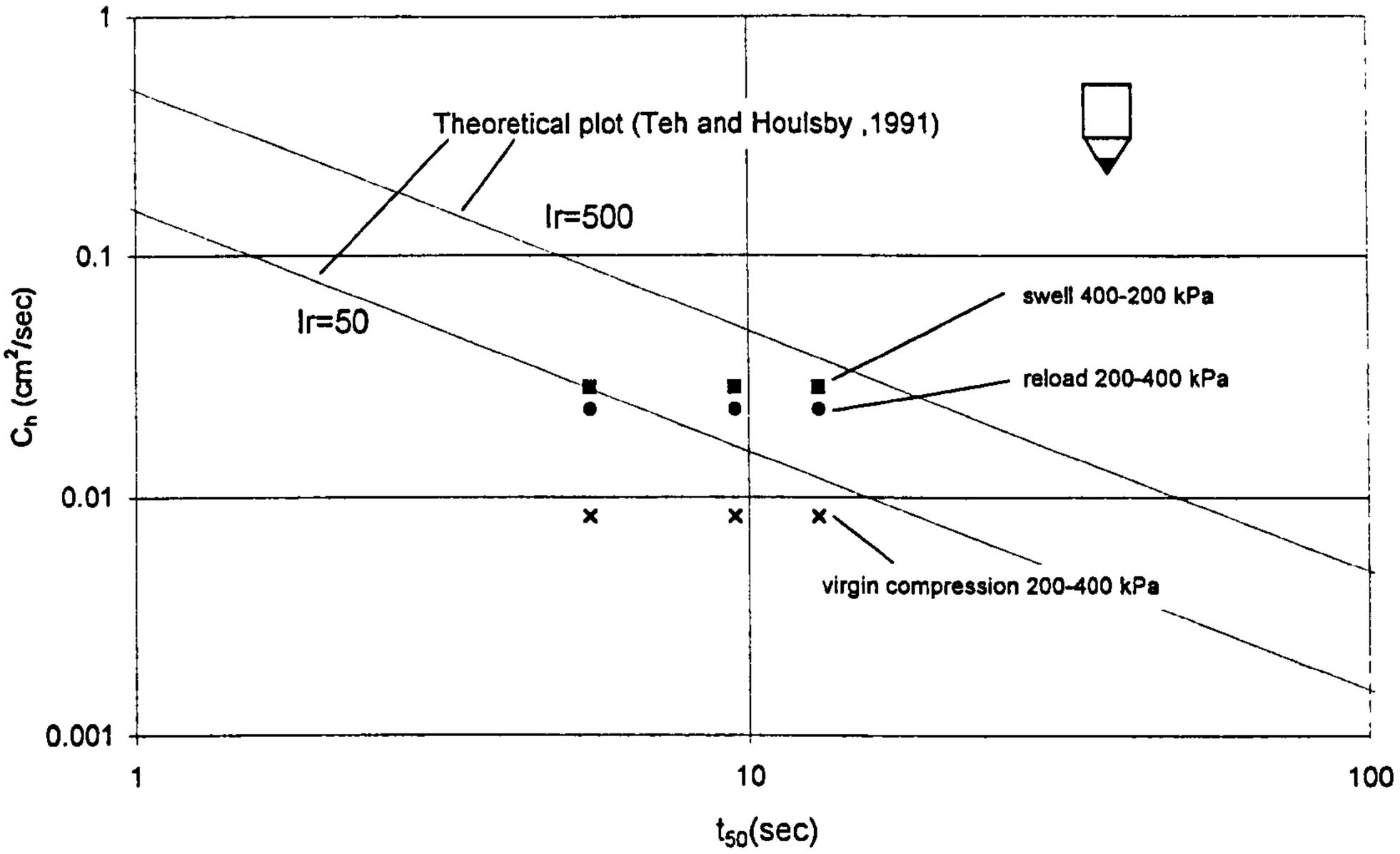

Figure 5.37 Values of c_h from Rowe cell tests related to piezocone dissipation measurments using the theory of Teh and Houlsby (1991) (tip filter in pure clay)

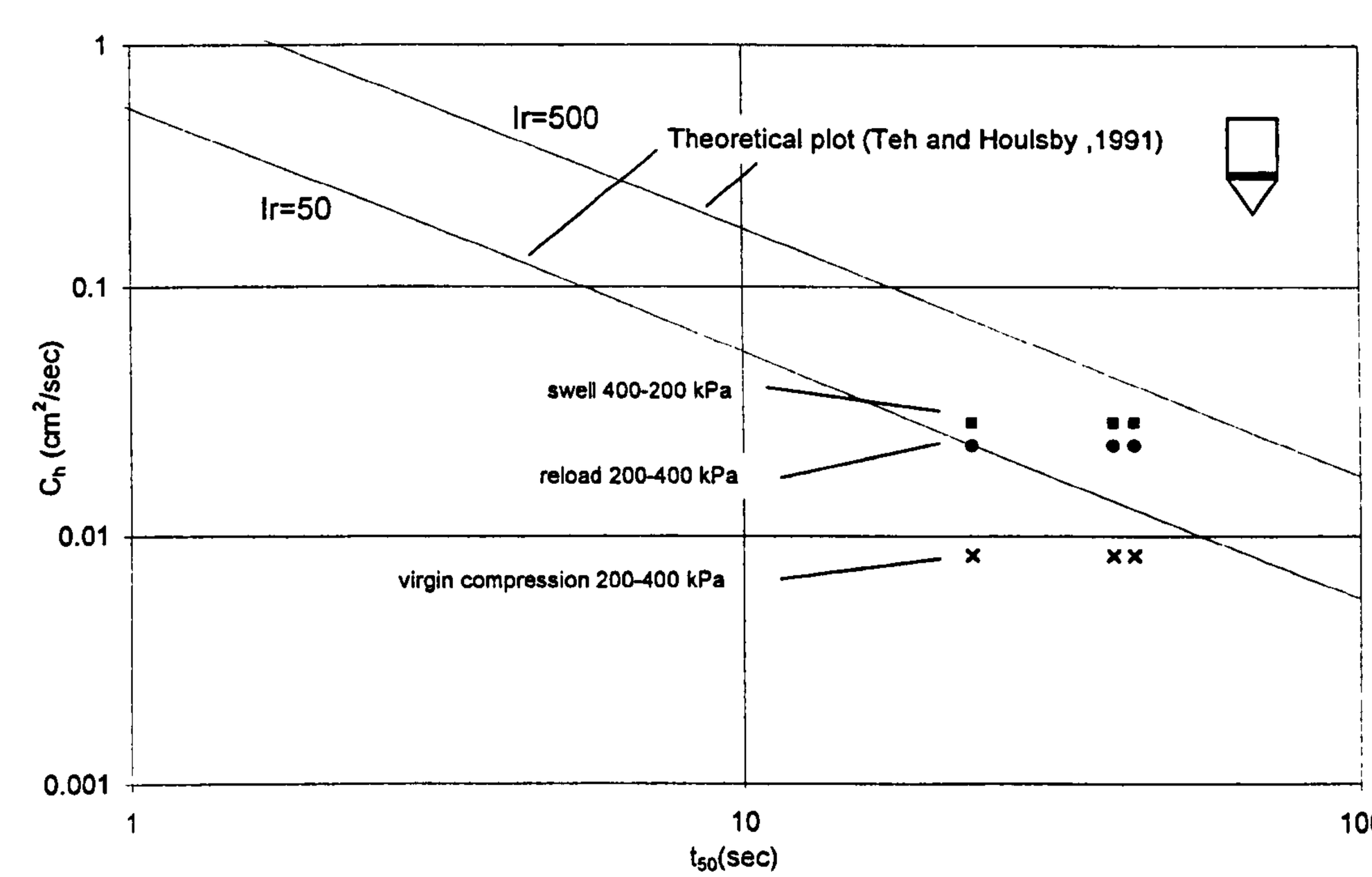

Figure 5.38 Values of c_h from Rowe cell tests related to piezocone dissipation measurments using the theory of Teh and Houlsby (1991) (shoulder filter in pure clay)

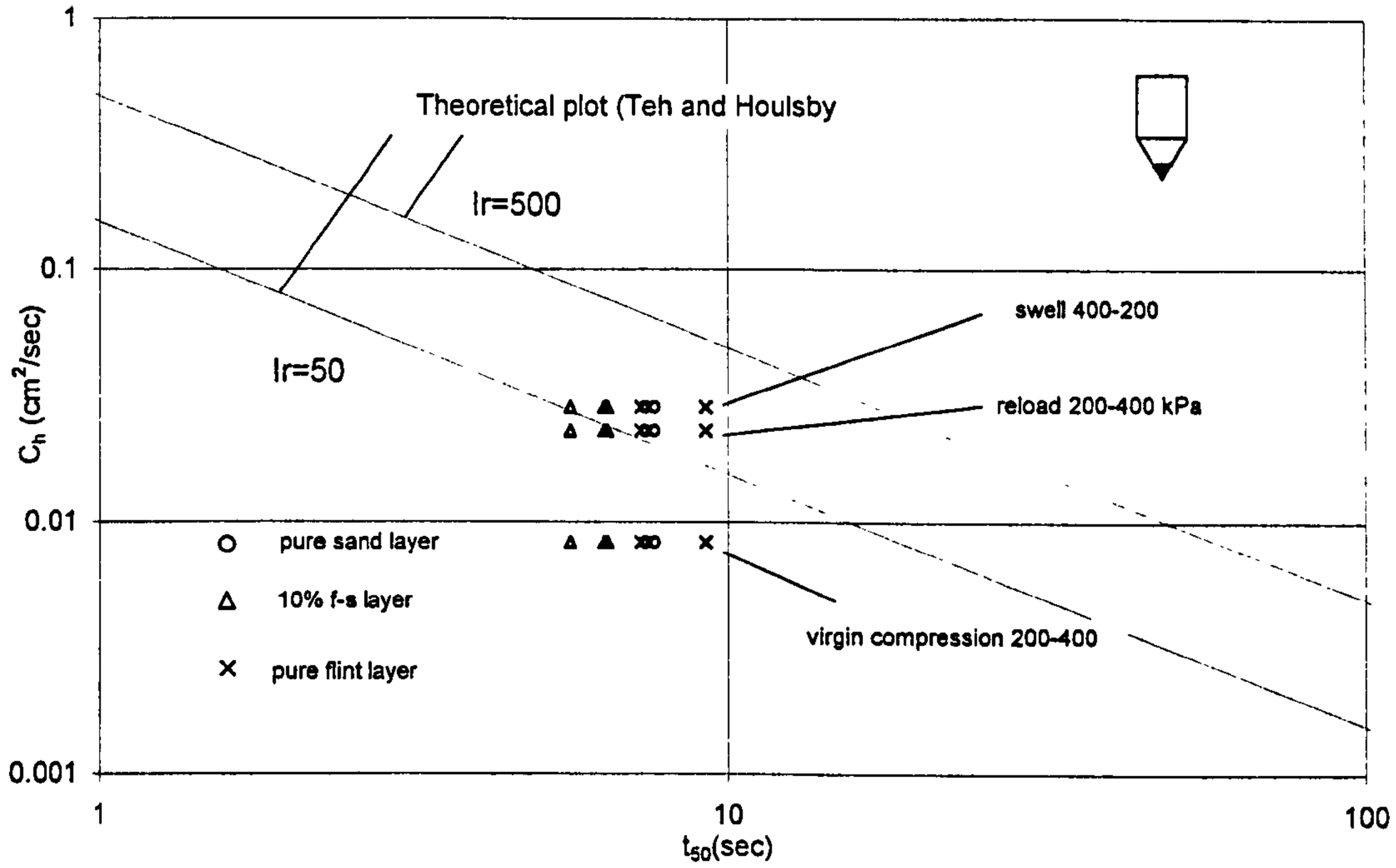

Figure 5.39 Values of c_h from Rowe cell tests related to piezocone dissipation measurments using the theory of Teh and Houlsby (1991) (tip filter in layered sample)

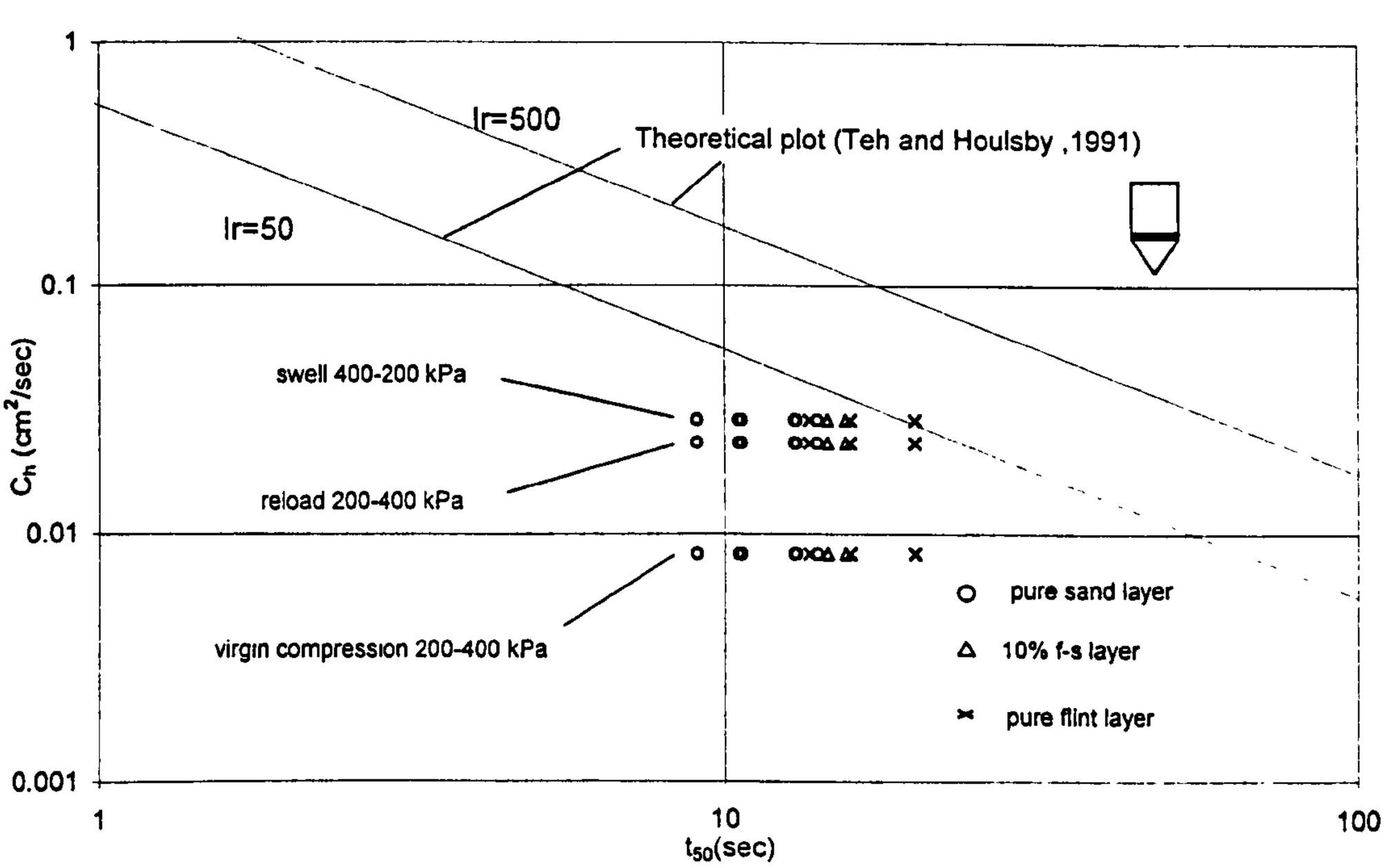

Figure 5.40 Values of c_h from Rowe cell tests related to piezocone dissipation measurments using the theory of Teh and Houlsby (1991) (shoulder filter in layered sample)

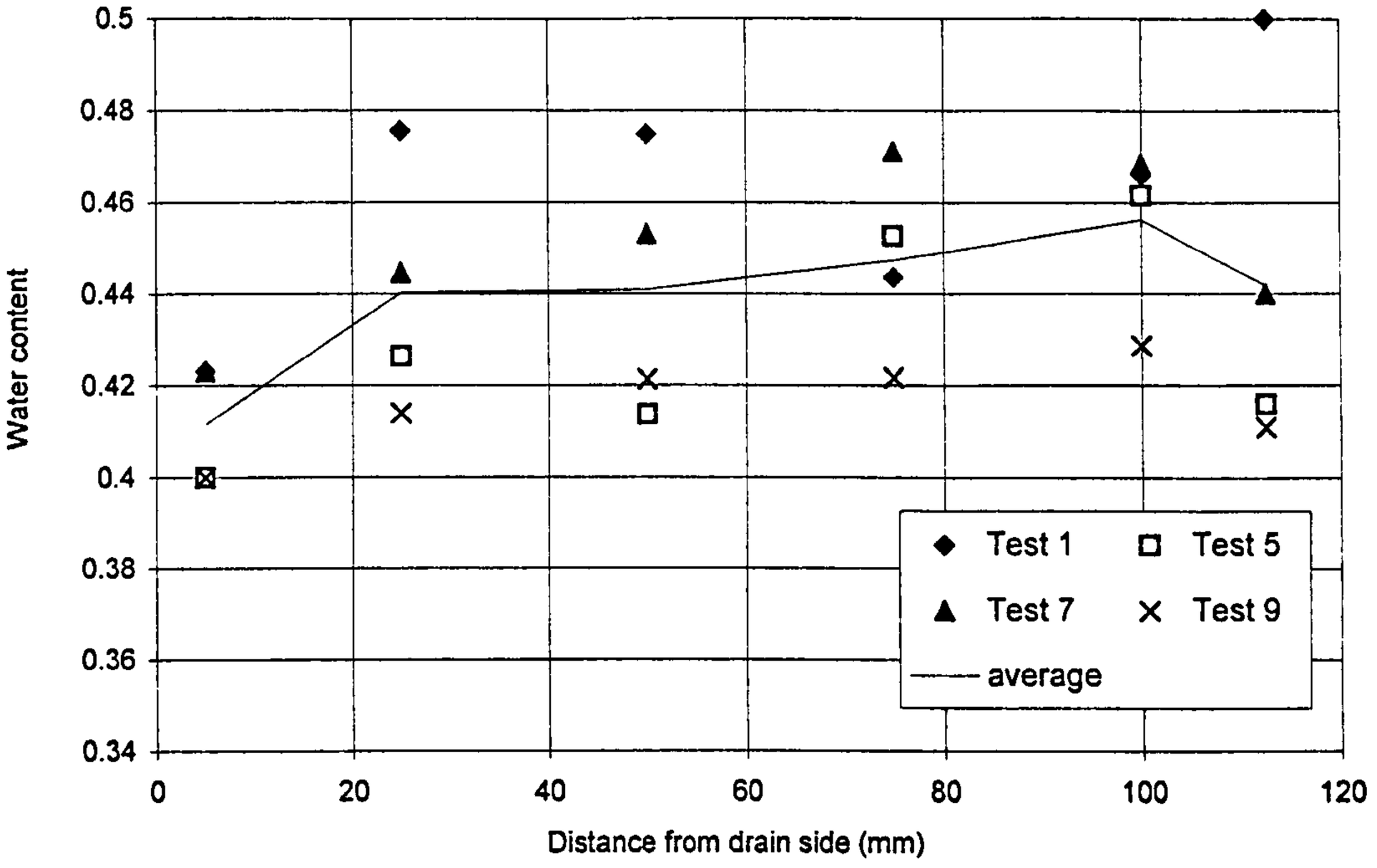

Figure 5.41 Final water content distribution in the samples with a circular drain

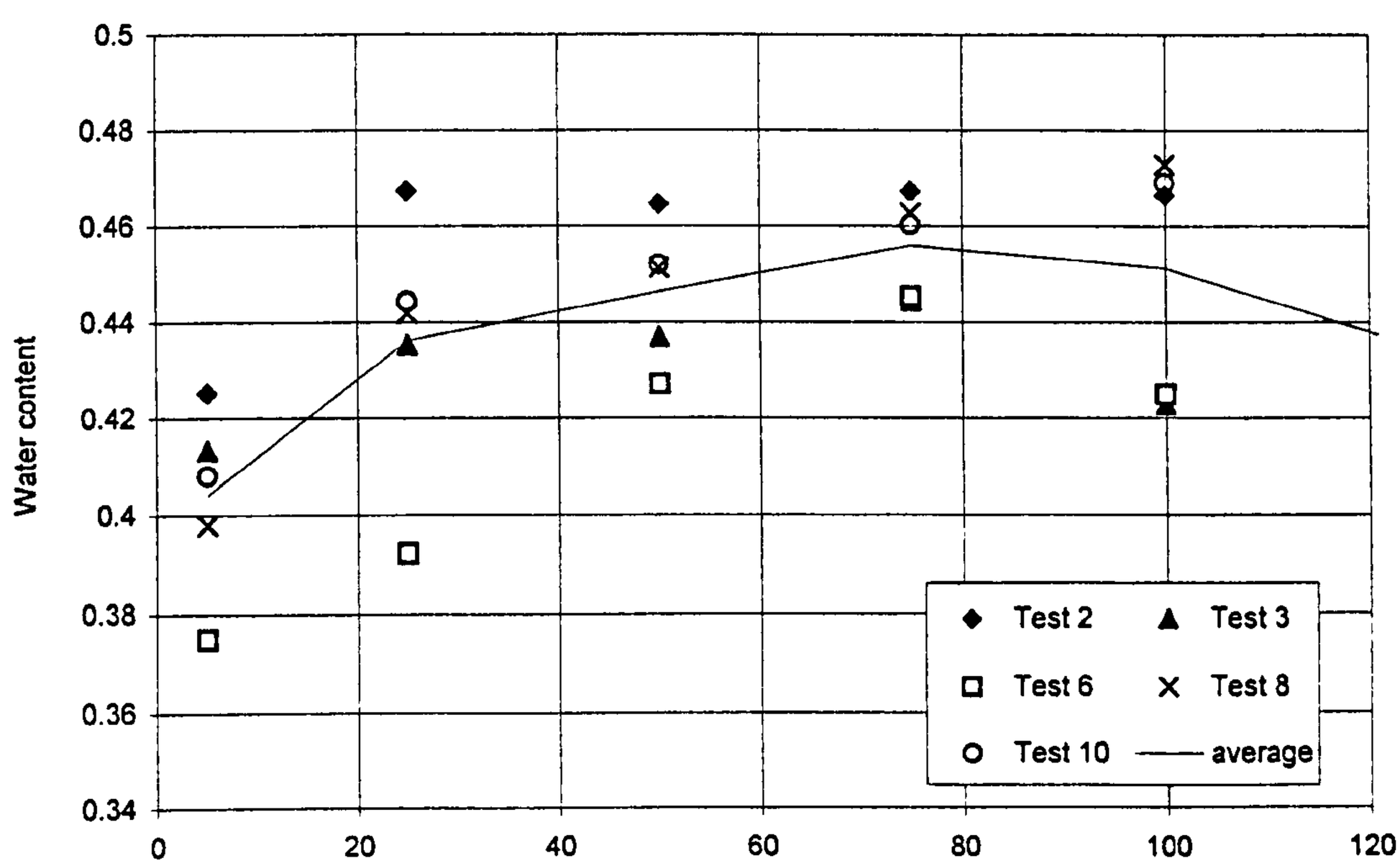

Figure 5.42 Final water content distribution in the samples with band drain

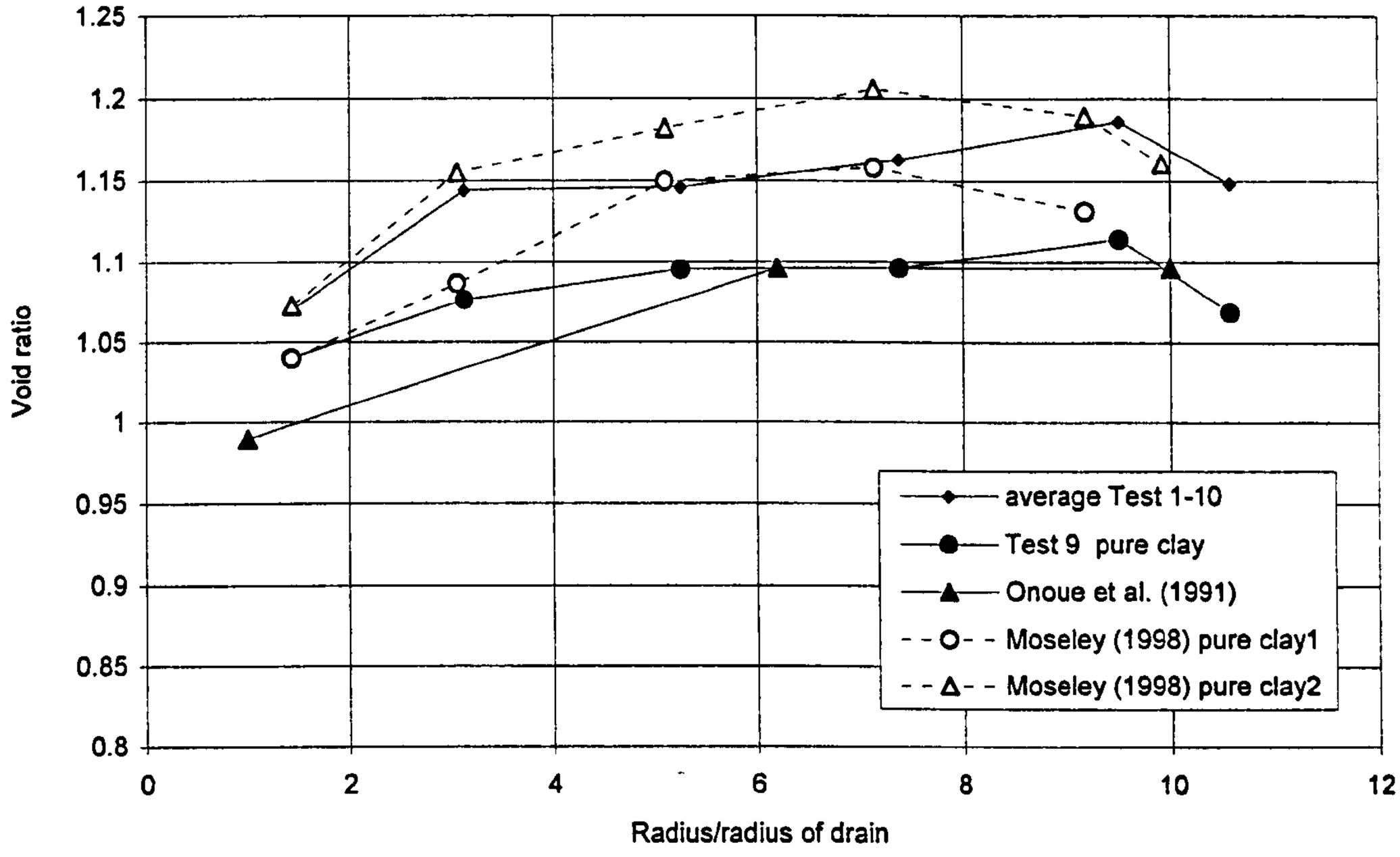

Figure 5.43 Comparison of void ratio distribution in clay in the samples with a circular drain

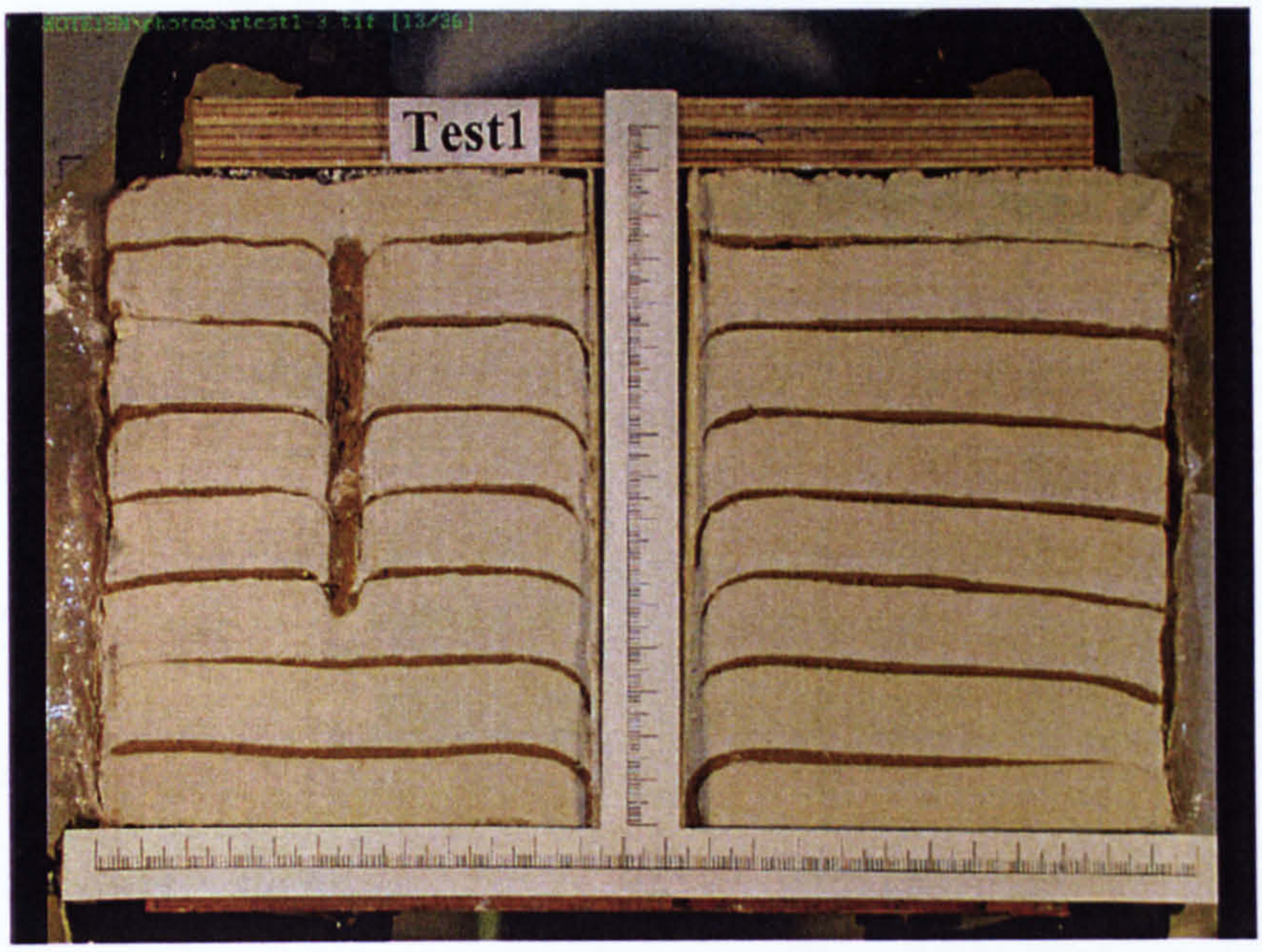

Note: piezocone drive hole visible on the left, infilled with sand

Figure 5.44 Section of sample with a circular drain (Test 1)

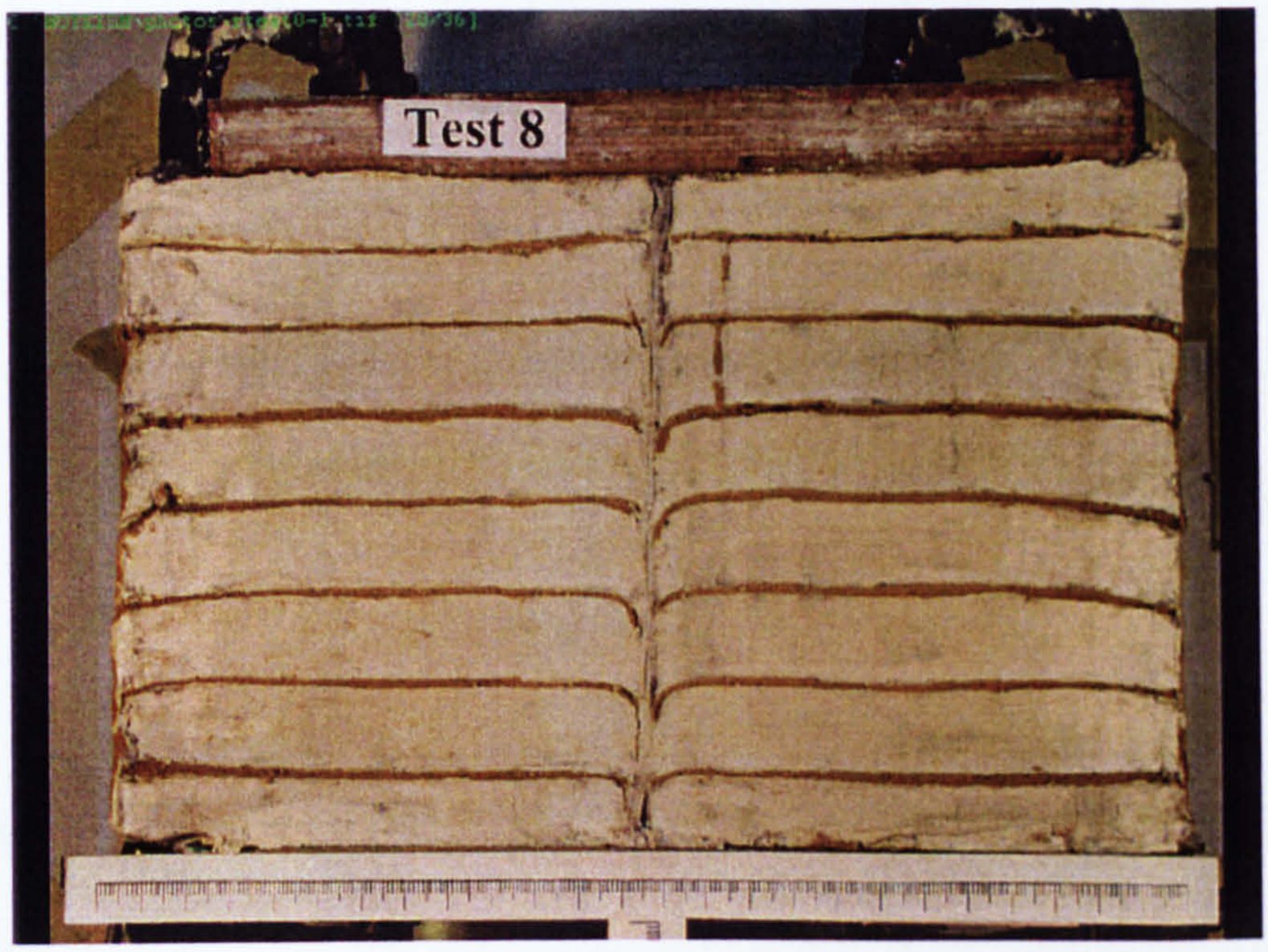

Figure 5.45 Section of sample with a band drain (Test 8)

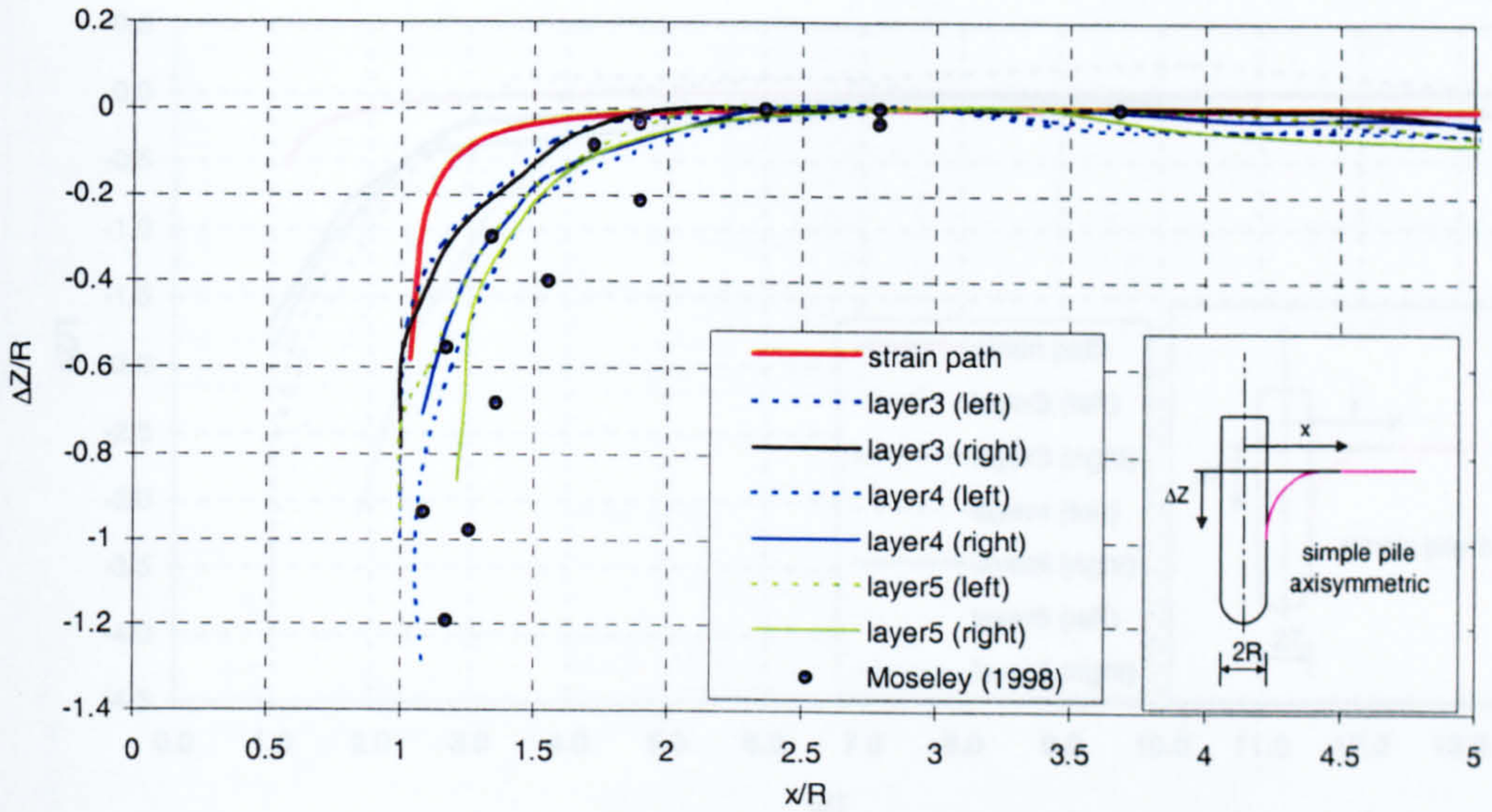

a) Test 5

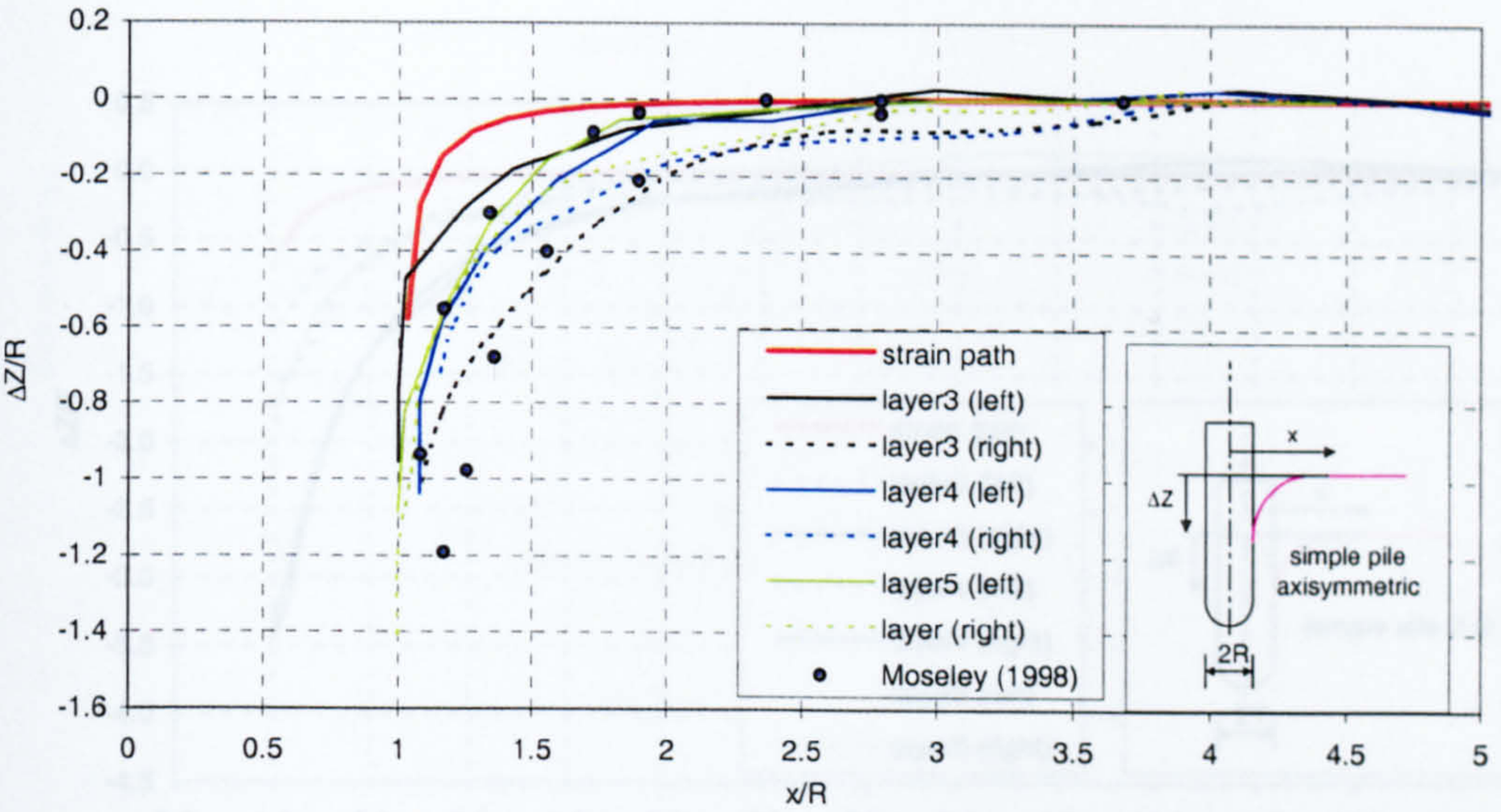

b) Test 7

Figure 5.46 Geometry of permeable layers penetrated by a circular drain

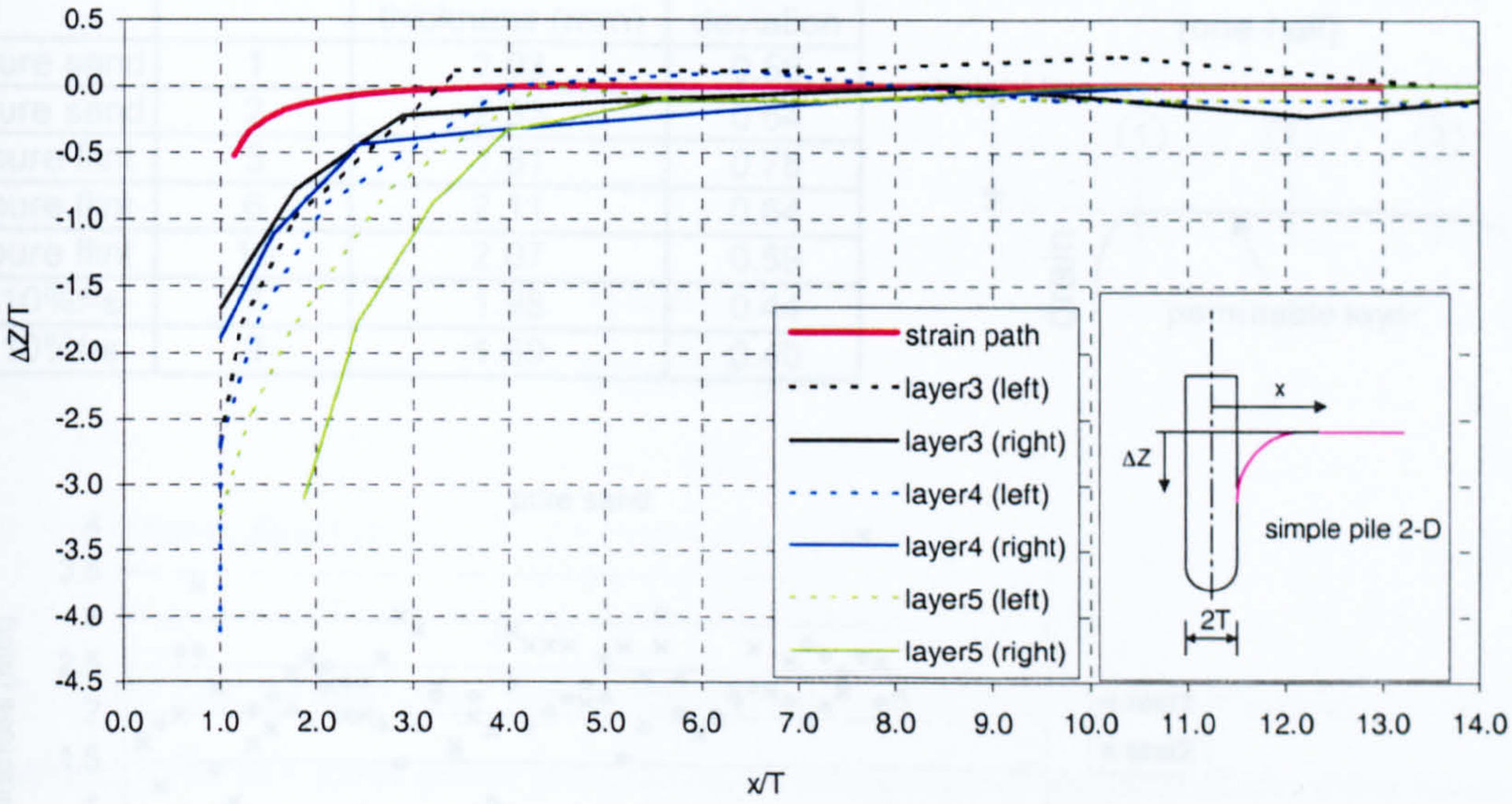

a) Test 6

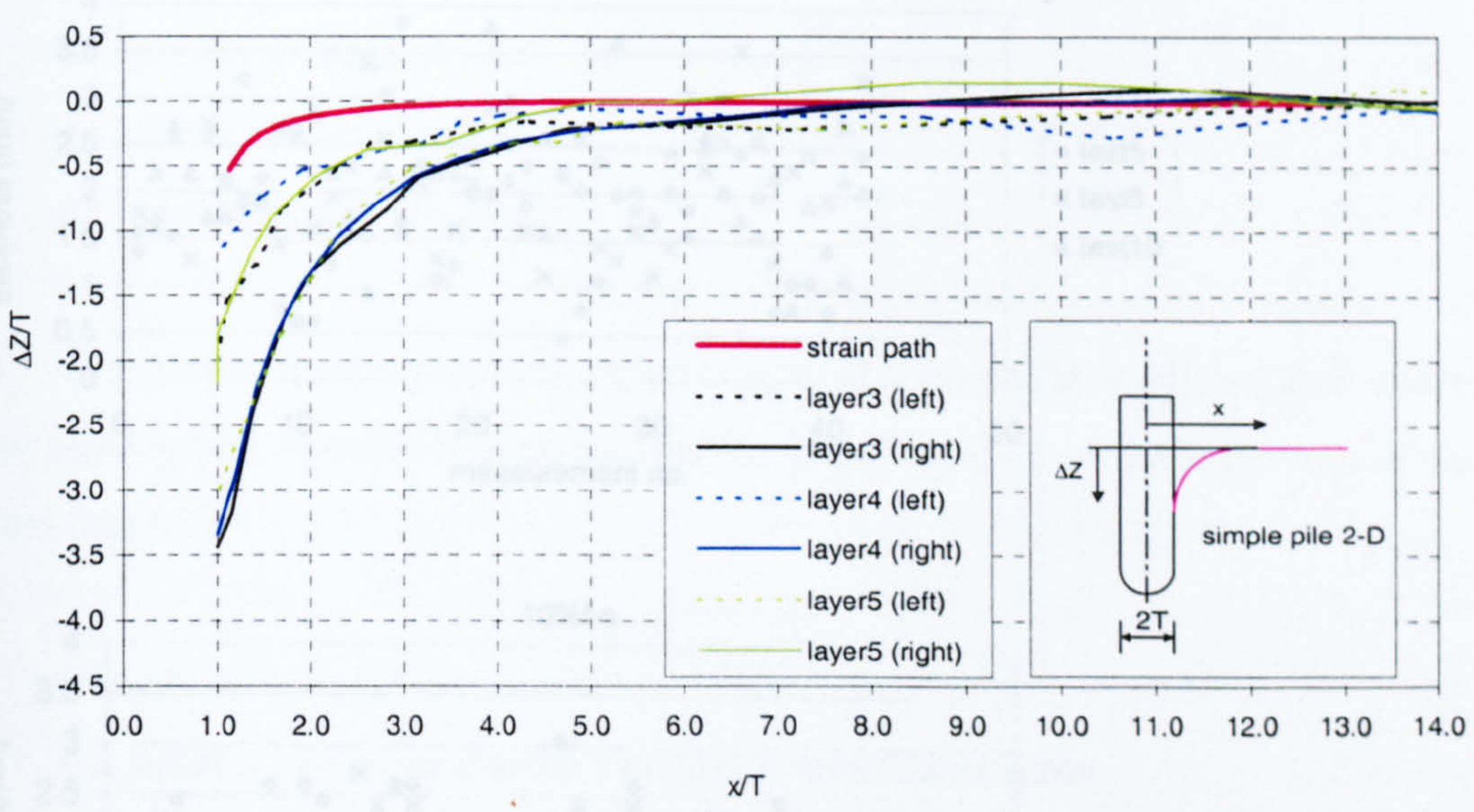

b) Test 8

Figure 5.47 Geometry of permeable layers penetrated by a band drain

Materials	test no.	average thickness (mm)	standard deviation
pure sand	1	2.03	0.56
pure sand	2	2.33	0.54
pure flint	5	1.81	0.78
pure flint	6	2.11	0.64
pure flint	10	2.07	0.59
10%f-s	7	1.98	0.44
10%f-s	8	1.89	0.40

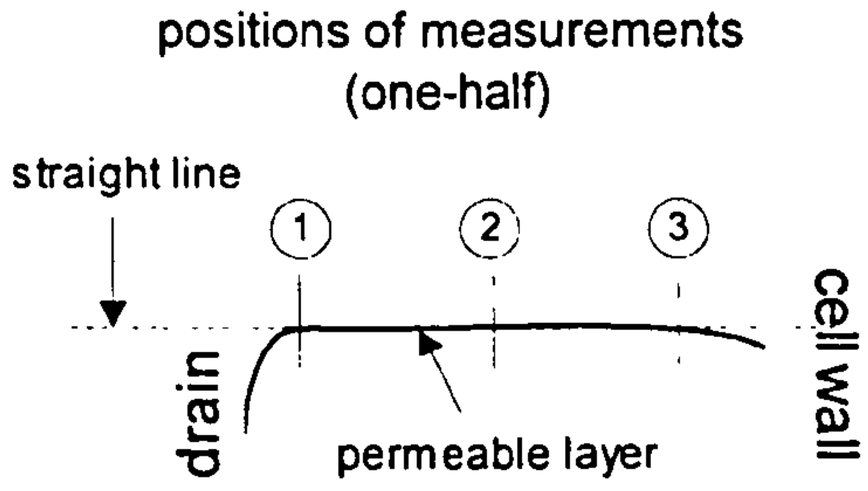

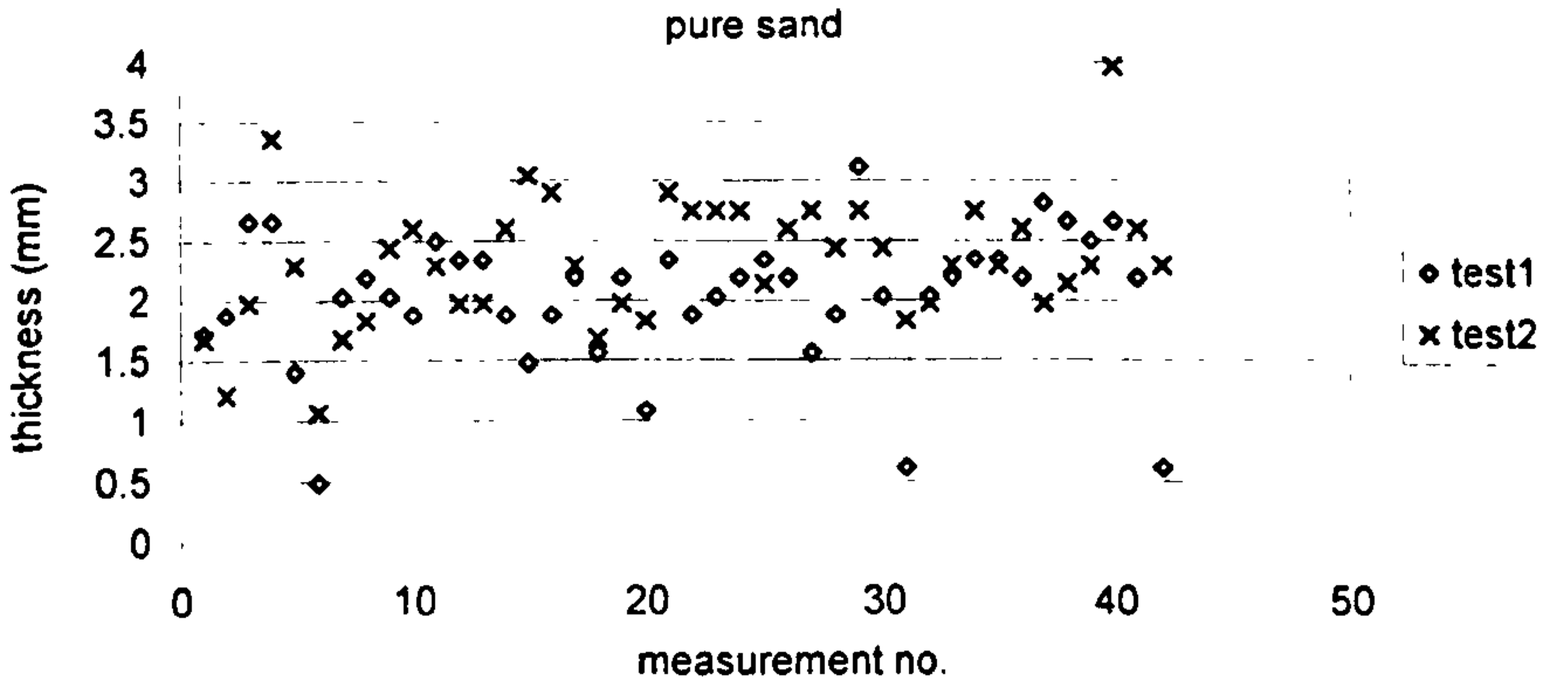

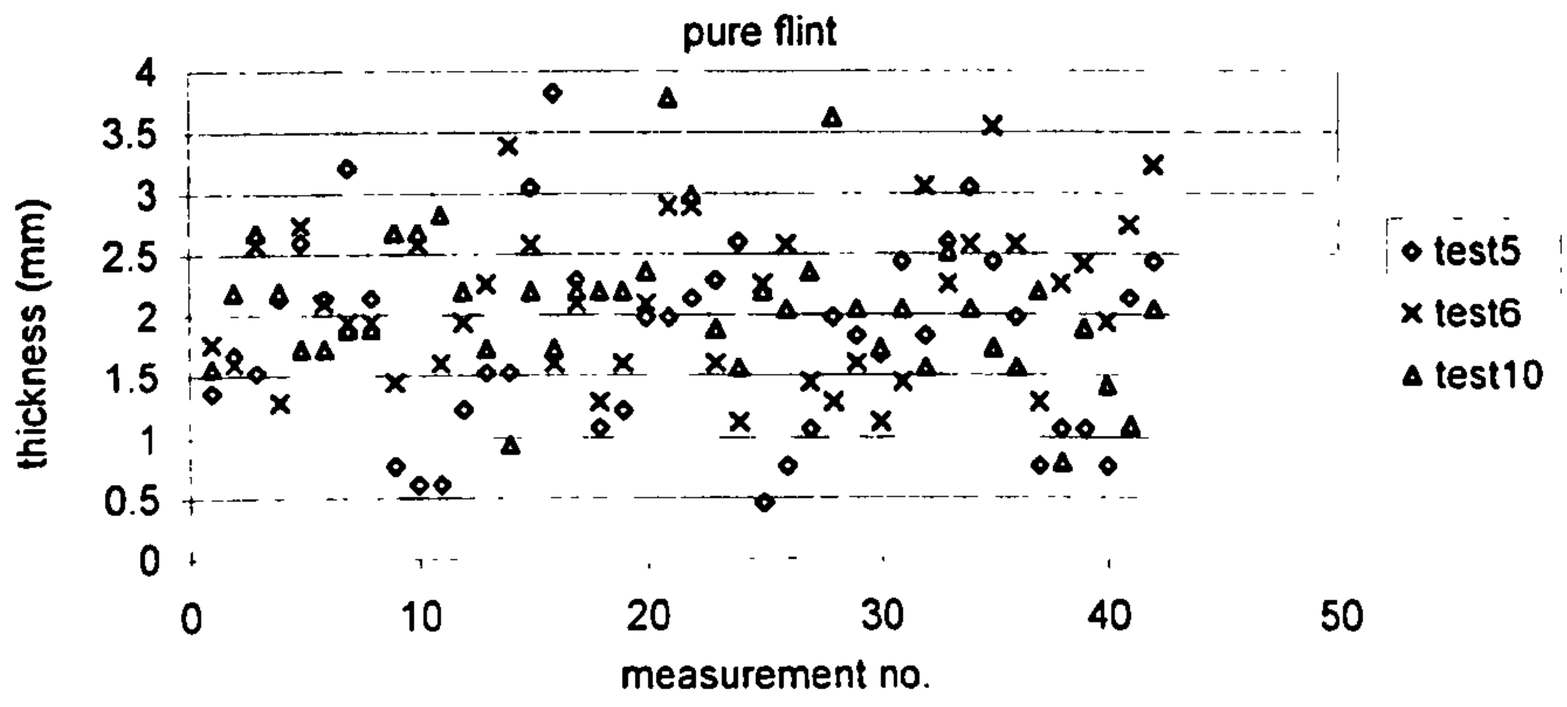

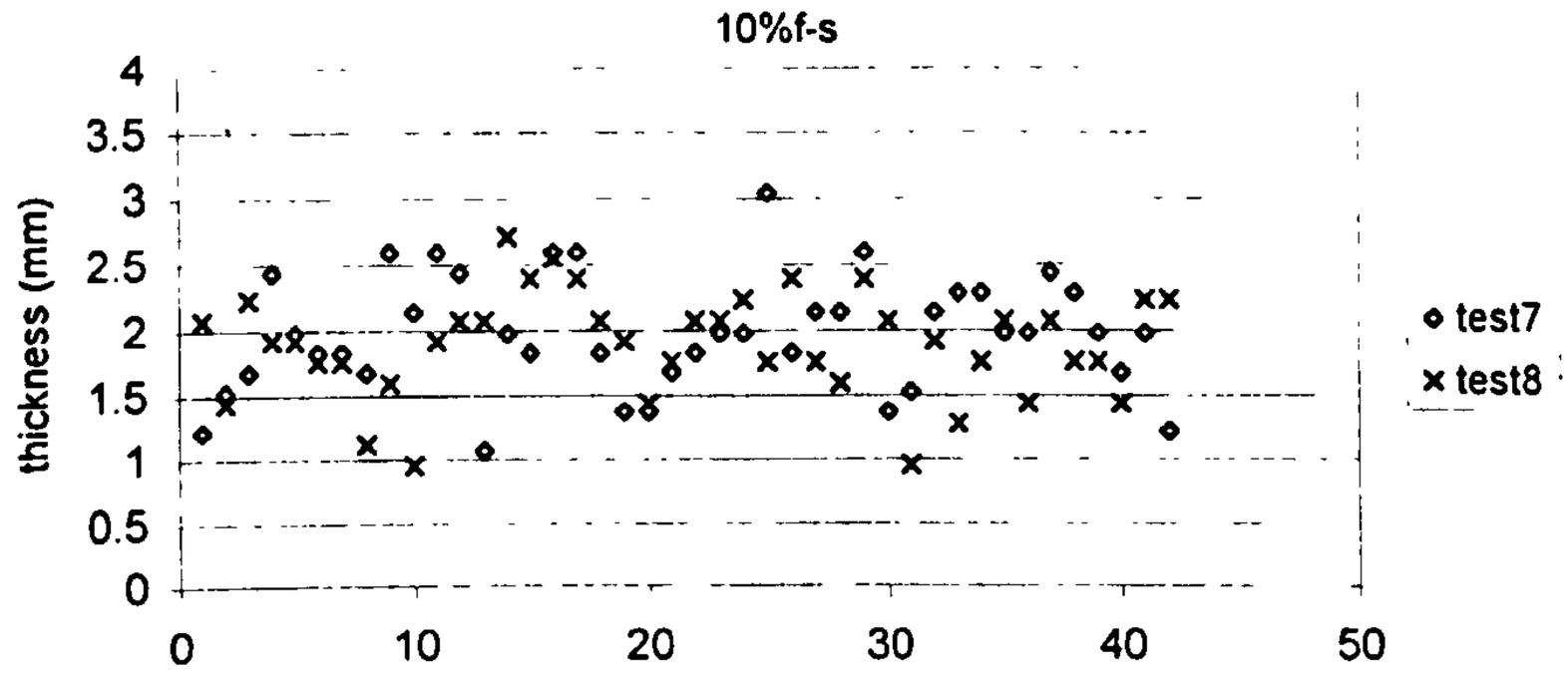

Figure 5.48 Permeable layer thicknesses

CHAPTER 6
DISCUSSION

6.1 Introduction

This chapter discusses the experimental results presented in Chapter 5. The discussion is in two main parts: the effects of smear due to vertical drain installation are discussed in Section 6.2, and the results of the miniature piezocone tests are discussed in Section 6.3.

In each part, there is discussion of the following:

- explanation the overall physical phenomena,
- practical implications,
- quality of test results,
- problems and limitations

Comparisons with previous experimental or theoretical work are also made, where appropriate, in order to demonstrate the improvements or contributions of the present research.

6.2 Effects of Smear due to Vertical Drain Installation

6.2.1 Physical effects of vertical drain penetration in soils

To quantify the effects of smear caused by installing vertical drains with different shapes into soil, band and circular drains were used as the penetrating objects (Section 3.3.11) and, to investigate the effects of the permeability ratio of the

layering materials on the degree of disturbance, materials with different permeabilities were used in constructing the soil samples.

The effects of smear were not only observed by performing the constant head distribution tests and permeability tests (Section 4.3.10) but also by visually investigating the deformation of the soil fabric after dissection of the sample (Section 4.3.12).

Figures 6.1 and 6.2 show close up photographs of horizontal sections through more permeable layers and clay layers penetrated by a circular drain and a band drain. The horizontal cut was made where the more permeable layer was curved down due to drain installation (i.e. approximately 6mm and 4mm below the original base of the permeable layer for the tests with the circular drain and the band drain respectively).

For the circular drain case (Figure 6.1), it can be seen that the more permeable layer curved down around the vertical drain is not continuous. Due to this non-uniformity (lack of symmetry), the more permeable layers do not all deform downwards to the same extent in the cross section (Figure 5.46). Moseley (1998) investigated the effects of smear due to the installation of a circular vertical drain in layered soil samples composed of clay and sand layers and also reported this phenomenon. He commented that the failure of the penetrated sand layers appeared similar to the so called "petalling" of metal plates penetrated by a rigid penetrator, as originally described by Backman and Goldsmith (1978). In this failure mode, as penetration proceeds, the plate bulges until its tensile strength is exceeded and star-shaped cracks develop. Then the individual sectors of the "star" are pushed back by the continuing motion of the penetrator to form the "petals". It should be noted, however, that this description is for penetration into a metal plate of which the material properties are very different from those of a sand layer.

For the band drain case (Figure 6.2), the more permeable material around the vertical drain is quite symmetrical and continuous. However, the more permeable layers still do not all deform downwards to the same extent in the cross section (Figure 5.47). This could be due to localised variation of the friction on the drain sheath and the thickness of the permeable layer (Section 6.2.4) in the area penetrated by the drain.

As reviewed in Chapter 2, several researchers have reported the effects of the shape of penetrating objects on the degree of disturbance of the soil. In the present research, the deflection of the thin sand layers in the layered sample was compared with the strain path solution (Baligh, 1985), for the deformations of uniform soil caused by deep penetration of a simple pile. Figures 5.46-5.47 show that the strain path solution underestimates the soil deformations. As pointed out by Baligh (1985), the surface roughness of the pile and viscosity of material surrounding the pile have been neglected in the analysis. The difference between the theoretical prediction and the experimental results was more obvious in the case of the band drain. This implies that the significance of friction effects for the overall deformation of the soil depends on the shape of the penetrating object. Deformation due to the displacement of the drain, in comparison with that due to frictional down-dragging, is more significant for the circular drain than for the band drain.

In Figure 6.3, using the trend line function provided in Microsoft Excel 97, lines were fitted to two sets of data points. The data points in each set represent the locations of three more permeable layers penetrated by a circular drain or a band drain. It can be seen that, although the equivalent diameter of the band drain (Sections 3.3.11 and 5.3.4) is comparable with the diameter of the circular drain, the overall magnitude of soil fabric deformation caused by installing the circular drain is more than that caused by installing the band drain. Consequently smaller smear effects were observed in the latter case.

Upon dissecting the sample and removing the porous plastic of the drain, it was found that a thin clay film covered almost the entire sample area contacted by the drain as illustrated for the circular drain in Figure 6.4. In the case of the band drain, when the drain was removed, parts of the clay film stuck to the drain and therefore the film could not be photographed. This phenomenon will be called "the smearing film" and can be attributed to the effect of friction between the drain sheath and the soil during the driving of the drain and the removal of the sheath.

Thus the smear zone in the soil surrounding the penetrating object consists of two major parts. The outer part is the deflected fabric zone caused by displacement of the soil. In this part, the degree of disturbance would be expected to be a maximum at the point closest to the drain and then decrease with distance. The inner

part is the smearing film caused by friction between the drain sheath and the soil. Figure 6.3 shows that the overall degree of smearing in the outer part depends on the shape of the drain. On the other hand, the smearing film may not be influenced by the drain shape but possibly depends on amount of friction between the soil and the drain. Effects of the smearing film are discussed below in Section 6.2.2.

6.2.2 Practical implications

The degree of smear due to drain installation in the soil sample was experimentally measured in terms of the change of permeability of the soil (Section 5.3.4) and the head loss in the smear zone, based on the pore water pressure distribution across the sample (Section 5.3.3).

Two independent parameters, h_s and r_s, were calculated to quantify the smear effect (Section 5.3.5). Theoretically, the values of both h_s and r_s should be the same providing the smear is consistent throughout the sample. A difference between h_s and r_s was possible because, to determine h_s, the pore water pressures were taken from only one permeable layer and differences in the degree of smear in each permeable layer could produce a variation in h_s.

Figures 5.19 and 5.20 show that at a given permeability ratio, the values of h_s and r_s of the band drain are lower than those of the circular drain. Therefore, the band drain does not only produce more uniform punching behaviour but also causes less disturbance to the penetrated soils. For both the band drain and the circular drain, it was shown in Figures 5.19 and 5.20 that h_s and r_s increased as the permeability ratio increased. Tentative curves expressing the relationships have been drawn in these two figures. Head losses due to the drain installation do not vary much where the permeability ratios (k_r) are between 1 and 100. Then they vary significantly with permeability ratios between 100 and 10000. At high permeability ratios a levelling off is observed, especially in the case of the circular drain.

For a layered sample, with known ranges of k_h of materials (Table 5.4) and assuming that for each material (the more permeable material and the clay) k_v is equal to k_h, the permeability anisotropy ratio of soil mass, r_k, (Section 2.2) can be estimated. The estimated r_k of samples with pure sand, 10%f-s and pure flint layers

are 673 to 897, 113 to 135 and 7.6 to 9.8 respectively. It can be seen that the realistic ranges of r_k of varved clays or laminated soils, as reviewed in Chapter 2, are comparable to that of the samples with pure flint layers but less that those of samples with sand and 10%f-s layers. As illustrated in Figures 5.19 and 5.20, the degree of smear due to drain installation is not much different in pure clay and flint layers. This implies that, for natural soils containing pure clay or thin permeable layers for which k_r is less than 100, the head loss due to smear in in-situ permeability tests should be in a range of 35%-45% for a circular piezometer with a comparable size to the laboratory device. If the soil contains thin more permeable layers producing a higher k_r, i.e. pure sand layers, the head loss due to smear could be much higher. However, in this case, Hird & Moseley (2000) reported that the thicknesses of the more permeable layer and clay layer could influence degree of smear.

For pure clay samples, in which there were no effects of differential smear of permeable layers, in the circular drain case, h_s is about 11% lower than r_s. For the band drain, r_s is about 44% lower than h_s. However, in the band drain case, it was found that this difference would reduce to 10% if the R/r_w (Section 5.3.4) of the band drain was reduced by 15% (i.e. from 8.59 to 7.30).

As described in Section 6.2.1, the smear zone in the soil surrounding the penetrating object consists of two major parts, the deflected fabric zone and the smearing film. It is difficult to define the effect of these two parts on h_s and r_s separately, because the permeability and size of each part could not be easily determined.

However, the head loss due to a smearing film in the sample can be investigated by assuming its permeability and thickness and calculating the head loss generated while the water is flowing through it with a given flow rate. Figure 6.5 presents the effect of a smearing film in the layered soil samples. In the analysis, the horizontal permeability of the smearing film is assumed to be 1×10^{-9} m/sec (approximately half of the horizontal permeability of the undisturbed kaolin). The flow rates measured in typical permeability tests on soil samples with different layering materials were used in the simulation. With a given flow rate, the head loss across the smearing film was calculated and then normalised by the corresponding applied head difference. The thickness of the film was varied to make the head loss vary between approximately

50% and 90% of the applied head difference. Figure 6.5 shows that, with the assumed permeability, a very thin film could by itself have produced the head losses observed in the tests. It should be noted that, in reality, the horizontal permeability of the film could be different from the assumed value because, during drain installation, kaolin around the drain may be mixed with the material of the more permeable layers.

With a given size of drain or piezometer, it is considered likely that the effects of a smearing film will be less as the penetrated more permeable layers become thicker. This is consistent with the trend reported by Hird & Moseley (2000).

6.2.3 Repeatability of test results

In order to check the repeatability of the test results, four tests in the present research and results from three tests carried out by Moseley (1998) and reported by Hird & Moseley (2000) were compared. Furthermore, in each soil sample, the permeability test was repeated at least four times with different applied heads across sample. It was found that, in accordance with Darcy's law, the flow rates were proportional to the applied heads. For the whole set of permeability tests, 37 tests in total, the average variation of the permeability values measured at different applied heads was only 3.1% of the corresponding mean value. The permeability values presented in the following section were the average values from tests on each sample.

For the sample with pure sand layers (Test 1 in Table 5.4), the measured permeability of the sample installed with a circular drain was 1.47×10^{-6} m/sec. Moseley (1998) carried out two tests using the same testing procedures and layered sample materials. The measured permeabilities in these tests were 1.34×10^{-6} m/sec and 1.28×10^{-6} m/sec. Based on the measured pore water pressure distribution (Section 5.3.3), the normalised head loss due to smear, h_s, caused by drain installation was 0.95 in Test 1 (Table 5.4) compared with 0.91 and 0.914 in the previous research. Furthermore, in these tests, the permeability of the sand layers was estimated (Section 5.3.4) by using the pore water pressure distribution across the

sample and found to be 1.65×10^{-5} m/sec in Test 1 (Figure 5.18) compared with an average of 1.50×10^{-5} m/sec in the previous research.

For the pure clay sample (Test 9 in Table 5.4), the permeability result, $k=1.16 \times 10^{-9}$ m/sec, was also comparable with that reported by Hird & Moseley (2000), $k=1.31 \times 10^{-9}$ m/sec. In these tests, the corresponding normalised head losses due to smear, h_s, were 0.34 and 0.33 respectively. The permeability of the clay estimated by using the pore water pressure distribution in Test 9 was 1.91×10^{-9} m/s, while the value reported by Hird & Moseley (2000) was 1.90×10^{-9} m/sec.

For two of the layered samples with pure flint layers (Test 6 and Test 10 in Table 5.4), a band drain was installed at the middle of the sample. To estimate the whole sample permeability, an equivalent diameter of the drain was assumed, based on FEM analysis (Section 5.3.4), and the water flow was assumed to be only in the flint layers. The permeabilities from these two tests were comparable, ($k=1.30 \times 10^{-7}$ m/sec in Test 6 and $k=1.24 \times 10^{-7}$ m/sec in Test 10). In terms of the pore water pressure distribution (Figure 5.16), some variation between these two tests was observed. The normalised head losses due to smear in Test 6 and test 10 were 0.166 and 0.310 respectively. As discussed in Section 6.2.2, because the pore water pressures were measured in only one permeable layer, a difference in the degree of smear due to drain installation in each layer could produce a variation in the h_s value.

It can be seen from the above comparisons that, in terms of the measured sample permeability, the results showed very satisfactory repeatability. In terms of the pore water pressure distribution across the sample, a lack of repeatability was occasionally observed, presumably because of differences in the degree of smear and local non-uniformity of the layers (Section 6.2.4).

6.2.4 Experimental problems and limitations

a) Head loss across peripheral drain

As mentioned in Section 5.3.3, pore water pressure readings across the sample were sometimes affected by a head loss at the peripheral drain. This head loss could be attributed to:

- smearing of clay on the peripheral drain.

It was found that this phenomenon could happen as the clay layers were placed into the test cell during the layered sample construction. Providing greater clearance between the drain and the soil could minimise this problem.

- smear at periphery due to consolidation.

After being assembled, a soil sample was consolidated in the test cell which was lined with porous plastic (Section 3.3.2). Evidence of friction generated during consolidation was observed during the sample dissection (Section 4.3.12). Figures 5.44 and 5.45 show that, at the periphery, the more permeable layers were curved due to the friction between the sample and the porous plastic.

- migration of suspended kaolin into the more permeable layers.

During layered sample preparation (Section 4.3.6), entrapping of clay particles in more permeable layers was countered by siphoning water with suspended kaolin out and replacing it with clean water before placing a more permeable layer. However, it was not possible to replace all the water and some kaolin could still have been trapped in the permeable layers, especially at the periphery where the water entered the layers.

b) Deformation of the top permeable layer

It can be seen from Figure 5.44 that the deformation of the uppermost permeable layer in the sample with a circular drain was not similar to that of the other more permeable layers. This phenomenon happened because, during the vertical drain installation, some kaolin from the top clay layer was forced into the gap between the drain and the cell base (now at the top of the sample). Therefore, there was not enough confined kaolin to push down the first permeable layer and form the "deflected fabric zone" (Section 6.2.1). In the samples tested by Moseley (1998), who had noted this phenomenon, the first clay layer was only 10mm thick. In order to reduce the effect in the present tests, the thickness of first clay layer was increased to 20mm. It was expected that the first permeable layer would still be smeared because of the formation of the "smearing film" (Section 6.2.1) as the drain was driven in and the sheath removed. Unfortunately, as also mentioned by Moseley (1998), this first layer was disturbed as the sample was separated from the cell base.

Therefore, the smearing film was usually disturbed and could not be clearly observed. Nevertheless, evidence of acceptable smear at the first permeable layer can be seen in Figure 5.19. If the first permeable layer had been smeared considerably less than the others, the reduction of the overall permeability (r_s) would have been much less than the head loss (h_s) based on the pore water pressure distribution measured in a more permeable layer near the mid-depth of the sample, especially for the cases of the layered samples with pure sand layers and 10%f-s layers. Such a difference was not observed.

For the band drain case, a very small amount of clay was forced into the gap at the top during the installation and, after the sample dissection, it was seen (e.g. Figure 5.45) that the deformation of the first permeable layer was not very different from that of the other layers.

c) Formation and uniformity of permeable layers

More permeable layers of pure sand, 10%f-s and pure flint were prepared in acrylic moulds as described in Section 4.3.3-4.3.5. Uniformity of thickness and density of the layers was aimed for in the preparation. To achieve these requirements, the material was sprinkled evenly into the mould, vibrated to densify it as much as possible and then frozen to prevent disturbance during placement in the test cell.

Thickness data for the permeable layers was presented in Figure 5.48. It can be seen that all the permeable layers, especially the pure flint, had a significant thickness variation, although the average values of thickness are not very different from the expected values (Section 5.2.2). Possible causes of the non-uniformity of the permeable layers could be as follows.

- Before freezing, movement of the materials in the mould during handling could have occurred, especially in the case of the pure flint, for which the mould lid did not directly press on the surface of the material.
- During the freezing process, ice crystal generated due to expansion of the water could have produced localised non-uniformity in the layers.

- Placement of the upper clay layers during sample assembly could have generated movement of the free water in the cell and, therefore, disturbed the de-frozen permeable layers already placed.

d) Segregation in 10%f-s layers

In the preparation of pure sand layers (Section 4.3.3), it was intended to minimise particle segregation by avoiding the use of gap-graded material (see Figure 3.1 for particle size distribution). After sprinkling the sand into the mould, a wide-toothed comb was dragged through the sand, not only to level the sand but also to produce more uniformity. For the flint layers, again, gap-graded material was avoided (see Figure 3.1). The flint slurry de-airing method (Section 4.3.4), in which a spinning magnet was used, coupled with wide-toothed comb dragging of slurry in the mould, encouraged uniformity in the flint layers.

In the case of 10%f-s, in order to get a required permeability, sand and flint were mixed. Due to the different particle sizes of these two materials, segregation in 10%f-s was considered to be potentially more likely. As described in Section 4.3.5, these two materials were mixed in a dry condition before they were mixed with de-aired water and vacuumed. To reduce potential segregation, the amount of water put into the mixture was kept as small as possible. Again, the spinning magnet was used during de-airing and, after the mixture was put into the mould, the wide-toothed comb dragging was performed. Once the material was in the mould, the cell lid was put in place and a slight pressure was applied to reduce the water content in the material and, therefore, minimise the risk of segregation.

Consideration of the permeable layer permeability data obtained using several test methods (Figure 5.18) shows that, for pure sand and pure flint layers, the horizontal permeability tests performed on the pure material provided the highest values, while the falling head tests gave lower values close to those predicted by the pore pressure probe readings in the layered samples. However, all these values were within approximately plus or minus 30% of the mean value.

However, for the 10%f-s, it was found that the values obtained from the falling head tests and the probe readings were much lower than that obtained from the horizontal permeability test. It was supposed that this phenomenon was due to

segregation. In the case of the falling head tests (Section 4.2.1), to prepare a sample, the material was uniformly sprinkled through water with a depth of less than 10mm in the test cell. Nevertheless, during this process segregation may have occurred and produced alternation of low permeability and high permeability layers in the cell. The layers of low permeability material would then have dominated the overall vertical permeability of the sample. In the case of the layered sample, due to segregation, a 10%f-s layer could have presented a horizontal permeability lower than that of a similar layer in the horizontal permeability test. This is because, in the layered samples, segregated 10%f-s layers could have had a high possibility of being subjected to clay particle migration. If the clay particles had migrated, even in a very small quantity, into the higher permeability part (presumably the lower part) of a layer, the overall permeability of the layer would have been greatly decreased.

e) Limitations

The most important limitations of the experiments to investigate the effects of smear due to vertical drain installation are that the effects of the sample configuration have not been studied and that the scaling relationships to larger vertical drains have not been established.

As reviewed in Chapter 2, Hird & Moseley (2000) reported that, in a layered sample with pure sand layers, the smear increases as the clay layer thickness, the sand layer thickness or the driving speed reduces. In the present research, variations of sample configuration (i.e. layer thickness) have not been studied. Only the permeability ratio of the layering materials was varied, while the thickness of the clay and the permeable layers, and the size of the drain, were kept constant. Furthermore, in the present research, the samples were confined under a single effective stress of 250kPa. The effects of a variation in stress level and over consolidation ratio (of the clay) have not been studied.

In terms of scaling relationships, the drains used in the present research are smaller than the drains used in the field, i.e. sand drains and pre-fabricated vertical drains. Although they are not geometrically scaled down from any particular drain used in practice, they could still be considered as small scale models for which it would be desirable to correctly scale the stresses and times of the installation event.

Generally in the physical modelling of geotechnical problems, if all the linear dimensions in the model have been reduced N times, in order to get the same stresses at equivalent depths of the model and full-scale soil (prototype), gravitational acceleration in the model must be N times the normal value (Atkinson, 1993; Powrie, 1997). This can be achieved using a centrifuge. However, in the present research, stresses in the samples were controlled using laboratory pressure systems (Section 3.3.12), and could be taken to represent conditions at a given depth.

For the times, i.e. the speed of installation, Steenfelt et al. (1981), referring to model pile tests in clay, stated that, since dissipation of pore pressure occurs at a rate inversely proportional to the square of the linear scale, the installation time of a model pile should be equal to the installation time of a full-scale pile divided by a factor of N^2. This implies faster absolute driving rates in the model (by a factor N) than in the field. In the present research, the vertical drain installation speed was kept at approximately 5mm/s which was actually lower than those used in the field (typically 150-500 mm/sec). Due to the limitations of the driving system, it would not be possible to scale the driving speed in the laboratory correctly to study full-scale vertical drains. However, as reported by Hird & Moseley (2000), the smear due to vertical penetration increases as the driving speed reduces. Therefore, it could be said that, with a lower penetration rate, the degree of smear obtained in the laboratory is higher than in the field and, that the experimental results are on the "safe side".

For the case of a push-in piezometer, the size of the piezometer and the pushing rate may be not much different from those of the drain used in the present experiment. In this case scaling effects would not be significant.

6.3 Miniature Piezocone Test in Layered Soils

6.3.1 Pore water pressure behaviour in layered soils

A miniature piezocone with a porous filter element located either at the tip or shoulder was driven into layered soil samples in order to investigate its performance in layer detection (Section 4.3.11).

The location of the filter element greatly influenced the performance of the piezocone in terms of layer detection. Considering typical test results, for example Figure 5.24, as the piezocone approached the more permeable layers, very sharp peaks of excess pore water pressure were observed at the cone tip, while these sharp peaks were not observed at the cone shoulder. Furthermore, once the cone was driven through the more permeable layers, it was found that the excess pore water pressure at the cone tip suddenly reduced, while the reduction at the cone shoulder took longer to develop. The reductions of the excess pore water pressure at the cone tip were not only quicker but also larger than at the cone shoulder.

As discussed by Lunne et al. (1997), soil adjacent to different parts of the piezocone will be subjected to different types of stress when the cone is driven into the soil. According to Lunne et al., the soil near the cone face will be mainly subjected to normal compressive stress while the soil near the shaft will be mainly subjected to shear stress. Therefore, in terms of the pore water pressure, the response at the cone face will be dominated by normal stresses, while the response at the shaft will be dominated by shear stresses. However, Burns & Mayne (1998) stated that, along the shaft, the normal compressive stress and shear stress induced components can be comparable in magnitude. Furthermore, in most saturated soil an increment of compressive stress will induce a positive excess pore water pressure, but a shear stress increment could yield either a negative or positive excess pore water pressure depending on the over consolidation ratio of the soil (Lunne et al., 1997; Burns & Mayne, 1998).

With the above knowledge, it may be postulated that as the piezocone approached the more permeable layers with a higher stiffness than the clay layers, the total compressive stress near the cone tip greatly increased and this led to an

increase of pore water pressure at the tip. It should be noted that this was a localised phenomenon happening in a small area around the cone tip. As the cone advanced, the excess pore water pressure would have started dissipating towards the permeable layer but, due to the low permeability of the clay, the dissipation rate was evidently smaller than the rate of increase due to the increase of compressive stress. However, once the cone tip contacted the permeable layer, from which drainage was allowed, the excess pore water pressure in the piezocone was suddenly dissipated through the layer. At the same time, once the permeable layer was penetrated, the compressive stress at the cone tip would have reduced and, therefore, a reduction of excess pore water pressure would have occurred. Furthermore, dilation of the penetrated permeable layer may have produced negative changes of excess pore water pressure that contributed to the reduction of excess pore water pressure at the cone tip.

Behind the cone tip, as described above, the excess pore water pressure developed during the piezocone driving was due to a combination of (possibly dominant) shear stress and compressive stress. The compressive stress increment at the cone tip as the cone approached the permeable layers was too localised to produce a sharp pore pressure increase at the cone shoulder. Also, it was found that the reduction of the excess pore water pressure at the shoulder sometimes started before the shoulder filter reached the permeable layer. Then the reduction gradually continued while the cone was passing the original level of the permeable layer. To account for this phenomenon, it should be realised that, before the cone shoulder reached the permeable layer position, the layer had already been penetrated and deformed (curved down) by the cone body and clay had possibly been smeared across the filter. As the cone shoulder was approaching the permeable layer, even if clay had smeared across the filter, the excess pore water pressure could still have been able to start dissipating through the smeared clay. Then the dissipation would have continued while the cone shoulder was passing the deformed layer. The minimum excess pore water pressure was thus reached after the cone shoulder had passed the original level at which the permeable layer was located. As the cone shoulder was passing the permeable layer, the permeable material was also continuously subjected to shear stress and, therefore, dilation of the permeable

material may again have been a factor contributing to the reduction of the pore water pressure.

These phenomena have also been recently investigated in tests using the same mini-piezocone in larger soil samples (Hird et al., 2001). It was found that thicker clay layers, 80mm rather than 20mm, made a difference only in terms of the establishment of the excess pore water pressure response in the clay. Because the spacing of the permeable layers in the present research was only about 20mm, the response in the clay was only just re-established after passing a permeable layer before the next permeable layer was encountered. A steady excess pore water pressure in clay was more clearly re-established with 80mm clay layers. However, the response during penetration of a permeable layer was essentially the same in each case.

6.3.2 Excess pore water pressure dissipation behaviour

At the end of driving, the piezocone was stopped with the filter element approximately at the middle of a clay layer and a dissipation test was performed (Section 4.3.11). During the dissipation test, drainage from the soil sample to the peripheral drain was allowed. Dissipation tests were performed in pure clay and layered samples so that the effects of the layers with different permeabilities on the dissipation behaviour could be investigated. Results from the dissipation test were eventually used to calculate the coefficient of consolidation of the clay as described in Section 5.4.2.

The test results from the dissipation tests in pure clay were presented in Figures 5.35 and 5.36. A couple of typical results are compared with the theoretical plot proposed by Teh & Houlsby (1991) in Figure 6.6. The Teh & Houlsby theory was selected for the comparison because it represents the most comprehensive theoretical study of the piezocone dissipation test.

To compare the theoretical and experimental curves, it was assumed that the experimental curve crossed the theoretical one at 50% dissipation. Then, based on the dissipation time, the dimensionless time factor, T^*, was calculated for the rest of

the experimental curve. However there are two important differences between the theoretical assumptions and the experimental situation as follows.

- During the dissipation of the excess pore water pressure, the total stresses in the soil surrounding the cone are assumed to be constant in the theoretical analysis. In the real situation, total stresses might be reduced due to relaxation of the soil or the driving system.

- Effects of smear due to the penetration are completely ignored in the theoretical analysis. In the present research (Section 5.3.5), it has been shown that smearing caused by penetration can considerably reduce the permeability of the soil surrounding the penetrating object. Therefore, in reality, the disturbance of the soil around the cone might significantly affect the pore water pressure dissipation behaviour.

a) <u>Dissipation behaviour at the piezocone tip</u>

Comparison of the theoretical curve and the typical experimental dissipation curve from the test performed in a pure clay sample, Figure 6.6, shows that the shapes of the two curves are quite different. An initial delay of the dissipation was observed experimentally and then the experimental dissipation proceeded at a faster rate than the theoretical one. During the last stages of dissipation, the rate of experimental dissipation was comparable to that of the theoretical dissipation. These results could be attributed to two mechanisms.

Firstly, as mentioned in Section 5.4.2, the start of the dissipation in the dissipation analysis was defined by choosing a point at which the excess pore water pressure was a maximum, before the excess pore water pressure continuously reduced. This was because it was difficult to define the starting point from the cone displacement data. In order to stop the piezocone at the end of driving, the power to the drive unit was manually switched off, as described in Section 4.3.11, and then the motorised driving system would slow down before stopping completely. As shown in Figure 6.7, the deceleration from switching off the power to a complete stop (point B), took about 0.3 second. By inspection of many test results, it was found that

dissipation of the excess pore water pressure actually started during the deceleration. Therefore, it was difficult to base the starting point of the dissipation on the cone movement. Selecting a point at which the excess pore water pressure was a maximum (point A), as the starting point of the dissipation was thought to be the best solution. However, due to the tiny further movement of the piezocone after the designated starting point, the rate of dissipation was initially slower than it would otherwise have been.

Secondly, once the piezocone was completely stopped, because of relaxation of the driving system or the soil surrounding the cone tip, the vertical total stress (expressed in terms of cone resistance) from the soil around the cone tip rapidly reduced, Figure 6.8. This stress reduction could have led to the rapid reduction of excess pore water pressure at the cone tip shortly after the beginning of the dissipation process. Later on, the vertical stress would often be observed to stabilise by increasing again to a constant value. However, the rate of this pressure increase was very slow and, therefore, could not have affected the pore water pressure response.

Dissipation tests were also performed in the clay layers of the layered samples to investigate the effects of the permeable layers. As described in Section 5.4.2, the results gained from the dissipation tests, both in the pure clay and layered samples, were used to determine the coefficient of consolidation of the clay. A summary of the $c_h / \sqrt{I_r}$ values determined by using three methods (logarithm of time (Equation 2.7), square root of time (Equation. 5.12) and least squares analysis) was presented in Table 5.5.

It can be seen in Table 5.5 that, for pore water pressure dissipation at the cone tip, analysis using the square root of time method gave very high $c_h / \sqrt{I_r}$ values compared with the other two methods. In the square root of time method, most of the data points used are from the early stages of the dissipation process. As noted above, this stage was possibly affected by the total vertical stress reduction caused by soil or driving system relaxation after the piezocone driving was stopped. The total vertical stress reduction could lead to a faster reduction of excess pore water pressure and, hence, to a higher calculated $c_h / \sqrt{I_r}$.

Furthermore, Table 5.5 shows that the $c_h / \sqrt{I_r}$ values of pure clay samples determined by using the logarithm of time method and the least squares analysis were not very different from those of the layered soils. Thus, the permeable layers did not obviously influence the dissipation behaviour. Nevertheless, due to the "deflected fabric" described in Section 6.2.1, part of a deformed permeable layer could still be close enough to the cone tip to influence the dissipation of the excess pore water pressure. Figure 6.9 shows a piezocone hole after a horizontal cut was made through a clay layer. It can be seen that the distribution of the permeable material surrounding the cone is similar to those in the case of a circular drain (Figure 6.1). This could have an unpredictable and erratic effect because, not only the permeability of the permeable layers, but also their deformed shape could affect the excess pore water pressure dissipation at the cone tip. Therefore the dissipation rate in a sample with pure sand layers may sometimes be lower than that in one with pure flint layers, as evident in Figure 5.31 and, in terms of t_{50}, in Table 5.6.

It should be noted that, for the pure clay case in Table 5.5, the $c_h / \sqrt{I_r}$ values determined by the square root of time method are not presented because, after the data was plotted, a straight-line portion on the curve could not be identified. This may be, again, an effect of the relaxation and reduction of the total vertical stress at the cone tip.

b) Dissipation behaviour at the piezocone shoulder

Comparison of the theoretical and the typical experimental results obtained from the dissipation tests in pure clay samples showed that the shapes of these curves were comparable, Figure 6.6.

A rapid change of the degree of consolidation is not initially predicted by the theory, so even though the deceleration of the driving system might initially slow down dissipation, as described above, there might not be any evidence of this in the comparison with theory. Also the total vertical stress reduction at the cone tip or face once the cone stopped might not have much effect on the pore water pressures at the cone shoulder.

The summary of the dissipation tests carried out by the piezocone with the filter at the cone shoulder, Table 5.5, shows that the $c_h / \sqrt{I_r}$ values calculated by the three calculation methods were very consistent. The effects of the permeable layers can be seen from the magnitude of $c_h / \sqrt{I_r}$. The values from tests in soil samples with pure sand layers are, on average, higher than those from tests in soil samples with 10%f-s layers and the latter are, on average, higher than those from tests in soil samples with pure flint layers. The $c_h / \sqrt{I_r}$ values from tests in pure clay samples are the lowest and are comparable to those obtained from tests in pure clay using the piezocone with a tip filter.

In the layered samples, it is likely that the excess pore water pressure dissipation at the cone shoulder, embedded in the middle of a clay layer, was affected by permeable material which was displaced downwards by the penetration. Compared with the tip, the cone shoulder filter area is larger and may be more easily influenced by parts of a deformed permeable layer.

Levadoux & Baligh (1986) explained that, while the piezocone is driven into normally consolidated clay, undrained shearing develops positive pore pressure which causes a negative mean effective stress change. Under undrained conditions, the reduction of the effective stress brings the clay surrounding the cone into an "artificial overconsolidated" state. Subsequently, the excess pore water pressure dissipates and, during early stages of consolidation, the soil surrounding the cone undergoes recompression. Therefore, the determined values of c_h could be higher than those obtained from tests involving virgin compression of normally consolidated clay. Lacasse & Lunne (1982) performed piezocone dissipation tests in two soft Norwegian marine clays, Onsφy clay and Drammen clay, and reported that the c_h values from field tests and the re-consolidation stages of oedometer tests agreed very well.

To validate the piezocone dissipation test results, independent consolidation tests were performed on kaolin in two Rowe cells, as described in Section 4.2.3. The horizontal coefficient of consolidation was directly measured under different loading conditions, namely virgin compression, swelling and re-compression. The values of time at 50% dissipation, t_{50}, from piezocone dissipation tests performed in pure clay

samples were plotted against the independent c_h value on a chart showing also the theoretical solution by Teh and Houlsby (1991), for a realistic range of the rigidity index (I_r = 50-500), as shown in Figures 5.37-5.38. It can be seen that, for c_h measured under swelling and re-compression conditions, the data plot in a realistic range of rigidity index whereas, for the c_h obtained from virgin compression stage, the data plot well below the expected range of I_r. The independent consolidation tests suggest that, once the piezocone was stopped in the clay after driving, the reduction of the excess pore water pressure around the cone was affected by the "artificial overconsolidation" described by Levadoux and Baligh (1986).

6.3.3 Cone resistance in clay and layered soil

In the present research, it was shown that, in terms of uncorrected cone resistance, the piezocone could not clearly detect the permeable layers in the soil sample. However, it was found that the uncorrected cone resistances of the layered samples are higher than those of the pure clay samples, e.g. compare Test 4 (Figure 5.25) and Test 3 (Figure 5.24). Lunne et al. (1997) explain that, because the cone will start to sense a change in material type before it reaches a new material and will continue to sense a previous material even when it has entered a new material, the transition of cone resistance responses from one material to another will not necessarily be sharp. The thickness of penetrated material that would be enough for the cone to respond fully, for soft and stiff materials, is 2-3 and 10-20 cone diameters respectively. Hence, it may be postulated that, in the present research, the more permeable layers could not be detected because their thickness was not enough for the cone response to be fully established. At the same time, clay layers in the layered sample were not thick enough for the cone resistance to be unaffected by the permeable layers

For the tests in pure clay (Tests 3 and 9, Figures 5.23 and 5.29), by averaging the results after approximately 60mm driving distance, the ratio of the excess pore water pressures measured at cone shoulder and at the cone tip, K, was determined. The calculated values were 0.71 and 0.66 for Test 3 and Test 9 respectively. These values are comparable to those (0.6 to 0.8) recommended for normally consolidated

clay by Lunne et al. (1997). It should be noted that piezocone drive1 of Test 3 was neglected because, due to the slow response at the initial stages, it was considered that full saturation of the filter was not achieved.

Cone resistances in the pure clay were corrected for the effect of water pressure acting over the area behind the cone (ISSMGE, 1999). Equation 2.1 was used in the correction. When the tip filter was used, the pore water pressure at the cone shoulder was calculated as follows.

$$u_2 = u_d + K(u_1 - u_d) \text{ ---------- } (6.1)$$

where u_1 is the pore water pressure measured at cone tip, u_d is the pore water pressure before driving, u_2 is the estimated pore water pressure at cone shoulder and K was assumed to be 0.7.

In Tests 3 and 9, the uncorrected cone resistances, q_c, and corrected cone resistances, q_t, after approximately 40mm of driving distance were then averaged, Table 6.1(a) (column 5). It was found that the q_t values from the piezocone with tip and shoulder filters were comparable. The highest q_t value was obtained from Test 3 drive3. This could be because, the soil sample was confined in the test cell for an unusually long period (10 days) before the piezocone test.

In Table 6.1(a), by substituting the average values of q_t (column 5) and the average undrained shear strength obtained from the vane tests (36kPa) (see Section 6.3.7) into Equation 2.5, the values of N_{kt} for Tests 3 and 9 were calculated (column 8). It should be noted that, due to the friction between the soil and the peripheral porous plastic, instead of using the total applied stress (450kPa), the total stress substituted into Equation 2.5 was the sum of the effective vertical stress in the kaolin estimated using the vane tests (average=190.5kPa) and the applied back pressure (200kPa). The N_{kt} values from Tests 3 and 9 were then compared with those predicted by theoretical solutions, Table 6.1(b), and empirical investigation, Table 6.1(c). It can be seen that the present N_{kt} values fall within all the empirical ranges and agree well with Yu's (1993) theoretical solution in which the roughness of the cone was considered. However, the present N_{kt} values are higher than those predicted by the remaining theoretical solutions. This is possibly because the latter do not consider the effect of friction between the cone and the penetrated soil.

Therefore, they overestimate s_u for the soil or, in the case that s_u is known, underestimate N_{kt}.

In the layered samples, as discussed in Section 5.4.1, it was difficult to obtain the proper cone resistance correction (Section 2.3.3) when a test was performed using the piezocone with a tip filter. In tests where the shoulder filter was used, corrections of cone resistance were made and changes of the response were investigated. No significant changes in the form of the responses were observed, e.g. Figure 6.10.

6.3.4 Practical aspects

During piezocone tests, responses in terms of cone resistance, excess pore water pressure and friction at the cone side are commonly used in the interpretation of ground conditions. The accuracy of the investigation is directly related to the quality of the data gained from the tests and their interpretation. In this section, relevant practical findings gained from the experimental work are discussed.

a) Saturating the piezocone

Saturation of the piezocone filter, and the cavity between the filter and the pore pressure transducer, is important because, once the piezocone is driven into the ground, changes in pore water pressure must be transmitted by the incompressible saturating fluid to the transducer inside the cone. Vacuum de-airing of the cone and the cone filters before use is widely accepted as a saturation technique (e.g. Lacasse & Lunne, 1982; Campanella & Robertson, 1988; Kurup, 1993; Moseley; 1998). With this saturation method, the piezocone is supposed to provide a full and rapid response to changes of pore water pressure during driving. In the current research, it was found that a rapid response of the piezocone to a change of pore pressure was not achieved immediately after the de-airing process (Section 3.3.13). A good response was obtained, however, after the piezocone was left in the saturation fluid under atmospheric pressure for about six hours. The following paragraph explains how this phenomenon may have occurred.

As described in Section 3.3.13, after the porous filter was de-aired under silicon oil, the cone was assembled under the silicon oil and de-aired by applying a vacuum. It was usually found that, after a period of vacuuming, some air bubbles were drawn out from the filter. Although good care was taken, very small air bubbles were possibly entrapped during the assembling processes. Under the negative pressure, any entrapped air bubbles in the cavity between the porous filter and the pore pressure transducer had to be expanded and expelled through the porous filter. At this stage, a space with a negative pressure might have developed in the cavity between the porous filter and the pore pressure transducer. Once the vacuum was released, the atmospheric pressure would have pushed the saturation fluid into the above space. It was considered that this process would take a time roughly equal to the time taken by the vacuum to pull the air bubbles out, i.e. 6 hours. Full and rapid responses of the cone to pressure changes would not be achieved if the space behind the filter was not replaced with saturation fluid.

Figure 6.11 presents the effect of not allowing enough time before taking the cone out of the saturation fluid after de-airing. Figure 6.11(a) is a result of a piezocone test performed by Moseley (1998) on a layered soil sample with 20mm clay and 2mm sand layers and Figure 6.11(b) is a preliminary test from the present research on a sample with 40mm clay and 2mm sand layers. These two results were obtained from tests performed using the same piezocone, with the same tip filter, and the same sample preparation procedures. However, whereas Moseley (1998) performed his test immediately after the de-airing process, before the test in Figure 6.11(b) the cone was left in the saturation fluid under atmospheric pressure for about six hours.. It can be seen that a much better performance was obtained in the latter case.

In practice, due to time constraints, the piezocone preparation procedures may be shortened. For example, according to Lunne et al. (1997), the procedures commonly used are to oven-dry the filter, vacuum the filter under the saturation fluid and assemble the cone under the saturation fluid. As mentioned before, unless very good care is taken, especially during the assembling process, air bubbles could be entrapped in parts of the piezocone and affect the test results. De-airing after assembling is advisable to ensure that the piezocone is fully saturated before testing.

The time that the piezocone needs to be left under the saturation fluid after de-airing may be shortened by applying a high positive pressure to the cone under the saturation fluid.

b) Response time as piezocone saturation indicator

It should be noted again at this point that saturation of the filters and the cavity between the filter and the pressure transducer is an extremely important factor affecting the piezocone response during penetration and dissipation. As mentioned by Campanella & Robertson (1988), one of the major difficulties with piezocone testing can be the evaluation of saturation. Loss of saturation of the piezocone could happen during cone assembly, handling or driving through unsaturated soils above the ground water table.

Several researchers, (Campanella et al., 1981; Lacasse & Lunne, 1982; Lunne et al, 1997) have published examples of the pore pressure response from a poorly saturated piezozone. Lacasse & Lunne (1982) reported that, for their piezocone tests in Onsøy and Drammen, the quality of the probe saturation was indicated by the rapidity with which the pore pressures recovered their pre-dissipation level after a dissipation test. It was stated that recovery within a penetration distance of 50mm indicated satisfactory probe saturation.

In the present research, it was considered that, with the standard driving speed of 20 mm/sec, the distance required for a full establishment of excess pore water pressure in the pure clay could be used as rough indicator to evaluate the quality of saturation of the piezocone. In the two tests on pure clay with a back pressure of 200kPa, Test 3 and Test 9 (Figures 5.23 and 5.29), it was found that a driving distance of approximately 10mm and 30mm was enough for the full establishment of excess pore water pressure measured at the cone tip and cone shoulder respectively. It should be noted that these results were obtained by performing the piezocone tests very carefully in the laboratory with the benefit of back pressure and that they are therefore unlikely to be bettered in the field.

In field tests, checking of the piezocone saturation by this method could be performed when driving is started, either at the beginning or after a dissipation test, in clay soils. To investigate the data in more detail at this stage, the logging speed

might usefully be set to at least 10 data/sec, which was also sufficient for soil fabric determination (Section 6.3.4(c)). The driving should be started after complete stabilisation of the pore water pressure measured by the piezocone.

Table 6.2 presents the penetration distances required for the measured pore water pressure to reach a steady value in the study by Kurup (1985) and the estimated c_h values from the associated dissipation tests. It is seen that all Kurup's estimated c_h values were much lower than the reference values for reloading obtained from separate consolidation tests, and almost all, except those obtained by using Chan's (1982) method, were also lower than reference values for virgin compression. As discussed in Section 6.3.2, the c_h values estimated from piezocone dissipation tests generally tend to be close to those from consolidation tests under recompression loading. In Table 6.2, the penetration distances at which the measured pore water reached a steady value are much larger than those in the present research and those reported by Lacasse&Lunne (1982). By considering these pieces of evidence, it is possible to conclude, assuming Kurup's soil samples were saturated, that the piezocone used in the experiments was not properly saturated.

c) Pore water pressure interpretation in soil fabric determination

The present research has shown that, in terms of the pore water pressure response, a mini-piezocone with the filter element located either at its tip or shoulder can detect layers of pure sand, 10%f-s or pure flint with a thickness as thin as approximately 2mm.

The test results showed that the pore water pressure change at the cone tip was very sensitive to localised effects. At this position, the excess pore water pressure would typically increase very quickly once the cone was penetrating a clay layer. Then a sharp peak and a reduction of the excess pore water pressure were observed as the cone approached and penetrated a more permeable layer. Positions of the permeable layers were clearly defined by these changes of pore pressure. In Section 6.3.1 the physical phenomena during the driving have been discussed.

The peak magnitude of the pore water pressure probably depends on the stiffness of the permeable layer that the piezocone is approaching. In the layered samples, the stiffness of the permeable layer could depend on its thickness, its

density and the properties of the material in the layer. The shear strength and stiffness of the permeable layers have not been investigated but it is known (Moseley; 1998 and Hird et al.; 2001), that the peak magnitude of the excess pore water pressure increased as the sand layer thickness increased.

It could be seen from the test results that the reduction of pore water pressure at the cone tip was largest as the cone was penetrating pure sand layers but that the reductions were not very different for penetration in 10%f-s and pure flint layers. Therefore, the magnitude of the pore water pressure reduction cannot be related only to the permeability of the permeable layers. As described in Section 6.3.1, the reduction of the excess pore water pressure at the cone tip results from the combination of factors which are a sudden reduction of total stress, dilation of the penetrated permeable layer and drainage through the permeable layer.

Concerning the layer thickness, although the piezocone with the tip filter showed a sharp response in detecting the permeable layers, it is still difficult to determine the exact layer thickness from the measured pore water pressure response. It was found that the vertical distance over which a reduction of the excess pore water pressure occurred was longer than the thickness of the permeable layer. This could be due to the effects of smear of the soil at the cone tip.

Due to the small size of the cone tip filter, the pore water pressure response at the tip could vary easily and, therefore, appear less consistent (see Section 6.3.5) if the piezocone is driven through thinner or thicker parts of the permeable layers, discontinuities or air pockets in the layers. Localised differences in the density of the layers could also affect the pore water pressure response at the tip, because the magnitude of the negative pore water pressure generated by dilation directly depends on the density. Furthermore, as in the case of circular vertical drain penetration (Section 6.2.1), breaking up of the permeable layer penetrated by the piezocone may not be symmetrical and consistent, Figure 6.9. This could also lead to inconsistency of the pore water pressure response at the cone tip. Therefore, in practice a comparison with the pore water pressure responses recorded at other locations, e.g. cone shoulder, could produce more confidence in the interpretation of fabric.

For the cone shoulder position, it could be seen that the maximum pore water pressures induced during the penetration in layered soil samples and pure clay

samples were approximately the same. Therefore, approaching stiffer layers in the soil may not obviously affect the pore water pressure measured at the shoulder location.

As described in Section 6.3.1, the reduction of the excess pore water pressure at the cone shoulder sometimes started before the filter reached the permeable layer. Then the reduction gradually continued while the cone was passing the position of the layer and the minimum excess pore water pressure was recorded after the filter had passed the level at which the layer was originally located. Due to this behaviour, prediction of the permeable layer thickness based on the pore water pressure response at the cone shoulder is very difficult. Furthermore, although the magnitude of the reduction of the pore water pressure seemed to increase as the permeability of the permeable layers increased, this trend was not very clearly seen. On the other hand, consideration of the results from the entire test series suggested that, for a given permeable layer type, the pore water pressure responses measured at the cone shoulder were more regular than those measured at the cone tip. This may be because the shoulder filter has a larger area than the tip filter and, therefore, the effects of localised variation in the soil are smaller.

The logging rate used during the piezocone test is one of the most important factors affecting the quality of the results. As described in Section 3.3.14, the logging rate used in the present research was 205 data/sec. Figure 6.12 shows results of piezocone drive 1 of Test 4 presented as if the data had been recorded using different logging rates. This has been achieved by sampling from the full data set. At a driving speed of 20mm/sec, it can be seen that the minimum logging rate that would probably suffice for the layer determination is 10 data/sec or one reading every 2mm. This minimum logging rate is 10 times faster than that recommended by ISSMGE (1999) for a first class piezocone test. Therefore, with logging speeds currently used in practice, pore water pressure responses obtained from a piezocone test cannot be used for detailed soil fabric determination.

d) Prediction of c_h in layered soil

By inspection of all the $c_h / \sqrt{I_r}$ values obtained from the dissipation tests (Table 5.5), it can be seen that the maximum value (Test 1 drive2) is different to the minimum value (Test 9 drive 4) only by a factor of 5. This indicates that although a soil may contain very high permeable layers with rather small spacing (i.e. about 2 cone diameter in the present case), if a dissipation test is performed when the cone filter is in a layer of clay, a low value of c_h may still be observed. Therefore, if this c_h value is used to predict the consolidation behaviour of the ground, the consolidation rate could be significantly underestimated.

e) Cone tip filter materials

As reported by Campanella & Robertson (1988), Jacobs & Coutts (1992), several different materials with different properties (i.e. rigidity, permeability, durability) have been used in the filter elements of piezocones. In the present research, as described in Section 3.3.13, sintered glass filters made from 45-90 μm glass beads were used at the cone tip. These glass filters have a number of advantages. Glass beads can be purchased at a low price from many different companies. The permeability of the sintered glass filter can be changed by varying the size of the glass beads and the heating time in the oven. Glass filters can be produced with a preferred permeability that suits the saturation fluid to maintain a fast response time and a high degree of saturation. With a suitable bead size and heating time, the sintered glass can easily be machined to make the piezocone tip filters. Therefore, the filters can be produced in large quantities and changed following each piezocone test. This is to ensure, as suggested by Campanella & Robertson (1988), that the results obtained are not affected by clogging of the filter.

In the present research the piezocone with the sintered glass tip filter was driven in soft clay with 2mm thick more permeable layers. After driving, no visible damage was noticed. In the field, piezocone tests are performed not only in soft clay but also in dense sand and gravelly soils in which high resistance to abrasion and toughness of the filter are required. Therefore, further investigation concerning the durability of the material would be needed before it could be used with confidence in the field.

6.3.5 Repeatability

The piezocone tests were performed in ten soil samples with four different configurations (Table 5.1). In each soil sample, four piezocone tests were carried out. In order to check the repeatability of the test results, for each different configuration and filter element location (tip or shoulder) on the piezocone, at least two tests were performed under the same applied back pressure, which was normally 200kPa.

As described in Section 3.3.13, the glass filters (Type A, B, C and D) used in the research were produced by sintering glass beads, at 680°C, for various lengths of time. Type A filters were used in Tests 3-5, Type B&C filters were used in Test 6 and Type D filters were used in Tests 7-10.

By inspection of Figures 5.21-5.30, in terms of pore water pressure, repeatability of the piezocone test results gained during driving was generally satisfactory. However, at a particular layer in layered samples, inconsistencies of the maximum and minimum magnitudes of the responses were observed (for example see Figure 5.24). It was found that variations of the maximum pore pressure were more obvious in case of the tip filter than in the case of the shoulder filter. For the minimum pore pressures, again, higher variations were observed at the tip. At the shoulder, maximum pore pressures were more consistent than the minimum values in a particular layer. As discussed in Section 6.3.4, inconsistency of the pore pressure responses was possibly due to thickness and density variation of the permeable layers and, due to small size of the filter, effects of these localised variations were more obvious when a tip filter was used. For the piezocone tests in pure clay samples (Figure 5.23 and 5.29), the pore water pressure responses, both at tip and shoulder, were very consistent except for Test 3 drive1 in which a slow response at the initial stages of the drive was observed. It was considered that full saturation of the filter was not achieved in this drive. Fluctuation of the pore pressure responses at the cone tip (e.g. Test 3 drive 3, Figure 5.23) was attributed to variation in the clay caused by assembling the sample in layers.

In terms of uncorrected cone resistance, it can be seen (e.g. Test 3 drive 3, Figure 5.23) that, the initial resistance value always decreased to a lower value during the first 10-20mm of driving distance. As described in Section 4.3.11, to

ensure saturation, before the cone was fully driven into the sample, the cone tip was embedded in the first clay layer (with a back pressure of 200kPa) for approximately 6 hours. It was thought that, due to this procedure, the penetrated clay surrounding the cone was re-consolidated and, therefore, stiffer than the clay in other parts of the sample.

In layered samples, inconsistency of the cone resistances was commonly observed, e.g. Test 4 in Figure 5.24. As described in Section 6.3.3, the clay layers and the permeable layers in the samples used in the present research may have been not thick enough for the cone responses to be fully established in either layer type. Therefore, in a sample with a small distance between soft (clay) and stiff (permeable) layers, the characteristics of the cone resistance could be erratic. Furthermore, not only distances between the layers but also non-symmetrical breaking up of the penetrated layers (Section 6.3.4) could lead to inconsistency of the cone resistances. In pure clay (Figure 5.23 and 5.29), much more consistent cone resistances were observed. It should be noted that, in Test 10 (Figure 5.30), possibly due to a cone load transducer fault, the results were very scattered and are considered not to be reliable.

6.3.6 Saturation of samples

It was considered that saturation of the soil samples was a very important factor affecting the piezocone performance. For example, any trapped air in the sample could have migrated into the piezocone filter, affecting the capacity of the piezocone to detect permeable layers and influencing the results of dissipation tests. While the piezocone was penetrating the permeable layers, any lack of saturation of these layers could have increased the pore fluid compressibility and influenced the pore pressure changes being measured.

To ensure that the clay layers were fully saturated, a vacuum of about 100kPa was applied to the slurry before consolidation (Section 4.3.2). With the known dry density of the slurry and specific gravity of the clay particles, the void ratio and degree of saturation of the slurry could be checked. It was found that the degree of saturation was very close to unity. During the layered sample construction, the

consolidated kaolin was wire-cut. There was no evidence of any air pockets or bubbles at this stage.

For the permeable layers, de-aired and de-ionised water was used in the preparation, as described in Sections 4.3.3-4.3.5. In the sand layer preparation, the material was uniformly sprinkled into the mould through the water. For the pure flint and 10%f-s layers, the material was mixed with the water and then the mixture was de-aired by applying a vacuum before it was put into the mould.

Furthermore, during the sample consolidation and most of the testing, including the piezocone tests, the back pressure was normally kept at 200kPa. All these procedures helped to ensure saturation of the layers.

In order to check the saturation of the permeable layers, in at least one piezocone test on most of the layered samples, a higher back pressure of 400kPa was applied to the sample. If the samples had not been saturated, the excess pore water pressure responses of the cone under 200kPa and 400kPa back pressures should have been different. However, obvious differences were not observed, e.g. compare drives 1&4 or drives 2&5 in Test 4 (Figure 5.24), drives 1&3 in Test 6 (Figure 5.26) and drives 2&4 in Test 8 (Figure 5.28).

6.3.7 Limitations of the piezocone tests

Limitations are mainly concerned with boundary conditions in the test cell.

a) Effects of side wall friction in the test cell

The layered soil samples were prepared and consolidated in a test cell lined with a 1mm porous plastic sheet to allow radial drainage during the consolidation stages, permeability tests and the piezocone tests.

It was realised that, as the soil sample was consolidated in the test cell, friction between soil sample and the porous plastic was generated. The wall friction at the periphery reduced the effective vertical stress towards the cell base from which the cone penetration started. The variation of effective stress caused non-uniformity in terms of undrained shear strength and over consolidation ratio in the sample.

To investigate the sample uniformity, laboratory vane tests were performed on a pure clay sample (Test 9) at three different depths. It was found that the vane shear strength, s_{uv}, varied from 27kPa to 45kPa, Figure 6.13. Rossato et al. (1992) proposed values of the normalised undrained shear strength of normally consolidated kaolin, s_u/σ'_v, based on the method of testing. For triaxial compression, triaxial extension and direct simple shear tests, the values were given as 0.197, 0.180 and 0.152 respectively. However, it has been shown by several authors, e.g. Vaid & Campanella (1974), Lefebvre et al. (1983), Wroth (1984) and Koutsoftas & Ladd (1985), that, at a given effective stress, s_u obtained from direct simple shear generally falls between those obtained from triaxial compression and triaxial extension. For this reason, the value of s_u/σ'_v for direct simple shear quoted by Rossata et al. (1992) is substantially lower than would be expected. Wroth (1984) suggested that s_u in a soft clay measured using the vane test would also fall between those obtained from triaxial compression and triaxal extension tests. Therefore, it could be postulated that s_{uv}/σ'_v was equal to about 0.189 (average of 0.197 and 0.180). Figure 6.13 shows that, at the cell base (point A), the s_{uv} value estimated by extrapolating the test results was 51.6kPa. If it was assumed that σ'_v at point A was equal to the confining pressure (250kPa), s_{uv}/σ'_v can be calculated as 0.20. This is slightly higher than the postulated value, possibly because torsional resistance was generated along the vane stem during the test. According to the vane test results shown in Figure 6.13, the friction between the soil sample and the porous plastic caused a reduction of about 57% in the vertical effective stress at the top of the sample as compared with the bottom.

The effect of the friction could be also seen from the pore water pressure response of the piezocone (Δu) to a change of cell pressure ($\Delta\sigma$) when the piezocone was located near the top and bottom of the sample. Figure 6.14 shows that when the cone was located near the cell base (before the drive) the recorded B value ($B = \Delta u/\Delta\sigma$) was only 0.8, but when the cone was located near the loading plate (after the drive) the B value was approximately unity. This was because, once the cell pressure increment was applied to the sample, the total stress increment at a particular position in the sample was reduced by the friction at the periphery. Under undrained conditions, the maximum total stress increment was highest in the soil

close to the loading plate and then decreased with distance to the cell base. Hence, assuming that no changes of effective stress occurred, the increment of pore water pressure due to the cell pressure increment was highest close to the loading plate.

It can be seen from Figure 6.14 that, initially and for a very short time, the B value measured close to the loading plate (after the drive) was higher than one. It was thought that, due to a small quantity of air bubbles trapped around the cell membrane or in the porous plastic, the sample was slightly compressible, although external drainage was not allowed during the cell pressure increment. Therefore, once the cell pressure increment was applied, a tiny relative moment of the soil and the cone could have occurred and generated an excess pore water pressure higher than the cell pressure increment. Thus, the calculated B value was higher than one.

Furthermore, it can be seen from the figure that the B values, measured at the top and bottom of the sample, slightly decreased with time. This was possibly because the excess pore water pressure generated by the cell pressure increment caused solution of some of the trapped air in the cell.

During the piezocone driving, the effects of the non-uniform vertical effective stress were not apparent in the uncorrected cone resistance. However, it was found that the excess pore water pressure generated in pure clay (Test 9) slightly increased as the piezocone was penetrating towards the loading plate. By drawing a straight line through the data points, a gradient of pore water pressure increment with driving distance could be determined and, if the piezocone had been driven through the whole sample, the maximum excess pore water pressure at the bottom of sample (loading plate level) could be predicted, Figure 6.15. The hypothetical excess pore water pressure at the top of the sample was determined by extrapolating the line backwards to the level of the cell base. Using measurements at the cone tip and cone shoulder, it was found that the excess pore water pressures at the top of sample were 455kPa and 322kPa and at the bottom of sample were 694kPa and 451kPa respectively. Assuming that the excess pore water pressures generated during the penetration were proportional to the vertical effective stress in the clay, based on the excess pore pressures at the cone tip and cone shoulder, the friction at the periphery of the sample generated a loss of effective stress of approximately 34% and 29% respectively. It can be seen that these values are lower than that deduced from the

vane tests. This could be because, as mentioned above, the vane test results could have been affected by torsional resistance between the soil and the vane stem. However, the available evidence implies that the clay at the top of the sample was lightly overconsolidated rather than normally consolidated.

b) Differentiating between layers and lenses

As discussed in section 6.3.1, a factor that could affect the performance of the piezocone in permeable layer detection is dilation of the penetrated layers. If dilation is the dominant factor or if drainage is localised as the piezocone passes through the layer, the drainage boundary conditions of the permeable layers in the sample during penetration may not have influenced the pore water pressure behaviour. To investigate the pore water pressure change while the piezocone was penetrating a permeable layer under undrained boundary conditions, two sand layers, the third and fourth layers from the start, in Test 4 (Figure 5.24) were isolated using a 242mm diameter brass ring pushed down during sample preparation to cut off the drainage to the porous plastic drain. It can be seen that both the tip and shoulder pore water pressure responses at these two layers were similar to those at other layers (with peripheral drainage). Therefore, it is likely that localised dilation and drainage in the penetrated sand layers dominated the pore water pressure response at the tip and the shoulder of the piezocone.

In natural soils, the drainage conditions of the permeable layers depend on their continuity. However, if drainage is very localised during penetration, the piezocone may not be able to differentiate between layers and lenses. This limitation could be a source of misinterpretation of the ground exploration data, whereby lenses are interpreted as layers. In this case the consolidation rate of the soil mass may be overestimated because the permeable layers in clay can speed up the consolidation by shortening drainage paths but the lenses cannot.

Further investigation of the performance of the piezocone in soil with permeable lenses is needed.

a) Cone resistance and cone factor of tests in pure clay sample

Sample	drive no.	filterlocation	average uncorrected cone resistance, q_c (kPa)	average corrected cone resistance, q_t (kPa)	average q_t		calculated N_{kt} Eq 2 5	average N_{kt}
					u1	u2		
Test no.3	1	u2	739.3	921.6			14.8	
	2	u2	681.09	900.76			14.2	
	3	u1	752.13	978.11	978.11	911.18	16.3	15.1
Test no.9	1	u2	683	892.12			13.9	
	2	u1	693.57	911.5			14.5	
	3	u1	658.15	886.25			13.8	
	4	u1	684.65	908.05	901.93	892.12	14.4	14.1

b) Theoretically predicted cone factors

Authors	$I_r = G/s_u$	Theories	predicted N_{kt}	average N_{kt}
Ladanyi & Johnston (1974)	50	Cavity expansion	8.3	
	500		11.3	9.8
Vesic'(1972,1977)	50	Cavity expansion	9.1	
	500		12.2	10 6
Yu (1993) smooth cone	50	Cavity expansion	8.5	
	500		11.2	9.9
Yu (1993) rough cone	50	Cavity expansion	13.8	
	500		16.4	15 1
Baligh (1985), Whittle (1992)	50	Strain path	9.3	
	500		13.9	11.6
Teh & Houlsby (1991)	50	Strain path	8.4	
	500		14.4	11.4

(equations were summansed by Yu & Honorary, 1998)

c) Empirical cone factors

Authors	empirical N_{kt}
Aas et al (1986)	8-16
La Rochelle et al.(1988)	11-18
Karlsrud et al (1996)	6-15

(from Lunne et al , 1997)

Table 6.1 Cone resistance and cone factor of tests in pure clay

Specimen	Test	Distance to reach steady state (mm)	Estimated $c_r x10^{-3}$ cm^2/sec				Reference $c_r x10^{-3}$ cm^2/sec	
			Tortensson (1975,1977)	Levadoux & Baligh (1986)	Houlsby & Teh (1988)	Chan (1982)	Virgin	Reload
1	1 (U2)	>90	10.89	10.01	7.16	29.3	14.1	78.8
	2 (U1)	>45	5.82	7.18	2.18	31.8		
2	3 (U2)	>80	4.86	9.9	4.33	29	28.3	141
	4 (U1)	>200	7.51	15.7	2.93	69.6		
3	5 (U2)	>100	7.68	11.14	5.97	32.6	14.1	78.8
	6 (U1)	>100	7.7	12.66	2.89	56.1		
4	7 (U2)	>40	9.09	5.09	5.31	14.9	26.4	105
	8 (U1)	>400	28.65	11.78	5.23	52.2		

U1 = Piezocone with tip filter
U2 = Piezocone with shoulder filter

Table 6.2 Dissipation test results (Kurup, 1985)

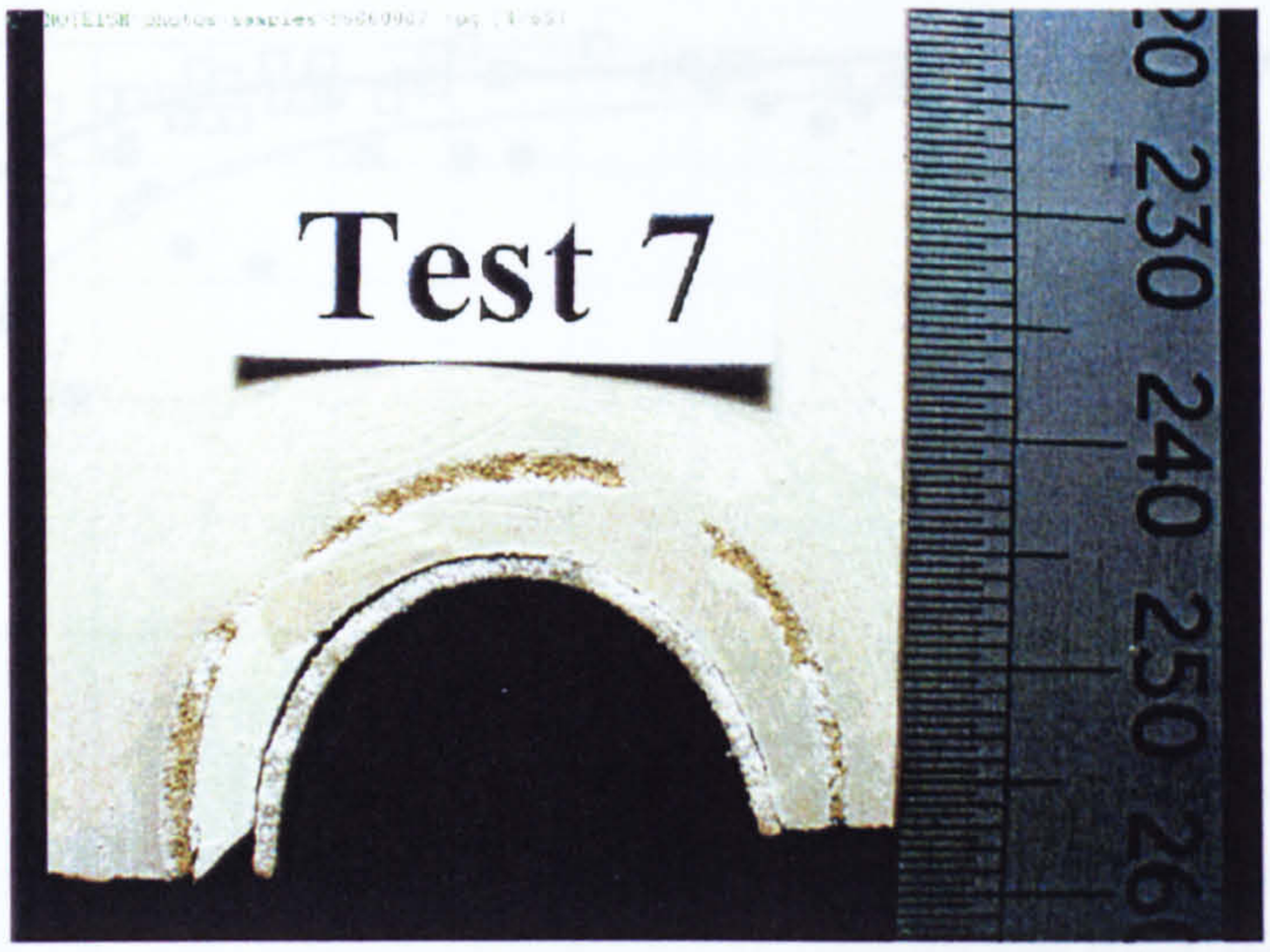

Figure 6.1 Circular drain after horizontal slice through clay layer 5 from cell base

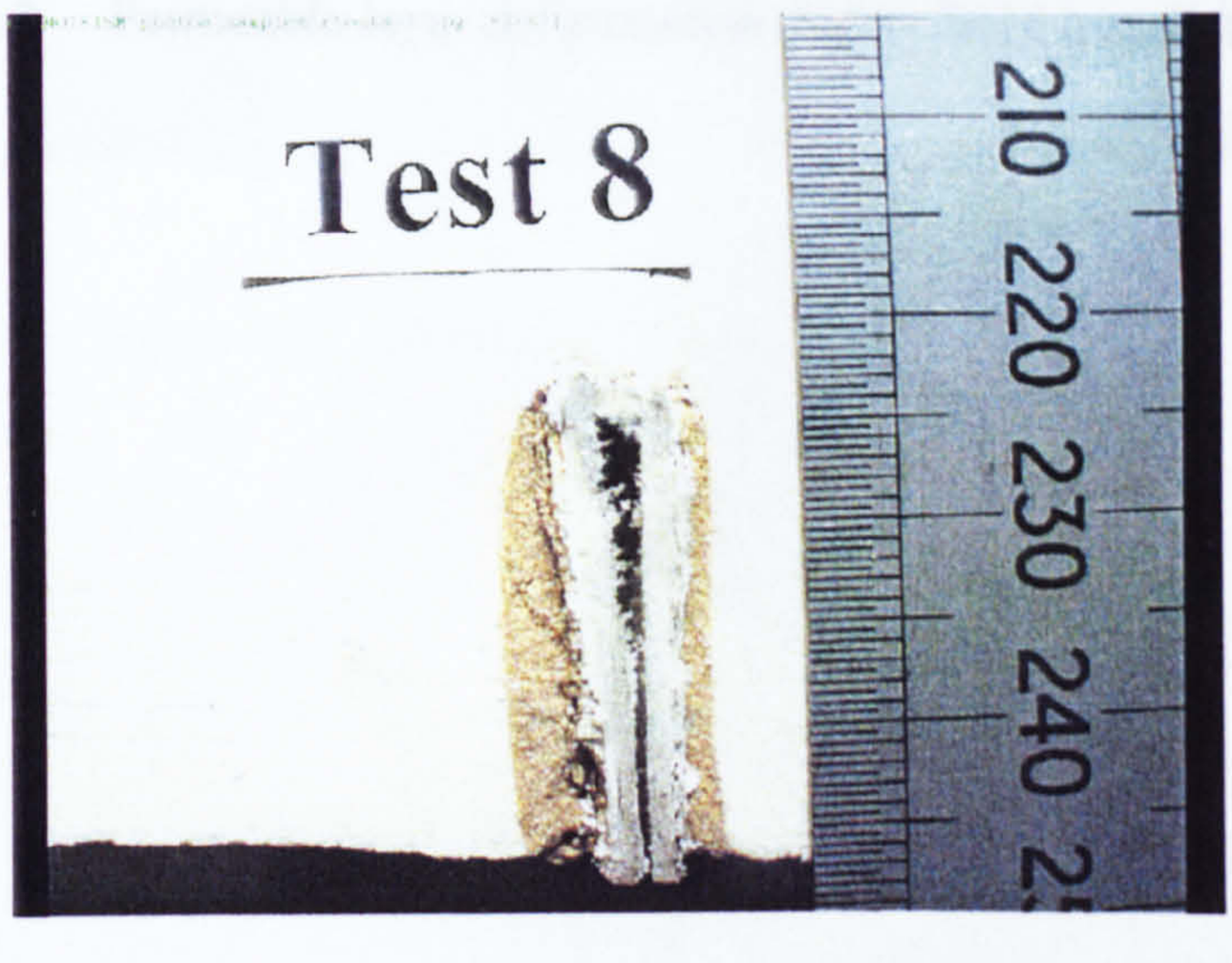

Figure 6.2 Band drain after horizontal slice through clay layer 6 from cell base

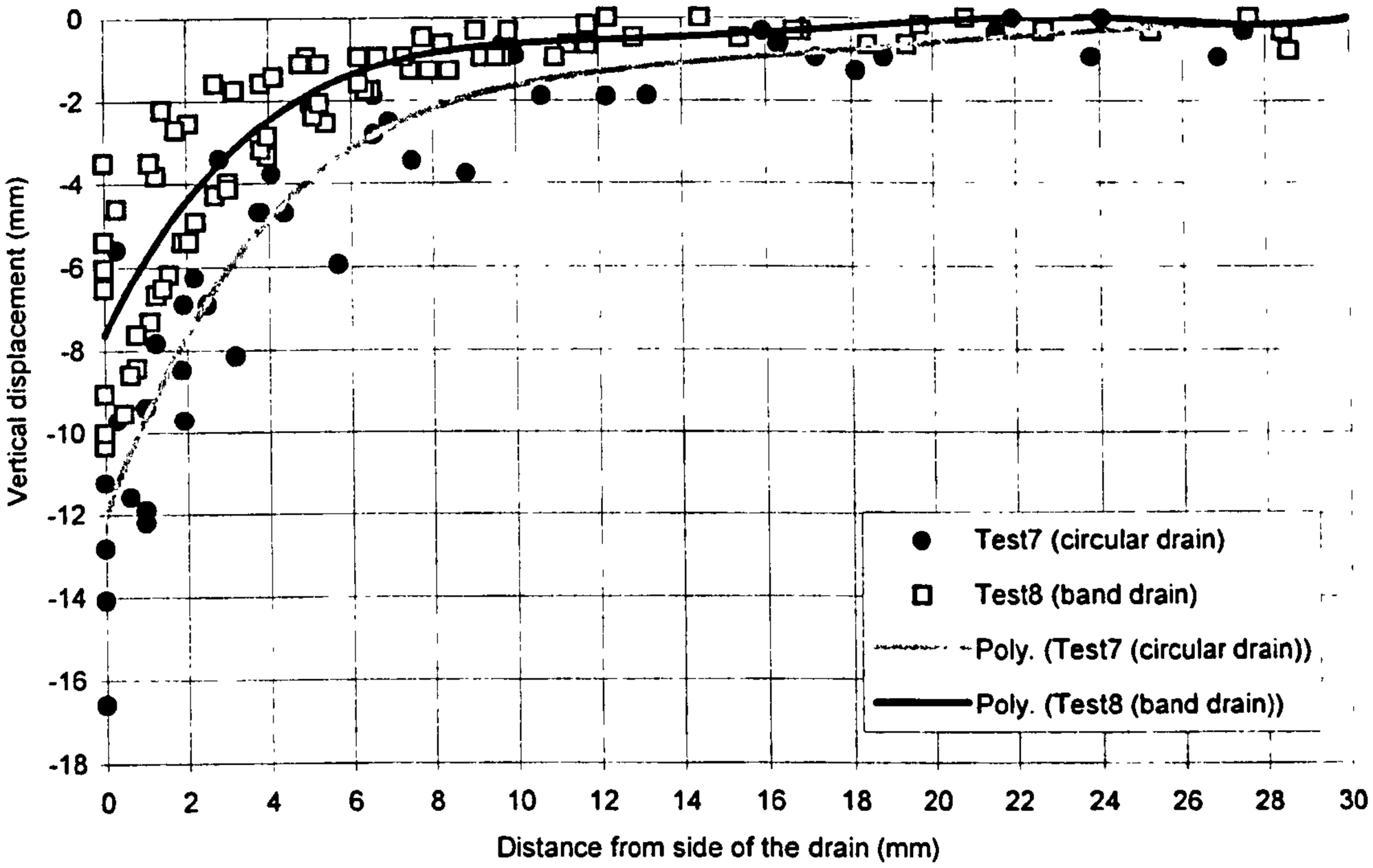

Figure 6.3 Permeable layer deformation due to drain installation

Figure 6.4 Smearing film of circular drain

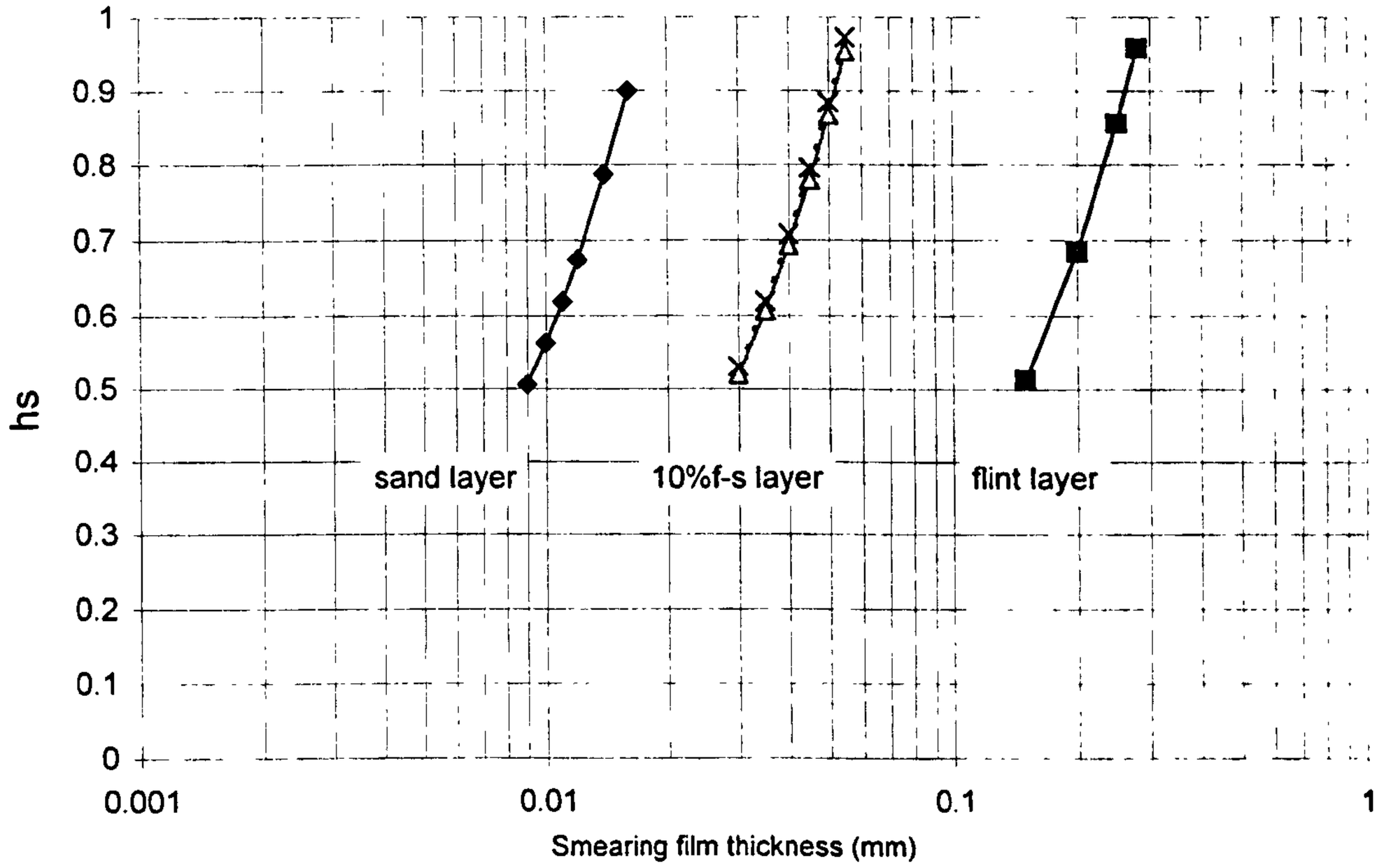

Figure 6.5 Effects of smearing film

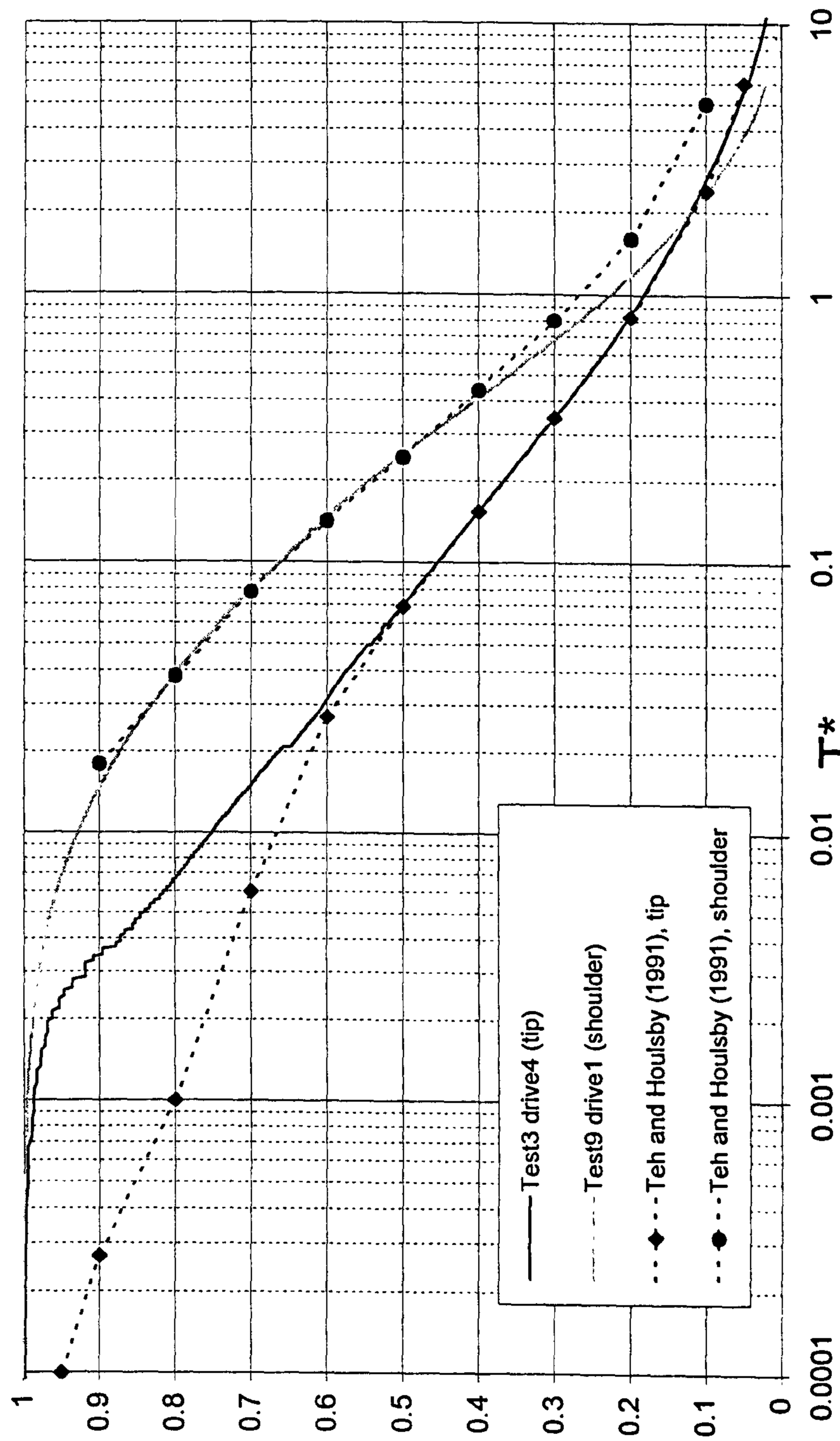

Figure 6.6 Comparison of theoretical and experimental dissipation curves

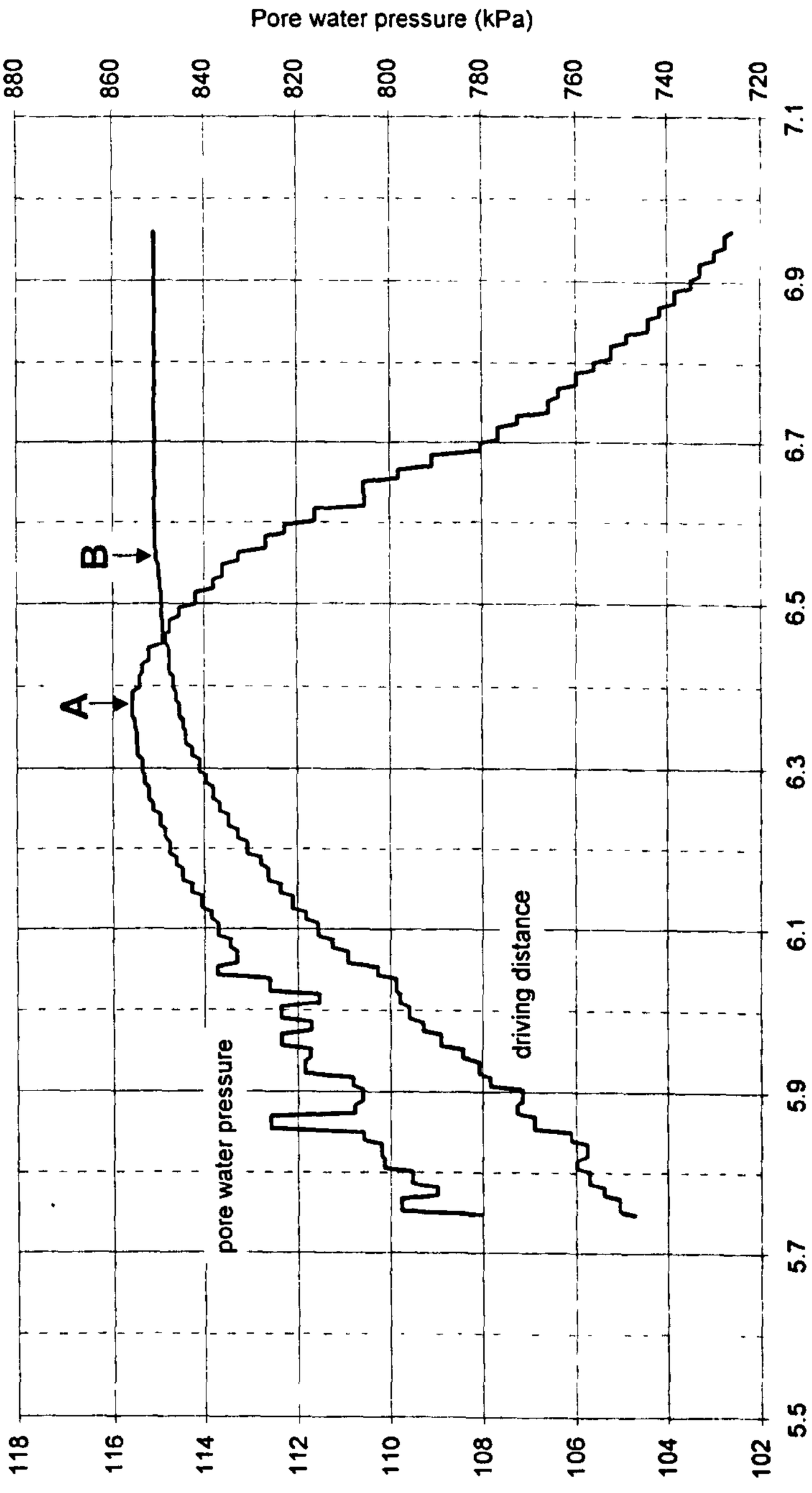

Figure 6.7 Typical pore water pressure at cone stop (Test3 drive4)

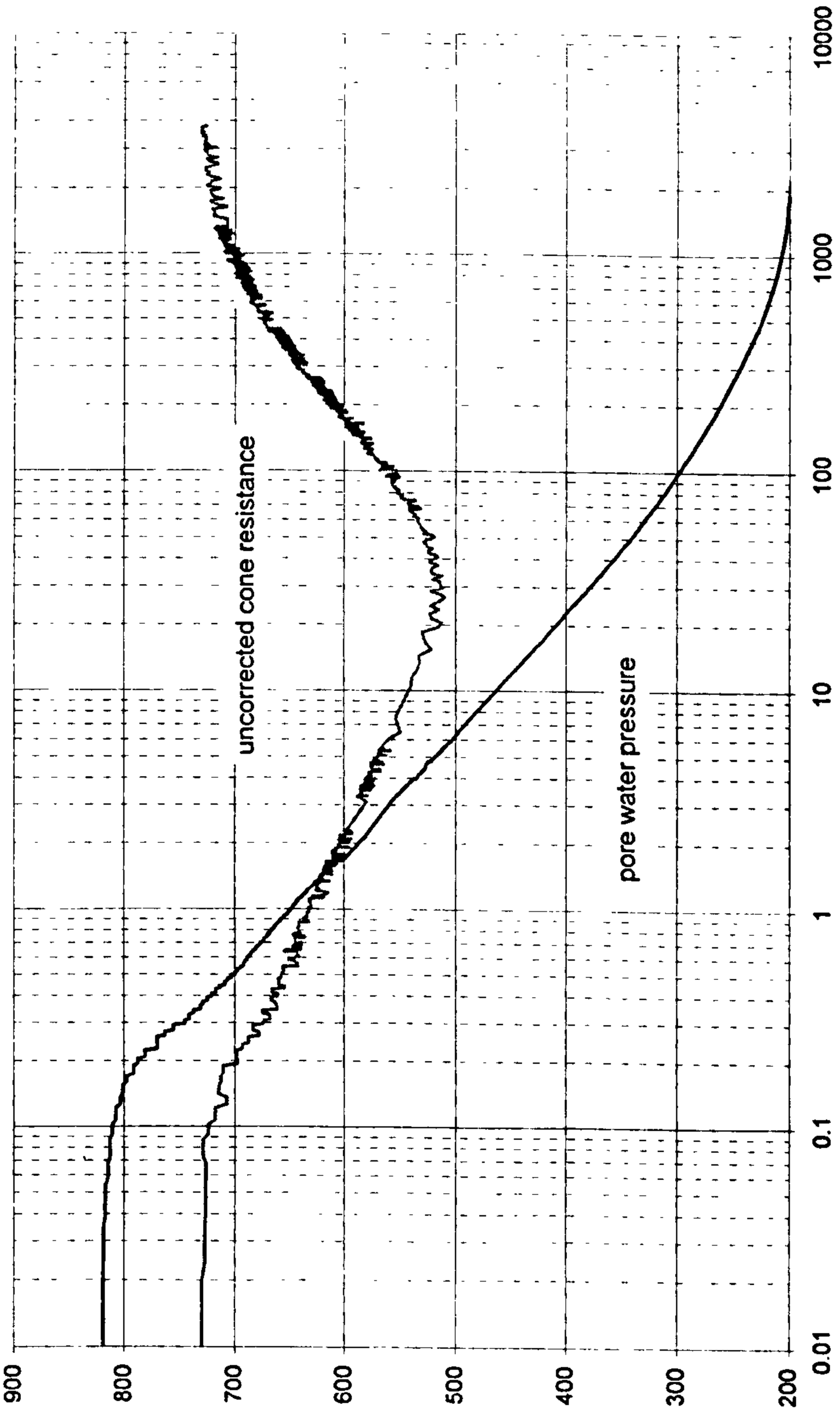

Figure 6.8 Typical cone resistance during dissipation test (Test3 drive4)

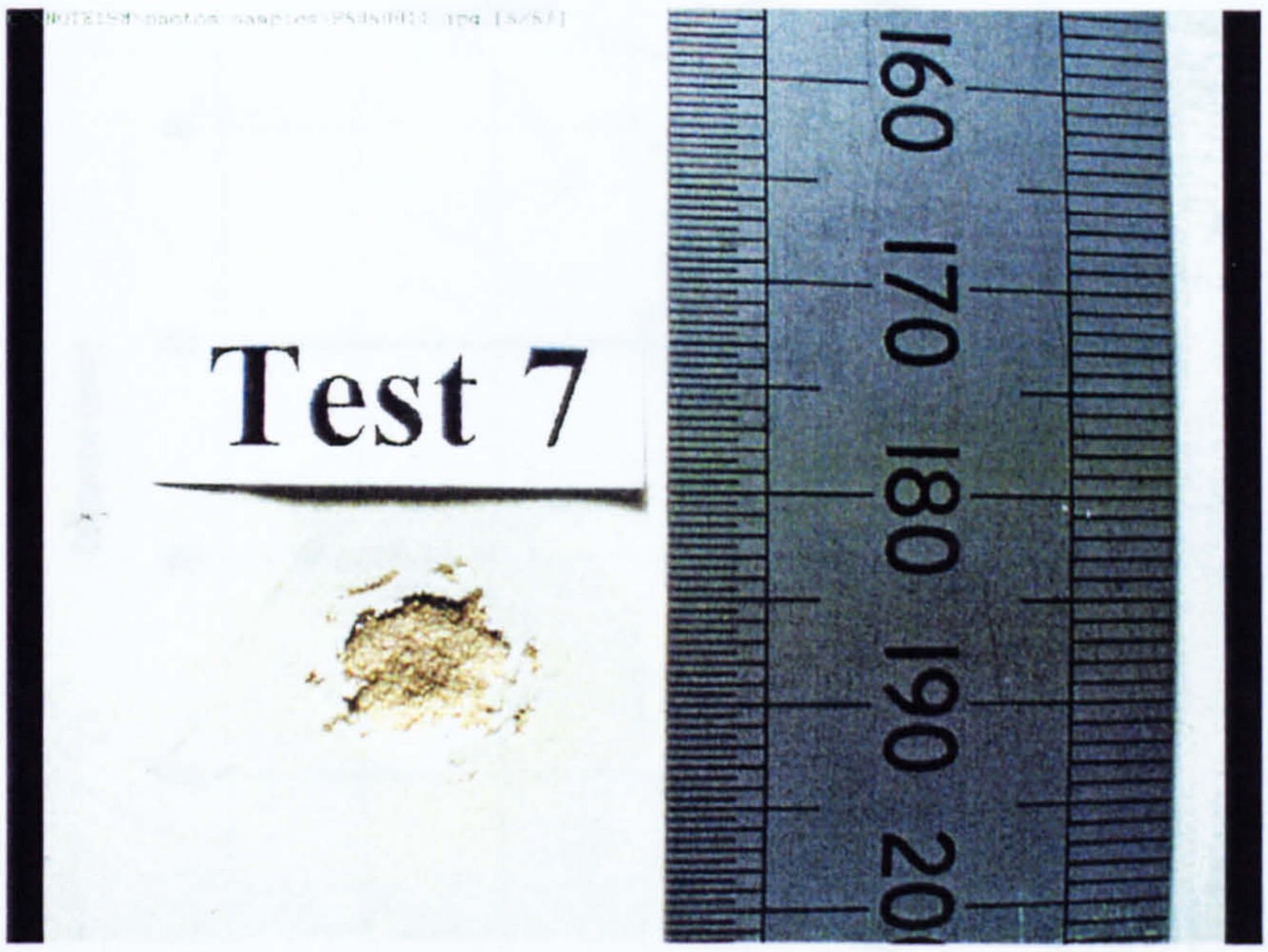

Figure 6.9 Piezocone hole after horizontal slice through clay layer 5 from cell base

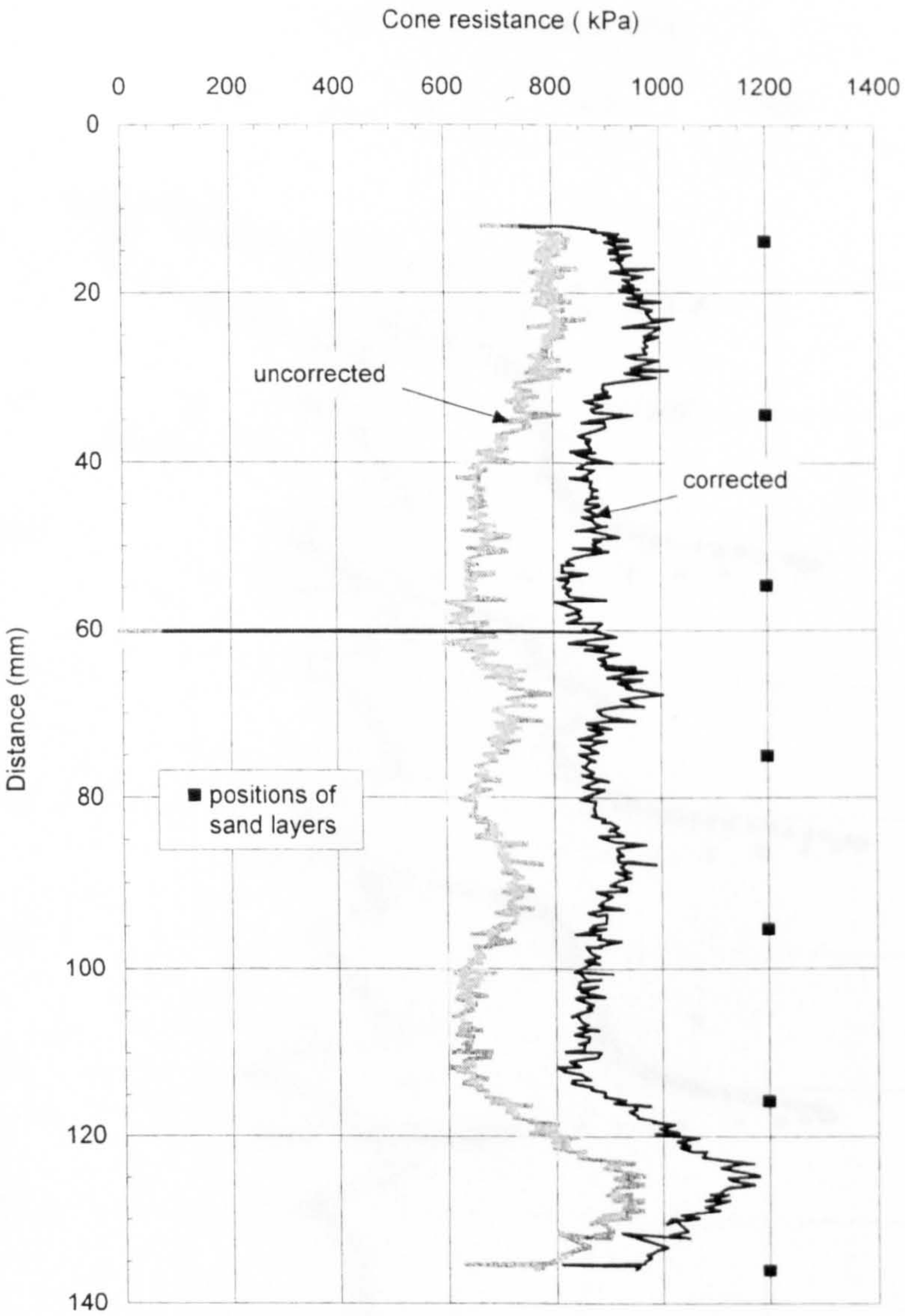

Figure 6.10 Corrected and uncorrected cone resistance (Test 4, drive2)

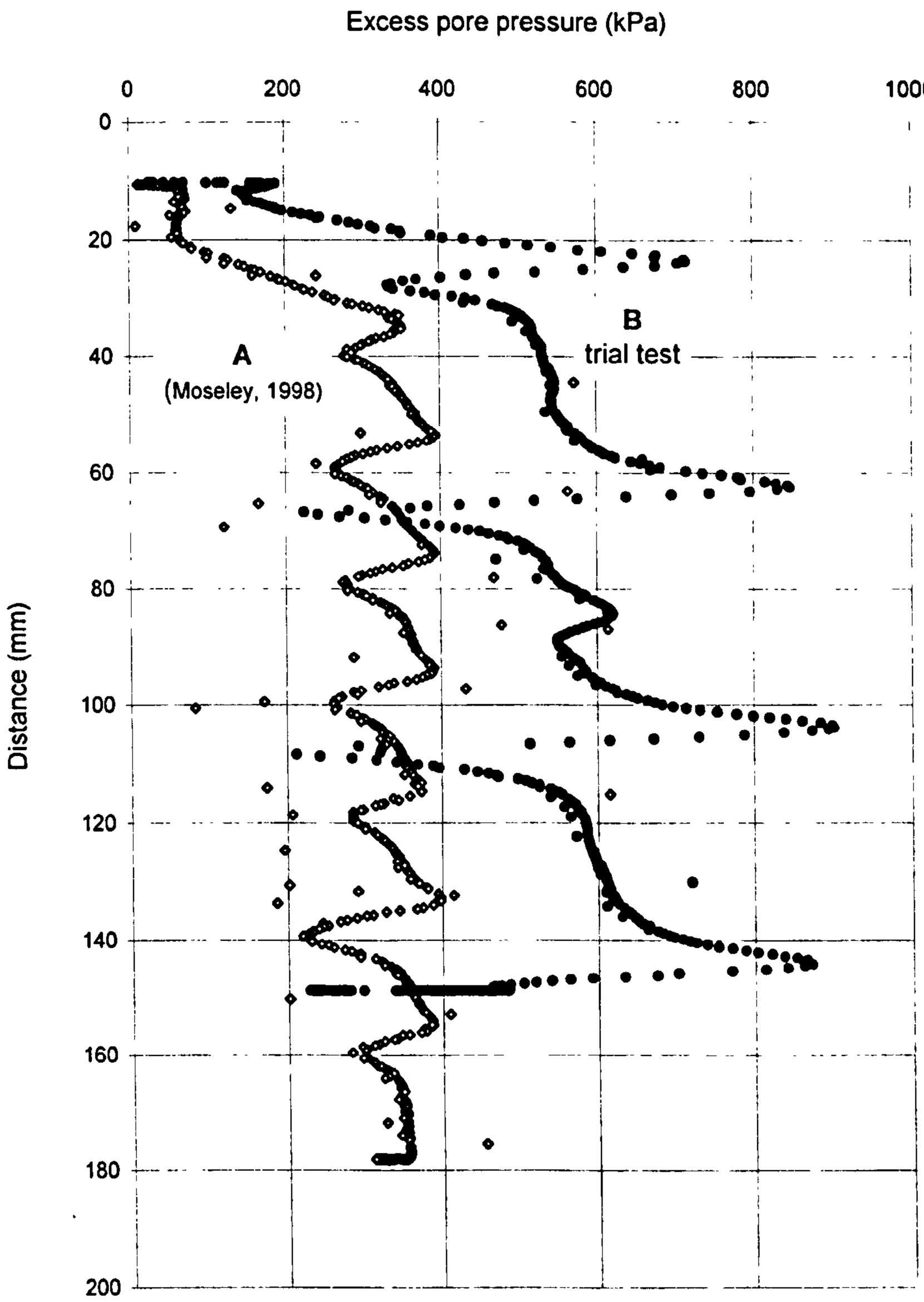

Figure 6.11 Comparison of piezocone pore pressure responses (Moseley (1998) & trial test of present research)

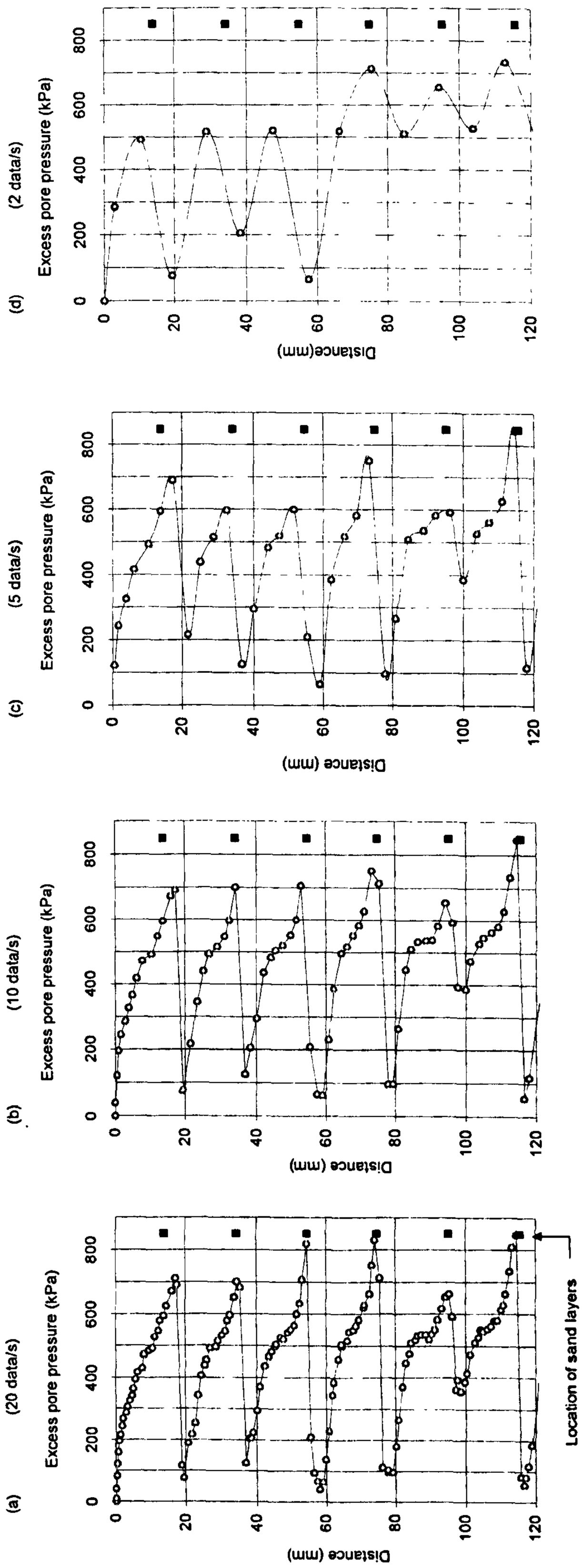

Figure 6.12 Effects of logging rate during cone driving (Test 4, drive 1)

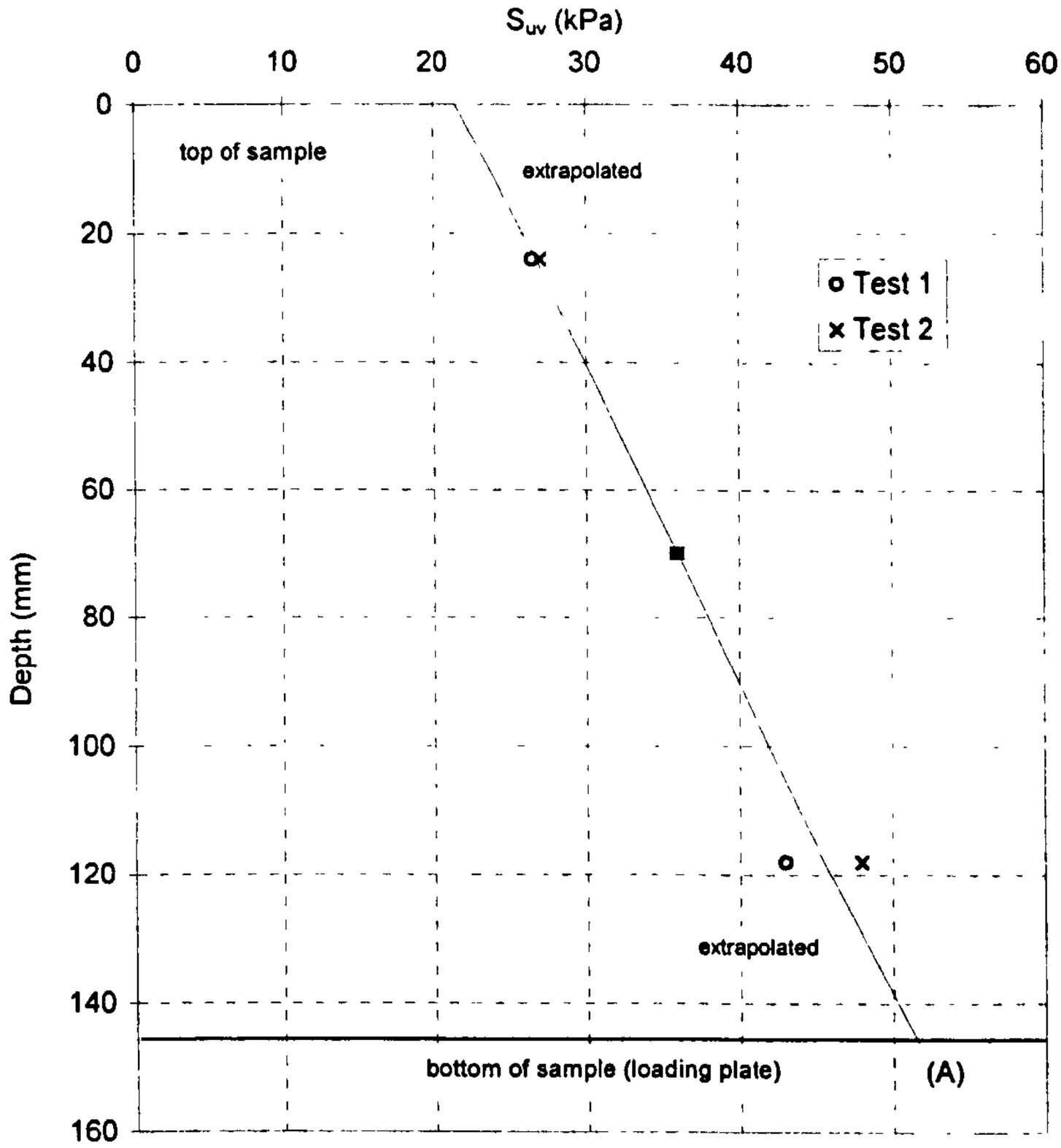

Figure 6.13 Laboratory vane test results from a pure kaolin sample

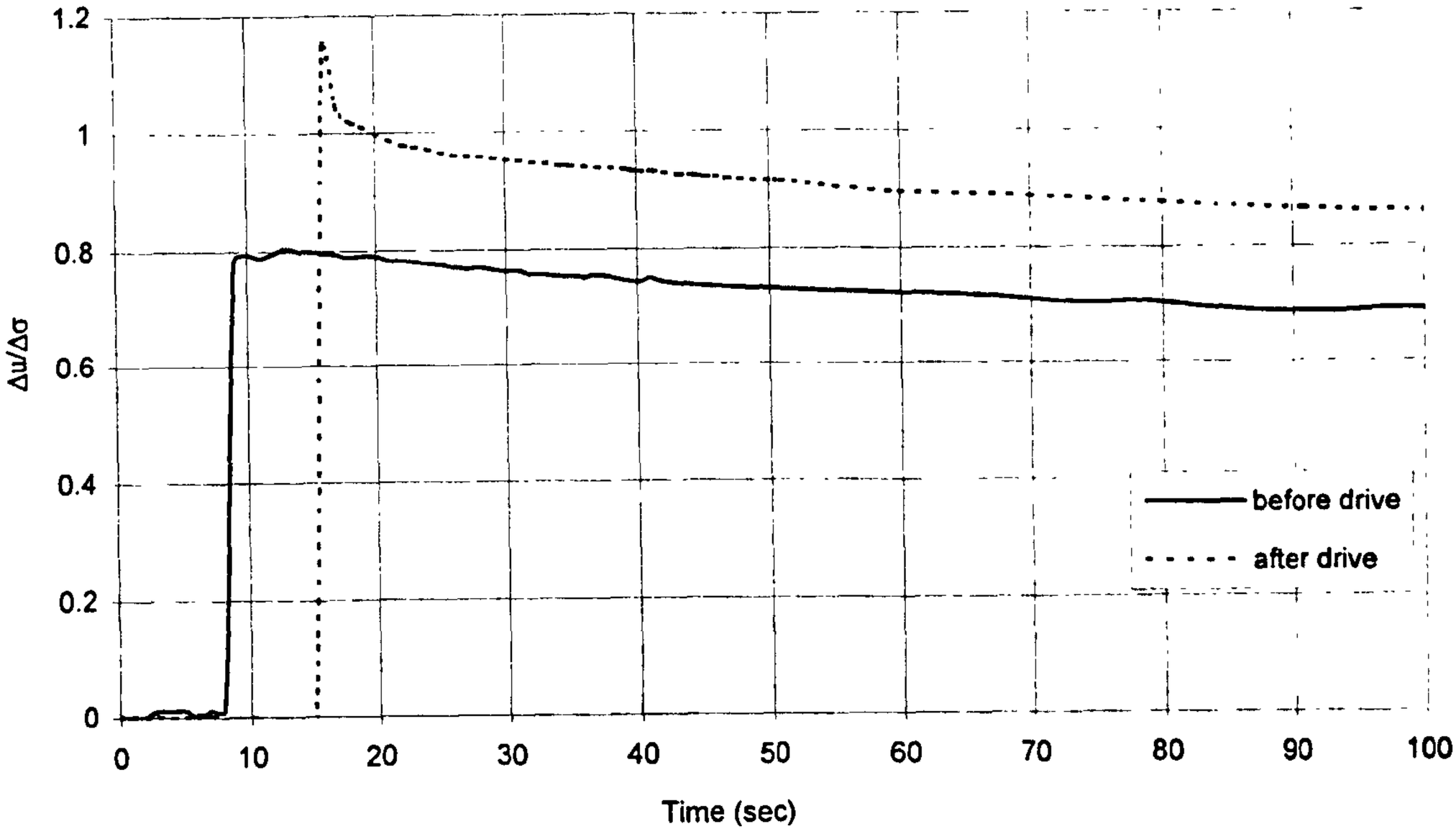

Figure 6.14 Piezocone pore water pressure response to a change of cell pressure in pure clay

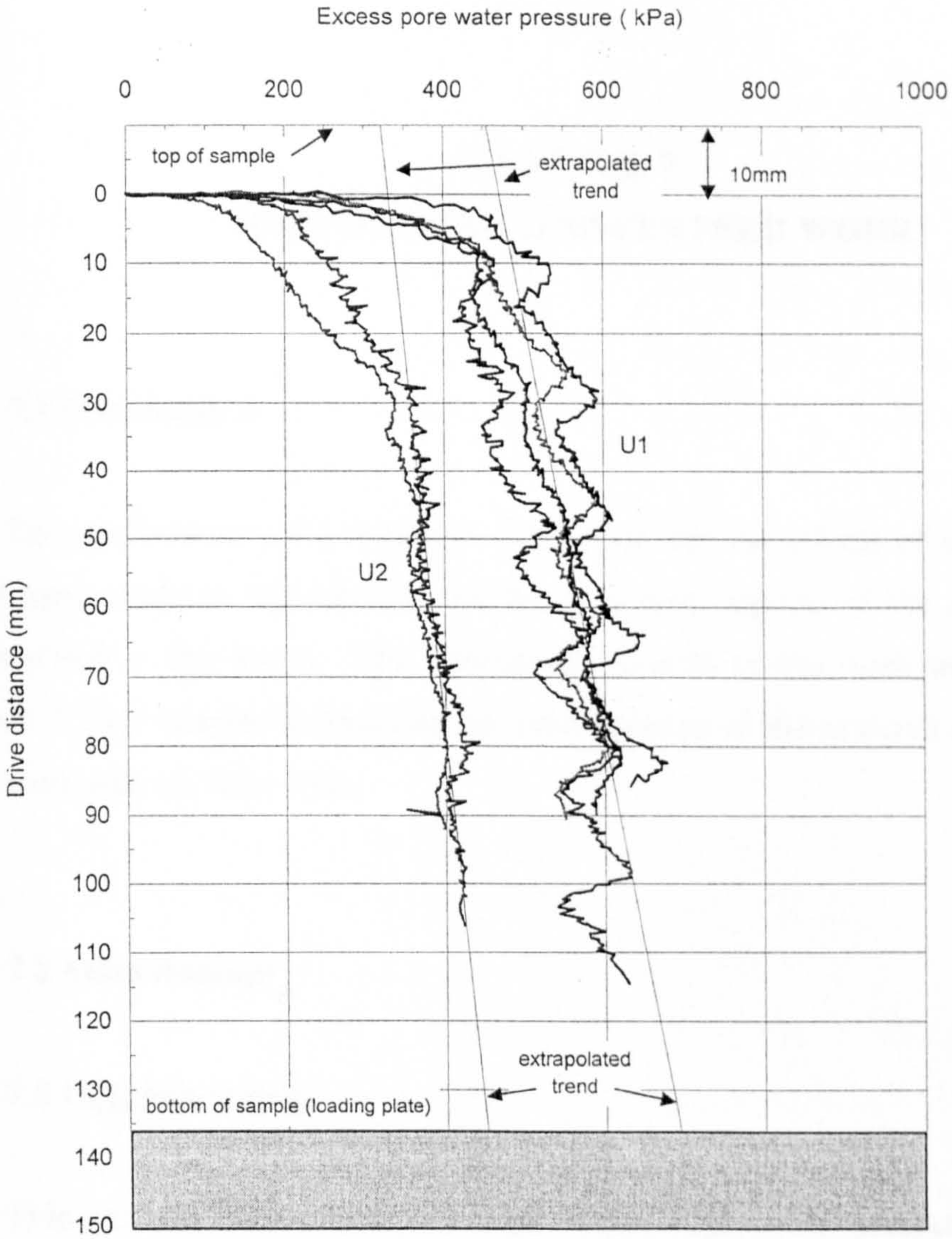

Figure 6.15 Estimating the friction loss at the cell wall using the piezocone pore pressure responses in pure clay

CHAPTER 7

MAIN FINDINGS AND FURTHER WORK

7.1 Introduction

The performance of a miniature piezocone and the effects of smear due to vertical penetration in layered soils are the two main aspects of the experimental work reported in this thesis. The corresponding aims of the work were given in Section 1.2. This chapter summarises the main findings of the research and suggests further work that could be done.

7.2 Main findings

7.2.1 Piezocone tests

1) In terms of the pore pressure response, the Fugro 1 cm^2 piezocone was able to detect more permeable layers (sand or silt) 2mm thick located with a spacing of about 20mm in a clay soil. As the piezocone approached the more permeable layers, very sharp peaks of excess pore water pressure were observed at the cone tip, while these sharp peaks were not observed at the cone shoulder. Once the cone was driven through the more permeable layers, the excess pore water pressure at the cone tip suddenly reduced, while the reduction at the cone shoulder took longer to develop. Dilation and localised drainage in the penetrated permeable layer may have produced negative changes of excess pore water pressure that contributed to the reduction of excess pore water pressure at both the cone tip and shoulder. At a driving speed of

20mm/sec, the minimum logging rate that would probably suffice for detailed profiling is 10 data/s or one reading every 2mm.

2) During dissipation tests, once the piezocone was completely stopped, because of relaxation in the soil surrounding the cone tip or in the driving system, the vertical total stress in the soil around the cone tip rapidly reduced. This stress reduction could have contributed to the rapid reduction of excess pore water pressure at the cone tip shortly after the beginning of the dissipation process. However, the stress reduction, being localised, might not have had much effect on the pore water pressures at the cone shoulder. During the dissipation tests in pure clay, the reduction of the excess pore water pressure around the cone was affected by the "artificial overconsolidation" described by Levadoux & Baligh (1985). Based on the time at 50% dissipation, independently measured c_h values for the clay (kaolin) under one-dimensional swelling and re-compression plotted in a realistic range of rigidity index (I_r = 50-500) on a chart derived from the theoretical solution by Teh & Houlsby (1991) whereas, for the independent c_h values obtained during virgin compression, the data plotted well outside the above range of I_r.

3) In the layered samples, the excess pore water pressure dissipation at the cone shoulder, embedded in the middle of a clay layer, was affected by permeable material which was displaced downwards by the penetration. However, the c_h values determined from a sample with pure sand layers were not much higher than those determined from a sample with no permeable layers. Therefore, although a clay deposit may contain very permeable layers with rather small spacing (approximately twice the cone diameter), if a dissipation test is performed when the cone filter is in a layer of clay, a low value of c_h may still be observed. For dissipation tests using the piezocone with a tip filter, due to the smaller size of the filter, effects of the more permeable layers were even less obvious.

4) During piezocone penetration in pure clay, the average ratio of the excess pore water pressures measured at the cone shoulder and at the cone tip was 0.69. This value is comparable to those recommended (0.6-0.8) for normally consolidated

clay by Lunne et al. (1997). In terms of cone resistance, the experimental values of the cone factor, N_{kt}, agreed well with Yu's (1993) theoretical solution in which the roughness of the cone was considered.

5) For piezocone tests in pure clay, the distance required for a full establishment of excess pore water pressure could be used as an indicator to evaluate the quality of piezocone saturation. With the best achievable saturation and the standard driving speed of 20 mm/sec, a driving distance of approximately 10mm and 30mm was enough for the full establishment of excess pore water pressure measured at the cone tip and cone shoulder respectively.

6) Sintered glass filters made from 45-90mμ glass beads were successfully used as tip filters. However, further investigation concerning the permeability and durability of the material would be needed before it could be used in practice

7.2.2 Vertical drain tests

1) The smear zone in the soil surrounding a penetrating object consists of two main parts. The inner part is the "smearing film" caused by friction between the object and the soil. The outer part is the "deflected fabric zone" caused by displacement of the soil. In the latter part, the degree of disturbance would be expected to be a maximum at the point closest to the drain and then to decrease with distance. The overall degree of smearing in the outer part depends on the shape of the object. The smearing film may not be influenced by the object shape but possibly depends on amount of friction between the soil and the object. The strain path solution (Baligh, 1985) underestimates the vertical displacement of the soil in the deflected fabric zone.

2) Head losses due to the circular drain and band drain installation increased as the permeability ratio (the ratio of the permeability of the more and less permeable layers) increased. The head losses did not vary much when the permeability ratios (k_r) lay between 1 and 100. Then they varied significantly with permeability ratios

between 100 and 10000. In most natural soils, the head losses for a circular drain are likely to be significantly larger than (almost twice as large as) those for a band drain of similar equivalent size. However, this is assuming that the mandrel shape is the same as the drain shape and that there is negligible inward movement of soil surrounding the drain after the mandrel is withdrawn.

3) For natural soils containing pure clay or thin permeable layers for which k_r is less than 100, the head loss due to smear in in-situ permeability tests should be in a range of 35%-45% for circular piezometers with a comparable size to the laboratory device.

7.3 Recommendations of Further Work

1) In profiling soil layers using the piezocone, due to dilation and localised drainage in the penetrated permeable layers, the piezocone may not be able to differentiate between layers and lenses (Section 6.3.1). A parametric study concerning the size, thickness and permeability of the lenses, the size of the piezocone and the location of the pore pressure filter should be performed to evaluate the influence of these factors on the performance of the piezocone. To create small lenses at the piezocone driving positions, parts of the permeable layers could be isolated using small brass rings installed during sample preparation, as mentioned in Section 6.3.7.

2) As mentioned in Section 6.3.1 and 6.3.4, due to the effects of smear at the cone tip and cone shoulder during penetration through a more permeable layer, the vertical distance over which a reduction of the excess pore water pressure occurred was greater than the thickness of the permeable layer. Further work is needed to determine the thickness of permeable layers from the pore water pressure responses obtained from the piezocone. This could be done by varying the thickness of the more permeable layers in the layered sample and, based on pore pressure responses, systematically analysing the error in predicting layer thickness.

3) Although the piezocone results from the present artificial samples are promising, the performance of the piezocone in determining fabric detail (in the form of thin layers) should be also investigated in natural soil deposits, in which the properties and spacing of the layers would be more variable than those in the artificial samples. In the artificial samples, the layering materials changed abruptly from one to another but in natural deposits this change is possibly more gradual (Kenney, 1963).

4) In practice, the piezocone may be driven through unsaturated soil and saturation of the cone filter may not be maintained. The effects of driving through unsaturated soil with various thicknesses and degrees of saturation on the effectiveness of a piezocone should be evaluated. Soil samples containing unsaturated sand or clay layer at the top could be constructed in a calibration chamber for this purpose.

5) Capability of the piezocone in detecting thin permeable layers in a clay soil may be different when the cone is driven at different speeds. Effects of driving speed on piezocone performance should be studied.

6) The effects of a smearing film caused by drain installation on consolidation of a layered soil could be evaluated by performing a parametric study using the finite element method. The influences of the thicknesses and permeability ratio of the layering materials, the thickness and permeability of the smearing film and the spacing of the vertical drain on the rate of consolidation could be considered.

REFERENCES

Al-Tabbaa, A. and Wood, D. M. (1987). Some measurements of the permeability of kaolin. Geotechnique, Vol. 37, No. 4, pp. 499-503.

Al-Tabbaa, A. (1994). Consolidation and swelling with combined vertical and horizontal drainage. International Conference on Computing Methods in Structural and Geotechnical Engineering, Hong Kong.

Ali, H. F. (1991). The influence of filter jacket and core geometry on the longitudinal permeability of a prefabricated vertical drain. Soils and Foundation, JSSMFE, Vol. 31, No. 3, pp. 120-126.

Ali, H. F. (1993). A method to test the performance of a prefabricated vertical drain. Soils and Foundation, JSSMFE, Vol. 33, No. 2, pp. 181-187.

Anderson, W. F., Pyrah, I. C. and Fryer, S. J. (1991). A clay calibration chamber for testing field devices. ASTM Geotechnical Testing Journal, Vol. 14, No. 4, pp. 440-450.

Asaoka, A. (1978). Observational procedure of settlement prediction. Soil and Foundation, Vol. 18, pp. 87-101.

Atkinson, J. H. (1993). An introduction to mechanics of soils and foundations. Published by McGRAW-HILL, Berkshire, UK.

Baguelin, F., Jezequal, J. F. & Le Mehaute, A (1974). Self-boring placement method of soil characteristics measurements. Proceeding of Engineering Foundation Conference on Subsurface Exploration for Underground Excavation and Heavy Construction, Henniker, N. H., pp. 312-332.

Baligh, M. M. (1985). The strain path method. Journal of Geotechnical Engineering, ASCE, Vol. 111, No. 9, pp. 1108-1136.

Baligh, M. M. & Levadoux, J. N. (1980). Pore pressure dissipation after cone penetration. R80-11, Department of Civil Engineering, MIT.

Baligh, M. M., Vivatrat, V. & Ladd, C. C. (1980). Cone penetration in soil profiling. Journal of the Geotechnical Engineering Division, ASCE, 106(GT4), pp. 447-61.

Barron, R. A. (1948). Consolidation of fine-grained soils by drain wells. Transactions of the American Society of Civil Engineers, Vol. 113, N°. 2346, pp. 718-742.

Bergado, D. T., Asakami, H., Alfaro, M. C. and Balasubramaniam, A. S. (1991). Smear effects of vertical drains on soft Bangkok clay. Journal of Geotechnical Engineering, ASCE, Vol. 117, No. 10, pp. 1509-1530.

Brown, M. (2001) Personal communication

Burns, S. E. & Mayne, P. W. (1998). Monotonic and dilatory pore – pressure decay during piezocone tests in clay. Canadian Geotechnical Journal, Vol. 35, pp. 1063-1073

Campanella, R. G. and Robertson, P. K. (1988). Current status of the piezocone test. Proceedings of the 1st International Symposium on Penetration Testing, ISOPT-1, Orlando, Vol. 1, pp. 93-116, Balkema Publications, Rotterdam.

Casagrande, A. & Fadum, R. E. (1940). Notes on soil testing for engineering purposes. Harvard University Graduate School Engineering Publication No. 8.

Chai, J. C. & Miura, N. (1997). A theoretical study on smear effect around vertical drain. Proceedings, 14th International Conference on Soil Mechanics and Foundation Engineering, Vol. 3, Hamburg, pp. 302-305.

Davies, J. A. & Humpheson, C. (1981). A comparison between the performance of two types of vertical drain beneath a trial embankment in Belfast. Geotechnique, Vol. 31, No.1, pp. 19-31.

DeGroot, D. J. & Lutenegger A. J. (1994). A comparison between field and laboratory measurements of hydraulic conductivity in a varved clay. Hydraulic conductivity and waste contaminant transport in soil, ASTM STP 1142.

Edge, M. J. & Sills, G. C. (1989). The development of layered sediment beds in the laboratory as an illustration of possible field processes. Q. Jl Engng Geol. Vol. 22, No. 4, pp. 271-279.

Eid, M. M. (1978). Expansion of cylindrical cavities in clay. Ph.D. thesis, University of Sheffield.

Hansbo, S. (1981). Consolidation of fine-grained soils by prefabricated drains. Proceedings of the 10th International Conference on Soil Mechanics, Stockholm 3, pp. 677-682.

Hird, C. C., Pyrah, I. C. & Russell, D. (1992). Finite element modelling of vertical drains beneath embankments on soft ground. Geotechnique, Vol. 42, No. 3, pp. 499-511.

Hird, C. C. & Moseley, V. J. (2000). Model study of seepage in smear zones around vertical drains in layered soil. Geotechnique, Vol. 50, No. 1, pp. 89-97.

Hird, C. C., Johnson, P. & Sangtian, N. (2001). Performance of a miniature piezocone in profiling thinly layered soil. Proceedings of the 15th International Conference on Soil Mechanics and Geotechnical Engineering, Vol.1, pp.113.

Hird, C. C. (2001) Personal communication.

Holtz, R. D., Jamiolkowski, M. B., Lancellotta, R. & Pedroni, R. (1991). Prefabricated Vertical Drains: Design and Performance. CIRIA. Published by Butterworth-Heinemann Ltd.

Horne, M. R. (1964). The consolidation of a stratified soil with vertical and horizontal drainage. International Journal of Mechanical Sciences, Vol. 6, pp 187-197.

Houlsby, G. T. & Teh, C. I. (1988). Analysis of the piezocone in clay. Proceedings of the 1st International Symposium on Penetration Testing, ISOPT-1, Orlando, Vol. 2, pp. 777-83, Balkema Publications, Rotterdam.

ISSMFE (1999). International reference test procedure for the cone penetration test (CPT) and cone penetration test with pore pressure (CPTU). Report of the ISSMFE technical committee 16 on ground property characterisation from in-situ testing.

ISSMFE (1989). Report of the ISSMFE technical committee on penetration testing of soils - TC 16 with reference test procedures. Published by the Swedish Geotechnical Institute.

Jacobs, P. A. and Coutts, J. S. (1992). A comparison of electric piezocone tips at the Bothkennar test site. Geotechnique, Vol. 42, No. 2, pp. 369-375.

Janbu, N. & Senneset, K. (1974). Effective stress interpretation of in situ static penetration tests. Proceedings of the European Symposium on Penetration Testing, ESOPT, Stockholm, 2.2, pp. 181-193.

Kenney, T. C. (1963). Permeability ratio of repeatedly layered soils. Geotechnique, Vol. 13, No. 4, pp. 325-333.

Kenney, T. C. & Chan, H. T. (1973). Field investigation of permeability ratio in New Liskard varved soil. Canadian Geotechnical Journal, Vol. 10(3), pp. 473-488

Kim, S. S., Jang, Y. S., Kang M. S. & Koh, K. H. (1997). Shape effect of mandrels on smear and well resistance of plastic drain boards. Proceeding of the 7th International Offshore and Polar Engineering Conference, Honolulu, USA.

Kjellman, W. (1948). Accelerating consolidation of fine grained soils by means of cardboard wicks. Proceedings, Second International Conference on Soil Mechanics and Foundation Engineering, Vol. 2, Rotterdam, pp. 302-305.

Koutsoftas, D. C. & Ladd, C. C. (1985). Design strength of an offshore clay. Journal of Geotechnical Engineering, ASCE, Vol. 111, No. 3, pp. 337-355.
Kurup, P. U. (1993). Calibration chamber studies of miniature piezocone penetration tests in cohesive soil specimens. Ph.D. thesis, Louisiana State University.

Lacasse, S. & Lunne, T. (1982). Penetration tests in two Norwegian clays. Proceedings of the 2nd European Symposium on Penetration Testing, ESOPT-II, Amsterdam, 2, pp. 661-9, Balkema Publications, Rotterdam.

Ladd (1990). Stability evaluation during staged construction. Revised Draft March (1990) to be published in the ASCE JGE.

Lambe T. W. & Whitman R. V. (1979). Soil mechanics, SI Version. Published by John Wiley & Sons, Inc.

Lefebvre, G., Ladd, C. C., Mesri, G. & Tavenas, F. (1983). Report of the testing subcommittee. Committee of specialists on sensitive clays on the NBR complex, SEBJ, Montre'al, Canada, Annexe I.

Leroueil, S., Lerat, P., Hight, D. W. & Powell, J. J. M. (1992). Hydraulic conductivity of a recent estuarine silty clay at Bothkennar. Geotechnique, Vol. 42, No. 2, pp. 275-288.

Levadoux, J. N. & Baligh, M. M. (1980). Pore pressure during cone penetration. R80-15, Department of Civil Engineering, MIT.

Levadoux, J. N. & Baligh, M. M. (1986). Consolidation after undrained piezocone penetration. I: Prediction & II: Interpretation. Journal of Geotechnical Engineering, ASCE, Vol. 112, No. 7, pp. 707-726.

Little, J. A., Muir Wood, D., Paul, M. A. & Bouazza, A. (1992). Some laboratory measurements of permeability of Bothkennar clay in relation to soil fabric. Geotechnique, Vol. 42, No. 2, pp. 355-361.

Lunne, T., Robertson, P. K. and Powell, J. J. M. (1997). Cone penetration testing in geotechnical practice. Published by Blackie Academic and Professional, London.

Madhav, M. R., Park, Y. M. & Miura, N. (1993). Modelling study of smear zones around band shaped drains. Soils and Foundations, JSSMFE, Vol. 33, No. 4, pp. 135-147.

May, R. E. (1987). A study of the piezocone penetrometer in normally consolidated clay. D.Phil. Thesis, Oxford University.

Meigh, A. C. (1987). Cone penetration testing. CIRIA, published by Butterworths.

Moseley (1998). Effects of smear during vertical penetration of layered soils. Ph.D. Thesis, University of Sheffield.

Nyirenda, Z. M. & Sills, G. C. (1988). Discussion on paper No. 15 (Interpretation and use of the piezocone test in UK clays by Powell, J. J. M. & Quarterman, R. S. T.) in Proceedings of the Geotechnology Conference: Penetration testing in the UK. Published by Thomas Telford, London.

Ong, Y. P. (1998). Finite element modelling of steady seepage to vertical drain with smear. Msc Dissertation, University of Sheffield.

Onoue, A (1988b). Consolidation by vertical drains taking well resistance and smear into consideration. Soils and Foundations, JSSMFE, Vol. 28, No. 4, pp. 165-174.

Onoue, A (1988). Consolidation of multilayered anisotropic soils by vertical drains with well resistance. Soils and Foundations, JSSMFE, Vol. 28, No. 3, pp. 75-90.

Onoue, A., Ting, N., Germaine, J. T. and Whitmann, R. V. (1991). Permeability of disturbed zone around vertical drains. In: ASCE Geotechnical Special Publication N°. 27, pp. 879-890.

Powrie, W. (1997). Soil mechanics. Published by E & FN Spon, London, UK

Rixner, J. J., Kraemer, S. R. & Smith, A. D. (1986). Prefabricated vertical drains. Vol.1, Engineering Guidelines, FWHA/RD-86/168, Federal Highway Administration, Washington, D. C.

Robertson, P. K. (1990). Soil classification using the cone penetration test. Canadian Geotechnical Journal, Vol. 27(1), pp. 151-158.

Robertson, P. K., Sully J. P., Woeller, D. J., Lunne, T., Powell J. J. M. & Gillespie D. G. Estimating coefficient of consolidation from piezocone tests. Canadian Geotechnical Journal, Vol. 29, pp. 539-550.

Rossato, G., Ninis, N. L. and Jardine, R. J. (1992). Properties of some kaolin based model clay soils. ASTM Geotechnical Testing Journal, Vol. 15, No. 2, pp. 166-179.

Rowe, P.W. (1972). The relevance of soil fabric to site investigation practice. Geotechnique, Vol. 22, No. 2, pp. 195-300

Roy, M., Tremblay, M., Tavenas, F. and La Rochelle, P. (1980). Induced pore pressure in static penetration tests in sensitive clay. Proceedings of the 33rd Canadian Geotechnical Conference, Calgary, Preprint Volume, 11.3.1 to 11.3.13.

Rust, E. & Clayton, C. R. I. (1999). Interpretation of incomplete dissipation data from piezocone tests. Proc. Instn Civ. Engrs. Geotech. Engng, 137, pp. 97-103.

Schaap, L. H. J. & Zuidberg, H. M. (1982). Mechanical and electrical aspects of the electric cone penetrometer tip. Proceedings of the 2nd European Symposium on Penetration Testing, ESOPT-II, Amsterdam, 2, pp. 841-51, Balkema Publications, Rotterdam.

Schmertmann, J. H. (1974). Penetration pore pressure effects on quasi-static cone bearing, q_c. Proceedings of the European Symposium on Penetration Testing, ESOPT, Stockholm, 2.2, pp. 345-351.

Senneset, K. and Jambu, N. (1985). Shear strength parameters obtained from static cone penetration tests. Strength Testing of Marine Sediments; Laboratory and In Situ Measurements. Symposium, San Diego 1984, ASTM Special Technical Publication, STP 883, pp. 41-54.

Senneset, K., Janbu, N. & Svano, G. (1982). Strength and deformation parameters from cone penetration tests. Proceedings of the 2nd European Symposium on Penetration Testing, ESOPT-II, Amsterdam, 2, pp. 863-70, Balkema Publications, Rotterdam.

Schnaid, F., Sills G. C., Soares, J. M. & Nyirenda, Z. (1997). Predictions of the coefficient of consolidation from piezocone tests. Canadian Geotechnical Journal, Vol. 34, pp. 315-327.

Sills, G. C., May, R. E., Henderson, T. and Nyirenda, Z. (1989). Piezocone measurements with four pore pressure positions. Proceedings of the Geotechnology Conference: Penetration Testing in the UK, Birmingham, pp. 247-250. Published by Thomas Telford, London.

Steenhuis, T.S., Kung, K.J.S. & Cathles, L.M. (1990). Finding layers in the soil. Ground-penetrating as a tool in studies of groundwater contamination. Engineering: Cornell Quarterly, Fall 1990, Vol.25, No.1, pp. 15-19

Tavenas, F., Tremblay, M., Larouche, G. & Leroueil, S. (1986). In situ measurement of permeability in soft clay. Proceeding of In Situ'86, Geotechnical special publication No.6, ASCE, Virginia, June 1986.

Taylor, D. W. (1942). Research on consolidation of clays, Serial No. 82. Department of Civil and Sanitary Engineering, MIT, Cambridge, Mass.

Taylor D. W. (1948). Fundamentals of soil mechanics. Published by John Wiley & Sons, Inc., New York, N.Y.

Teh, C. I. (1987). An analytical study of the cone penetration test. D.Phil. Thesis, Oxford University.

Terzaghi, K. & Peck, R. B. (1967). Soil mechanics in engineering practice. John Wiley, New York, second edition.

Tomlinson (1995). Foundation design & construction. Published by Longman Singapore Publishers (Pte) Ltd.

Torstensson, B. A. (1975). Pore pressure sounding instrument. Proceeding in the ASCE Specialty Conference on In Situ Measurement of Soil Properties, Raleigh, North Carolina, 2, pp. 48-54, American Society of Engineers (ASCE).
Torstensson, B. A. (1984). A new system for ground water monitoring. Ground water monitoring review, Vol. 4, No.4, pp. 131-138.

Torstensson, B. A. & Petsonk, A. M. (1986). A device for in situ measurement of hydraulic conductivity. Proceeding in 4th International Geotechnical Seminar on Field Instrumentation and in situ Measurements, Singapore, pp. 157-162.

Vaid, Y. P. & Campanella, R. G. (1974). Triaxial and plane strain behavior of natural clay. Journal of Geotechnical Engineering, ASCE, Vol. 100, No. 3, pp. 207-224.

Van den Berg, P. (1994). Analysis of soil penetration. Delft University Press.

Wissa, A. E. Z., Martin, R. T. & Garlanger, J. E. (1975). The piezometer probe. Proceeding in the ASCE Specialty Conference on In Situ Measurement of Soil Properties, Raleigh, North Carolina, 1, pp. 536-545, American Society of Engineers (ASCE).

Whittle, A. J. & Aubeny, C. P. (1991). Pore pressure fields around piezocone penetrometers installed in clay. Proceedings of the 7th International Symposium on Computer Methods and Advances in Geomechanics, Cairns, 1, pp. 285-90. Balkema Publications, Rotterdam.

Wroth, C. P. (1984). The interpretation of in situ soil tests. Geotechnique, Vol. 34, No. 4, pp. 449-489.

Worth, C. P. (1988). Penetration testing – a more rigorous approach to interpretation. Proceedings of the 1st International Symposium on Penetration Testing, ISOPT-1, Orlando, Vol. 1, pp. 303-11, Balkema Publications, Rotterdam.

Yu, H. S. (1993). Discussion on: singular plastic fields in steady penetration of rigid cone. J. Appl. Mech., 60, 1061-1062